MONOGENIC DIABETES: FROM GENETICS AND CELL BIOLOGY TO CLINICAL PRACTICE

EDITED BY: Ming Liu, Jiajun Zhao, Fabrizio Barbetti and Simone Baltrusch
PUBLISHED IN: Frontiers in Endocrinology

frontiers Research Topics

frontiers

ISSN 1664-8714
ISBN 978-2-83250-199-3
DOI 10.3389/978-2-83250-199-3

About Frontiers

Frontiers is more than just an open-access publisher of scholarly articles: it is a pioneering approach to the world of academia, radically improving the way scholarly research is managed. The grand vision of Frontiers is a world where all people have an equal opportunity to seek, share and generate knowledge. Frontiers provides immediate and permanent online open access to all its publications, but this alone is not enough to realize our grand goals.

Frontiers Journal Series

The Frontiers Journal Series is a multi-tier and interdisciplinary set of open-access, online journals, promising a paradigm shift from the current review, selection and dissemination processes in academic publishing. All Frontiers journals are driven by researchers for researchers; therefore, they constitute a service to the scholarly community. At the same time, the Frontiers Journal Series operates on a revolutionary invention, the tiered publishing system, initially addressing specific communities of scholars, and gradually climbing up to broader public understanding, thus serving the interests of the lay society, too.

Dedication to Quality

Each Frontiers article is a landmark of the highest quality, thanks to genuinely collaborative interactions between authors and review editors, who include some of the world's best academicians. Research must be certified by peers before entering a stream of knowledge that may eventually reach the public - and shape society; therefore, Frontiers only applies the most rigorous and unbiased reviews.
Frontiers revolutionizes research publishing by freely delivering the most outstanding research, evaluated with no bias from both the academic and social point of view. By applying the most advanced information technologies, Frontiers is catapulting scholarly publishing into a new generation.

What are Frontiers Research Topics?

Frontiers Research Topics are very popular trademarks of the Frontiers Journals Series: they are collections of at least ten articles, all centered on a particular subject. With their unique mix of varied contributions from Original Research to Review Articles, Frontiers Research Topics unify the most influential researchers, the latest key findings and historical advances in a hot research area! Find out more on how to host your own Frontiers Research Topic or contribute to one as an author by contacting the Frontiers Editorial Office: frontiersin.org/about/contact

MONOGENIC DIABETES: FROM GENETICS AND CELL BIOLOGY TO CLINICAL PRACTICE

Topic Editors:
Ming Liu, Tianjin Medical University General Hospital, China
Jiajun Zhao, Shandong Provincial Hospital, China
Fabrizio Barbetti, University of Rome Tor Vergata, Italy
Simone Baltrusch, University Hospital Rostock, Germany

Citation: Liu, M., Zhao, J., Barbetti, F., Baltrusch, S., eds. (2022). Monogenic Diabetes: From Genetics and Cell Biology to Clinical Practice. Lausanne: Frontiers Media SA. doi: 10.3389/978-2-83250-199-3

Table of Contents

frontiers | Frontiers in Endocrinology

TYPE Editorial
PUBLISHED 31 August 2022
DOI 10.3389/fendo.2022.1022611

OPEN ACCESS

EDITED AND REVIEWED BY
Åke Sjöholm,
Gävle Hospital, Sweden

*CORRESPONDENCE
Ming Liu
mingliu@tmu.edu.cn

SPECIALTY SECTION
This article was submitted to Clinical Diabetes, a section of the journal Frontiers in Endocrinology

RECEIVED 18 August 2022
ACCEPTED 19 August 2022
PUBLISHED 31 August 2022

CITATION
Ding L, Barbetti F and Liu M (2022) Editorial: Monogenic diabetes: from genetics and cell biology to clinical practice.
Front. Endocrinol. 13:1022611.
doi: 10.3389/fendo.2022.1022611

Editorial: Monogenic diabetes: from genetics and cell biology to clinical practice

Li Ding[1], Fabrizio Barbetti[2] and Ming Liu[1]*

[1]Department of Endocrinology and Metabolism of Tianjin Medical University General Hospital, Tianjin, China, [2]Department of Experimental Medicine, University of Rome Tor Vergata, Rome, Italy

KEYWORDS

monogenic diabetes, maturity-onset diabetes of the young, personalized medicine, clinical characterisation, pathogenesis

Editorial on the Research Topic
Monogenic diabetes: from genetics and cell biology to clinical practice

Monogenic diabetes mellitus (MDM) is a special type of diabetes caused by a single gene mutation. MDM accounts for approximately 1-5% of all causes of diabetes. MDM can be classified as neonatal diabetes mellitus (NDM), maturity-onset diabetes of the young (MODY), mitochondrial diabetes, and some rare genetic syndromes associated with diabetes. To date, mutations in more than 60 genes have been reported to cause MDM. Most of the genes are critical for pancreatic beta cell function, development, and survival. Pathogenetic mutations in the genes involved in insulin action can also cause MDM. Over the past decades, significant advances have been made in MDM awareness, diagnosis, and management. However, patients with MDM are easily misdiagnosed as type 1 diabetes or type 2 diabetes, and may not receive appropriate management. There are significant unmet medical needs for improving recognition, appropriate clinical/genetic testing/diagnosis and management, as well as better understanding of the underlying mechanisms of MDM. In this special issue, we have come together an array of reports encompassing disease spectrum and clinical characteristics of monogenic diabetes, as well as novel techniques for functional analysis of variants.

A series of studies in this Research Topic expanded our knowledge regarding genetic etiology and pathogenesis of monogenic diabetes. Yang et al. identified a novel, heterozygous INS nonsense mutation, preproinsulin R46X in two unrelated patients with early onset diabetes. Mechanistically, despite with an intact signal peptide, R46X failed to be efficiently translocated into the ER, highlighting that proinsulin domain downstream of signal peptide plays an important unrecognized role in preproinsulin translocation. Given the fact that some family members carrying R46X do not develop diabetes, further studies are warranted to determine additional genetic and/or environmental factors contributing to the development and progression of diabetes in the patients carrying R46X. In an intriguing case report, Zhou et al. described a Chinese family of Woodhouse-Sakati syndrome presented with diabetes mellitus,

hypogonadotropic hypogonadism, central hypothyroidism, alopecia, and intellectual disability, caused by a novel biallelic deletion mutation of the DCAF17 gene. Jiang et al. identified a novel missense mutation GCK p.A259T, which cosegregated with diabetes in a Chinese MODY2 pedigree. The authors conducted extensive kinetic and thermal stability analysis, and showed that the mutation impaired the affinity, catalytic capability, and cooperativity for the glucose substrate. Koneshamoorthy et al. described a novel GCK activating mutation in an adult with hypoglycemia. The variant segregated with hypoglycemia in the pedigree, and morphological changes were observed in the islet of the patient, along with accentuated glucose stimulated insulin secretion, cytosolic calcium response to glucose, and changes in single cell transcriptomics in the pancreatic islets.

Functional analysis of variants identified is vital in confirmation of disease causality and pursuit of treatment options, but can be difficult. In a two-part series, Dhayalan et al. proposed a single-chain peptide model, "DesDi", that comprised 49 residues and a single disulfide bridge, optimized for efficiency of disulfide pairing. The platform enabled comparative biophysical studies, regarding α-helix contents, thermal unfolding profiles, thermodynamic stabilities, and NMR resonance properties, of mutations that cause Mutant INS-gene Induced Diabetes of the Young (MIDY). Location and degree of structural perturbation that the MIDY variants caused, assessed by the peptide model, correlated with degree of ER stress and age of diabetes onset. Taken together, the model allows molecular dissection of phenotype-genotype relationships of MIDY variants. Guo et al. developed a scalable dual fluorescence assay in cells, that enables functional characterization of HNF-4α missense variants, with respect to transcription activity and expression abundance, identified in exome sequencing. In combination with cloning and Sanger sequencing, the method allows quantitative and high-throughput interpretation of HNF-4α variants.

Monogenic diabetes is under-diagnosed. Awareness of clinical presentations of monogenic diabetes is a prerequisite for recognition of the condition, and subsequent diagnosis and personalized management. In a comprehensive review, Li et al. discussed the pathogenesis and treatment of maturity-onset diabetes of the young type 3, and the association of HNF1A single nucleotide polymorphisms with type 2 diabetes and gestational diabetes. Zhao et al. reviewed the literature extensively, and investigated the clinical presentations of patients with HNF1-alpha MODY. The authors found that clinical manifestations of HNF1-alpha MODY differed by geographical regions and HNF1-alpha mutations. Ge et al. reviewed the clinical presentations and gene mutations of MODY5, in the literature, and concluded that testing for MODY5 should be prioritized in patients with early-onset diabetes, low or normal BMI, renal cysts, hypomagnesemia, and pancreatic dysplasia. Yang et al. reviewed literature, and investigated the genetic spectrum and the clinical features of maternally inherited diabetes and deafness caused by deleterious mitochondrial mutations. The authors found that the heteroplasmy levels of the m.3243A>G mutation in the peripheral blood was negatively correlated with age at the onset of diabetes, and argued that young onset of diabetes with low or normal BMI, maternal inheritance and presence of impairments of multiple systems should prompt a genetic testing for maternally inherited diabetes and deafness. Zhao et al. found that plasma lactate immediately and 30 minutes after exercise could contribute to the differential diagnosis of mitochondrial diabetes and type 1 diabetes. In longitudinal follow-up, fasting C-peptide in patients with mitochondrial diabetes declined rapidly within the first 5 years after diagnosis, and stabilized at low levels 10 years after diagnosis. Abreu et al. investigated the proportion and genetic spectrum of monogenic diabetes in a cohort of patients in Brazil, providing evidence for screening for monogenic diabetes in such a population with mixed ethnic backgrounds.

The field of monogenic diabetes is rapidly evolving. We hope this Research Topic will motivate doctors/researchers in promoting wider recognition, timely diagnosis, and proper management of monogenic diabetes.

Author contributions

All authors listed have made a substantial, direct, and intellectual contribution to the work and approved it for publication.

Funding

This work was supported by the National Natural Science Foundation of China 446 (81830025), and also by Tianjin Key Medical Discipline 451 (Specialty) Construction Project (TJYXZDXK-030A).

Conflict of interest

The authors declare that the research was conducted in the absence of any commercial or financial relationships that could be construed as a potential conflict of interest.

Publisher's note

frontiers in Endocrinology

REVIEW
published: 25 November 2021
doi: 10.3389/fendo.2021.728043

The Mutations and Clinical Variability in Maternally Inherited Diabetes and Deafness: An Analysis of 161 Patients

Mengge Yang[1,2], Lusi Xu[1,2], Chunmei Xu[1,2], Yuying Cui[3], Shan Jiang[4], Jianjun Dong[4] and Lin Liao[1,2]**

[1] Cheeloo College of Medicine, Shandong University, Department of Endocrinology and Metabolology, Shandong Provincial Qianfoshan Hospital, Shandong Key Laboratory of Rheumatic Disease and Translational Medicine, Shandong Institute of Nephrology, Ji-nan, China, [2] Department of Endocrinology and Metabolology, The First Affiliated Hospital of Shandong First Medical University & Shandong Provincial Qianfoshan Hospital, Ji-nan, China, [3] College of Traditional Chinese Medicine, Shandong University of Traditional Chinese Medicine, Ji-nan, China, [4] Division of Endocrinology, Department of Internal Medicine, Qilu Hospital of Shandong University, Ji-nan, China

OPEN ACCESS

Edited by:
Ming Liu,
Tianjin Medical University General Hospital, China

Reviewed by:
Mouna Tabebi,
Linköping University Hospital, Sweden
Chen-Chi Wu,
National Taiwan University Hospital, Taiwan

***Correspondence:**
Lin Liao
liaolin@sdu.edu.cn
Jianjun Dong
dongjianjun@sdu.edu.cn

Specialty section:
This article was submitted to Clinical Diabetes, a section of the journal Frontiers in Endocrinology

Received: 20 June 2021
Accepted: 01 November 2021
Published: 25 November 2021

Citation:
Yang M, Xu L, Xu C, Cui Y, Jiang S, Dong J and Liao L (2021) The Mutations and Clinical Variability in Maternally Inherited Diabetes and Deafness: An Analysis of 161 Patients. Front. Endocrinol. 12:728043. doi: 10.3389/fendo.2021.728043

Aims: To investigate the clinical features and mitochondrial mutations for maternally inherited diabetes and deafness.

Methods: PubMed, Embase, Medline, Web of Science, the China National Knowledge Infrastructure, and Wanfang were searched with the following search terms: "Maternally inherited diabetes and deafness" OR "MIDD" OR "Mitochondrial diabetes". The mutations and clinical features were analyzed. Correlation between the heteroplasmy levels of the m.3243A>G mutation in the peripheral blood and age at the onset of diabetes was conducted by Spearman test. The significance level was set as $p < 0.05$. Statistical analysis was performed using the Statistical Package for the Social Sciences version 26 for Windows.

Results: Totally 161 patients with 21 different mitochondrial mutations were enrolled. The most common mutation was the m.3243A>G mutation in 136 cases. Of 142 patients, 120 (84.51%) had family histories of diabetes or hearing loss. Hearing loss presented in 85.71% of the patients with mitochondrial mutations. Central nervous system diseases were found in 29.19%, myopathy in 22.98%, oculopathy in 23.60%, cardiac disease in 23.60%, and nephropathy in 13.66% of the patients. Forty-two of 101 (41.58%) patients were underweight. A significant negative correlation was found between the heteroplasmy levels of the m.3243A>G mutation in the peripheral blood and age at the onset of diabetes.

Conclusions: The young onset of diabetes with low or normal BMI, maternal inheritance, and presence of impairments of multiple systems should prompt a genetic testing in order to differentiate MIDD from other types of diabetes earlier.

Keywords: treatment, diagnosis, mitochondrial gene mutations, heteroplasmy, maternally inherited diabetes and deafness

INTRODUCTION

Diabetes mellitus is one of the most important chronic non-communicable disease, which has been a significant global public health problem. The incidence of monogenic diabetes mellitus has increased in recent years due to greater awareness and wider availability of genetic testing. Monogenic diabetes mellitus comprises a heterogeneous group of diabetes which are caused by a single gene defect (1). A subtype of monogenic diabetes associated with mutations in the mitochondrial DNA is referred to as maternally inherited diabetes and deafness (MIDD), which was first described in 1992 by Van den Ouveland et al. (2). The abnormality of glucose metabolism in MIDD is associated with a gradual decrease in insulin secretion due to reduced ATP production in pancreatic β-cells with abnormal mitochondria (3). The diagnosis and differentiation of MIDD from type 1 and type 2 diabetes are important in view of the implications for treatment and prognosis as well as for identification of family members at risk of diabetes (2). However, the clinical features of MIDD are variable, and MIDD is frequently misdiagnosed as other types of diabetes. Thus, it is extremely essential to recognize MIDD among the diabetic patients. It is a pity that there is no systematic summary about the disease up to now. Our study summarized the clinical features and mutations in reported MIDD to help the doctors better diagnose and manage these patients.

SUBJECTS AND METHODS

PubMed, Embase, Medline, Web of Science, the China National Knowledge Infrastructure (CNKI), and Wanfang were searched from the date of their inception to February 10, 2021, without language restrictions. The key words used were "Maternally inherited diabetes and deafness" OR "MIDD" OR "Maternally inherited diabetes" OR "Mitochondrial diabetes." Eligible studies met the following criteria: (1) Mitochondrial mutations were confirmed by genetic testing, and detection of the mutation was based on polymerase chain reaction (PCR) amplification. (2) The mutation sites were described. (3) The main clinical data of patients were described. The flow chart (**Supplementary Data Figure S1**) showed the reasons for identification of eligible studies.

From the eligible studies, the following data were extracted: (1) country, (2) gender, (3) age at onset of diabetes and hearing loss, (4) family history, (5) therapies, (6) BMI, (7) fasting C-peptide, (8) mutation sites, (9) antibodies, (10) the heteroplasmy levels in tissues.

Abbreviations: MIDD, maternally inherited diabetes and deafness; mtDNA, mitochondrial DNA; tRNA, transfer RNA; PCR, polymerase chain reaction. GADA, glutamic acid decarboxylase antibody; IAA, insulin autoantibody; ICA, islet cell antibody; OHA, oral hypoglycemic agents; MELAS, mitochondrial encephalopathy lactic acidosis and stroke like episodes; CPEO, chronic progressive external ophthalmoplegia; FSGS, focal glomerulosclerosis.

Statistical Analyses

Correlation between the heteroplasmy levels of the m.3243A>G mutation in the peripheral blood and age at the onset of diabetes was conducted by Spearman test. The significance level was set as $p < 0.05$. Statistical analysis was performed using the Statistical Package for the Social Sciences version 26 for Windows (SPSS).

RESULTS

Epidemiological Characteristics and Gene Mutations

One hundred and sixteen studies including 161 patients were eligible with the aforementioned search terms. Among them, Asian cases accounted for the largest part (108 cases, 67.08%), followed by European (43 cases, 26.71%), North American (5 cases, 3.11%), South American (3 cases, 1.86%), African and Oceania (1 case, 0.62%, respectively). Among the Asian, cases from China, Japan, India, Iran, and Korea accounted for 39.75, 25.47, 0.62, 0.62, and 0.62%, respectively. Totally 21 different mtDNA mutations were identified. Most of the patients (158/161, 98.14%) had one mutation, and three (3/161, 1.86%) had two mutations. The most common mutation was the m.3243A>G mutation, which accounted for 84.47% of the cases, while other mutations were quite rare. The detailed information of enrolled countries and individuals are described in **Table S1** (**Supplementary Materials**) and **Figure 1**.

Clinical Characteristics

The clinical data at diagnosis of the patients are shown in **Table S2** (**Supplementary Materials**) and **Figures 2** and **3**. Among the 161 patients, 60.25% (97/161) were female and 39.75% (64/161) were male. Family histories were mentioned in 142 patients, and among them, 59.86% (85/142) had family histories of both diabetes and hearing loss; 21.83% (31/142) had family history of diabetes; 2.82% (4/142) had family history of hearing loss. Mitochondrial mutations were detected in 3.52% (5/142) of patients' relatives who had no hyperglycemia or hearing loss. The body-mass-index (BMI) at diagnosis were available in 101 patients. Their BMI ranged from 12.5 to 36.89 kg/m² (mean 19.41 kg/m²). The group of underweight (<18.5 kg/m^2), normal weight, overweight (25~29.9 kg/m^2), or obese (≥30 kg/m^2) accounted for 41.58, 51.49, and 6.93%, respectively, according to WHO standard.

Fasting C-peptide data were available in 42 patients, with a mean of 0.83 ng/ml, lower than the normal range (1.1~4.4 ng/ml). Diabetes antibodies were reported in 50 patients, and among them, only five (10.00%) patients had positive results (one case had GADA, two cases had IAA, and two cases had ICA).

The clinical manifestations of MIDD patients are shown in **Table S3** (**Supplementary Materials**). Hearing impairment presented in 138 (85.71%) patients. Central nervous system diseases were found in 47 (29.19%) patients, including encephalatrophy (11.18%), cerebellar ataxia (6.21%), basal ganglia calcification (2.48%), migraine (4.97%), and cerebral infarction (5.59%). Peripheral neuropathy was found in 28 (17.39%) patients. Myopathy was presented in 37 (22.98%)

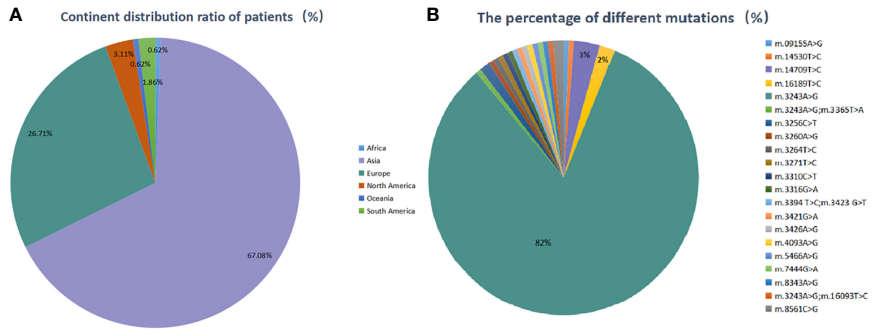

FIGURE 1 | **(A)** Geographical country distribution ratio among the patients (%), **(B)** the percentage of different mutation sites (%).

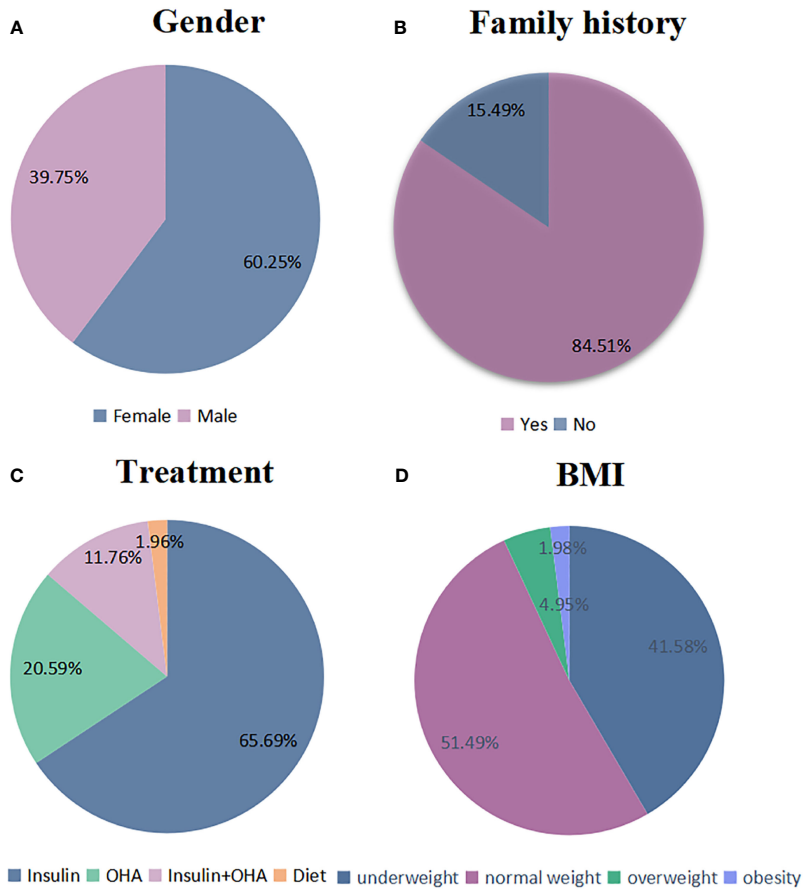

FIGURE 2 | Clinical characteristics of patients with mitochondrial mutations. **(A–D)** The proportion of several clinical characteristics in enrolled patients: **(A)** gender (N: 161), **(B)** family histories (N: 142), **(C)** treatment (N: 102), and **(D)** BMI (N: 101).

patients manifesting muscle weakness (14.91%), myophagism (4.97%), ptosis (2.48%). Ragged red fibers on muscle biopsy were seen in 26 (16.15%) patients. Oculopathy was observed in 38 (23.60%) patients, and the prevalence of macular degeneration (9.32%) was higher than proliferative retinopathy (5.59%). Cardiac disease was present in 38 (23.60%) patients, and 19 (11.80%) patients had a manifestation of ventricular hypertrophy and 15 (9.32%) patients had a manifestation of arrhythmia. Nephropathy, defined by the presence of albuminuria and/or impairment in renal function, was found in 22 (13.66%) patients.

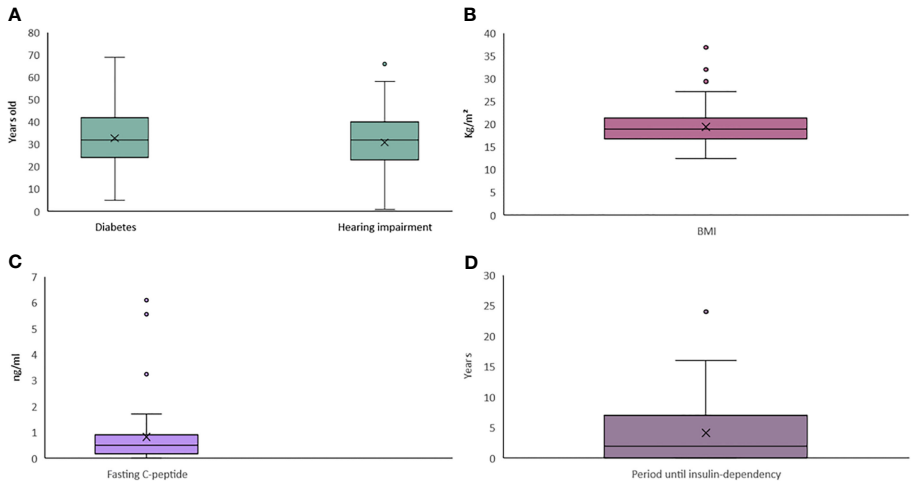

FIGURE 3 | Whisker plot for continuous clinical data of patients with mitochondrial mutations. **(A–D)** Continuous data for the variables of **(A)** Age at onset, **(B)** BMI, **(C)** Fasting C peptide, and **(D)** Period until insulin dependency.

Gastrointestinal symptoms were observed in 9 (5.95%) patients. In addition to diabetes, other endocrine disorders involving hypogonadism (1.86%) and osteoporosis (2.48%) were observed.

Treatment

The treatments of 102 patients were provided in the original articles. Seventy-nine patients (79/102, 77.45%) injected insulin, and 23 patients (23/102, 22.55%) did not. Among them, 67 patients (67/102, 65.69%) received insulin without oral hypoglycemic agent. Twenty-two patients (21/102, 20.59%) received oral hypoglycemic agents (OHA) without insulin, and 12 (12/102, 11.76%) received both insulin and OHA. Two patients (2/102, 1.96%) underwent diet therapy only. Among the patients who received insulin, 37.18% (29/78) initiated once diabetes was diagnosed. The mean time from the diagnosis of diabetes to insulin therapy was 4.15 years. Onset of the diabetes usually occurred at an early age with a mean age of 32.79 years, and the mean age of onset of hearing impairment was 30.84 years.

Heteroplasmy Levels

The heteroplasmy levels of the m.3243A>G mutation in different tissues are shown in **Table 1**. The blood heteroplasmy levels in 27 patients ranged from 0.102 to 58%, with a mean value of 26.97%. The mean heteroplasmy levels in urothelium, muscle, hair follicle, buccal mucosa, nail, and myocardium were 58.13, 49.53, 41.35, 48.25, 32.00, and 67.50% respectively. We used different colors representing different mutations in the scattergram, which showed a negative correlation between blood heteroplasmy levels and age at the onset of diabetes (**Figure 4**). A significant negative correlation was found between the blood mutation levels of the m.3243A>G mutation and age at the onset of diabetes ($P<0.01$) (**Table 2**).

DISCUSSION

Since MIDD was first described, there have been some reports about this disease. However, most studies about MIDD involved only a small series of patients. Unlike previous studies, we summarized the clinical features and mutations of 161 patients with mitochondrial mutations. Our study demonstrated the MIDD patients with most mutations had the following clinical characteristics: (1) high incidence of progressive neurosensory deafness (85.71%); (2) early onset of diabetes and deafness; (3)

TABLE 1 | The heteroplasmy levels of the m.3243A>G mutation in different tissues.

Tissue	N	Heteroplasmy levels (%)		
		Min	Max	Mean
Peripheral blood leukocyte	27	0.102	58	26.97
Urothelium	3	31.4	76	58.13
Muscle	7	0.024	90	49.53
Buccal mucosa	4	40	58	48.25
Hair follicle	2	12.7	70	41.35
Nail	1	32	32	32.00
Myocardium	2	60	75	67.50

N, number of patients.

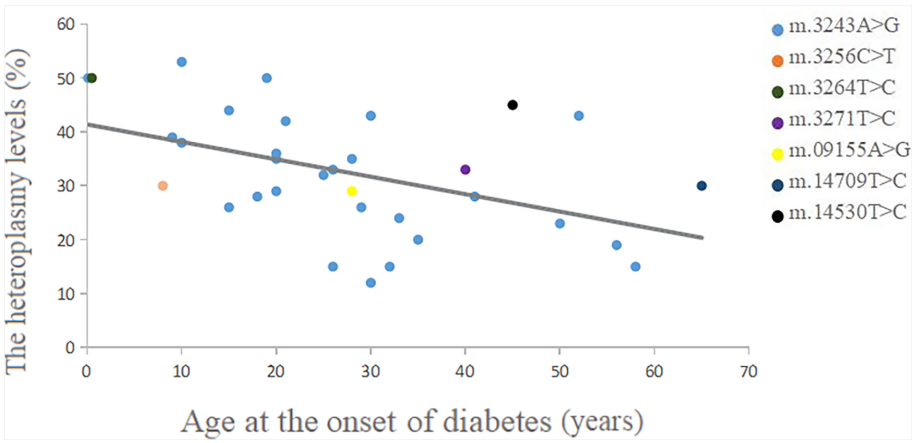

FIGURE 4 | Correlation between blood heteroplasmy levels and age at the onset of diabetes.

TABLE 2 | Correlation between blood heteroplasmy levels of the m.3243A>G mutation and age at the onset of diabetes.

Age at onset	The heteroplasmy levels in peripheral blood	blood
	r	p
Diabetes	−0.612	0.001**

$^{**}p < 0.01$

high incidence of maternal inheritance (84.51%); (4) thin and short stature (41.58%); (5) absence of diabetes antibodies (90.00%); (6) progressive insulin secretory defect.

But not all patients with mitochondrial mutations met the above characteristics. The m.3426 A>G and m.16189T>C mutation were considered as susceptibility factors for insulin resistance and T2DM, which were also maternal inherited (4–6). The patients with m.3426 A>G mutation did not have deafness and had late onset age of diabetes (mean 42.14 years) with the BMI above the normal range (mean 27.14 kg/m^2) and usually had no complications (4). In addition, the laboratory characteristics of patients with m.3426A>G mutation was that they had normal levels of fasting C-peptide and usually took oral hypoglycemic agents for treatment (4, 6). The patients with m.16189T>C mutation were also usually overweight (mean BMI 28.12 kg/m^2) and had high HOMA-IR (5). The reason for the above differences is not clear yet. Previous studies have demonstrated the m.3243A>G mutation is associated with both insulin deficiency and reduced insulin sensitivity in patients with MIDD (7). Sequential follow-up of patients with the 3243 mutation documented decreased sensitivity to insulin prior to the development of insulin deficiency (7). A presumable supposition is that reduced sensitivity to insulin could be a consequence of minor mitochondrial dysfunction, and deficiency only occurred with a severe defect. The mutations 3426A>G and 16189T>C have less impact on mitochondrial function than 3243A>G.

MtDNA is passed from the mother to offspring; therefore, it is generally accepted mitochondrial diabetes is also maternally inherited (8, 9). However, in our study, 22 patients were sporadic cases without family histories of diabetes and hearing loss. Among the 22 patients, mitochondrial mutations were detected in five patients' relatives who had no hyperglycemia or hearing loss. One possible reason for this seems to be that mitochondrial inheritance is characterized by heteroplasmy and threshold (10). The percentage of affected mitochondria is variable among different tissues and among cells within a given tissue, which is called heteroplasmy (11). Typically, the carrier exhibits clinical phenotypes when the mutant mtDNA reaches more than 60%, which is the threshold (12). The other reason is that the patient was the propositus and had the first mutation in his family (13).

In addition to diabetes mellitus and hearing loss, other clinical phenotypes may present differently since there are variabilities in heteroplasmy in different tissues (14, 15). Mitochondria are presented in every cell of the human body except red blood cells, so the organs depending on energy metabolism are subjected to be affected in patients with MIDD, such as central nervous system, retina, skeletal muscle, heart, kidney, and endocrine. We found some complications involving other systems are characteristic, which might help to identify MIDD from other types of diabetes.

The prevalence of macular dystrophy (9.32%) was higher than proliferative retinopathy (5.59%), which was consistent with a previous study (16). Macular pattern dystrophy might protect against the development of diabetic retinopathy through a reduction in retinal metabolism and a decrease in oxygen consumption in the retina (17). Macular dystrophy is thought be used as a marker to select the MIDD patients (17). This typical retinal dystrophy should raise suspicion as to the diagnosis for MIDD. Therefore, it is of clinical importance for diabetes to perform specific examinations by a trained ophthalmologist.

Our results also suggested a high frequency of myopathy, especially muscle weakness and myophagism. Skeletal muscle requires a great deal of ATP to function, and when patients increase the demand on the muscles, the dysfunctional mitochondria are unable to meet the demand and develop muscular symptoms (18). Further, ragged red fibers on muscle biopsy are typically seen in MIDD, which indicate damaged muscles and are thought to be pathognomonic of mitochondrial disease (19). Muscle biopsy may show ragged-red fibers that are characteristic of mitochondrial disorders and contribute to the diagnosis of MIDD (20).

In the UK MRC Mitochondrial Disease Patient Cohort Study involving 129 patients with the m.3243A>G mutation, the patients were associated with other clinical syndromes involving the nervous and muscular systems including mitochondrial encephalopathy lactic acidosis and stroke-like episodes (MELAS) and chronic progressive external ophthalmoplegia (CPEO). Thirty percent had MIDD, 6% MELAS/MIDD, and 5% MIDD/CPEO overlap syndromes (21). Our study also showed high prevalence of central nervous system involvement (29.19%) and myopathy (22.98%) in MIDD patients. Brain and skeletal muscle are susceptible to be affected due to a great demand for ATP (3). Basal ganglia high signal lesions (2.48%) or encephalatrophy (11.18%) on the brain computerized tomography (CT) are specific manifestations, which might have implications for the diagnosis.

Cardiac abnormalities in MIDD mainly manifested as cardiomyopathy or arrhythmias. The decrease in ATP leads to a decrease in contractility and subsequently results in decreased stroke volume. The increase in end diastolic volume and pressure in the left ventricle causes further left ventricular remodeling, most often, left ventricular hypertrophy (22). Cardiac conductance disorders might occur by a rearrangement of the cardiac conductance system induced by the mitochondrial dysfunction. Common cardiac conduction abnormalities seen in MIDD include Wolff Parkinson White syndrome, frequent ventricular extrasystoles, and atrial fibrillation (20, 22). Cardiac conductance disorders might contribute to sudden deaths; therefore, patients diagnosed with MIDD should undergo a comprehensive cardiac examination to avoid adverse outcomes (15).

Although the prevalence of nephropathy (13.66%) and gastrointestinal symptoms (5.59%) was relatively lower, it was not insignificant. Renal biopsy of MIDD often shows focal glomerulosclerosis (FSGS), not typical diabetic nephropathy, and is the most prevalent finding (23). The main gastrointestinal symptoms were usually mild and presented as constipation, diarrhea, or succession of both. Intestinal pseudo-obstruction is a rare but serious complication of mitochondrial disease of alimentary localization with a mortality rate of approximately 50% (24). In addition, there have also been rare reports of pancreatitis, which may be related to MIDD (25, 26). Apart from diabetes, the most common endocrine manifestation of MIDD was short stature. Hypothyroidism and hypogonadism were also observed in MIDD (27–29). For MIDD patients, in addition to glycemic control, other endocrine function should be cared.

In clinical practice, testing for mutations in mitochondrial DNA is routinely done in DNA isolated from blood; however, the level of mutation may be low and even undetectable in blood. Our study indicated that mutational loads of m.3243A>G varied widely among different tissues. The mean mutation levels of m.3243A>G in urothelium, muscle, hair follicle, buccal mucosa, nail, and myocardium were 58.13, 49.53, 41.35, 48.25, 32.00, and 67.50%. DNA from urothelium, myocardium, and buccal mucosa had the higher while blood had the lowest proportion of mutant genomes. These results are consistent with a previous research (20). Each time a somatic cell undergoes mitosis, mtDNA will be randomly distributed to the progeny cells along with mitochondria. Therefore, the mutation load of mtDNA in the tissue will change with the division of the tissue cells (30, 31). The above results indicate that buccal mucosa and urinary sediment are tissues of choice for the diagnosis of mtDNA mutations, as they are easy to obtain and their mutation loads are greater than blood.

Five patients were positive for diabetes antibodies. The patient with GADA positive was diagnosed as MIDD combined with latent autoimmune diabetes in adults (LADA) (32). The two patients with ICA positive were diagnosed as MIDD. The original literatures considered that metabolic damage to beta cells could possibly trigger an autoimmune response and ICA might be a secondary phenomenon in mitochondrial diseases (33, 34). As for two patients with IAA positive, one was diagnosed as MIDD (32). The other patient repeated antibody tests, and the results were negative for all antibodies in the first test and positive for IAA in the second test. Since the patient had high HOMA-IR, the patient was diagnosed as T2DM combined with mitochondrial gene mutation (35). Actually, the three diabetes antibodies all have false-positive rates, which can be positive in some patients without diabetes, and some drugs such as methimazole could result in positive antibodies (36, 37).

We investigated the correlation between the heteroplasmy levels in the peripheral blood and age at the onset of diabetes. The scattergram showed an overall trend that the age at onset of diabetes was negatively correlated with the heteroplasmies in the peripheral blood. Especially the age at onset of m.3243A>G was significantly negatively correlated with the heteroplasmies in the peripheral blood, which was consistent with previous studies (38). The heteroplasmy load of the m.3243A>G mutation declines with age in blood leukocytes at a mean rate of 1.4% per year (39). Moreover, as the patient's age increased, all tissue showed a declining proportion of mutant mtDNA (40), which might indicate that early genetic testing is easier to detect mutations, and the positive rate of detection decreases with age. And one previous study suggested age-adjusted blood m.3243A>G mutation load might be an indicator of disease burden (41).

For MIDD patients, the clinical management is also a complicated issue to be discussed. Our study showed that most of the MIDD patients (79/102,77.45%) received insulin therapy, 37.18% (29/78) initiated insulin once diabetes was diagnosed, and less than one-fourth (24/102,23.53%) did not use insulin. The mean time from the diagnosis of diabetes to insulin therapy was 4.15 years. Our results might indicate that only minority of MIDD patients did not need insulin injection as they were

diagnosed. As islet function declines, insulin is usually required. There is a research suggesting a cocktail therapy combining CoQ10, lipoic acid, L-carnitine, and thiamine (42). CoQ10 is an antioxidant and mitochondrial cofactor that plays an important role in the mitochondrial respiratory chain, which may enhance insulin secretion, slow hearing loss, improve symptoms of myopathy and congestive heart failure in the setting of mitochondrial disease (43–45). Some drugs should be avoided, such as metformin as it might increase the risk of lactic acidosis (46). Additionally, some antibiotics such as tetracycline (47) and chloramphenicol (48), antiepileptic drugs such as sodium valproate phenytoin and phenobarbital (49), antiretroviral drugs (50), and statins (51) should be taken carefully due to their mitochondrial toxicity, which may exacerbate mitochondrial damage. For hearing impairment, cochlear implantation could improve listening in patients of all ages, provided there are intact neural components to function (52).

Our study has several limitations. First, to analyze the characteristics of patients with MIDD, studies with insufficient information were excluded, so that we were unable to analyze the characteristics of some rare mutations. Second, this study might have selective bias, because typical or more severe patients tend to be reported. Additionally, the mechanism of different mutations leading to various clinical features still remains unclear. Further studies are needed for the purpose of explaining the more precise molecular mechanism of MIDD.

CONCLUSIONS

In summary, our study shows that MIDD is a heterogeneous disease which is various in clinical features and treatment. The age of onset of diabetes is negatively correlated with the heteroplasmies in the peripheral blood. These patients who present with low body mass index, young onset of diabetes but without positive antibodies, multiple systems involved especially hearing loss should prompt an investigation for MIDD and genetic counseling as soon as possible.

AUTHOR CONTRIBUTIONS

MY contributed to the conception and design of the study. CX, YC, and LX performed the literature search and study selection. LX performed the data extraction. MY and SJ performed the statistical analyses. MY, LL, SJ and JD drafted the manuscript and revised it critically. SJ polished the draft. All authors gave final approval for submitted manuscript content and agreed to be accountable for all aspects of the work in ensuring that questions related to the accuracy or integrity of any part of the work are appropriately investigated and resolved.

FUNDING

This work was funded by the National Natural Science Foundation of China (81770822).

SUPPLEMENTARY MATERIAL

The Supplementary Material for this article can be found online at: https://www.frontiersin.org/articles/10.3389/fendo.2021.728043/full#supplementary-material

REFERENCES

1. Henzen C. Monogenic Diabetes Mellitus Due to Defects in Insulin Secretion. *Swiss Med Wkly* (2012) 142:w13690. doi: 10.4414/smw.2012.13690
2. van den Ouweland JM, Lemkes HH, Ruitenbeek W, Sandkuijl LA, de Vijlder MF, Struyvenberg PA, et al. Mutation in Mitochondrial Trna(Leu)(UUR) Gene in a Large Pedigree With Maternally Transmitted Type II Diabetes Mellitus and Deafness. *Nat Genet* (1992) 1(5):368–71. doi: 10.1038/ng0892-368
3. Murphy R, Turnbull DM, Walker M, Hattersley AT. Clinical Features, Diagnosis and Management of Maternally Inherited Diabetes and Deafness (MIDD) Associated With the 3243A>G Mitochondrial Point Mutation. *Diabetes Med* (2008) 25(4):383–99. doi: 10.1111/j.1464-5491.2008.02359.x
4. Yu P, Yu D. Study on a New Point Mutation of Nt3426 a→G of Mitochondrial DNA in a Diabetes Mellitus Family. *Chin J Med Genet* (2003) 03):63–5. Chinese.
5. Poulton J, Brown MS, Cooper A, Marchington DR, Phillips DI. A Common Mitochondrial DNA Variant Is Associated With Insulin Resistance in Adult Life. *Diabetologia* (1998) 41(1):54–8. doi: 10.1007/s001250050866
6. Shin CS, Kim SK, Park KS, Kim WB, Kim SY, Cho BY, et al. A New Point Mutation (3426, a to G) in Mitochondrial NADH Dehydrogenase Gene in Korean Diabetic Patients Which Mimics 3243 Mutation by Restriction Fragment Length Polymorphism Pattern. *Endocr J* (1998) 45(1):105–10. doi: 10.1507/endocrj.45.105
7. Gebhart SS, Shoffner JM, Koontz D, Kaufman A, Wallace D. Insulin Resistance Associated With Maternally Inherited Diabetes and Deafness. *Metabolism* (1996) 45(4):526–31. doi: 10.1016/s0026-0495(96)90231-0
8. Greenfield A, Braude P, Flinter F, Lovell-Badge R, Ogilvie C, Perry ACF. Corrigendum: Assisted Reproductive Technologies to Prevent Human Mitochondrial Disease Transmission. *Nat Biotechnol* (2018) 36(2):196. doi: 10.1038/nbt0218-196b
9. van den Ameele J, Li AYZ, Ma H, Chinnery PF. Mitochondrial Heteroplasmy Beyond the Oocyte Bottleneck. *Semin Cell Dev Biol* (2020) 97:156–66. doi: 10.1016/j.semcdb.2019.10.001
10. Dimauro S, Davidzon G. Mitochondrial DNA and Disease. *Ann Med* (2005) 37(3):222–32. doi: 10.1080/07853890510007368
11. Laloi-Michelin M, Meas T, Ambonville C, Bellanné-Chantelot C, Beaufils S, Massin P, et al. The Clinical Variability of Maternally Inherited Diabetes and Deafness Is Associated With the Degree of Heteroplasmy in Blood Leukocytes. *J Clin Endocrinol Metab* (2009) 94(8):3025–30. doi: 10.1210/jc.2008-2680
12. Bacman SR, Kauppila JHK, Pereira CV, Nissanka N, Miranda M, Pinto M, et al. Mitotalen Reduces Mutant MtDNA Load and Restores tRNA(Ala) Levels in a Mouse Model of Heteroplasmic Mtdna Mutation. *Nat Med* (2018) 24 (11):1696–700. doi: 10.1038/s41591-018-0166-8
13. Maassen JA, Biberoglu S, t Hart LM, Bakker E, de Knijff P. A Case of a *De Novo* A3243G Mutation in Mitochondrial DNA in a Patient With Diabetes and Deafness. *Arch Physiol Biochem* (2002) 110(3):186–8. doi: 10.1076/apab.110.3.186.8294
14. Li HZ, Li RY, Li M. A Review of Maternally Inherited Diabetes and Deafness. *Front Biosci (Landmark Ed)* (2014) 19:777–82. doi: 10.2741/4244
15. Robinson KN, Terrazas S, Giordano-Mooga S, Xavier NA. The Role of Heteroplasmy in the Diagnosis and Management of Maternally Inherited

Diabetes and Deafness. *Endocr Pract* (2020) 26(2):241–6. doi: 10.4158/ep-2019-0270
16. Massin P, Virally-Monod M, Vialettes B, Paques M, Gin H, Porokhov B, et al. Prevalence of Macular Pattern Dystrophy in Maternally Inherited Diabetes and Deafness. GEDIAM Group. *Ophthalmology* (1999) 106(9):1821–7. doi: 10.1016/s0161-6420(99)90356-1
17. Guillausseau PJ, Massin P, Dubois-LaForgue D, Timsit J, Virally M, Gin H, et al. Maternally Inherited Diabetes and Deafness: A Multicenter Study. *Ann Intern Med* (2001) 134(9 Pt 1):721–8. doi: 10.7326/0003-4819-134-9_part_1-200105010-00008
18. Tanaka K, Takada Y, Matsunaka T, Yuyama S, Fujino S, Maguchi M, et al. Diabetes Mellitus, Deafness, Muscle Weakness and Hypocalcemia in a Patient With an A3243G Mutation of the Mitochondrial DNA. *Intern Med* (2000) 39 (3):249–52. doi: 10.2169/internalmedicine.39.249
19. Lien LM, Lee HC, Wang KL, Chiu JC, Chiu HC, Wei YH. Involvement of Nervous System in Maternally Inherited Diabetes and Deafness (MIDD) With the A3243G Mutation of Mitochondrial DNA. *Acta Neurol Scand* (2001) 103 (3):159–65. doi: 10.1034/j.1600-0404.2001.103003159.x
20. Fukao T, Kondo M, Yamamoto T, Orii KE, Kondo N. Comparison of Mitochondrial A3243G Mutation Loads in Easily Accessible Samples From a Family With Maternally Inherited Diabetes and Deafness. *Mol Med Rep* (2009) 2(1):69–72. doi: 10.3892/mmr_00000063
21. Nesbitt V, Pitceathly RD, Turnbull DM, Taylor RW, Sweeney MG, Mudanohwo EE, et al. The UK MRC Mitochondrial Disease Patient Cohort Study: Clinical Phenotypes Associated With the M.3243A>G Mutation–Implications for Diagnosis and Management. *J Neurol Neurosurg Psychiatry* (2013) 84(8):936–8. doi: 10.1136/jnnp-2012-303528
22. Hoptasz M, Szczuciński A, Losy J. Heterogeneous Phenotypic Manifestations of Maternally Inherited Deafness Associated With the Mitochondrial A3243G Mutation. Case Report. *Neurol Neurochir Pol* (2014) 48(2):150–3. doi: 10.1016/j.pjnns.2013.12.007
23. Cao XY, Wei RB, Wang YD, Zhang XG, Tang L, Chen XM. Focal Segmental Glomerulosclerosis Associated With Maternally Inherited Diabetes and Deafness: Clinical Pathological Analysis. *Indian J Pathol Microbiol* (2013) 56(3):272–5. doi: 10.4103/0377-4929.120392
24. Narbonne H, Paquis-Fluckinger V, Valero R, Heyries L, Pellissier JF, Vialettes B. Gastrointestinal Tract Symptoms in Maternally Inherited Diabetes and Deafness (MIDD). *Diabetes Metab* (2004) 30(1):61–6. doi: 10.1016/s1262-3636(07)70090-3
25. Schleiffer T, t Hart LM, Schürfeld C, Kraatz K, Riemann JF. Maternally Inherited Diabetes and Deafness (MIDD): Unusual Occult Exocrine Pancreatic Manifestation in an Affected German Family. *Exp Clin Endocrinol Diabetes* (2000) 108(2):81–5. doi: 10.1055/s-2000-5800
26. Verny C, Amati-Bonneau P, Letournel F, Person B, Dib N, Malinge MC, et al. Mitochondrial DNA A3243G Mutation Involved in Familial Diabetes, Chronic Intestinal Pseudo-Obstruction and Recurrent Pancreatitis. *Diabetes Metab* (2008) 34(6 Pt 1):620–6. doi: 10.1016/j.diabet.2008.06.001
27. Finsterer J, Frank M. The Tip of the Iceberg in Maternally Inherited Diabetes and Deafness. *Oman Med J* (2018) 33(5):437–40. doi: 10.5001/omj.2018.80
28. Kytövuori L, Lipponen J, Rusanen H, Komulainen T, Martikainen MH, Majamaa K. A Novel Mutation M.8561C>G in MT-ATP6/8 Causing a Mitochondrial Syndrome With Ataxia, Peripheral Neuropathy, Diabetes Mellitus, and Hypergonadotropic Hypogonadism. *J Neurol* (2016) 263 (11):2188–95. doi: 10.1007/s00415-016-8249-2
29. Moraes CT, Ciacci F, Bonilla E, Jansen C, Hirano M, Rao N, et al. Two Novel Pathogenic Mitochondrial DNA Mutations Affecting Organelle Number and Protein Synthesis. Is the Trna(Leu(UUR)) Gene an Etiologic Hot Spot? *J Clin Invest* (1993) 92(6):2906–15. doi: 10.1172/jci116913
30. Cao L, Shitara H, Horii T, Nagao Y, Imai H, Abe K, et al. The Mitochondrial Bottleneck Occurs Without Reduction of Mtdna Content in Female Mouse Germ Cells. *Nat Genet* (2007) 39(3):386–90. doi: 10.1038/ng1970
31. Chinnery PF, Howell N, Lightowlers RN, Turnbull DM. MELAS and MERRF. The Relationship Between Maternal Mutation Load and the Frequency of Clinically Affected Offspring. *Brain* (1998) 121(Pt 10):1889–94. doi: 10.1093/brain/121.10.1889
32. Rong Y. *Mitochondrial Diabetes Mellitus With 3 Cases*. Hebei Medical University (2011). MA thesis. Hebei, Chinese.
33. Xiu L. Clinical Characterizations of Familial Diabete Mellitus Associated With Mitochondrial Gene Mutation. *Natl Med J China* (1997) 06:111–3. doi:CNKI : SUN:ZHYX.0.1997-06-007. Chinese. doi: 10.13471/j.cnki.j.sun.yat-sen.univ (med.sci).2002.0036
34. Oexle K, Oberle J, Finckh B, Kohlschütter A, Nagy M, Seibel P, et al. Islet Cell Antibodies in Diabetes Mellitus Associated With a Mitochondrial Trna(Leu (UUR)) Gene Mutation. *Exp Clin Endocrinol Diabetes* (1996) 104(3):212–7. doi: 10.1055/s-0029-1211445
35. Yu Z, Li J. Islet Cell Antibodies in Diabetes Mellitus Associated With a Mitochondrial Trnal(U) Gene Mutation. *Int J Endocrinol Metab* (2020) 40 (04):279–83. Chinese.
36. Hu L. The Clinical Significance of Serum Autoantibodies to Pancreatic Islet in One Thousand and Four Hundreds Patients With Diabetes. *J Modern Lab Med* (2006) 02):15–7. doi:CNKI : SUN:SXYN.0.2006-02-007Chinese. doi: 10.3969/j.issn.1671-7414.2006.02.005
37. Di Mario U, Perfetti R, Anastasi E, Contreas G, Crisà L, Tiberti C, et al. Autoantibodies to Insulin do Appear in Non-Diabetic Patients With Autoimmune Disorders: Comparison With Anti-Immunoglobulin Antibodies and Other Autoimmune Phenomena. *Acta Endocrinol (Copenh)* (1990) 122(3):303–8. doi: 10.1530/acta.0.1220303
38. Suzuki S, Oka Y, Kadowaki T, Kanatsuka A, Kuzuya T, Kobayashi M, et al. Clinical Features of Diabetes Mellitus With the Mitochondrial DNA 3243 (a-G) Mutation in Japanese: Maternal Inheritance and Mitochondria-Related Complications. *Diabetes Res Clin Pract* (2003) 59(3):207–17. doi: 10.1016/s0168-8227(02)00246-2
39. van Essen EH, Roep BO, 't Hart LM, Jansen JJ, Van den Ouweland JM, Lemkes HH, et al. HLA-DQ Polymorphism and Degree of Heteroplasmy of the A3243G Mitochondrial DNA Mutation in Maternally Inherited Diabetes and Deafness. *Diabetes Med* (2000) 17(12):841–7. doi: 10.1046/j.1464-5491.2000.00379.x
40. Liou CW, Huang CC, Wei YH. Molecular Analysis of Diabetes Mellitus-Associated A3243G Mitochondrial DNA Mutation in Taiwanese Cases. *Diabetes Res Clin Pract* (2001) 54 Suppl 2:S39–43. doi: 10.1016/s0168-8227(01)00334-5
41. Grady JP, Pickett SJ, Ng YS, Alston CL, Blakely EL, Hardy SA, et al. MtDNA Heteroplasmy Level and Copy Number Indicate Disease Burden in M.3243A>G Mitochondrial Disease. *EMBO Mol Med* (2018) 10(6):e8262. doi: 10.15252/emmm.201708262
42. Rodriguez MC, MacDonald JR, Mahoney DJ, Parise G, Beal MF, Tarnopolsky MA. Beneficial Effects of Creatine, Coq10, and Lipoic Acid in Mitochondrial Disorders. *Muscle Nerve* (2007) 35(2):235–42. doi: 10.1002/mus.20688
43. Fragaki K, Chaussenot A, Benoist JF, Ait-El-Mkadem S, Bannwarth S, Rouzier C, et al. Coenzyme Q10 Defects may be Associated With a Deficiency of Q10-Independent Mitochondrial Respiratory Chain Complexes. *Biol Res* (2016) 49:4. doi: 10.1186/s40659-015-0065-0
44. Salles JE, Moisés VA, Almeida DR, Chacra AR, Moisés RS. Myocardial Dysfunction in Mitochondrial Diabetes Treated With Coenzyme Q10. *Diabetes Res Clin Pract* (2006) 72(1):100–3. doi: 10.1016/j.diabres.2005.09.005
45. Suzuki S, Hinokio Y, Ohtomo M, Hirai M, Hirai A, Chiba M, et al. The Effects of Coenzyme Q10 Treatment on Maternally Inherited Diabetes Mellitus and Deafness, and Mitochondrial DNA 3243 (a to G) Mutation. *Diabetologia* (1998) 41(5):584–8. doi: 10.1007/s001250050950
46. Kim NH, Siddiqui M, Vogel J. MELAS Syndrome and MIDD Unmasked by Metformin Use: A Case Report. *Ann Intern Med* (2021) 174(1):124–5. doi: 10.7326/l20-0292
47. Chatzispyrou IA, Held NM, Mouchiroud L, Auwerx J, Houtkooper RH. Tetracycline Antibiotics Impair Mitochondrial Function and its Experimental Use Confounds Research. *Cancer Res* (2015) 75(21):4446–9. doi: 10.1158/0008-5472.Can-15-1626
48. Leiter LM, Thatte HS, Okafor C, Marks PW, Golan DE, Bridges KR. Chloramphenicol-Induced Mitochondrial Dysfunction Is Associated With Decreased Transferrin Receptor Expression and Ferritin Synthesis in K562 Cells and Is Unrelated to IRE-IRP Interactions. *J Cell Physiol* (1999) 180 (3):334–44. doi: 10.1002/(sici)1097-4652(199909)180:3<334::Aid-jcp4>3.0.Co;2-q
49. Lam CW, Lau CH, Williams JC, Chan YW, Wong LJ. Mitochondrial Myopathy, Encephalopathy, Lactic Acidosis and Stroke-Like Episodes (MELAS) Triggered by Valproate Therapy. *Eur J Pediatr* (1997) 156 (7):562–4. doi: 10.1007/s004310050663

50. Moyle G. Mitochondrial Toxicity: Myths and Facts. *J HIV Ther* (2004) 9(2):45–7.
51. Okuyama H, Langsjoen PH, Hamazaki T, Ogushi Y, Hama R, Kobayashi T, et al. Statins Stimulate Atherosclerosis and Heart Failure: Pharmacological Mechanisms. *Expert Rev Clin Pharmacol* (2015) 8(2):189–99. doi: 10.1586/17512433.2015.1011125
52. Sinnathuray AR, Raut V, Awa A, Magee A, Toner JG. A Review of Cochlear Implantation in Mitochondrial Sensorineural Hearing Loss. *Otol Neurotol* (2003) 24(3):418–26. doi: 10.1097/00129492-200305000-00012

Conflict of Interest: The authors declare that the research was conducted in the absence of any commercial or financial relationships that could be construed as a potential conflict of interest.

Publisher's Note: All claims expressed in this article are solely those of the authors and do not necessarily represent those of their affiliated organizations, or those of the publisher, the editors and the reviewers. Any product that may be evaluated in this article, or claim that may be made by its manufacturer, is not guaranteed or endorsed by the publisher.

frontiers in Endocrinology

ORIGINAL RESEARCH
published: 09 December 2021
doi: 10.3389/fendo.2021.803992

Functional Characterization of a Novel Heterozygous Mutation in the Glucokinase Gene That Causes MODY2 in Chinese Pedigrees

Feng Jiang[1†], *Jing Yan*[1†], *Rong Zhang*[1], *Xiaojing Ma*[1], *Yuqian Bao*[1], *Yujuan Gu*[2*] and *Cheng Hu*[1,3*]

[1] Department of Endocrinology, Shanghai Diabetes Institute, Shanghai Key Laboratory of Diabetes Mellitus, Shanghai Clinical Center for Diabetes, Shanghai Jiao Tong University Affiliated Sixth People's Hospital, Shanghai, China, [2] Department of Endocrinology, Affiliated Hospital of Nantong University, Jiangsu, China, [3] Department of Endocrinology, Fengxian Central Hospital Affiliated to Southern Medical University, Shanghai, China

OPEN ACCESS

Edited by:
Jiajun Zhao,
Shandong Provincial Hospital, China

Reviewed by:
Maurizio Delvecchio,
Giovanni XXIII Children's Hospital, Italy
Lin Liao,
Shandong University, China
Huiqing Li,
Huazhong University of Science and Technology, China

***Correspondence:**
Cheng Hu
alfredhc@sjtu.edu.cn
Yujuan Gu
desette@ntu.edu.cn

[†]*These authors have contributed equally to this work*

Specialty section:
This article was submitted to Diabetes: Molecular Mechanisms, a section of the journal Frontiers in Endocrinology

Received: *28 October 2021*
Accepted: *22 November 2021*
Published: *09 December 2021*

Citation:
Jiang F, Yan J, Zhang R, Ma X, Bao Y, Gu Y and Hu C (2021) Functional Characterization of a Novel Heterozygous Mutation in the Glucokinase Gene That Causes MODY2 in Chinese Pedigrees. Front. Endocrinol. 12:803992. doi: 10.3389/fendo.2021.803992

Background: Glucokinase (GCK) plays a central role in glucose regulation. The heterozygous mutations of *GCK* can cause a monogenic form of diabetes, maturity-onset diabetes of the young (MODY) directly. In our study, we aimed to explore the mechanism of the novel mutation *GCK* p.Ala259Thr leading to glucokinase deficiency and hyperglycemia.

Methods: Thirty early-onset diabetes pedigrees were referred to whole exome sequencing for novel mutations identification. Purified wild-type and mutant GCK proteins were obtained from *E.coli* systems and then subjected to the kinetic and thermal stability analysis to test the effects on GCK activity.

Results: One novel missense mutation *GCK* p.Ala259Thr was identified and co-segregated with diabetes in a Chinese MODY2 pedigree. The kinetic analysis showed that this mutation result in a decreased affinity and catalytic capability for glucose. The thermal stability analysis also indicated that the mutant protein presented dramatically decreased activity at the same temperature.

Conclusion: Our study firstly identified a novel MODY2 mutation p.Ala259Thr in Chinese diabetes pedigrees. The kinetic and thermal stability analysis confirmed that this mutation caused hyperglycemia through severely damaging the enzyme activities and protein stability.

Keywords: glucokinase, MODY, mutation, A259T, mechanism

INTRODUCTION

Maturity Onset Diabetes of the Young (MODY) is a heritable and heterogeneous group of monogenic diabetes mellitus that are characterized by autosomal dominant inheritance, early onset and beta cell dysfunction. Mutations in at least 14 different genes (*HNF4A, GCK, HNF1A, PDX1, HNF1B, NEUROD1, KLF11, CEL, PAX4, INS, BLK, ABCC8, KCNJ11* and *APPL1*) have been shown to cause MODY subtypes 1–14 (1–3).

The *GCK* gene (7p15.3–p15.1) encodes the glucokinase (GCK) enzyme, which is a rate-limiting enzyme of glycolysis that is responsible for phosphorylating glucose to glucose-6-phosphate. GCK has unique kinetic characteristics, including a low affinity for glucose ($S_{0.5}$ = 5-8 mmol/L) (4), cooperativity with its glucose substrate (Hill coefficient, h=1.7), and a lack of inhibition by its product glucose-6-phosphate (G-6-P). In pancreatic β cells, GCK maintains glucose homeostasis through regulating glucose-stimulated insulin secretion in response to the intracellular glucose concentration (5–7). In the liver, GCK stimulates glucose disposal and glycogen storage (8). In addition, the crystal structures of human GCK present both active and inactive forms according to the glucose levels. Katama and colleagues revealed that GCK had a small and large domain that were separated by a deep cleft; these domains undergo a large conformational change through rotation of the small domain, which is induced by binding to glucose (9, 10).

Given its central role in glucose regulation, mutations in the gene encoding glucokinase can cause both hyper- and hypoglycaemia. Heterozygous activating GCK mutations can cause persistent hyperinsulinaemic hypoglycaemia of infancy (PHHI) (11). Furthermore, homozygous inactivating GCK mutations leading to complete GCK deficiency present as permanent neonatal diabetes mellitus (12), whereas heterozygous inactivating mutations are the underlying causes of MODY2 (13).

MODY is the most common type of monogenic diabetes, accounting for 2% to 5% of all diabetes cases in Europe (14). Previous studies indicate that *GCK*-MODY2, *HNF1A*-MODY3, *HNF4A*-MODY1 and *HNF1B*-MODY5 account for more than 95% cases of MODY in Caucasians, but only account for just 10–20% of MODY cases in Asia (including China, Japan and Korea) (15). An epidemiological investigation in Chinese hyperglycemia pedigrees that fulfilling the clinical diagnostic criteria for MODY show that the MODY subtype detection rate was 18.42% for GCK (16). Heterozygous mutations in *GCK* lead to decreased glucokinase activity and thus deficient sensitivity to glucose in β cells and impaired glycogen synthesis in the liver (17). GCK/MODY2 occurs with a mild non-progressive hyperglycaemia, which generally is asymptomatic and develops without an increased risk of late complications, such as diabetic retinopathy or nephropathy (18, 19). Due to the unapparent symptoms, MODY2 is often misdiagnosed and treated inappropriately. However, a molecular genetic diagnosis can change the management, since patients with *GCK* mutations rarely require pharmacological treatment. Thus, a correct genetic diagnosis is important for guidance of the prediction of asymptomatic relatives and personalized treatment for those with diabetes. To date, although more than 600 different GCK/MODY2 mutations have been reported, including nonsense, missense, and frameshift mutations, less than 20% of these mutations have been functionally characterized (20–22). Pathophysiological studies on naturally occurring GCK missense mutations will provide further clues to help elucidate the mechanisms of glycaemic disorders and investigate the biological characteristics of this enzyme.

In this study, we report the novel *GCK* missense mutation Ala259Thr, which co-segregates with diabetes in Chinese MODY families for the first time. This mutation, which alters alanine to threonine at the 259th amino acid, is located proximal to the glucose-binding site but has not been investigated biochemically. Herein, we discovered that the Ala259Thr mutation exerted effects on the catalytic activity and protein thermostability of glucokinase.

MATERIALS AND METHODS

Subjects

The retrospective study included 30 early-onset diabetes pedigrees referred for genetic testing. All pedigrees were clinically diagnosed with MODY according to the following classic criteria (23, 24): a family history diabetes for at least two consecutive generations, early-onset of diabetes before the age of 25 years, no need for insulin therapy, and negative for type 1 diabetes antibodies. The diagnosis was made based on an oral glucose tolerance test (OGTT). The fasting blood glucose (FPG), 2h blood glucose (2h PG), fasting insulin (FINS), 2h insulin (2h-INS) and glycated hemoglobin (HbA1c) levels were measured in all family members available for testing.

The study was performed according to the Declaration of Helsinki and was approved by our institutional review boards. Informed consent was obtained from all family members.

Identification of Glucokinase Gene Mutations by Whole Exome Sequencing

Genomic DNA was extracted from peripheral lymphocytes using a Qiagen DNA extraction kit (Qiagen, Frankfurt, Germany). Whole exome sequencing was performed to explore novel mutation and direct sequencing was used to validate the positive mutation. The coding regions of exons 1a-10 and the intron-exon boundaries of the GCK gene were amplified by PCR using self-designed primers (**Table 1**). PCR products were purified using QIAquick PCR purification columns (Qiagen, Frankfurt, Germany), and both strands were sequenced using the BigDye Terminator Cycle Sequencing Kit (Applied Biosystems, CA, UK) according to the manufacturer's recommendations.

Production and Purification of Recombinant Wild-Type and Mutant Glucokinase

Recombinant human wild-type liver GCK was constructed with a His tag at the NH2 terminal and ligated into the pET-28a(+) vector. The Ala259Thr mutation was generated based on the His-GCK construct by PCR using a kit (QuikChange II Site-Directed Mutagenesis Kit, Stratagene, CA, USA). The following oligonucleotide was used to generate the Ala259Thr mutation: forward primer (5' CGAGTGGGGCACCTTCGGGGACTC CGGCGAGCTGGACGAGTT 3') and reverse primer (TCCCC GAAGGTGCCCCACTCGGTATTGACGCACATGCGGC CCT). The wild-type and mutant GCK sequences were verified using the ABI 3500xl DNA sequencer (Applied Biosystems,

TABLE 1 | Amplification and sequencing primers for the *GCK* exons.

Exon	Forward primers (3'-5')	Reverse primers (3'-5')	Product length (bp)
Exon-1a	TCCACTTCAGAAGCCTACTG	GTTTGAGCCTCAGAATCTGA	195
Exon-1b	AGCAGGCAGGAGCATCTCTG	CTTTGCACTGGGAGAGCAGC	149
Exon-1c	GAACTCGGGCCTCACATG	GGATTGTTAGGACAGCCTG	252
Exon 2	TGTGCAGATGCCTGGTGA	CACTCCCAGACTCACAGCC	343
Exon 3	TAATATCCGGGCTCAGTCACCT	CAAGGCCATGCAGGATCTCAG	298
Exon 4	TAGCTTGGCTTGAGGCCGTG	CCAGAGGAACTCTGCCTTCA	272
Exon 5	GCAGCCACGAGGCCTATCTC	CAGCACTGCCTGCCTTTCTC	195
Exon 6	CCAGCACTGCAGCTTCTGTG	CTTCCAGACTGCTGAGGCTC	176
Exon 7	AGCCGCCTTTCCATTGTT	AAAAGCAAACTGACAATCCGTT	451
Exon 8	CCTCCCTCGTGCCTGCTGAT	ACTTGGTCTCAGGGCGACG	279
Exon 9	ACTGTCGGAGCGACACTCAG	TGCGGTTCCCAAGCTCCAAG	367
Exon 10	CGCCCGGTAATGAATGTGG	CCACAGCACCCAGGCTCCAT	269

USA). The wild-type and mutant GCKs with His tags were transformed into *E. coli* (BL21-CodonPlus (DE3)-RIPL chemically competent cells) and then purified from 30-g cell pellet. Two-step affinity chromatography was used with Ni-NTA beads to bind the fusion protein, which was eluted with Ni-NTA and loaded onto the Superdex^{TM} 200 16/60 column. Both the wild-type and mutant His-GCK purified proteins showed a single band on SDS-PAGE gels. The purified proteins were quantified using the Bradford method (Bradford Protein Assays, Thermo Fisher Scientific, USA) using standard methods and stored at -80°C in 30% glycerol, 5 mmol/L glutathione, 5 mmol/L dithiothreitol (DTT), 200 mmol/L KCl, and 50 mmol/L Tris buffer (pH 7.4).

Kinetic Analysis

GCK activity was measured spectrophotometrically based on the ADP-Glo^{TM} Kinase Assay (Promega, USA). The luminescent signal generated is proportional to the ADP concentration produced and is correlated with the kinase activity. Kinetic parameters were also determined according to the assay as follows. First, standard ATP/ADP mixtures representing different conversion percentages were prepared to generate the standard curve for conversion of ATP to ADP. Second, ten serial two-fold dilutions of glucose in the assay buffer (final concentration starting from 200 mM) in the presence of 1 mM ATP were generated to determine the optimal glucose concentration when the half maximal velocity (V_{max}) of the reaction was reached. The assay buffer contained 50 mM Tris, 100 mM KCl and 10 mM $MgCl_2$ (pH 7.5). GraphPad Prism 7.0 (GraphPad Software, La Jolla, CA, USA) was used to calculate the glucose-K_m ($S_{0.5}$), glucose-K_{cat}, ATP-K_m, ATP-K_{cat}, Hill coefficient (h) and inflection point of glucose. The relative activity index and the glucose concentration at the inflection point were also calculated.

Thermal Stability Analysis

The thermal stability of the mutant and wild-type His-GCK enzymes was assessed using the ADP-Glo^{TM} Kinase Assay with 3 mM (for the wild-type)/11 mM (for the mutant) glucokinase and 1 mM ATP. The enzymes were incubated in a water bath at 25, 30, 35, 40, 45, 50, 55, and 60°C for 30 min or 50°C for 0, 5, 10, 15, 20, 25, and 30 min. Luminescence was measured to represent the glucokinase activity as described above.

Statistical Analysis

All results are presented as the mean ± SD. Student's two-tailed unpaired t test was used to assess differences between groups. The Mann-Whitney test was used to evaluate differences in clinical parameters between the mutants and non-mutants. The statistical analyses were performed using SAS 8.0 (SAS institute, Cary, NC, USA). A two-tailed p value less than 0.05 was considered significant.

RESULTS

Identification of a Novel Missense Mutation in the *GCK* Gene

The 12 exons of the *GCK* gene were scanned for the validation of mutations using direct sequencing for each of the affected families. A novel heterozygous missense mutation in GCK gene exon 7 (codon 259 GCC➔ACC; **Figure 1**) resulting in an amino acid substitution (Ala^{259}➔Thr) was identified in the proband. The same mutation was also identified in the proband's father and grandfather. Conversely, this mutation was not found in the four unrelated healthy individuals used as controls.

Clinical Profiles of the Patients

The male proband (III:2) was diagnosed with diabetes at 5 years of the age and presented with fasting hyperglycemia. Biochemical studies showed elevated fasting plasma glucose (FPG) (8.0 mmol/L), 2h plasma glucose (2h PG)(12.8 mmol/L) after oral glucose tolerance test (OGTT), and glycatedhemoglobin A1c (HbA1c) (7%). In contrast, fasting insulin (FINS) and 2h insulin (2h-INS) decreased (FINS: <0.2 uU/ml, 2h-INS: 2.23 uU/ml). The proband's father (II:3) and grandfather (I:2) were diagnosed with fasting hyperglycaemia at the ages of 33 and 47 years, respectively, during routine screening (FGP=7.8 and 9 mmol/L, respectively). The HbA1c level was elevated in proband's grandfather (7.5%), but was normal in proband's father (6%). Both FINS and 2h-INS were normal in proband's father and grandfather. The proband's paternal aunt (II:2) presented with gestational diabetes mellitus (GDM) during her first pregnancy according to the previous medical history. But it is unavailable for us to get her biochemical results. None of the diabetic patients received hypoglycemic drugs. The rest of the

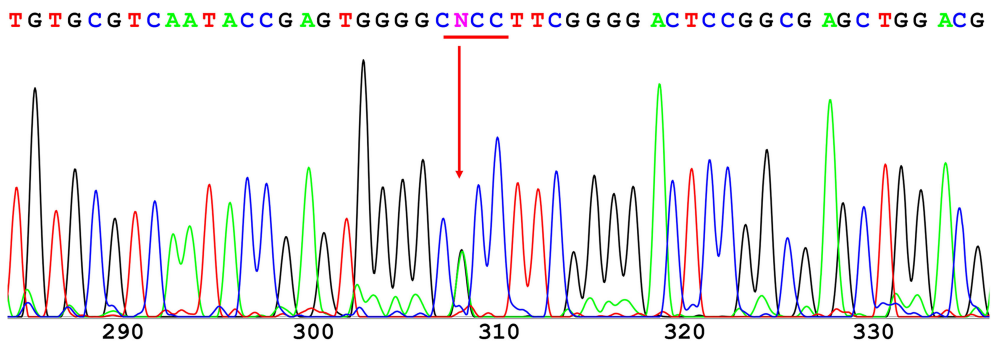

FIGURE 1 | Direct sequencing of GCK exon 7. A novel heterozygous missense mutation was found in codon 259 and resulted in a substitution of alanine (GCC) to threonine (ACC).

family were normal glucose regulation (NGT) individuals with normal blood glucose and insulin levels (**Figure 2**).

Production of Recombinant Wild-Type and Mutant Glucokinase

The recombinant wild-type and mutant enzymes were expressed in an *E. coli* system (BL21(DE3)-Gold). Nine preparations of the His-fusion protein were purified with a Ni-NTA column, thrombin digestion and Superdex^{TM} 200 column, with yields of 11.5 mg/L and 10 mg/L for the wild-type and mutant proteins, respectively. All His-GCK proteins were proven to be essentially pure based on the presence of a single band at 75 kDa on a SDS-PAGE gel.

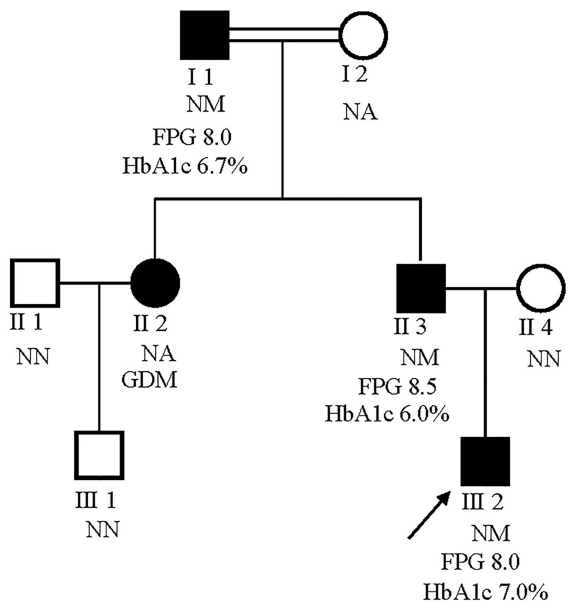

FIGURE 2 | Pedigrees for a MODY2 family showing co-segregation of the Ala259Thr GCK mutation with diagnosed diabetes. Circles represent females, and squares represent males. Black shaded shapes represent diabetic individuals. The number under each member represents the sample identifier. NN, no mutation; NM, heterozygous for Ala259Thr mutation; NA, not available for testing. The FPG and HbA1c values are shown where available.

Kinetic Analysis

Both the purified wild-type and mutant GCKs were subjected to kinetic analysis using glucose and ATP as substrates. The response curves of GCK for a series of glucose or ATP concentrations, which indicate the affinity of GCK for the substrates, are shown in **Figure 3** (glucose as substrate) and **Figure 4** (ATP as substrate). The kinetic parameters, including the substrate affinities ($S_{0.5}$ for glucose and ATP-K_m for ATP), catalytic constants (glucose-K_{cat} and ATP-K_{cat}, respectively), Hill coefficients and inflection points of glucose, are shown in **Table 1**. The Ala259Thr mutant showed a 2.3-fold lower affinity for glucose ($S_{0.5}$ for mutant and wild-type, 2.42 ± 0.14 vs. 7.95 ± 0.92, p=0.0005), but a similar affinity to the second substrate ATP (ATP-Km for mutant and wild-type, 1.00 ± 0.25 vs. 1.00 ± 0.24, p>0.05). Moreover, the glucose-K_{cat} was significantly higher for the wild-type than for the mutant (33.2 ± 0.6 vs. 30.3 ± 1.2, p=0.0201), whereas the ATP-K_{cat} was similar between the two groups (43.8 ± 3.9 vs. 45.2 ± 4.1, p=0.6903), indicating a decreased catalytic capability of the mutant enzyme for glucose but not for ATP. In addition, the Ala259Thr mutant presented a significantly higher inflection point than the wild-type enzyme (3.78 ± 0.44 vs. 1.69 ± 0.10, p=0.0013), indicating a greater demand for glucose when the maximal velocity was reached in the reaction system. Finally, the mutant showed a lower Hill coefficient than the wild-type enzyme (2.44 ± 0.29 vs. 1.75 ± 0.30, p=0.0457), implying decreased cooperativity for the glucose substrate (**Table 2**).

Thermal Stability Analysis

The thermostability tests of the wild-type and mutant His-GCK enzymes were performed at different temperatures to investigate protein stability, which was also a key determinant of enzyme function. The enzyme activity of wild-type GCK was stable under a temperature of 45°C with a sharp decline at 50°C (**Figure 5A**). In contrast, the Ala259Thr mutant maintained activity under a temperature of 40°C but decreased dramatically at 45°C (**Figure 5A**). However, the mutant maintained decreased

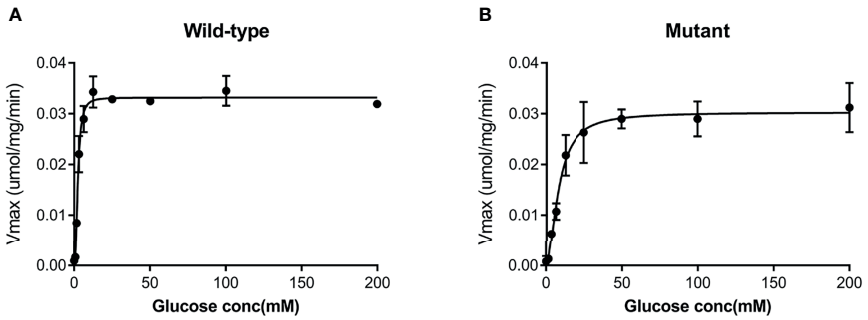

FIGURE 3 | Response curve of GCK for a series of glucose concentrations. **(A)** Wild-type GCK, **(B)** mutant GCK. The Ala259Thr mutation showed a lower maximum reaction velocity than the wild-type GCK, indicating a lower affinity for glucose.

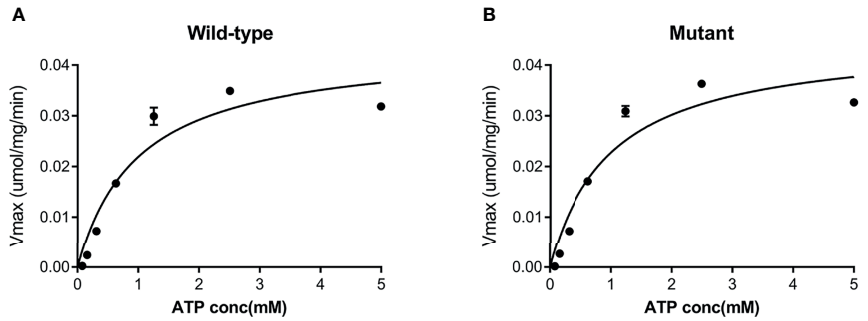

FIGURE 4 | Response curve of GCK for a series of ATP concentrations. **(A)** Wild-type GCK, **(B)** mutant GCK. The wild-type GCK and Ala259Thr mutation showed a similar maximum reaction velocity, indicating a similar affinity for the second substrate (ATP).

TABLE 2 | Kinetic parameters of the wild-type and mutant forms of His-GCK.

	$S_{0.5}$ (mM)*	ATP-Km (mM)	Glucose-K_{cat}*	ATP-K_{cat}	Hill coefficient (h) *	Inflection point (mM)*
Wild-type	2.42 ± 0.14	1.00 ± 0.24	33.2 ± 0.6	43.8 ± 3.9	2.44 ± 0.29	1.69 ± 0.10
Mutant	7.95 ± 0.92	1.00 ± 0.25	30.3 ± 1.2	45.2 ± 4.1	1.75 ± 0.30	3.78 ± 0.44

Means ± SD are given. The S0.5 value, ATP-Km, Kcat value for glucose (Glucose-Kcat), ATP (ATP-Kcat), Hill coefficient and inflection point were obtained from the allosteric sigmoidal equation. Note that the Hill coefficient (h) is unitless.
*$p < 0.05$.

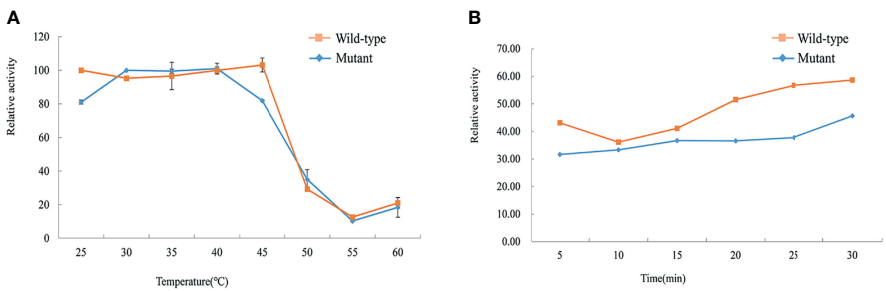

FIGURE 5 | Assessment of thermal instability of the wild-type and mutant GCK proteins. Squares represent wild-type GCK, and circles represent mutant GCK. **(A)** Relative activity of the wild-type and mutant GCKs at different temperatures in the kinase reaction. **(B)** Stability of the wild-type and mutant GCKs at 50°C in the kinase reaction.

enzyme activity similar to the wild-type enzyme at 50°C that was maintained for 30 min (**Figure 5B**). The statistical analyses were performed with SAS 8.0 (SAS Institute, Cary, NC, USA). A two-tailed p value <0.05 was considered significant.

DISCUSSION

MODY is an autosomal dominant form of diabetes that is characterized by early onset, pancreatic dysfunction and a non-insulin-dependent diabetes status. Heterozygous mutations in *GCK* were first recognized as the intrinsic cause of MODY2 in 1992 (13, 25). *HNF1A*, *GCK*, *HNF4A*, and *HNF1B are the most common types* in Europeans. MODY2 accounts for approximately 80% of MODY patients in Span (22), 38-86% in Italy (26–28), 56% in France (29) and 32% in United Kingdom (30). However, MODY2 is rarely reported in Asian patients, with a prevalence of 1% in Japanese (31), 2% in Korean (32) and 1-4% in Hong Kong Chinese patients (33, 34).

In our study, we recruited 30 early-onset diabetes pedigrees for genetic testing and discovered the novel mutation Ala259Thr in *GCK*, which was accompanied by hyperglycaemia and was in accordance with autosomal dominant inheritance. Three of the four diabetic patients in this pedigree were characterized by mild hyperglycaemia. The patients with Ala259Thr mutations did not require treatment, but could be managed with diet or exercise. Although we could not confirm whether the remaining female patient was a mutation carrier, since her DNA sample was not available, this patient was definitely diagnosed with GDM during her first pregnancy and returned to a normal glucose level after delivery. Therefore, this family was confirmed to be a MODY2 pedigree linked to a novel *GCK* p.Ala259Thr mutation.

Different MODY2 mutations have been reported to impair GCK function through different mechanisms, including kinetics, enzymatic activity or protein thermostability (18, 22, 35–38). Therefore, we investigated the functional characteristics of the Ala259Thr recombinant protein to elucidate the potential mechanism resulting in hyperglycaemia. In the kinetic analysis, Ala259Thr presented a higher $S_{0.5}$ value and inflection point, which indicated that a high glucose concentration was required to achieve the V_{max}. Moreover, the lower Hill coefficient and K_{cat} of the Ala259Thr mutation revealed a decreased affinity and catalytic activity when glucose was used as the substrate. However, when ATP was used as the substrate, the K_m-ATP and K_{cat} showed no significant differences between the mutant and wild-type recombinant proteins, which suggested that the Ala259Thr mutation affected the binding or catalytic capacity for glucose but not ATP. No mutation was reported in the same position previously, but the nearby mutations p.Trp257Arg and p.Gly261Arg presented decreased K_{cat} values (39, 40).

Most of the GCK mutations reported were found to be kinetically inactive, with alterations of one or more kinetic parameters (22, 35, 40). However, kinetic inactivation may not be the only factor that causes hyperglycaemia. Different MODY2 mutations have been reported to impair GCK function through different mechanisms, including kinetics, enzymatic activity or protein thermostability (36, 37). In our study, we also performed a thermal analysis. The wild-type GCK recombinant protein was stable under a temperature of 45°C, whereas the mutant protein presented dramatically decreased activity at the same temperature. Since the temperature for protein thermostability exceeds the normal temperature of the human body, the effect of thermal stability on hyperglycemia remained to be confirmed. As for the investigation of enzyme function, biochemical experiments are still the first choice in most literature reports since researchers can directly obtain recombinant protein and perform kinetic and thermal stability analysis to evaluate the activity and stability of the enzyme. However, it might be better to perform functional experiments *in vivo* to demonstrate the mechanism that the mutation contributing to hyperglycemia.

In addition, the glucokinase regulatory protein (GKRP) could act as a competitive inhibitor of glucose and regulate GCK activity through protein-protein interactions (41). Posttranslational regulation of GCK could also influence GCK activation (14). For example, cytoplasmic Ca(2+) levels may regulate GCK activation and therefore glucose metabolism and insulin secretion (42). The GCK-R369P and GCK-V367M mutations could impair glucose-stimulated insulin secretion through posttranslational regulation of GCK S-nitrosylation (14). However, whether these mechanisms participate in *GCK* p.Ala259Thr activity needs to be elucidated.

In the present study, we identified the novel mutation GCK p.Ala259Thr that co-segregated with diabetes in a Chinese MODY2 pedigree. Our study illustrated that the GCK p.Ala259Thr mutation had an immediate impact on the kinetic inactivity and thermal instability of the GCK enzyme, which led to hyperglycaemia in the mutation carriers of this pedigree. Other potential mechanisms, such as posttranslational regulation or crystal structure crystallographic analysis, need to be assessed in future studies.

DATA AVAILABILITY STATEMENT

The data analyzed in this study is subject to the following licenses/restrictions: Datasets consist of data routinely recorded in clinical practice. Requests to access these datasets should be directed to Cheng Hu, alfredhc@sjtu.edu.cn.

ETHICS STATEMENT

Ethical approval was granted by the Institutional Review Board of Shanghai Jiao Tong University Affiliated Sixth People's Hospital. Written informed consent to participate in this study was provided by the participants' legal guardian/next of kin.

AUTHOR CONTRIBUTIONS

CH and YG contributed to the study design, acquisition and interpretation of data, reviewed and edited the manuscript. FJ

focused on the biological experiments, analysis and interpretation of data, drafted and edited the manuscript. JY contributed to the biological experiments. RZ, XM, and YB contributed to the pedigree collection, genetic testing and clinical diagnosis. All authors contributed to the article and approved the submitted version.

FUNDING

This work was supported by the National Science Foundation of China (NSFC) (31500955, 81800702), the Shanghai Outstanding Academic Leaders (20XD1433300) and the Interdisciplinary Program of Shanghai Jiao Tong University (YG2021ZD20) and Nantong Municipal Science and Technology Project (MS22019005).

ACKNOWLEDGMENTS

The authors are grateful to the patients who participated in this research and gratefully acknowledge the skillful technical support from the nursing and medical staff at the Shanghai Clinical Centre for Diabetes and Department of Endocrinology and Metabolism. The authors are grateful to the HapMap, dbSNP, and 1000 Genome Project data sets.

REFERENCES

1. Bonnefond A, Philippe J, Durand E, Dechaume A, Huyvaert M, Montagne L, et al. Whole-Exome Sequencing and High Throughput Genotyping Identified KCNJ11 as the Thirteenth MODY Gene. *PloS One* (2012) 7(6):e37423. doi: 10.1371/journal.pone.0037423
2. Gao R, Liu Y, Gjesing AP, Hollensted M, Wan X, He S, et al. Evaluation of a Target Region Capture Sequencing Platform Using Monogenic Diabetes as a Study-Model. *BMC Genet* (2014) 15:13. doi: 10.1186/1471-2156-15-13
3. Prudente S, Jungtrakoon P, Marucci A, Ludovico O, Buranasupkajorn P, Mazza T, et al. Loss-Of-Function Mutations in APPL1 in Familial Diabetes Mellitus. *Am J Hum Genet* (2015) 97(1):177–85. doi: 10.1016/j.ajhg.2015.05.011
4. Mahalingam B, Cuesta-Munoz A, Davis EA, Matschinsky FM, Harrison RW, Weber IT. Structural Model of Human Glucokinase in Complex With Glucose and ATP: Implications for the Mutants That Cause Hypo- and Hyperglycemia. *Diabetes* (1999) 48(9):1698–705. doi: 10.2337/diabetes.48.9.1698
5. Matschinsky F, Liang Y, Kesavan P, Wang L, Froguel P, Velho G, et al. Glucokinase as Pancreatic Beta Cell Glucose Sensor and Diabetes Gene. *J Clin Invest* (1993) 92(5):2092–8. doi: 10.1172/JCI116809
6. Matschinsky FM. Regulation of Pancreatic Beta-Cell Glucokinase: From Basics to Therapeutics. *Diabetes* (2002) 51(Suppl 3):S394–404. doi: 10.2337/diabetes.51.2007.S394
7. Gidh-Jain M, Takeda J, Xu LZ, Lange AJ, Vionnet N, Stoffel M, et al. Glucokinase Mutations Associated With Non-Insulin-Dependent (Type 2) Diabetes Mellitus Have Decreased Enzymatic Activity: Implications for Structure/Function Relationships. *Proc Natl Acad Sci USA* (1993) 90(5):1932–6. doi: 10.1073/pnas.90.5.1932
8. Postic C, Shiota M, Niswender KD, Jetton TL, Chen Y, Moates JM, et al. Dual Roles for Glucokinase in Glucose Homeostasis as Determined by Liver and Pancreatic Beta Cell-Specific Gene Knock-Outs Using Cre Recombinase. *J Biol Chem* (1999) 274(1):305–15. doi: 10.1074/jbc.274.1.305
9. Kamata K, Mitsuya M, Nishimura T, Eiki J, Nagata Y. Structural Basis for Allosteric Regulation of the Monomeric Allosteric Enzyme Human Glucokinase. *Structure* (2004) 12(3):429–38. doi: 10.1016/j.str.2004.02.005S0969212604000474
10. Choi JM, Seo MH, Kyeong HH, Kim E, Kim HS. Molecular Basis for the Role of Glucokinase Regulatory Protein as the Allosteric Switch for Glucokinase. *Proc Natl Acad Sci USA* (2013) 110(25):10171–6. doi: 10.1073/pnas.1300457110
11. Glaser B, Kesavan P, Heyman M, Davis E, Cuesta A, Buchs A, et al. Familial Hyperinsulinism Caused by an Activating Glucokinase Mutation. *N Engl J Med* (1998) 338(4):226–30. doi: 10.1056/NEJM199801223380404
12. Njolstad PR, Sovik O, Cuesta-Munoz A, Bjorkhaug L, Massa O, Barbetti F, et al. Neonatal Diabetes Mellitus Due to Complete Glucokinase Deficiency. *N Engl J Med* (2001) 344(21):1588–92. doi: 10.1056/NEJM200105243442104
13. Froguel P, Vaxillaire M, Sun F, Velho G, Zouali H, Butel MO, et al. Close Linkage of Glucokinase Locus on Chromosome 7p to Early-Onset Non-Insulin-Dependent Diabetes Mellitus. *Nature* (1992) 356(6365):162–4. doi: 10.1038/356162a0
14. Ding SY, Tribble ND, Kraft CA, Markwardt M, Gloyn AL, Rizzo MA. Naturally Occurring Glucokinase Mutations are Associated With Defects in Posttranslational S-Nitrosylation. *Mol Endocrinol* (2010) 24(1):171–7. doi: 10.1210/me.2009-0138
15. Kleinberger JW, Pollin TI. Undiagnosed MODY: Time for Action. *Curr Diabetes Rep* (2015) 15(12):110. doi: 10.1007/s11892-015-0681-7
16. Liang H, Zhang Y, Li M, Yan J, Yang D, Luo S, et al. Recognition of Maturity-Onset Diabetes of the Young in China. *J Diabetes Investig* (2021) 12(4):501–9. doi: 10.1111/jdi.13378
17. Dimitriadis G, Boutati E, Raptis SA. The Importance of Adipose Tissue in Diabetes Pathophysiology and Treatment. *Horm Metab Res* (2007) 39(10):705–6. doi: 10.1055/s-2007-990269
18. Ellard S, Bellanne-Chantelot C, Hattersley ATMODY group. Best Practice Guidelines for the Molecular Genetic Diagnosis of Maturity-Onset Diabetes of the Young. *Diabetologia* (2008) 51(4):546–53. doi: 10.1007/s00125-008-0942-y
19. Hattersley A, Bruining J, Shield J, Njolstad P, Donaghue KC. The Diagnosis and Management of Monogenic Diabetes in Children and Adolescents. *Pediatr Diabetes* (2009) 10(Suppl 12):33–42. doi: 10.1111/j.1399-5448.2009.00571.x
20. Stenson PD, Mort M, Ball EV, Howells K, Phillips AD, Thomas NS, et al. The Human Gene Mutation Database: 2008 Update. *Genome Med* (2009) 1(1):13. doi: 10.1186/gm13
21. Osbak KK, Colclough K, Saint-Martin C, Beer NL, Bellanne-Chantelot C, Ellard S, et al. Update on Mutations in Glucokinase (GCK), Which Cause Maturity-Onset Diabetes of the Young, Permanent Neonatal Diabetes, and Hyperinsulinemic Hypoglycemia. *Hum Mutat* (2009) 30(11):1512–26. doi: 10.1002/humu.21110
22. Estalella I, Garcia-Gimeno MA, Marina A, Castano L, Sanz P. Biochemical Characterization of Novel Glucokinase Mutations Isolated From Spanish Maturity-Onset Diabetes of the Young (MODY2) Patients. *J Hum Genet* (2008) 53(5):460–6. doi: 10.1007/s10038-008-0271-5
23. McDonald TJ, Ellard S. Maturity Onset Diabetes of the Young: Identification and Diagnosis. *Ann Clin Biochem* (2013) 50(Pt 5):403–15. doi: 10.1177/0004563213483458
24. American Diabetes, A. 2. Classification and Diagnosis of Diabetes: Standards of Medical Care in Diabetes-2021. *Diabetes Care* (2021) 44(Suppl 1):S15–33. doi: 10.2337/dc21-S002
25. Hattersley AT, Turner RC, Permutt MA, Patel P, Tanizawa Y, Chiu KC, et al. Linkage of Type 2 Diabetes to the Glucokinase Gene. *Lancet* (1992) 339(8805):1307–10. doi: 10.1016/0140-6736(92)91958-B
26. Delvecchio M, Ludovico O, Menzaghi C, Di Paola R, Zelante L, Marucci A, et al. Low Prevalence of HNF1A Mutations After Molecular Screening of Multiple MODY Genes in 58 Italian Families Recruited in the Pediatric or Adult Diabetes Clinic From a Single Italian Hospital. *Diabetes Care* (2014) 37(12):e258–60. doi: 10.2337/dc14-1788
27. Bitterman O, Giuliani C, Festa C, Napoli A. Glucokinase Deficit Prevalence in Women With Diabetes in Pregnancy: A Matter of Screening Selection. *Front Endocrinol (Lausanne)* (2020) 11:268. doi: 10.3389/fendo.2020.00268
28. Delvecchio M, Mozzillo E, Salzano G, Iafusco D, Frontino G, Patera PI, et al. Monogenic Diabetes Accounts for 6.3% of Cases Referred to 15 Italian

Pediatric Diabetes Centers During 2007 to 2012. *J Clin Endocrinol Metab* (2017) 102(6):1826–34. doi: 10.1210/jc.2016-2490
29. Froguel P, Zouali H, Vionnet N, Velho G, Vaxillaire M, Sun F, et al. Familial Hyperglycemia Due to Mutations in Glucokinase. Definition of a Subtype of Diabetes Mellitus. *N Engl J Med* (1993) 328(10):697–702. doi: 10.1056/NEJM199303113281005
30. Shields BM, Hicks S, Shepherd MH, Colclough K, Hattersley AT, Ellard S. Maturity-Onset Diabetes of the Young (MODY): How Many Cases are We Missing? *Diabetologia* (2010) 53(12):2504–8. doi: 10.1007/s00125-010-1799-4
31. Nishi S, Hinata S, Matsukage T, Takeda J, Ichiyama A, Bell GI, et al. Mutations in the Glucokinase Gene are Not a Major Cause of Late-Onset Type 2 (Non-Insulin-Dependent) Diabetes Mellitus in Japanese Subjects. *Diabetes Med* (1994) 11(2):193–7. doi: 10.1111/j.1464-5491.1994.tb02019.x
32. Hwang JS, Shin CH, Yang SW, Jung SY, Huh N. Genetic and Clinical Characteristics of Korean Maturity-Onset Diabetes of the Young (MODY) Patients. *Diabetes Res Clin Pract* (2006) 74(1):75–81. doi: 10.1016/j.diabres.2006.03.002
33. Xu JY, Dan QH, Chan V, Wat NM, Tam S, Tiu SC, et al. Genetic and Clinical Characteristics of Maturity-Onset Diabetes of the Young in Chinese Patients. *Eur J Hum Genet* (2005) 13(4):422–7. doi: 10.1038/sj.ejhg.5201347
34. Ng MC, Lee SC, Ko GT, Li JK, So WY, Hashim Y, et al. Familial Early-Onset Type 2 Diabetes in Chinese Patients: Obesity and Genetics Have More Significant Roles Than Autoimmunity. *Diabetes Care* (2001) 24(4):663–71. doi: 10.2337/diacare.24.4.663
35. Shen Y, Cai M, Liang H, Wang H, Weng J. Insight Into the Biochemical Characteristics of a Novel Glucokinase Gene Mutation. *Hum Genet* (2011) 129(3):231–8. doi: 10.1007/s00439-010-0914-4
36. Garcia-Herrero CM, Galan M, Vincent O, Flandez B, Gargallo M, Delgado-Alvarez E, et al. Functional Analysis of Human Glucokinase Gene Mutations Causing MODY2: Exploring the Regulatory Mechanisms of Glucokinase Activity. *Diabetologia* (2007) 50(2):325–33. doi: 10.1007/s00125-006-0542-7
37. Wang Z, Diao C, Liu Y, Li M, Zheng J, Zhang Q, et al. Identification and Functional Analysis of GCK Gene Mutations in 12 Chinese Families With Hyperglycemia. *J Diabetes Investig* (2019) 10(4):963–71. doi: 10.1111/jdi.13001
38. Fajans SS, Bell GI, Polonsky KS. Molecular Mechanisms and Clinical Pathophysiology of Maturity-Onset Diabetes of the Young. *N Engl J Med* (2001) 345(13):971–80. doi: 10.1056/NEJMra002168
39. Takeda J, Gidh-Jain M, Xu LZ, Froguel P, Velho G, Vaxillaire M, et al. Structure/function Studies of Human Beta-Cell Glucokinase. Enzymatic Properties of a Sequence Polymorphism, Mutations Associated With Diabetes, and Other Site-Directed Mutants. *J Biol Chem* (1993) 268(20):15200–4. doi: 10.1016/S0021-9258(18)82456-5
40. Davis EA, Cuesta-Munoz A, Raoul M, Buettger C, Sweet I, Moates M, et al. Mutants of Glucokinase Cause Hypoglycaemia- and Hyperglycaemia Syndromes and Their Analysis Illuminates Fundamental Quantitative Concepts of Glucose Homeostasis. *Diabetologia* (1999) 42(10):1175–86. doi: 10.1007/s001250051289
41. Park JM, Kim TH, Jo SH, Kim MY, Ahn YH. Acetylation of Glucokinase Regulatory Protein Decreases Glucose Metabolism by Suppressing Glucokinase Activity. *Sci Rep* (2015) 5:17395. doi: 10.1038/srep17395
42. Markwardt ML, Seckinger KM, Rizzo MA. Regulation of Glucokinase by Intracellular Calcium Levels in Pancreatic Beta Cells. *J Biol Chem* (2016) 291(6):3000–9. doi: 10.1074/jbc.M115.692160

Conflict of Interest: The authors declare that the research was conducted in the absence of any commercial or financial relationships that could be construed as a potential conflict of interest.

Publisher's Note: All claims expressed in this article are solely those of the authors and do not necessarily represent those of their affiliated organizations, or those of the publisher, the editors and the reviewers. Any product that may be evaluated in this article, or claim that may be made by its manufacturer, is not guaranteed or endorsed by the publisher.

frontiers in Endocrinology

CASE REPORT
published: 23 December 2021
doi: 10.3389/fendo.2021.770871

Case Report: A Chinese Family of Woodhouse-Sakati Syndrome With Diabetes Mellitus, With a Novel Biallelic Deletion Mutation of the DCAF17 Gene

Min Zhou[1,2†], Ningjie Shi[3,4†], Juan Zheng[3,4†], Yang Chen[3,4], Siqi Wang[3,4], Kangli Xiao[3,4], Zhenhai Cui[3,4], Kangli Qiu[3,4], Feng Zhu[5,6] and Huiqing Li[3,4]*

[1] Department of Pulmonary and Critical Care Medicine, Tongji Hospital, Tongji Medical College, Huazhong University of Science and Technology, Wuhan, China, [2] Key Laboratory of Respiratory Diseases, National Ministry of Health of the People's Republic of China and National Clinical Research Center for Respiratory Disease, Wuhan, China, [3] Department of Endocrinology, Union Hospital, Tongji Medical College, Huazhong University of Science and Technology, Wuhan, China, [4] Hubei Provincial Clinical Research Center for Diabetes and Metabolic Disorders , Wuhan, China, [5] Clinic Center of Human Gene Research, Union Hospital, Tongji Medical College, Huazhong University of Science and Technology, Wuhan, China, [6] Department of Cardiology, Union Hospital, Tongji Medical College, Huazhong University of Science and Technology, Wuhan, China

OPEN ACCESS

Edited by:
Ming Liu,
Tianjin Medical University General Hospital, China

Reviewed by:
Rabia Habib,
COMSATS University, Pakistan
Suleyman Nahit Sendur,
Hacettepe University, Turkey

***Correspondence:**
Huiqing Li
lhqing5@126.com

†These authors have contributed equally to this work and share first authorship

Specialty section:
This article was submitted to Clinical Diabetes, a section of the journal Frontiers in Endocrinology

Received: *05 September 2021*
Accepted: *25 November 2021*
Published: *23 December 2021*

Citation:
Zhou M, Shi N, Zheng J, Chen Y, Wang S, Xiao K, Cui Z, Qiu K, Zhu F and Li H (2021) Case Report: A Chinese Family of Woodhouse-Sakati Syndrome With Diabetes Mellitus, With a Novel Biallelic Deletion Mutation of the DCAF17 Gene. Front. Endocrinol. 12:770871. doi: 10.3389/fendo.2021.770871

Woodhouse–Sakati syndrome (WSS) (OMIM#241080) is a rare multi-system autosomal recessive disease with homozygous mutation of the DCAF17 gene. The main features of WSS include diabetes, hypogonadism, alopecia, deafness, intellectual disability and progressive extrapyramidal syndrome. We identified a WSS family with a novel DCAF17 gene mutation type in China. Two unconsanguineous siblings from the Chinese Han family exhibiting signs and symptoms of Woodhouse-Sakati syndrome were presented for evaluation. Whole-exome sequencing revealed a homozygous deletion NM_025000.4: c.1488_1489delAG in the DCAF17 gene, which resulted in a frameshift mutation that led to stop codon formation. We found that the two patients exhibited low insulin and C-peptide release after glucose stimulation by insulin and C-peptide release tests. These findings indicate that the DCAF17 gene mutation may cause pancreatic β cell functional impairment and contribute to the development of diabetes.

Keywords: Woodhouse–Sakati syndrome, diabetes, intellectual disability, alopecia, hypogonadism

INTRODUCTION

WSS, which is a rare autosomal recessive genetic disease, was first reported in 1983 (1). Previous, reports revealed the presence of hypogonadism (100%), diabetes mellitus (66%), intellectual disability (58%), sensorineural hearing loss (62%), and extrapyramidal movements (65%) (2). To date, 88 cases from more than 40 families have been reported (2). Most of these families originate from the Middle East (3, 4), particularly Saudi Arabia. Some cases have also been recognized in other areas such as Europe, Turkey, India, Pakistan, Portugal, France, and Japan. The disease is caused by mutations in the DCAF17 gene (also known as C2orf37), which

is located on chromosome 2q22.3-q35 (5). The DCAF17 gene contains at least 14 exons and encodes a nuclear transmembrane protein whose specific function is unclear (6). Eighteen types of pathogenic mutations have been identified, including three nonsense, five intronic, nine frameshift and one start loss mutation, all of which result in truncated nonfunctional protein products. Based on the hypothesis of Alazami et al. (2008), the mutation of DCAF17 impairs the function of the nucleolus, which causes disruptions of normal cell routines such as cell cycle regulation, cellular senescence, and apoptosis, which may underlie the pathogenesis of WSS (5).

We identified a WSS family in China and found a novel DCAF17 deletion mutation *via* genetic testing. Two patients in this family were affected with clinical features of diabetes, alopecia, intellectual disability, hypogonadism, anemia and thrombocytopenia.

CASE DESCRIPTION

Case 1

There were two affected individuals in this family line, whose parents were not consanguineously married (Family **Figure 1A**). The proband born on October 24, 1984, was found to have elevated blood glucose and edema throughout the body in November 2018 and was admitted to the hospital for treatment. Physical examination showed sparse scalp hair and eyebrows, absence of axillary and pubic hair, infantile external genitalia, generalized edema and intellectual disability (**Figures 2A, B**). Other data were normal, including bedside hearing and sensory testing (although formal assessment was not performed). Laboratory tests showed that the fasting glucose was 40.22 mmol/L (reference range: 3.9-6.1 mmol/L), and the glycosylated hemoglobin (HbA1c) was 13.8% (reference range: < 6.4%). Sex hormone tests revealed low levels of luteinizing hormone (LH), follicle stimulating hormone (FSH) and estradiol. Routine blood tests suggested that the patient had anemia and thrombocytopenia (**Table 1**). Insulin and C-peptide release tests showed that the patient's insulin and C-peptide secretion had no peak (**Supplementary Table 1A**). The OGTT-based measures of insulin secretion index homeostasis model assessment- β (HOMA-β = 20 × Ins0/(Glu0-3.5) was low (**Table 1**). Thyroid hormone tests revealed normal thyroid-stimulating hormone (TSH), low free thyroxine (FT4), and a low free triiodothyronine level (FT3). Pancreatic CT indicated a slightly atrophied pancreas (**Figure 3A**). While ultrasound showed that the uterus was absent. The patient was treated with insulin injection, and the blood glucose was poorly controlled.

Case 2

The brother of the proband, who was born on October 29, 1986, was found to have elevated blood glucose in 2019 and admitted to our hospital for a closed fracture in January 2020. Physical examination also showed sparse scalp hair and eyebrows (**Figures 2C, D**), absence of axillary and pubic hair, hypotrophy testicles, small penis, and intellectual disability. Laboratory tests revealed that his fasting glucose was 14.91 mmol/L, HbA1c was 9.0%, he had negative insulin antibodies, low IGF-1 level of 43 ng/ml (reference range: 111-320 ng/ml), low testosterone and LH. Routine blood tests also suggested that the patient had anemia and thrombocytopenia. Insulin and C-peptide release tests showed low insulin, C-peptide secretion (**Supplementary Table 1B**) and low HOMA-β. Thyroid

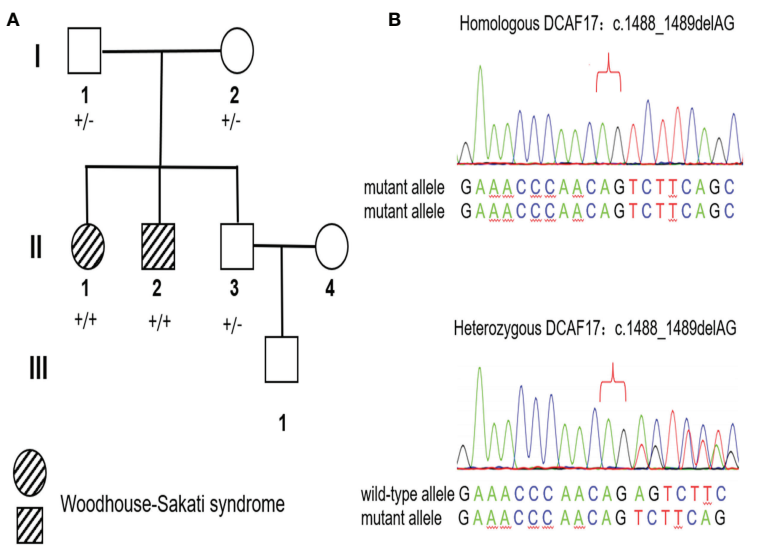

FIGURE 1 | Pedigree and Sanger sequencing chromatograms of the identified disease-causing variants. **(A)** Pedigree of the WSS family. Marks '+/+' and '+/-' indicate the homozygous status and heterozygous status of the identified the DCAF17:c.1488_1489delAG respectively. **(B)** Sanger sequencing chromatograms of the DCAF17: c.1488_1489delAG in homozygous status (above) and heterozygous status (below).

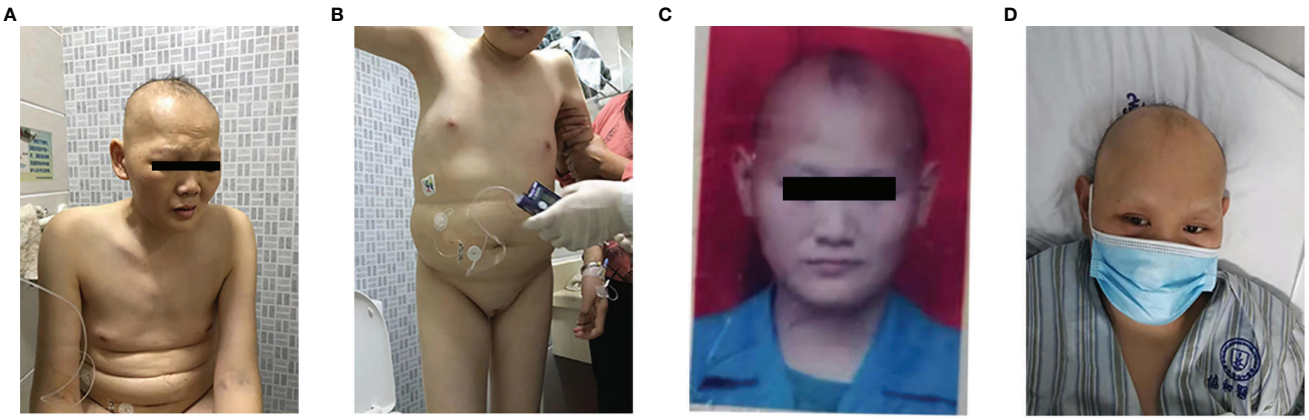

FIGURE 2 | Photographs of the WSS patients. **(A, B)** The proband's hair, eyebrows and eyelashes are sparse, and infantile external genitalia. **(C, D)** The brother of proband: childhood-onset hair thinning, His hair, eyebrows and eyelashes are further sparse in adulthood.

TABLE 1 | Clinical features of affected individuals in the family.

Clinical features	Affected individuals		Normal reference range	
	II-1	II-2		
Sex	female	male		
Age(at first diagnosis of diabetes)	34	33		
Height (cm)	162	N/A		
Weight (kg)	54	45		
Clinical manifestations				
Alopecia	+	+		
Intellectual Disability	+	+		
Hypogonadism	+	+		
Diabetes Mellitus	+	+		
Anemia	+	+		
Thrombocytopenia	+	+		
Hypothyroidism	–	–		
Other Neurophysiology findings	–	–		
Sensorineural hearing loss	–	–		
Progressive extrapyramidal movements	–	–		
Laboratory tests				
Fasting blood glucose (mmol/L)	40.22	14.91	3.9-6.1	
HbA1c %	13.8	9.0	<6.4	
Islet beta-cell autoantibodies	N/A	–		
HOMA-β (%)	4.63	21.69		
IGF-1 (ng/ml)	N/A	43	115-320	
Hb (g/L)	81	105	115-150	
PLT (G/L)	63	89	125-350	
Sexual hormones			Male	Female (follicular phase)
Progesterone (ng/ml)	0.2	0.2		0.10-0.30
FSH (mIU/ml)	4.23	0.99	0.95-11.95	3.03-8.08
PRL (ng/ml)	11.17	5.4	3.46-19.40	5.18-26.53
Estradiol (pg/ml)	20	14	11-44	21-251
Testosterone (nmol/l)	1.6	0.89	4.94-32.01	0.38-1.97
LH (mIU/ml)	0.78	0.16	1.14-8.75	2.39-6.60
ECG abnormalities	+	+		

HbA1c, Glycated hemoglobin; Hb, Hemoglobin; PLT, Platelet; FSH, Follicle-stimulating hormone; PRL, Prolactin; LH, Luteinizing hormone; ECG, Electrocardiographic; N/A, not available; +, positive; -, negative.

hormone tests revealed normal thyroid function. The patient exhibited an uneven pancreatic density by abdominal CT scan (**Figure 3B**), empty sella by pituitary MRI (**Figures 3C, D**), and osteoporosis that was not consistent with actual age by hip CT scan (**Figure 3E**). Before admission to the hospital, the patient had oral hypoglycemic agents to control glucose, and insulin pump treatment was given after admission to the hospital, but the glucose control was poor.

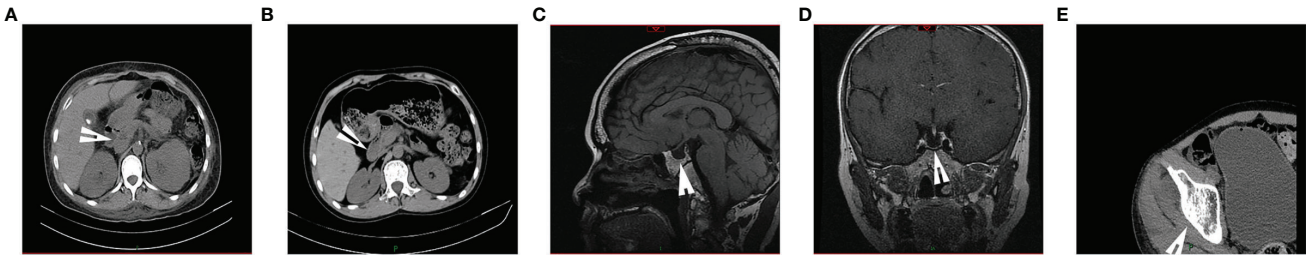

FIGURE 3 | The images of the WSS patients. **(A)** Computed tomography of the abdomen of the proband demonstrated atrophy of the pancreas. **(B)** Computed tomography of the abdomen of the brother of proband showed uneven pancreatic density. **(C, D)** Pituitary MR of the brother of proband indicated the empty sella and none pituitary gland. **(E)** Hip CT of the brother of proband suggested osteoporosis that was not consistent with actual age. (arrows).

Genetic Sequencing and Bioinformatics Analysis

5ml venous blood was collected from the proband (II-1, **Figure 1A**) and her family members (I-1, I-2, II-2 and II-3, **Figure 1A**). Whole Exome sequencing (WES) was performed on proband using the xGen® Exome Research Panel v1.0 (IDT, USA) on the Illumina NovaSeq6000. Genomic DNA was extracted from whole blood, then sheared by sonication and hybridized for enrichment. And the library was enriched for target regions, sequencing was performed to generate 150 bp paired-end reads. To identify mutations, sequencing data was analyzed and annotated according to an in-house pipeline which we describe before (7). Based on the variant annotations, a series of prioritization strategies were applied to identify candidate variants associated with the phenotypes. The detailed steps were as follows: (1) excluding variants outside exonic and splicing regions; (2) excluding variants with minor allele frequency >=0.01 according to public databases (GnomAD, 1000 Genomes and ExAC); (3) excluding synonymous variants; (4) excluding variants not presenting damaging results in the function prediction from clinPred (8). To prioritize the most likely candidate disease-causing gene, all candidate genes were then ranked by Phenolyzer (9). Human Phenotype Ontology (HPO) Identifiers of the proband's disease phenotype (anemia, HP:0001903; alopecia, HP:0001596; diabetes mellitus, HP:0000819; hypogonadism, HP:000013; intellectual disability, HP:0001249) were input as phenotype terms into Phenolyzer. To confirm the candidate disease-causing variant, we PCR-amplified the genomic DNA fragments in the proband (II-1) and her family members (I-1, I-2, II-4 and III-2), then sequenced them by Sanger sequencing. The PCR primer pairs were uses as followings: forward 5′–TCCTGGGTCCAGAGTTCTTT–3′, reverse 5′–TGGGGTGTTTGGCTAAAAGT–3′).

Identification of Variants Associated With Disease Phenotypes of the Proband

Based on the aligned reads, 76,241 single nucleotide variants (SNVs) and 13,038 indels (deletions and insertions, <50bp) were identified by WES. After three filters of prioritization strategies, 271 variants from 244 genes were kept. Both these genes and HPO Identifiers of phenotypes of the proband were input Phenolyzer. Phenolyzer suggested that WSS was the most likely disease that can explain the syndrome phenotypes of the proband, and the DCAF17 gene was the candidate gene (**Supplementary Figure 1**). A homozygous deletion DCAF17: c.1488_1489delAG was detected at genomic position 172,337,546-172,337,547 of chromosome 2 (GRCh37/Hg19), resulting in frameshift in reading frame in exon 14 leading to premature stop codon (**Figure 1B**). The full-length DDB1 and CUL4 associated factor 17 contains 520 amino acids. The premature termination was predicted to cause a truncated protein comprising 506 amino acids. The first 495 residues corresponding to the normal protein and the other extra 11 derived from the frameshift deletion. Sanger sequencing analysis showed the identified c.1488_1489delAG (deletion of nucleotide AG in coding region 1488-1489) was segregated with the disease in this family, which was in homozygous status in the proband's affected sibling (II-2) and heterozygous status in the proband's unaffected parents (I-1 and I-2) and sibling (II-3) (**Figure 1A**). Additionally, the identified variant allele has been recorded in the database of gnomAD with an extremely low allele frequency at 3/251,124 (dbSNP rs778488574). According to the ACMG/AMP criteria, the raw homozygous frameshift variant DCAF17: c.1488_1489delAG was classified as a pathogenic variant for WSS.

DISCUSSION

The clinical features of WSS patients are not entirely consistent. Most patients present extrapyramidal symptoms, intellectual disability, hypogonadism, alopecia and diabetes. We found two patients in a Chinese national lineage who exhibited diabetes mellitus, intellectual disability, hair thinning, and hypogonadism but no symptoms of progressive extrapyramidal dysfunction. The boosted whole exome gene sequencing technique suggested the presence of the NM_025000.4:c.1488_1489delAG variant in the DCAF17 gene (sequencing **Figure 1B**), which established the diagnosis of WSS in this lineage. We further performed insulin and C-peptide release tests and found pancreatic β cell functional impairment in both patients. We identified a WSS lineage in China with a novel DCAF17 gene mutation pattern and suggested that pancreatic β cell functional impairment might

be one of the major mechanisms in the pathogenesis of WSS diabetes.

The prevalence of diabetes mellitus in patients with WSS has been reported to be as high as 66%, and it mostly starts from adolescents to young adults (2). There are few studies on the pathogenesis of diabetes mellitus in WSS. Sendur SN et al. (2019) analyzed adolescent-onset diabetes mellitus in WSS case and found no significant increase in C-peptide release levels (10). Rachmiel M et al. (2011) detected low C-peptide levels and pancreatic atrophy when imaging some patients with abnormally elevated blood glucose (11). Both patients with WSS that we reported had diabetes in young adulthood with reduced insulin and C-peptide levels, negative insulin-related antibodies, and pancreatic atrophy from abdominal CT. HOMA-β was applied to assess β-cell function, HOMA-β was less than 100% and lower than type 2 diabetes in the two cases (12). Low insulin, low C-peptide levels, low HOMA-β and an atrophic pancreas suggest that WSS patients may have pancreatic β cell function defects. Therefore, we speculate that the DCAF17 gene is important for the maintenance of pancreatic β cell function. DCAF17 gene mutations may cause β cell functional defects, which may be one of the main mechanisms in the pathogenesis of diabetes in patients with WSS. However, the underlying pathological mechanism requires further study.

Thirty percent of individuals, typically around age 20 years, have hypothyroidism in patients with WSS (2). The proband showed low FT3 and FT4 with normal TSH. We observed decreased cortisol secretion in patients, which might indicate hypopituitarism.

In these two patients, we reported that the homozygous nucleotide variant changed the codon for the compilation of amino acid Arg 429 to Ser (NP_079276.2:p.Arg496SerfsX12), which prematurely terminated the peptide chain synthesis as a deletion variant and resulted in a truncated nonfunctional protein. These two patients had no significant extrapyramidal symptoms, dystonia or hearing loss. However, the proband's brother had osteoporosis not previously described in this WSS. Their clinical features are not entirely consistent with previously reported cases. The length of the truncated proteins does not parallel the phenotypes reported in patients with WSS. Ali RH et al. (2016) proposed that the cellular clearance of the truncated DCAF17 version rescued the unexpected outcomes of cellular events through nonsense-mediated decay (NMD) of mRNAs, which could be perturbed by an inefficient interaction of the truncated protein (13). A truncated DCAF17 protein with missing domains and motifs that are necessary to interact with the DDB1-CUL4 ubiquitin ligase complex and ultimately recruit substrates was formed.

The treatment of WSS patients is currently individualized and managed in a multi-disciplinary pattern (2). Since specific mechanisms and drug targets that are responsible for the pathogenesis of WSS remain unclear, the current therapeutic principles are only symptomatic treatments. For hypogonadism, estrogen or androgen replacement therapy is indicated. For patients with WSS complicated by diabetes, the main treatment principle is to control the blood glucose levels and delay the development of diabetes-related complications. We have found that β cell function defects may be the main mechanism for the development of diabetes in WSS, which suggests that insulin should probably be the main treatment for patients with WSS when diabetes occurs.

The current study has certain limitations. First, the number of cases in this study slightly less, to reflect the results of the accuracy and comprehensiveness. Second, there was no dynamic detection of changes in hormone levels. Third, in this study the indices of insulin sensitivity and secretion were obtained from OGTT, not the euglycemic-hyperinsulinemic and the hyperglycemic clamp technique. Fourth, further experimental studies are necessary to reveal the exact pathogenic mechanisms of how these genes affect different tissues.

CONCLUSIONS

Woodhouse-Sakati syndrome is a very rare autosomal recessive hereditary metabolic disorder. We observed the presence of impaired pancreatic (β cells) and gonadal function in patients with WSS. Further tests revealed the presence of low insulin secretion, which suggests that β cell functional defects due to DCAF17 gene mutation are among possible mechanisms for the development of diabetes in WSS. In this study, we reported a new pathogenic sequence variant in DCAF17, NM_025000.4: c.1488_1489delAG, which may expand the spectrum of DCAF17 variants. In addition to the endocrine findings of hypogonadism and diabetes mellitus, the decreased β cell function and osteoporosis observed are novel findings with unknown mechanisms. We have no neurologic findings of progressive extrapyramidal movements, or moderate bilateral postlingual sensorineural hearing loss other than intellectual disability. Whether phenotypes are associated with different mutation types requires further study.

DATA AVAILABILITY STATEMENT

The datasets presented in this study can be found in online repositories. The names of the repository/repositories and accession number(s) can be found in the article/**Supplementary Material**.

ETHICS STATEMENT

This study was approved by the ethics committee of Tongji Medical College, Huazhong University of Science and Technology, Wuhan, P.R China and informed consent was obtained from the patients and their parents. Written informed consent was obtained from the individual(s) for the publication of any potentially identifiable images or data included in this article.

AUTHOR CONTRIBUTIONS

All the authors have contributed significantly. HL designed the study. MZ, NS, and JZ wrote the manuscript. MZ, NS, JZ, YC,

SW, KX, ZC, KQ, and FZ collected and analyzed the clinical data, participated in discussion. HL supervised the study and corrected the manuscript. All authors contributed to the article and approved the submitted version.

FUNDING

This work was supported by the grant from the National Natural Science Foundation of China (grant numbers 81974111 to HL).

REFERENCES

1. Woodhouse NJ, Sakati NA. A Syndrome of Hypogonadism, Alopecia, Diabetes Mellitus, Mental Retardation, Deafness, and ECG Abnormalities. *J Med Genet* (1983) 20(3):216–9. doi: 10.1136/jmg.20.3.216
2. Bohlega SA, Abusrair A. Woodhouse-Sakati Syndrome. 2016 Aug 4 [Updated 2021 Jul 8]. In: MP Adam, HH Ardinger, RA Pagon, SE Wallace, LJH Bean, G Mirzaa, A Amemiya, editors. *GeneReviews®*. Seattle (WA: University of Washington, Seattle (1993–2021).
3. Habib R, Basit S, Khan S, Khan MN, Ahmad W. A Novel Splice Site Mutation in Gene C2orf37 Underlying Woodhouse-Sakati Syndrome (WSS) in a Consanguineous Family of Pakistani Origin. *Gene* (2011) 490(1-2):26–31. doi: 10.1016/j.gene.2011.09.002
4. Ben-Omran T, Ali R, Almureikhi M, Alameer S, Al-Saffar M, Walsh CA, et al. Phenotypic Heterogeneity in Woodhouse-Sakati Syndrome: Two New Families With a Mutation in the C2orf37 Gene. *Am J Med Genet A* (2011) 155A(11):2647–53. doi: 10.1002/ajmg.a.34219
5. Alazami AM, Al-Saif A, Al-Semari A, Bohlega S, Zlitni S, Alzahrani F, et al. Mutations in C2orf37, Encoding a Nucleolar Protein, Cause Hypogonadism, Alopecia, Diabetes Mellitus, Mental Retardation, and Extrapyramidal Syndrome. *Am J Hum Genet* (2008) 83(6):684–91. doi: 10.1016/j.ajhg.2008.10.018
6. Alazami AM, Schneider SA, Bonneau D, Pasquier L, Carecchio M, Kojovic M, et al. C2orf37 Mutational Spectrum in Woodhouse-Sakati Syndrome Patients. *Clin Genet* (2010) 78(6):585–90. doi: 10.1111/j.1399-0004.2010.01441.x
7. Sun D, Liu Y, Cai W, Ma J, Ni K, Chen M, et al. Detection of Disease-Causing SNVs/Indels and CNVs in Single Test Based on Whole Exome Sequencing: A Retrospective Case Study in Epileptic Encephalopathies. *Front Pediatr* (2021) 9:635703. doi: 10.3389/fped.2021.635703
8. Yang H, Robinson PN, Wang K. Phenolyzer: Phenotype-Based Prioritization of Candidate Genes for Human Diseases. *Nat Methods* (2015) 12(9):841–3. doi: 10.1038/nmeth.3484
9. Alirezaie N, Kernohan KD, Hartley T, Majewski J, Hocking TD. ClinPred: Prediction Tool to Identify Disease-Relevant Nonsynonymous Single-Nucleotide Variants. *Am J Hum Genet* (2018) 103(4):474–83. doi: 10.1016/j.ajhg.2018.08.005
10. Sendur SN, Oguz S, Utine GE, Dagdelen S, Oguz KK, Erbas T, et al. A Case of Woodhouse-Sakati Syndrome With Pituitary Iron Deposition, Cardiac and Intestinal Anomalies, With a Novel Mutation in DCAF17. *Eur J Med Genet* (2019) 62(8):103687. doi: 10.1016/j.ejmg.2019.103687
11. Rachmiel M, Bistritzer T, Hershkoviz E, Khahil A, Epstein O, Parvari R. Woodhouse-Sakati Syndrome in an Israeli-Arab Family Presenting With Youth-Onset Diabetes Mellitus and Delayed Puberty. *Horm Res Paediatr* (2011) 75(5):362–6. doi: 10.1159/000323441
12. Gao Z, Yan W, Fang Z, Zhang Z, Yuan L, Wang X, et al. Annual Decline in β-Cell Function in Patients With Type 2 Diabetes in China. *Diabetes Metab Res Rev* (2021) 37(2):e3364. doi: 10.1002/dmrr.3364
13. Ali RH, Shah K, Nasir A, Steyaert W, Coucke PJ, Ahmad W. Exome Sequencing Revealed a Novel Biallelic Deletion in the DCAF17 Gene Underlying Woodhouse Sakati Syndrome. *Clin Genet* (2016) 90(3):263–9. doi: 10.1111/cge.12700

SUPPLEMENTARY MATERIAL

The Supplementary Material for this article can be found online at: https://www.frontiersin.org/articles/10.3389/fendo.2021.770871/full#supplementary-material

Supplementary Figure 1 | A snapshot of the output from the Phenolyzer. **(A)** The interactive gene-disease-term network indicates the WSS is the most likely disease that can explain the syndrome phenotypes, which including anemia, alopecia, diabetes mellitus, hypogonadism, and intellectual disability. **(B)** The interactive gene-disease-term network indicates the DCAF17 is the candidate gene.

Conflict of Interest: The authors declare that the research was conducted in the absence of any commercial or financial relationships that could be construed as a potential conflict of interest.

Publisher's Note: All claims expressed in this article are solely those of the authors and do not necessarily represent those of their affiliated organizations, or those of the publisher, the editors and the reviewers. Any product that may be evaluated in this article, or claim that may be made by its manufacturer, is not guaranteed or endorsed by the publisher.

frontiers in Endocrinology

ORIGINAL RESEARCH
published: 05 January 2022
doi: 10.3389/fendo.2021.774634

A Novel Nonsense *INS* Mutation Causes Inefficient Preproinsulin Translocation Into the Endoplasmic Reticulum

Ying Yang[1†], Hua Shu[1†], Jingxin Hu[1†], Lei Li[2], Jianyu Wang[1], Tingting Chen[1], Jinyang Zhen[1], Jinhong Sun[1], Wenli Feng[1], Yi Xiong[3], Yumeng Huang[1], Xin Li[1], Kai Zhang[4], Zhenqian Fan[5], Hui Guo[2*] and Ming Liu[1*]*

[1] Department of Endocrinology and Metabolism, Tianjin Medical University General Hospital, Tianjin, China, [2] Department of Endocrinology, The Second Part of Jilin University First Hospital, Jilin, China, [3] Division of Metabolism, Endocrinology and Diabetes, University of Michigan Medical School, Ann Arbor, MI, United States, [4] Department of Technology Services, RSR Tianjin Biotech Co., Tianjin, China, [5] Department of Endocrinology and Metabolism, The Second Hospital of Tianjin Medical University, Tianjin, China

Preproinsulin (PPI) translocation across the membrane of the endoplasmic reticulum (ER) is the first and critical step of insulin biosynthesis. Inefficient PPI translocation caused by signal peptide (SP) mutations can lead to β-cell failure and diabetes. However, the effect of proinsulin domain on the efficiency of PPI translocation remains unknown. With whole exome sequencing, we identified a novel *INS* nonsense mutation resulting in an early termination at the 46th residue of PPI (PPI-R46X) in two unrelated patients with early-onset diabetes. We examined biological behaviors of the mutant and compared them to that of an established neonatal diabetes causing mutant PPI-C96Y. Although both mutants were retained in the cells, unlike C96Y, R46X did not induce ER stress or form abnormal disulfide-linked proinsulin complexes. More importantly, R46X did not interact with co-expressed wild-type (WT) proinsulin in the ER, and did not impair proinsulin-WT folding, trafficking, and insulin production. Metabolic labeling experiments established that, despite with an intact SP, R46X failed to be efficiently translocated into the ER, suggesting that proinsulin domain downstream of SP plays an important unrecognized role in PPI translocation across the ER membrane. The study not only expends the list of *INS* mutations associated with diabetes, but also provides genetic and biological evidence underlying the regulation mechanism of PPI translocation.

Keywords: *INS* gene, mutation, diabetes, preproinsulin, translocation

OPEN ACCESS

Edited by:
Sangeeta Dhawan,
City of Hope National Medical Center, United States

Reviewed by:
Michael A. Weiss,
Indiana University, United States
Tatyana Gurlo,
University of California, Los Angeles, United States

****Correspondence:***
Ming Liu
mingliu@tmu.edu.cn
Zhenqian Fan
fanzhenqian2003@163.com
Hui Guo
ghui@jlu.edu.cn

†These authors have contributed equally to this work and share first authorship

Specialty section:
This article was submitted to Diabetes: Molecular Mechanisms, a section of the journal Frontiers in Endocrinology

Received: *12 September 2021*
Accepted: *06 December 2021*
Published: *05 January 2022*

Citation:
Yang Y, Shu H, Hu J, Li L, Wang J, Chen T, Zhen J, Sun J, Feng W, Xiong Y, Huang Y, Li X, Zhang K, Fan Z, Guo H and Liu M (2022) A Novel Nonsense INS Mutation Causes Inefficient Preproinsulin Translocation Into the Endoplasmic Reticulum. Front. Endocrinol. 12:774634. doi: 10.3389/fendo.2021.774634

INTRODUCTION

Insulin is an essential hormone for maintaining glucose homeostasis of the body. In pancreatic β-cells, the insulin biosynthesis starts from its precursor, preproinsulin (PPI), which is composed of the N-terminal signal peptide (SP) followed by the C-terminal proinsulin domain. Newly synthesized PPI driven by its SP translocates across the membrane of the endoplasmic reticulum

(ER) through the Sec61 translocon. Upon delivery into the ER, SP of PPI is cleaved by signal peptidase at the luminal side of the ER membrane, forming another insulin precursor, proinsulin (PI) (1). In the oxidized ER lumen, PI undergoes rapid oxidative folding, forming three highly conserved disulfide bonds (B7-A7, B19-A20, and A6-A11). Well-folded PI exits from the ER and traffics through the Golgi to the secretory granules where it is processed by prohormone convertase (PC1/3 and PC2) and carboxypeptidase E (CPE), forming mature insulin and C-peptide (2–4). It takes approximately 30–150 min to finish these intracellular processes. Among these events, the earliest step during which PPI translocation into the ER had been long thought to be very efficient and exclusively through the signal recognition particle (SRP)-dependent co-translational translocation (5). However, recent evidence indicates that, as a small secretory protein with a suboptimal signal sequence, the fully synthesized PPI may not be efficiently recognized by SRP and co-translationally translocated into the ER. SRP independent post-translational translocation then functions as an important backup to enhance PPI translocation (4, 6, 7). The pathophysiological significance of inefficient PPI translocation is highlighted by recent evidence showing that deficiency of TRAPα [translocon associated protein alpha, a type 2 diabetes associated gene (8)], TRAPβ, and/or TRAPδ impairs PPI translocation and insulin production (9, 10), and also by the discoveries of PPI SP mutations that impair PPI translocation causing β-cell failure and diabetes in humans (2, 11–14).

In addition to the PPI SP mutations, at least 70 *INS* gene mutations located in the proinsulin domain have been reported to be associated with diabetes in humans (15–20). The majority of these mutations impair proinsulin oxidative folding in the ER, causing proinsulin misfolding, and decreasing insulin production (21–24). However, no *INS* mutation located in the proinsulin domain has been reported to affect translocation of PPI. Herein, we identified a novel nonsense *INS* mutation causing an early termination at the 46th residue of PPI (PPI-R46X) in two unrelated patients with early-onset diabetes. We found that, unlike other proinsulin domain mutations, R46X did not appear to induce strong ER stress or form abnormal disulfide-linked proinsulin complexes (DLPC) with co-expressed wild-type (WT) proinsulin in the ER. Metabolic labeling experiments established that, despite with an intact SP, R46X failed to be efficiently translocated into the ER, suggesting an important unrecognized role of proinsulin domain in determining the efficiency of PPI translocation. Genetic testing, pedigree analysis, and clinical presentations revealed a broad spectrum of diabetes phenotypes among the members carrying R46X in the two families, suggesting that other genetic and environmental factors may contribute to actual clinical presentations associated with R46X. This study not only expends the list of *INS* mutations associated with diabetes, but also provides genetic and biological evidence underlying the regulation mechanism of PPI translocation.

MATERIALS AND METHODS

Patients

Two unrelated patients with early-onset diabetes were referred for genetic testing of the monogenic diabetes. The clinical information was collected and recorded by the Tianjin Medical University General Hospital and the second Part of Jilin University First Hospital. The clinical information of these two probands and their family members is described in **Tables 1**–**3**.

TABLE 1 | Clinical characterization of the patients with INS-R46X mutation.

		Proband1	Proband2
Gender		Female	Female
At diagnosis	Age (years)	17	8
	BMI (kg/m^2)	24.8	20.9
	FBG (mmol/L)	9.4	14
	C-Peptide (ng/ml)	3.3	2.06
	HbA1c (%, mmol/mol)	7.8, 62	13, 119
	Symptoms of diabetes	polydipsia, polyphagia, polyuria	No
	75g-OGTT		
	Glucose (mmol/L)	9.16 (0 h)–18.13 (1 h)–18.01 (2 h)	6.1 (0 h)–15.7 (1 h)–15.4 (2 h)
	C-peptide (ng/ml)	3.3 (0 h)–5.02 (1 h)–5.8 (2 h)	1.1 (0 h)–4.45 (1 h)–4.18 (2 h)
	GADA	(-)	(-)
	ICA	(-)	(-)
	IA-2A	(-)	(-)
	ZnT8A	(-)	(-)
	Treatment	Insulin 0.71 (U/kg/day)	Insulin 0.73 (U/kg/day)
At present	Age (years)	20	11
	FBG (mmol/L)	7.76	16.7
	Insulin (mU/L)	28.26	26.88
	C-Peptide (ng/ml)	-	0.94
	HbA1c (%, mmol/mol)	7.1, 54.1	14.3, 133
	Treatment	Metformin	Insulin 1.87 (U/kg/day)
Family history		Maternal uncle had diabetes	Maternal grandmother, maternal uncle, mother, and older sister had diabetes

BMI, body mass index; FBG, fasting blood glucose; GADA, glutamate decarboxylase antibody; ICA, islet cell antibody; IA-2A, protein tyrosine phosphatase-like protein antigen; ZnT8A, Zinc transporter 8 antibody.

TABLE 2 | Clinical characterization of the subjects with INS-R46X mutation from family 1.

	Mother	Brother
Age (years)	53	28
BMI (kg/m^2)	24.2	33.6
FBG (mmol/L)	5.4	5.7
C-Peptide (ng/ml)	2.26	4.85
HbA1c (%, mmol/mol)	5.9, 41	5.7, 38.8
75g-OGTT		
Glucose (mmol/L)	5.36 (0 h)–8.40 (1 h)–7.88 (2 h)	5.73 (0 h)–10.5 (1 h)–8.03 (2 h)
Insulin (mU/L)	7.4 (0 h)–28.7 (1 h)–31.0 (2 h)	23.4 (0 h)–108.9 (1 h)–135.4 (2 h)
C-peptide(ng/ml)	2.26 (0 h)–6.17 (1 h)–7.9 (2 h)	4.85 (0 h)–11.65 (1 h)–13.79 (2 h)

BMI, body mass index; FBG, fasting blood glucose.

TABLE 3 | Clinical information of patients with diabetes from family 2.

		Elder sister	Mother	Maternal uncle
At diagnosis	Age (years)	20	40	40
	BMI (kg/m^2)	29.4	25.3	21.3
	FBG (mmol/L)	17	17	10
	C-peptide (ng/ml)	1.17	1.77	NA
	HbA1c (%, mmol/mol)	15.1, 142	12.9, 117	NA
	Symptoms of diabetes	Polydipsia, polyuria	Polydipsia, polyuria	Polydipsia, polyphagia, polyuria, loss of weight
	Treatment	Insulin 0.61 (U/kg/day)	Metformin	Metformin
At present	Age (years)	24	44	46
	FBG (mmol/L)	18.5	17	11
	Treatment	Insulin 0.61 (U/kg/day)	Metformin	Metformin

BMI, body mass index; FBG, fasting blood glucose; NA, not available.

An informed consent has been signed by patients and their families. The study was approved by Tianjin Medical University General Hospital Ethics Committee (No. IRB2017-047-01).

Genetic Testing and Analyses

Targeted gene capture followed by whole exome sequencing with massively parallel next-generation sequencing (NGS) was performed with the genomic DNA extracted from white blood cells. The identified *INS* gene mutation was confirmed by Sanger sequencing with the primer: Forward 5'-TCAGCCCTG CCTGTCTCC-3', Reverse 5'-AAAAGTGCACCTGAC CCCCTG-3'. The members of the two families of two probands were recruited and tested for the mutation by Sanger sequencing.

Reagents and Antibodies

Lipofectamine 2000, Lipofectamine 3000, and 4–12% NuPage gel were purchased from Invitrogen (Carlsbad, CA, USA). Protein A-Agarose was from Santa Cruz Biotechnology (Dallas, TX, USA). Guinea pig anti-insulin was from Merck Millipore (Billerica, MA, USA). Rabbit anti-Human proinsulin was from Biogot (Nanjing, China). Rabbit anti-Myc antibody was from Immunology Consultants Laboratories (Portland, OR, USA). Mouse anti-Hsp90 and anti-GFP antibody were from Sungene Biotech (Tianjin, China). Goat anti-guinea pig IgG Alexa Fluor 488 and goat anti-rabbit IgG Alexa Fluor 555 was bought from Invitrogen (Carlsbad, CA, USA). Enhanced chemiluminescence Western blotting substrate was from Millipore (Billerica, MA, USA). Trans^{35}S label and pure ^{35}S-methionine were from PerkinElmer (Waltham, MA, USA). Met/Cys-deficient Dulbecco's modified Eagle's medium (DMEM) was from Invitrogen (Thermo Fisher, Waltham, MA, USA).

Construction of Plasmids Encoding Preproinsulin Wild-Type and Mutants

The plasmids encoding human PPI WT with GFP-tag in the C-peptide were described previously (6). The DNA sequences of human PPI WT with or without Myc-tag in C-peptide and mutants (C96Y, R46X, G44R, P52L, H29T, and H29T/R46X) with Myc-tag were synthesized and introduced into the vector pcDNA3.1 (Tsingke Biological Technology, Beijing, China). All mutations were confirmed by DNA sequencing with primers: CMV-F 5'-CGCAAATGGGCGGTAGGCGTG-3', BGH-R 5'-TAGAAGGCACAGTCGAGG-3'.

Cell Culture and Transfection, ^{35}S-Met/Cys Metabolic Labeling, and Immunoprecipitation/Co-Immunoprecipitation

Human embryonic kidney 293T (HEK293T) cells and INS1 rat insulinoma cells were purchased from ATCC (Manassas, VA, USA). 293T cells were cultured in Dulbecco's Modified Eagle Medium (DMEM) with 10% fetal bovine serum (FBS), penicillin (100 units/ml), and streptomycin (100 μg/ml). The INS1 cells were cultured in RPMI 1640 (containing D-Glucose 2000 mg/L) supplemented with 10% FBS and 0.05 mM 2-mercaptoethanol (Sigma, St Louis, MO, USA). For the transfection, 293T cells were seeded into 12-well plates 1 day before the transfection. For each well, a total of 1 μg of plasmid DNA was transfected using

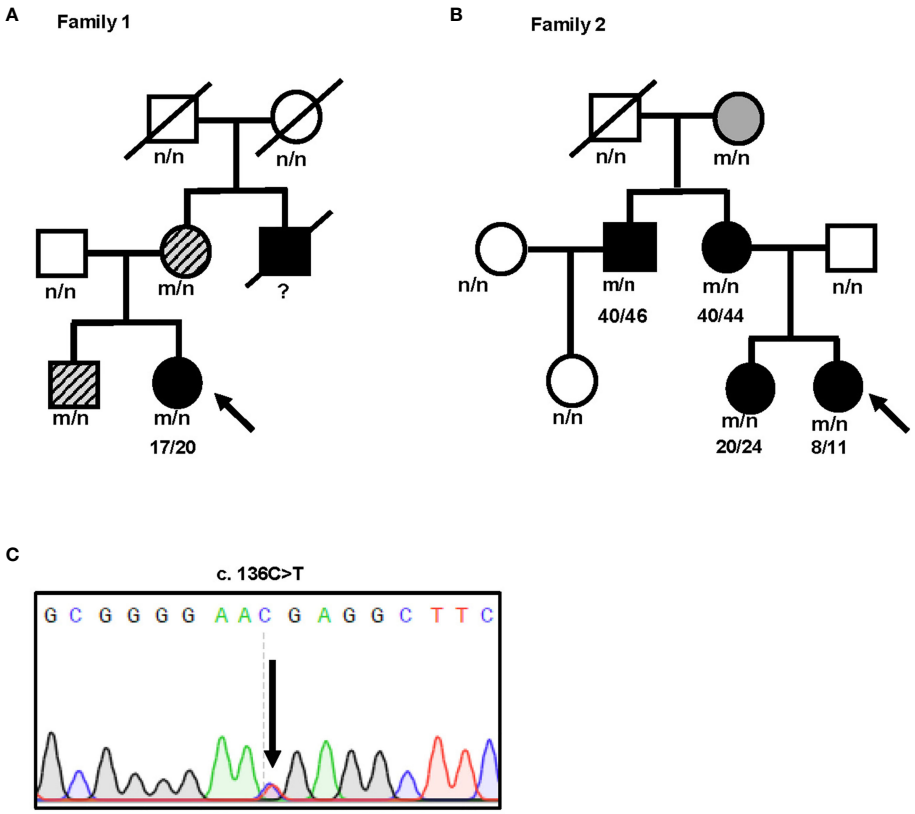

FIGURE 1 | Identification of a novel nonsense *INS* mutation R46X associated with diabetes in two unrelated patients. **(A, B)** Pedigree and genotypes of two families with early-onset diabetes. Subjects carrying R46X mutation without diabetes are shown in gray. Subjects carrying R46X mutation but just diagnosed as impaired glucose regulation are shown in gray with slash. Subjects with diabetes are shown in black. Black arrow indicates the probands. n, normal allele; m, mutant allele. **(C)** DNA sequences of the *INS* mutation c.136 C>T found in both probands.

Lipofectamine 2000. For metabolic labeling experiments, at 48 h post-transfection, the cells were pulse labeled with ^{35}S-Met or ^{35}S-(Met+Cys) and chased for the times indicated. The cells were harvested and lysed. Trichloroacetic acid (TCA)-precipitable counts were performed to normalize the amount of the total proteins among samples. The cell lysates were immunoprecipitated with anti-insulin antibody overnight at 4°C, and analyzed using 4%–12% NuPage gel under reducing condition as previously described (25). For co-immunoprecipitation (Co-IP), the cells were lysed with co-IP buffer (100 mM NaCl, 25 mM Tris, pH 7.0, 0.1% Triton X-100, 5 mM EDTA, and protease inhibitors mixture). Ninety percent of the total lysates were immunoprecipitated with anti-GFP at 4°C for 3 h. The remaining 10% of the total lysates were used to determine the expression levels of Myc-tagged and GFP-tagged PPI WT and Myc-tagged mutants. The immunoprecipitates and the total lysates were resolved using 4%–12% NuPage gel under reducing conditions followed by immunoblotted with anti-Myc and anti-proinsulin antibodies as indicated.

Immunofluorescence Assay

An immunofluorescence assay was employed in INS832/13 cells transfected with plasmids encoding Myc-tagged PPI WT or mutants (C96Y and R46X). Briefly, transfected INS832/13 cells grown on coverslips were fixed with 4% paraformaldehyde for 30 min at room temperature, followed by permeabilization with 0.2% Triton for an additional 15 min and then blocking with 5% BSA. The cell samples were incubated with primary antibodies (Anti-Myc 1:3000 dilution, anti-insulin 1:5,000 dilution) followed by appropriate secondary antibodies conjugated with different fluor as indicated. Immunofluorescence images were acquired by using Axio Imager M2 (ZEISS, Baden-Württemberg, Germany).

Statistical Analysis

All data were processed with GraphPad Prism 8 and presented as means ± SEM. One-way ANOVA test was used to determine significance between the groups. A p-value < 0.05 was considered as statistically significant.

RESULTS

Identification of a Novel Nonsense *INS* Mutation R46X Associated With Diabetes in Two Unrelated Patients

We identified an *INS* gene mutation (NM_001042376.2: p. Arg46*/c.136C>T) in two unrelated patients with early-onset

diabetes (**Figure 1**). Whole genome sequencing indicated that no additional known gene mutations associated with monogenic diabetes was found. Their clinical features at diagnosis of diabetes are shown in **Table 1**. The proband 1 was diagnosed with diabetes at the age of 17 due to the symptoms of polyuria, polydipsia, polyphagia with elevated fasting blood glucose (9.4 mmol/L), and diabetic ketosis. Her BMI was 24.8 kg/m^2 and the common T1DM autoantibodies (glutamate decarboxylase antibody [GADA], islet cell antibody [ICA], protein tyrosine phosphatase-like protein antigen [IA-2A], and Zinc transporter 8 antibody [ZnT8A]) were all negative. She was treated with insulin (0.71 U/kg/day) at the time of diagnosis. Self-monitoring of blood glucose (SMBG) showed that her fasting blood glucose (FBG) was 4–5 mmol/L and 2 h postprandial blood glucose (2hPBG) was 6–9 mmol/L, suggesting that her diabetes was well controlled. Subsequently 1 year later, she withdrew insulin without doctor's advice and only took metformin 1.5 g/day. Her HbA1c was 7.1% at the last visit. Notably, the proband's mother and older brother were found to carry the same mutation but only had impaired glucose regulation (**Figure 1A** and **Table 2**). Her maternal uncle was diagnosed with diabetes at the age of 40. Unfortunately, his blood sample was unavailable for genetic testing because he has passed away. The second proband was diagnosed with diabetes when she was 8 years old. She was accidentally found to have hyperglycemia when she had an upper respiratory tract infection. At the time of diabetes diagnosis, her BMI was 20.9 kg/m^2 and HbA1c was 13% without typical symptoms of diabetes. She was initiated insulin therapy (0.73 U/kg/day). However, the patient adherence was low and her blood glucose was poorly controlled even with a high dose of insulin therapy (1.87 U/kg/day). Except for her maternal grandmother whose fasting blood glucose were 6–7 mmol/L, her family members carrying this mutation were all diagnosed with diabetes at various onset ages (**Figure 1B** and **Table 3**).

R46X Mutant Impaired Secretion of the Mutant but Did Not Affect Secretion or Production of Bystander Proinsulin-WT, nor Did It Impair Production of Endogenous Insulin

At least 70 *INS* mutations in the coding region of the proinsulin domain have been reported to cause mutant *INS* gene induced diabetes of youth (MIDY). Most of them impair proinsulin folding and intracellular trafficking (2). We therefore firstly examined the secretion of R46X in transfected 293T cells and INS1 cells. An established proinsulin mutant PPI-C96Y (also called *Akita* proinsulin), which causes proinsulin misfolding and neonatal diabetes (19, 23), was used as a positive control. Although the total amount of proinsulin was comparable (**Figure 2A**, left panel), both R46X and C96Y failed to be secreted from the cells to the media in transfected cells (**Figures 2A, B**). This secretion defect was further confirmed in INS1 cells transfected with PPI-WT and mutants (**Figures 2C, D**). Theoretically, the amount of insulin expressed by a single allele is enough for control blood glucose *in vivo* (2). However, most diabetes causing *INS* mutants are heterozygous and present as autosomal dominant fashion, indicating trans-dominant negative effect of proinsulin mutants on bystander proinsulin-WT. We have previously reported that C96Y could interact with co-expressed WT proinsulin and prevent its ER export (26). We therefore asked whether this mechanism also applies for R46X mutant. We co-expressed WT-untagged with WT-Myc or mutants (C96Y-Myc and R46X-Myc) in 293T cells. Consistent with our previous observation, C96Y blocked secretion of co-expressed proinsulin-WT. In contrast, although R46X could not be secreted from the cells, it did not impair the secretion of bystander proinsulin-WT (**Figures 2E, F**). Next, we asked whether R46X could generate a dominant negative effect on insulin production from endogenous proinsulin in β cells. We transfected WT-Myc or mutants (C96Y-Myc and R46X-Myc) into INS832/13 cells. In the cells expressing C96Y-Myc (red), endogenous insulin (green) was significantly decreased compared with the neighboring control cells. However, although R46X itself displayed a diffused pattern within the cells, it did not appear to affect the insulin content of β cells (**Figure 2G**). Together, these results indicated that although the secretion efficiency of R46X was reduced, R46X did not affect secretion or production of bystander proinsulin-WT, nor did it impair insulin production from endogenous proinsulin.

R46X Did Not Form Disulfide-Linked Proinsulin Complexes, nor Did It Interact With Proinsulin-WT

In order to examine the effect of R46X on the folding of the mutant, we expressed Myc-tagged PPI-WT mutants in 293T cells and INS1 cells, and analyzed their oxidative folding under non-reducing conditions. Consistent with our previous reports (21, 27), we found that C96Y formed more misfolded disulfide-linked proinsulin complexes (DLPC, including dimer, trimer, tetramer, and high-molecular-weight proinsulin complexes) than that of WT. Surprisingly, however, unlike C96Y, R46X did not form DLPC itself in 293T cells (**Figures 3A, B**). Similar results were confirmed in INS1 cells transfected with Myc-tagged PPI-WT, C96Y, or R46X (**Figures 3C, D**). To examine whether R46X interacts with co-expressed PPI-WT, we co-expressed untagged PPI-WT with empty vector or Myc-tagged PPI-WT, or mutants (C96Y-MYC and R46X-Myc) in 293T cells. We found that, under non-reducing conditions, untagged PPI-WT and Myc-tagged PPI-WT could form disulfide-linked homodimers (marked as D and D', respectively) as well as heterodimers (arrow, and also marked as "H"). Importantly, C96Y-Myc not only formed more disulfide-linked homodimers, but also formed heterodimers with co-expressed untagged PPI-WT (**Figure 3E**). On the contrary, R46X-Myc did not form homodimers by itself or form heterodimers with untagged PPI-WT (**Figure 3E**). To further confirm whether R46X interacted with proinsulin-WT in the ER, we performed co-immunoprecipitation experiments, in which GFP-tagged PPI-WT with Myc-tagged PPI-WT or mutants (C96Y-MYC and R46X-Myc) were expressed in 293T cells. We found that C96Y-Myc and WT-Myc could be co-immunoprecipitated by GFP-tagged PI-WT (WT-GFP). However, R46X could not be pulled down by PI-WT-GFP

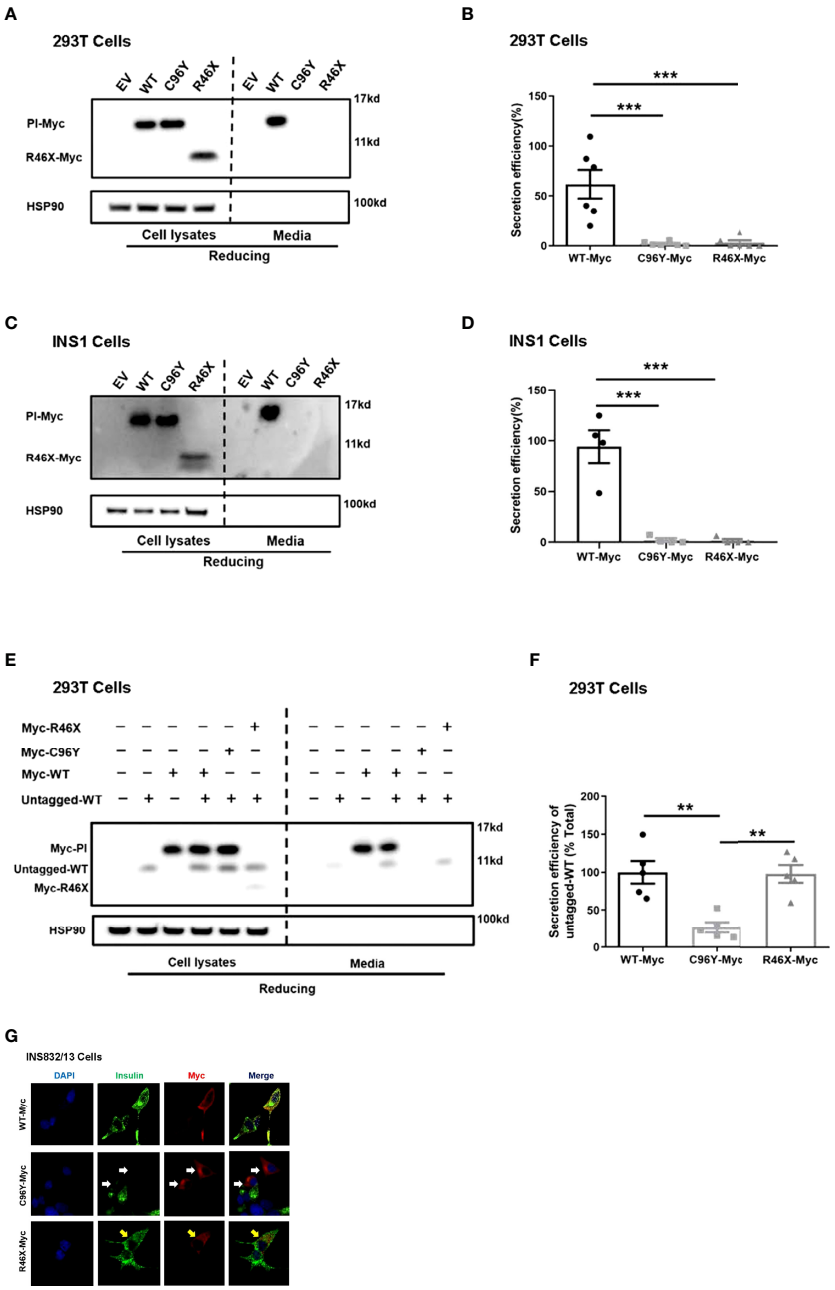

FIGURE 2 | R46X impaired secretion efficiency of the mutant but did not affect secretion or production of bystander proinsulin-WT or production of endogenous insulin. **(A)** 293T cells were transiently transfected with empty vector (EV) or Myc-tagged plasmids encoding PPI-WT or mutants (C96Y-Myc, R46X-Myc). The culture media were changed at 24 h post-transfection. After an additional 24 h of incubation, both cell lysates (left panel) and media (right panel) were subjected to Western blotting under reducing conditions with anti-Myc antibody. **(B)** The secretion efficiency of proinsulin-WT and mutants (media/cells) in panel A was quantified and calculated. The results were shown as mean ± SEM from 6 independent experiments. *** indicates $p < 0.001$ compared to WT-Myc. **(C)** Similar experiments of panel A were performed in INS1 cells. **(D)** The secretion efficiency of PI-WT and mutants (media/cells) in panel C was quantified and calculated. The results were shown as mean ± SEM from 4 independent experiments. *** indicates $p < 0.001$ comparing to WT-Myc. **(E)** 293T cells were transiently co-transfected with untagged PPI-WT (WT-untagged) and Myc tagged PPI-WT or mutants (WT-Myc, C96Y-Myc and R46X-Myc). The culture media were changed at 24 h post-transfection. After an additional 24 h of incubation, both cell lysates (left panel) and media (right panel) were subjected to Western blotting under reducing conditions. **(F)** The co-expressed WT-untagged in cell lysates and media were quantified using ImageJ. The secretion efficiency of WT-untagged in panel E (media/cells) was calculated. The results were shown as mean ± SEM from 5 independent experiments. ** indicates $p < 0.01$. **(G)** INS832/13 cells were transfected with plasmids encoding Myc-tagged PPI-WT and mutants as indicated. At 48 h post-transfection, the cells were fixed and permeabilized. Confocal immunofluorescence microscopy was performed after double-stained with anti-Myc (red) and anti-insulin (green). White and yellow arrows indicated that β cells were successfully transfected to express C96Y and R46X, respectively.

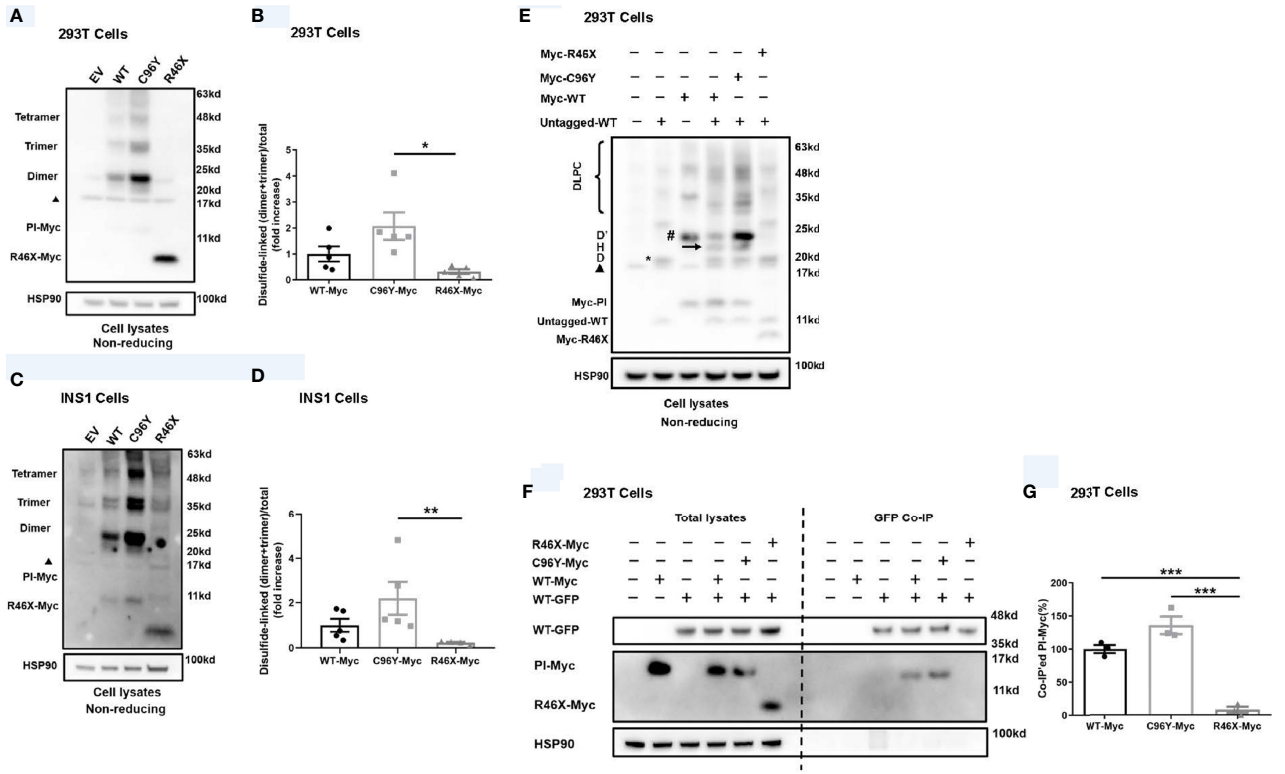

FIGURE 3 | R46X did not form disulfide-linked proinsulin complexes itself, nor did it interact with co-expressed proinsulin-WT. **(A)** 293T cells were transiently transfected with empty vector (EV) or Myc-tagged plasmids encoding PPI-WT (WT-Myc) or mutants (C96Y-Myc, R46X-Myc). Cell lysates were subjected to Western blotting with anti-Myc antibody under non-reducing conditions. The non-specific bands at ~17 Kd were marked with a black triangle. **(B)** The disulfide-linked dimer and trimer under non-reducing conditions in panel A and total proinsulin under reducing condition in were quantified. The ratios (dimer + trimer/total proinsulin) were calculated and that of PI-WT was set to "1". The results were shown as mean ± SEM from 4 independent experiments. * indicates $p < 0.05$. **(C)** Similar experiments to panel A were performed in INS1 cells. **(D)** The disulfide-linked dimer and trimer under non-reducing conditions in panel C and total proinsulin under reducing condition in were quantified. The ratios (dimer + trimer/total proinsulin) were calculated and that of proinsulin-WT was set to "1". The results were shown as mean ± SEM from 4 independent experiments. ** indicates $p < 0.01$. **(E)** 293T cells were co-transfected with plasmids encoding untagged PPI-WT (WT-untagged) and Myc-tagged PPI-WT or mutants (WT-Myc, C96Y-Myc, and R46X-Myc). The monomer, disulfide-linked proinsulin dimers (D refers to homodimers formed by WT-Untagged, D' refers to homodimers formed by Myc-tagged proinsulin, and H refers to heterodimers formed by Myc-tagged and untagged PI), and high-molecular-weight disulfide-linked proinsulin complexes (DLPC) were analyzed under non-reducing conditions. The non-specific bands at ~17 Kd were marked with a black triangle. **(F)** 293T cells were co-transfected with plasmids encoding GFP-tagged PPI-WT (WT-GFP) and Myc-tagged PPI-WT or mutants (WT-Myc, C96Y-Myc, and R46X-Myc) as indicated. At 48 h post-transfection, the cells were lysed and immunoprecipitated (IP) with anti-GFP antibody in co-IP buffer. The immunoprecipitants were resolved in 4%–12% NuPage gel and immuno-blotted with anti-proinsulin or anti-Myc antibodies under reducing conditions. **(G)** Myc-tagged PI in the total lysates and co-precipitated Myc-tagged PI (PI-Myc) were quantified using ImageJ. The percentages of co-precipitated Myc-tagged PI were calculated. The results were shown as mean ± SEM from 3 independent experiments. *** indicates $p < 0.001$.

(**Figures 3F, G**), indicating that R46X did not interact with PI-WT in the ER. Furthermore, we explored the effect of R46X mutation on ER stress and β-cell survival. We used an established ER stress reporter (21, 25, 28, 29) Bip-promoter driven luciferase assay to evaluate ER stress response in both INS1 and Min6 cells expressing Myc-tagged PPI-WT or mutants. We found that unlike other *INS* mutations, R46X mutation did not induce significant increases in ER stress response (**Supplemental Figures 1A, B**). In order to examine whether R46X could affect β-cell survival, we have examined cleaved caspase 3 in Min6 cells expressing PPI-WT and mutants. Min6 cells treated with ER stress inducer thapsigargin was used as a positive control. We found that R46X did not increase cleaved caspase 3, a critical executioner of apoptosis, suggesting that it did not cause β-cell apoptosis (**Supplemental Figures 1C, D**). Together, those data indicate that R46X does not interact and affect co-expressed PI-WT and does not induce strong enough ER stress as other tested mutations do, which does not appear to lead to apoptosis at least based on the short-term *in vitro* assays in cell lines. The future *in vivo* experiments using transgenic/knock-in mice expressing R46X may bring more certainty regarding the effect of the mutant on β-cell stress responses and survival.

R46X Causes an Inefficient Translocation Into the ER and Is Less Stable in the Cells

To further investigate biological behavior of R46X, we performed metabolic labeling experiments. Since the two methionine

residues present only in the signal peptide of PPI and six cysteine residues locate in the proinsulin domain (**Figure 4A**, upper panel), ^{35}S-methionine (^{35}S-Met only) can only label signal peptide attached PPI, but not proinsulin, whereas ^{35}S-methionine/cysteine (^{35}S-Met/Cys) mixture can label both PPI and proinsulin. As shown in **Figure 4A**, the newly synthesized PPI-WT and R46X were successfully detected in the cells labeled with ^{35}S-Met/Cys. However, only R46X was detected in the cells

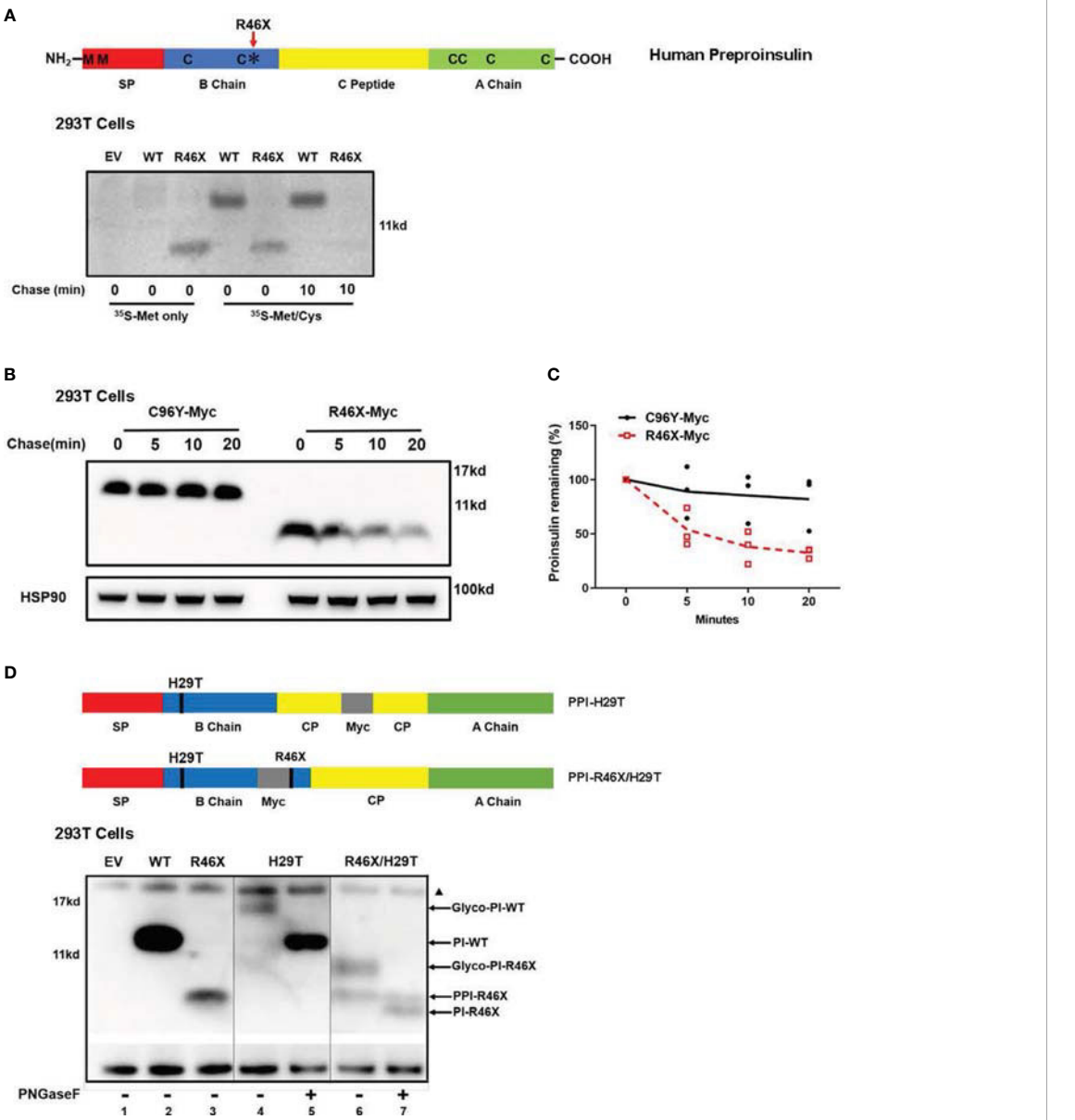

FIGURE 4 | R46X causes an inefficient translocation into the ER and is less stable in the cells. **(A)** A sketch of PPI (upper panel): The signal peptide (SP, red), insulin B chain (blue), C peptide (yellow), and insulin A chain (green). Two methionines (M) locate only in the SP of human PPI. Six cysteines **(C)** present in both human PPI and PI. Bottom panel: 293T cells were transfected with plasmids encoding empty vector (EV), Myc-tagged PPI-WT, or R46X. At 48 h post-transfection, the cells were pulse-labeled with either pure ^{35}S-Met or ^{35}S-Cys/Met as indicated for 10 min followed by 0 or 10 min chase. The newly synthesized PPI and PI were immunoprecipitated with anti-Myc and analyzed by 4%–12% NuPage under reducing conditions. **(B)** 293T cells were transfected with plasmids encoding Myc-tagged PPI-C96Y or R46X. After 48 h transfection, cells were treated with 20 μg/ml cycloheximide (CHX) for the indicated times, and the cell lysates were collected and analyzed by Western blotting with anti-Myc. **(C)** The expression levels of C96Y and R46X in panel B were quantified with ImageJ. The results were presented as mean ± SEM from 4 independent experiments. **(D)** PPI mutants with N-linked glycosylation sites were shown in the upper panel. 293T cells were transfected with empty vector (lane 1) or plasmids encoding PPI-WT (lane 2), R46X (lane 3), H29T (lanes 4 and 5) or R46X/H29T (lanes 6 and 7). Forty-eight hours post-transfection, the cell lysates were treated with or without PNGaseF before analyzing using Western blotting under reducing conditions. The non-specific bands at ~17 Kd were marked with a black triangle.

labeled with ^{35}S-Met only, suggesting that the signal peptide was still attached to the proinsulin domain of the R46X mutant (**Figure 4A**, the first five lanes of the bottom panel). Upon 10 min chase, a majority of the newly synthesized R46X was degraded (**Figure 4A**, the last two lanes of the bottom panel), suggesting that R46X was not stable in transfected 293T cells. Indeed, when we compared the stability of C96Y and R46X by Western blotting, we found that up to 60% of R46X was degraded in 20 min (**Figures 4B, C**).

At least two possible reasons can cause failure of signal peptide removal of PPI-R46X (**Figure 4A**). First, R46X caused inefficient translocation; therefore, the signal peptide cleavage site was not exposed to signal peptidase at the luminal side of the ER membrane. Second, R46X is successfully translocated into the ER; however, it cannot be efficiently cleaved by signal peptidase. To distinguish these possible causes, we mutated histidine to threonine at the 5th residue of proinsulin domain, generating an "N-X-T" *N-linked* glycosylation site (named as H29T). Consistent with our previous report (28), proinsulin WT was glycosylated as demonstrated by glycosylated proinsulin-WT that was deglycosylated upon the digestion with PNGase F (**Figure 4D**, lanes 4 vs. 5). However, R46X/H29T generated two bands (**Figure 4D**, lane 6). The upper band shifted down upon digestion of PNGase F, establishing that it entered the ER and acquired an *N-linked* glycan (**Figure 4D**, lane 7), whereas the lower band in the lane 6 did not shift upon treatment of PNGaseF, suggesting that it did not enter the ER lumen and was not glycosylated (**Figure 4D**. lanes 6 vs. 7). It is worth noting that, compared with R46X, more than 50% of the double mutant R46X/H29T did translocate into the ER and acquire an N-linked glycan (**Figure 4D**, lanes 3 vs. 6), suggesting that mutating histidine to threonine appeared to improve translocation efficiency of R46X. We have previously shown that increased PPI N-terminal charge gradient was favorable for translocation of PPI (6, 11). Therefore, the improvement of translocation efficiency of R46X/H29T was likely caused by mutation of histidine that increased charge gradient of PPI N-terminus. Altogether, these results established that R46X caused inefficient translocation and revealed an important role of proinsulin domain in determining translocation efficiency of PPI.

DISCUSSION

To date, at least 70 *INS* mutations have been reported to cause autosomal dominant diabetes in humans (2, 20, 30). Some additional mutations that disrupt transcription and translation of insulin gene due to *INS* deletion, promoter inactivation, and loss of translation initiation cause neonatal diabetes only when both *INS* alleles were affected (31), suggesting that one insulin gene allele may be sufficient to maintain normoglycemia under normal physiological conditions, although these recessive *INS* mutations are linked to an increased risk of diabetes (32, 33). Most dominant *INS* mutations are located in the proinsulin domain, impairing proinsulin oxidative folding and causing proinsulin misfolding in the ER (2, 16, 24, 34). Two main mechanisms underlie β-cell failure and diabetes caused by misfolded proinsulin mutants. First, misfolded proinsulin may accumulate in the ER, disturbing ER protein homeostasis, inducing chronic ER stress that may activate apoptotic pathway, leading to a decrease of β-cell mass (24, 35–37). Second, misfolded proinsulin can abnormally interact with co-expressed proinsulin-WT *via* proinsulin dimerization interface, impairing folding and the ER export of proinsulin-WT, decreasing insulin production, and leading to insulin-deficient diabetes (16, 21, 23, 28). More recently, a study shows that misfolded proinsulin may impair intracellular trafficking and processing of the precursor of insulin receptor, causing an impairment of insulin signaling in β cells, which may also contribute to β-cell failure caused by *INS* mutations (38). Interestingly, the clinical phenotypes associated with different *INS* mutations or even with same mutations range from severe neonatal diabetes to mild adult-onset diabetes, or some even without overt diabetes as the time of studies (2, 13, 16, 22, 39–42). In this report, we identified a novel nonsense *INS* mutation PPI-R46X associated with early-onset diabetes in two unrelated patients. Pedigree analysis showed a broad spectrum of clinical presentations among the members carrying R46X in the two families (**Figure 1** and **Tables 1**, **3**), suggesting that other factors that need to be further determined may contribute to actual clinical presentations associated with R46X. Functional studies showed that, although R46X failed to be secreted from the cells, unlike the mutations causing neonatal diabetes, R46X did not form DLPC, did not affect PPI-WT secretion and insulin production, and did not appear to induce strong ER stress or cause β-cell apoptosis (**Figures 2**, **3** and **Supplemental Figure 1**). In addition, R46X is less stable in the cells compared with C96Y (**Figures 4B, C**). All these data suggest that R46X may not be exposed to the oxidative ER environment. Indeed, two independent approaches demonstrated that, despite with an intact SP, R46X failed to be efficiently translocated into the ER (**Figures 4A, D**), highlighting a critically unrecognized role of proinsulin domain in efficient PPI translocation. Together, pedigree and functional analyses suggest that additional contributors may be required for developing diabetes in the patients carrying R46X. Further whole exome sequencing with linkage analysis among family members with or without R46X mutation, combined with functional studies, may shed light on better understanding what and how multiple genetic and/or environmental risk factors in concert with R46X lead to the development and progression of diabetes.

Preproinsulin is a small secretory protein with a suboptimal signal sequence that may not be efficiently recognized by the SRP and undergo SRP-dependent co-translational translocation across the ER membrane (7, 11). SRP-independent post-translational translocation is an important backup for efficient PPI translocation. However, the factors that determine the route and efficiency of PPI translocation remain to be further elucidated. PPI signal peptide mutations provide excellent molecular models and great opportunities to address these fundamental biological questions. To date, PPI signal peptide

mutations that have been experimentally established to affect PPI translocation are PPI-R6C/H. These two mutations locate in the n-region of the PPI signal peptide, resulting in a decrease of charge gradient from PPI N-terminus to proinsulin domain. This charge gradient has been shown to play an important role in orientating PPI signal peptide in the Sec61 translocon during translocation (11), and it is more important for small secretory proteins including PPI for the post-translational translocation, because of the large secretory proteins that do not depend on the N-terminal positive charge for their translocation (6, 43), suggesting that the length of secretory proteins may also play a role in selecting the translocation pathway and efficiency. Indeed, R46X results in translating a very small truncated PPI, causing inefficient translocation. However, increasing a charge gradient in the N-terminus of R46X by mutating histidine to threonine at the 5th residue of proinsulin domain improves efficiency of R46X translocation by more than 50%, supporting the notion that both N-terminal positive charge and the length of PPI are important for efficient PPI translocation.

In summary, this study reveals that PPI translocation efficiency is affected not only by the natural property of its signal sequence, but also by its downstream of proinsulin domain. To the best of our knowledge, this is the first report to experimentally demonstrate that a mutation in the proinsulin domain causes PPI translocation inefficiency, which may underlie increased risk of diabetes-associated R46X. This study not only expends the list of *INS* mutations associated with diabetes, but also provides genetic and biological evidence underlying the regulation mechanism of PPI translocation.

DATA AVAILABILITY STATEMENT

The data sets generated during and analyzed during the current study are available from the corresponding author upon reasonable request. The data presented in this study are deposited in the GenBank repository, accession number PRJNA787369. The information will be accessible with the following link: https://www.ncbi.nlm.nih.gov/sra/PRJNA787369.

ETHICS STATEMENT

The studies involving human participants were reviewed and approved by Tianjin Medical University General Hospital Ethics Committee (IRB2017-047-01 of 4 April 2017). Written informed consent to participate in this study was provided by the participants' legal guardian/next of kin.

AUTHOR CONTRIBUTIONS

YY, HS, JH, LL, JW, TC, JZ, ZF, HG, KZ, and YX generated research data. JS, WF, YH, and XL contributed to discussion and reviewed/edited the manuscript. ML initiated and designed the research project, reviewed the data, and wrote the manuscript. ML is the guarantor of this work and, as such, had full access to all the data in the study and take responsibility for the integrity of the data and the accuracy of the data analysis. All authors contributed to the article and approved the submitted version.

FUNDING

This work was supported by the National Natural Science Foundation of China (81620108004, 81830025, 81700699, 81870533, and 81900720), the Ministry of Science and Technology of China (2019YFA0802502), the Tianjin Municipal Science and Technology Bureau (17ZXMFSY00150 and 18JCYBJC93900), the Second Hospital of Tianjin Medical University Youth Program (2017YDEY19), the Scientific Research Project of Tianjin Educational Committee (2020KJ47), and the Fundamental Research Funds for the Central Universities of Peking Union Medical College (3332021083). The funders were not involved in the study design, collection, analysis, interpretation of data, the writing of this article or the decision to submit it for publication.

ACKNOWLEDGMENTS

We thank all probands and their families for their participating actively that enabled this work. We thank the RSR Tianjin Biotech Company's technical support. We thank professor Zhuoxian Meng at Zhejiang University for providing Min6 cells to us.

SUPPLEMENTARY MATERIAL

The Supplementary Material for this article can be found online at: https://www.frontiersin.org/articles/10.3389/fendo.2021.774634/full#supplementary-material

REFERENCES

1. Liu M, Wright J, Guo H, Xiong Y, Arvan P. Proinsulin Entry and Transit Through the Endoplasmic Reticulum in Pancreatic Beta Cells. *Vitam Horm* (2014) 95:35–62. doi: 10.1016/B978-0-12-800174-5.00002-8
2. Liu M, Sun J, Cui J, Chen W, Guo H, Barbetti F, et al. INS-Gene Mutations: From Genetics and Beta Cell Biology to Clinical Disease. *Mol Aspects Med* (2015) 42:3–18. doi: 10.1016/j.mam.2014.12.001
3. Dodson G, Steiner DF. The Role of Assembly in Insulin's Biosynthesis. *Curr Opin Struct Biol* (1998) 8:189–94. doi: 10.1016/S0959-440X(98)80037-7
4. Liu M, Huang Y, Xu X, Li X, Alam M, Arunagiri A, et al. Normal and Defective Pathways in Biogenesis and Maintenance of the Insulin Storage Pool. *J Clin Invest* (2021) 131(2):e142240. doi: 10.1172/JCI142240
5. Okun M, Shields D. Translocation of Preproinsulin Across the Endoplasmic Reticulum Membrane. The Relationship Between Nascent Polypeptide Size and Extent of Signal Recognition Particle-Mediated Inhibition of Protein Synthesis. *J Biol Chem* (1992) 267:11476–82. doi: 10.1016/S0021-9258(19)49934-1
6. Guo H, Sun J, Li X, Xiong Y, Wang H, Shu H, et al. Positive Charge in the N-Region of the Signal Peptide Contributes to Efficient Post-Translational

Translocation of Small Secretory Preproteins. *J Biol Chem* (2018) 293:1899–907. doi: 10.1074/jbc.RA117.000922
7. Lakkaraju AKK, Thankappan R, Mary C, Garrison JL, Taunton J, Strub K. Efficient Secretion of Small Proteins in Mammalian Cells Relies on Sec62-Dependent Posttranslational Translocation. *Mol Biol Cell* (2012) 23:2712–22. doi: 10.1091/mbc.e12-03-0228
8. Replication DIG, Meta-analysis CC. Asian Genetic Epidemiology Network Type 2 Diabetes, C. South Asian Type 2 Diabetes, C. Mexican American Type 2 Diabetes and C. Type 2 Diabetes Genetic Exploration by Next-Generation Sequencing in Multi-Ethnic Samples, et al. Genome-Wide Trans-Ancestry Meta-Analysis Provides Insight Into the Genetic Architecture of Type 2 Diabetes Susceptibility. *Nat Genet* (2014) 46:234–44. doi: 10.1038/ng.2897
9. Huang Y, Xu X, Arvan P, Liu M. Deficient Endoplasmic Reticulum Translocon-Associated Protein Complex Limits the Biosynthesis of Proinsulin and Insulin. *FASEB J* (2021) 35:e21515. doi: 10.1096/fj.202002774R
10. Li X, Itani OA, Haataja L, Dumas KJ, Yang J, Cha J, et al. Requirement for Translocon-Associated Protein (TRAP) Alpha in Insulin Biogenesis. *Sci Adv* (2019) 5:eaax0292. doi: 10.1126/sciadv.aax0292
11. Guo H, Xiong Y, Witkowski P, Cui J, Wang LJ, Sun J, et al. Inefficient Translocation of Preproinsulin Contributes to Pancreatic Beta Cell Failure and Late-Onset Diabetes. *J Biol Chem* (2014) 289:16290–302. doi: 10.1074/jbc.M114.562355
12. Hussain S, Mohd Ali J, Jalaludin MY, Harun F. Permanent Neonatal Diabetes Due to a Novel Insulin Signal Peptide Mutation. *Pediatr Diabetes* (2013) 14:299–303. doi: 10.1111/pedi.12011
13. Meur G, Simon A, Harun N, Virally M, Dechaume A.L., Bonnefond AL, et al. Insulin Gene Mutations Resulting in Early-Onset Diabetes: Marked Differences in Clinical Presentation, Metabolic Status, and Pathogenic Effect Through Endoplasmic Reticulum Retention. *Diabetes* (2010) 59:653–61. doi: 10.2337/db09-1091
14. Boesgaard T, Pruhova S, Andersson E, Cinek O, Obermannova B, Lauenborg J, et al. Further Evidence That Mutations in INS Can Be a Rare Cause of Maturity-Onset Diabetes of the Young (MODY). *BMC Med Genet* (2010) 11:42. doi: 10.1186/1471-2350-11-42
15. Støy J, Steiner D, Park S-Y, Ye H, Philipson L, Bell G. Clinical and Molecular Genetics of Neonatal Diabetes Due to Mutations in the Insulin Gene. *Rev Endocr Metab Disord* (2010) 11:205–15. doi: 10.1007/s11154-010-9151-3
16. Liu M, Hodish I, Haataja L, Lara-Lemus R, Rajpal G, Wright J, et al. Proinsulin Misfolding and Diabetes: Mutant INS Gene-Induced Diabetes of Youth. *Trends Endocrinol Metab* (2010) 21:652–9. doi: 10.1016/j.tem.2010.07.001
17. Polak M, Dechaume A, Cavé H, Nimri R, Crosnier H, Sulmont V, et al. Heterozygous Missense Mutations in the Insulin Gene Are Linked to Permanent Diabetes Appearing in the Neonatal Period or in Early Infancy. *Diabetes* (2008) 57:1115–9. doi: 10.2337/db07-1358
18. Colombo C, Porzio O, Liu M, Massa O, Vasta M, Salardi S, et al. Seven Mutations in the Human Insulin Gene Linked to Permanent Neonatal/Infancy-Onset Diabetes Mellitus. *J Clin Invest* (2008) 118:2148–56. doi: 10.1172/JCI33777
19. Stoy J, Edghill EL, Flanagan SE, Ye H, Paz VP, Pluzhnikov A, et al. And Neonatal Diabetes International Collaborative Group, Insulin Gene Mutations as a Cause of Permanent Neonatal Diabetes. *Proc Natl Acad Sci* (2007) 104:15040–4. doi: 10.1073/pnas.0707291104
20. Støy J, De Franco E, Ye H, Park SY, Bell GI, Hattersley AT. In Celebration of a Century With Insulin - Update of Insulin Gene Mutations in Diabetes. *Mol Metab* (2021) 52:101280. doi: 10.1016/j.molmet.2021.101280
21. Sun J, Xiong Y, Li X, Haataja L, Chen W, Mir SA, et al. Role of Proinsulin Self-Association in Mutant INS Gene-Induced Diabetes of Youth. *Diabetes* (2020) 69:954–64. doi: 10.2337/db19-1106
22. Liu M, Haataja L, Wright J, Wickramasinghe NP, Hua QX, Phillips NF, et al. Mutant INS-Gene Induced Diabetes of Youth: Proinsulin Cysteine Residues Impose Dominant-Negative Inhibition on Wild-Type Proinsulin Transport. *PloS One* (2010) 5:e13333. doi: 10.1371/journal.pone.0013333
23. Liu M, Hodish I, Rhodes CJ, Arvan P. Proinsulin Maturation, Misfolding, and Proteotoxicity. *Proc Natl Acad Sci* (2007) 104:15841–6. doi: 10.1073/pnas.0702697104
24. Dhayalan B, Chatterjee D, Chen YS, Weiss MA. Structural Lessons From the Mutant Proinsulin Syndrome. *Front Endocrinol (Lausanne)* (2021) 12:754693. doi: 10.3389/fendo.2021.754693
25. Wang H, Saint-Martin C, Xu J, Ding L, Wang R, Feng W, et al. Biological Behaviors of Mutant Proinsulin Contribute to the Phenotypic Spectrum of Diabetes Associated With Insulin Gene Mutations. *Mol Cell Endocrinol* (2020) 518:111025. doi: 10.1016/j.mce.2020.111025
26. Liu M, Hodish I, Rhodes CJ, Arvan P. Proinsulin Maturation, Misfolding, and Proteotoxicity. *Proc Natl Acad Sci USA* (2007) 104:15841–46 doi: 10.1073/pnas.0702697104
27. Arunagiri A, Haataja L, Pottekat A, Pamenan F, Kim S, Zeltser LM, et al. Proinsulin Misfolding Is an Early Event in the Progression to Type 2 Diabetes. *Elife* (2019) 8:e44532. doi: 10.7554/eLife.44532
28. Liu M, Lara-Lemus R, Shan SO, Wright J, Haataja L, Barbetti F, et al. Impaired Cleavage of Preproinsulin Signal Peptide Linked to Autosomal-Dominant Diabetes. *Diabetes* (2012) 61:828–37. doi: 10.2337/db11-0878
29. Tirasophon W, Welihinda AA, Kaufman RJ. A Stress Response Pathway From the Endoplasmic Reticulum to the Nucleus Requires a Novel Bifunctional Protein Kinase/Endoribonuclease (Ire1p) in Mammalian Cells. *Genes Dev* (1998) 12:1812–24. doi: 10.1101/gad.12.12.1812
30. Liu M, Weiss MA, Arunagiri A, Yong J, Rege N, Sun JH, et al. Biosynthesis, Structure, and Folding of the Insulin Precursor Protein. *Diabetes Obes Metab* (2018) 20:28–50. doi: 10.1111/dom.13378
31. Garin I EE, Akerman I, Rubio-Cabezas O, Rica I, Locke JM, Maestro MA, et al. Recessive Mutations in the INS Gene Result in Neonatal Diabetes Through Reduced Insulin Biosynthesis. *Proc Natl Acad Sci USA* (2010) 107:3105–10. doi: 10.1073/pnas.0910533107
32. Raile K, O'Connell M, Galler A, Werther G, Kühnen P, Krude H, et al. Diabetes Caused by Insulin Gene (INS) Deletion: Clinical Characteristics of Homozygous and Heterozygous Individuals. *Eur J Endocrinol* (2011) 165:255–60. doi: 10.1530/EJE-11-0208
33. Demiral M, Demirbilek H, Çelik K, Okur N, Hussain K, Ozbek MN. Neonatal Diabetes Due to Homozygous INS Gene Promoter Mutations: Highly Variable Phenotype, Remission and Early Relapse During the First 3 Years of Life. *Pediatr Diabetes* (2020) 21:1169–75. doi: 10.1111/pedi.13079
34. Meng Y, Eirin A, Zhu X-Y, Tang H, Chanana P, Lerman A, et al. The Metabolic Syndrome Alters the miRNA Signature of Porcine Adipose Tissue-Derived Mesenchymal Stem Cells. *Cytometry A* (2018) 93:93–103. doi: 10.1002/cyto.a.23165
35. Oyadomari S, Koizumi A, Takeda K, Gotoh T, Akira S, Araki E, et al. Targeted Disruption of the Chop Gene Delays Endoplasmic Reticulum Stress-Mediated Diabetes. *J Clin Invest* (2002) 109:525–32. doi: 10.1172/JCI0214550
36. Park S-Y, Ye H, Steiner DF, Bell GI. Mutant Proinsulin Proteins Associated With Neonatal Diabetes Are Retained in the Endoplasmic Reticulum and Not Efficiently Secreted. *Biochem Biophys Res Commun* (2010) 391:1449–54. doi: 10.1016/j.bbrc.2009.12.090
37. Weiss MA. Diabetes Mellitus Due to the Toxic Misfolding of Proinsulin Variants. *FEBS Lett* (2013) 587:1942–50. doi: 10.1016/j.febslet.2013.04.044
38. Liu S, Li X, Yang J, Zhu R, Fan Z, Xu X, et al. Misfolded Proinsulin Impairs Processing of Precursor of Insulin Receptor and Insulin Signaling in β Cells. *FASEB J* (2019) 33:11338–48. doi: 10.1096/fj.201900442R
39. Støy J, Edghill EL, Flanagan SE, Ye H, Paz VP, Pluzhnikov A, et al. Insulin Gene Mutations as a Cause of Permanent Neonatal Diabetes *Proc Natl Acad Sci USA* (2007) 04:15040–44 doi: 10.1073/pnas.070729110
40. Polak M, Dechaume A, Cave H, Nimri R, Crosnier H, Sulmont V, et al. Heterozygous Missense Mutations in the Insulin Gene Are Linked to Permanent Diabetes Appearing in the Neonatal Period or in Early Infancy: A Report From the French ND (Neonatal Diabetes) Study Group. *Diabetes* (2008) 57:1115–9. doi: 10.2337/db07-1358
41. Edghill EL, Flanagan SE, Patch AM, Boustred C, Parrish A, Shields B, et al. Insulin Mutation Screening in 1,044 Patients With Diabetes: Mutations in the INS Gene Are a Common Cause of Neonatal Diabetes But a Rare Cause of Diabetes Diagnosed in Childhood or Adulthood. *Diabetes* (2008) 57:1034–42. doi: 10.2337/db07-1405
42. Molven A, Ringdal M, Nordbo AM, Raeder H, Stoy J, Lipkind GM, et al. Mutations in the Insulin Gene can Cause MODY and Autoantibody-Negative Type 1 Diabetes. *Diabetes* (2008) 57:1131–5. doi: 10.2337/db07-1467

43. Okamoto Y, Shikano S. Positive Zip Coding in Small Protein Translocation. *J Biol Chem* (2018) 293:1908–9. doi: 10.1074/jbc.H118.001415

Conflict of Interest: Author KZ is employed by RSR Tianjin Biotech Co., Ltd.

The remaining authors declare that the research was conducted in the absence of any commercial or financial relationships that could be construed as a potential conflict of interest.

Publisher's Note: All claims expressed in this article are solely those of the authors and do not necessarily represent those of their affiliated organizations, or those of the publisher, the editors and the reviewers. Any product that may be evaluated in this article, or claim that may be made by its manufacturer, is not guaranteed or endorsed by the publisher.

frontiers in Endocrinology

METHODS
published: 14 February 2022
doi: 10.3389/fendo.2022.812747

Scalable Dual-Fluorescence Assay for Functional Interpretation of HNF-4α Missense Variants

Yiming Guo[1], Jing Zhao[1], Rong Huang[2], Tao Xu[1,2,3,4], Kaixin Zhou[1,2]* and Li Zheng[3]**

[1] College of Life Sciences, the University of Chinese Academy of Sciences, Beijing, China, [2] Guangzhou Laboratory, Guangzhou, China, [3] Key Laboratory of RNA Biology, Center for Big Data Research in Health, Institute of Biophysics, Chinese Academy of Sciences, Beijing, China, [4] Shandong First Medical University & Shandong Academy of Medical Sciences, Jinan, China

Aim: The study aimed to develop a scalable dual-fluorescence assay in cells to enable the functional interpretation of HNF-4α missense variants identified in exome sequencing, which can be used to guide clinical diagnosis.

Methods: Using mOrange2 and GFP fluorescence proteins to track the expression of HNF-4α (HNF-4α-mOrange2) and reporter activity under the control of the HNF-1α promoter (pHNF1A-GFP), respectively, we designed a dual-fluorescence assay to evaluate the expression level, cellular localization, and transcriptional function of HNF-4α simultaneously in live cells. To assess the scalable characteristic of the assay, a small library containing five previously reported mutations and wild-type HNF-4α was constructed. Cells infected with this library were sorted into different populations through fluorescence-activated cell sorting (FACS) according to the transcription activity and expression abundance. Cloning and Sanger sequencing were used to detect the mutations of the different groups. High content screening (HCS) assay was used for the validation of individual mutants in the function and expression point of view.

Results: HNF-4α-mOrange2 exhibited nuclear localization and transactivation capability on the HNF-1α promoter as physical HNF-4α does. The expression of HNF-4α-mOrange2 shows a 6-fold induction of GFP expression compared to the control without HNF-4α-mOrange2, which was significantly abolished by the known loss-of-function mutant M373R. The different performances of wild-type and mutant M373R made them distinguishable in the FACS system, empowering the scalable capability of this assay for classifying large numbers of variants combining functional stratification and sequencing. Further application of the assay in the small library showed that three cell populations were seen grouped as Normal (same transactivation as wild type), Reduced^{exp_nor} (reduced transactivation with normal or higher expression), and Reduced^{exp_low} (reduced transactivation with lower expression). Subsequently, Sanger sequencing showed that wild-type HNF-4α was in the Normal group, two mutations (M373R and G79C) were enriched in the Reduced^{exp_nor} group, and three mutations (C115S, L272P, and F83C) belonged to the Reduced^{exp_low} group. These results were validated by further imaging data using HCS assay for individual mutation.

OPEN ACCESS

Edited by:
Fabrizio Barbetti, University of Rome Tor Vergata, Italy

Reviewed by:
Hongwen Zhou, Nanjing Medical University, China
Cheng Hu, Shanghai Jiao Tong University, China

***Correspondence:**
Li Zheng
zhengli@ibp.ac.cn
Kaixin Zhou
zhoukx@ucas.ac.cn
Tao Xu
xutao@ibp.ac.cn

Specialty section:
This article was submitted to Diabetes: Molecular Mechanisms, a section of the journal Frontiers in Endocrinology

Received: *10 November 2021*
Accepted: *17 January 2022*
Published: *14 February 2022*

Citation:
Guo Y, Zhao J, Huang R, Xu T, Zhou K and Zheng L (2022) Scalable Dual-Fluorescence Assay for Functional Interpretation of HNF-4α Missense Variants. Front. Endocrinol. 13:812747. doi: 10.3389/fendo.2022.812747

Conclusions: Our study proposes a scalable and informative approach for the characterization of the variants in HNF-4α genes in a quantitative and high-throughput manner.

Keywords: HNF-4α, scalable, dual-fluorescence assay, high-throughput, functional interpretation

INTRODUCTION

HNF-4α belongs to the nuclear receptor (NR) superfamily, which comprises the DNA-binding domain (DBD), ligand-binding domain (LBD), activation function domain (AF), and F domain (F) (1). As an important transcription factor, HNF-4α is potentially involved in the regulation of about 40% of transcripts in the liver and controls nearly 11% of genes in pancreatic islets (2–5). Various deleterious mutants in HNF-4α had been shown to cause autosomal dominantly inherited maturity-onset diabetes of the young (MODY1), diazoxide-responsive hyperinsulinemic hypoglycemia (HH), or the development of carcinomas (6–11). More importantly, MODY1 patients are sensitive to treatment with oral sulfonylureas and proper clinical actions could be taken upon the right diagnosis (12, 13). Genetic testing was also highly recommended for HH in the first week of life as HNF-4α mutations are often the underlining cause (10, 13). Therefore, genetic testing of HNF-4α would be valuable for molecular diagnosis, precision treatment, and family genetic counseling.

With the fast-falling of sequencing cost, the number of cataloged genetic variants in public databases such as the Genome Aggregation Database had increased dramatically. The vast majority of missense variants are rare with only 2% of them having a clinical interpretation in ClinVar (14, 15). Within the HNF-4α gene, more than 300 variants have been reported in ClinVar with over 40% of them considered as variants of uncertain clinical significance (VUS). Given that no mutation hotspots were revealed, more VUS are expected to be found and the functional characterization of these VUS would post a significant challenge to the HNF-4α genetic testing and molecular diagnosis.

Although various *in silico* scoring methods such as SIFT and LRT have been developed to assist the functional interpretation of VUS, consensus was hard to achieve between them and they were rarely in agreement with clinical observations (16, 17). Rigorous functional evaluations of VUS *in vitro* are therefore considered a strong line of evidence for molecular diagnosis according to the current ACMG guideline (18).

So far, the functional characterization of HNF-4α variants has mostly utilized mutant plasmid-based assays to evaluate four readouts including transcription activity, protein abundance, cellular localization, and DNA-binding affinity (19). Although such studies were informative to the molecular diagnosis, the assays required to derive them are time consuming and resource intensive, making it difficult to combine different assays or evaluate multiple mutants simultaneously. Given that more VUS of HNF-4α are expected with the easier access of HNF-4α genetic testing, there is an urgent need to develop a scalable assay that could be used to systematically screen all possible HNF-4α mutants in advance.

Here we set out to develop a high-throughput assay for the functional evaluations of HNF-4α variants. Bearing in mind that the transcriptional activity appears to be a superior readout which may be affected by an abnormal expression level, cellular localization, and DNA-binding affinity, we developed a dual-fluorescence reporter assay which could reliably monitor the transactivation activity of an HNF-4α variant together with its expression level and localization in live cells. To fulfill the requirement of scalability, this assay was designed to classify cells, each of which carries a single mutation according to transactivation activity and expression levels using FACS and subsequent sequence using Sanger or next-generation sequencing to distinguish variants with functional change.

MATERIALS AND EQUIPMENT

Materials

The following reagents were purchased from Gibco: Dulbecco's modified Eagle's medium (DMEM), fetal bovine serum (FBS), penicillin G sodium and streptomycin, and TrypLE Express. Lipofectamine 3000 Reagent and OMEM were from Life Technologies (Carlsbad, CA, USA). PLP1, PLP2, and PLP-VSVG were kindly gifted from Dr. Ruirui Kong. pcDNA3.1-Flag-HNF-4α (GenBank: NM_000457.6) was purchased from the Public Protein/Plasmid Library (PPL00188-2c), and pRRL.sin-18.ppt.STAT3-GFP.pre (Addgene, #110495) was from Addgene. PQCXIP, VSVG, and Phit were from our lab. Polybrene was from Sigma (St. Louis, MO, USA). The anti-mCherry antibody (26765-1-AP), anti-GFP antibody (50430-2-AP), and anti-GAPDH antibody (60004-1-Ig) were purchased from Proteintech (Wuhan, China). Anti-HNF4A (sc-374229) was from Santa Cruz (Dallas, TX, USA). The PVDF membrane was from Millipore (Bedford, MA, USA). Enhanced chemiluminescence (ECL) was from Promega (Madison, WI, USA).

Equipment

An influx cell sorter (BD, Biosciences, San Jose, CA, USA) equipped with solid-state lasers for 488- and 561-nm excitation was used. The Opera Phenix High Content Screening (HCS) System is from PerkinElmer, Waltham, MA. FV1200 is from OLYMPUS (Tokyo, Japan).

METHODS

Cloning and Construction of Plasmids

Wild-type human HNF-4α cDNA was PCR amplified from pcDNA3.1-Flag-HNF-4α, and the HNF-4α2 site mutation variants c.235G>T (p.Gly79Cys), c.248T>G (p.Phe83Cys), c.344G>C (p.Cys115Ser), c.815T>C (p.Leu272Pro), and c.1118T>G (p.Met373Arg) were introduced by site-directed mutagenesis. Expression vectors for human HNF-4α2-WT or mutants were constructed by ligating cDNA fragments directly into the NotI and BamHI sites of PQCXIP-mOrange2. The pTOP-HNF1A-TATA-GFP (pHNF1A-GFP) reporter was constructed by replacing the four repeats of the M67 sequences on pRRL.sin-18.ppt.STAT3-GFP.pre (STAT3-GFP) with the proximal promoter of human hepatocyte nuclear factor-1α (*HNF-1α*) (-105~+30)) with the following sequence: TGTCCCTCTCCGC TGCCATGAGGCCTGCACTTTGCAGGGCTGAA GTCCAAAGTTCAGTCCCTTCGCTAAGCACACGGATAA ATATGAACCTTGGAGAATTTCCCCAGCTCCAATGT AAACAGAACAGGCAGGGGC (20).

Cell Culture and Transfection

HEK 293T cells were cultured in DMEM supplemented with 10% FBS, 100 units/ml penicillin G sodium, and 100 μg/ml streptomycin. During routine passaging, cells were washed with PBS (pH 7.4) and dissociated with TrypLE Express. For transient transfection, cells were plated and were transfected with plasmids as indicated using Lipofectamine 3000 Reagent.

Viral Preparation and Infection

For virus packaging, the lentivirus system containing transfer plasmid pHNF1AP1-GFP and packing vectors (PLP1, PLP2, PLP-VSVG) or the retrovirus system containing PQCXIP-HNF-4α, VSVG, and Phit were co-transfected into HEK 293T cells with 4×10^6 cells in a 100-mm dish using Lipofectamine 3000. Media were replaced 24 h later, and viral supernatants were collected at 48 and 72 h, centrifuged at 1,300 rpm for 5 minutes, passed through a 0.45-μm filter (Millipore), and concentrated by lentivirus concentration solution (YEASEN). The virus should be used with optimal virus volumes (MOI of 0.1–0.2) or frozen at -20°C or -80°C for long-term storage. Cells were infected with the virus in the presence of polybrene at a concentration of 1 μg/ml.

Analytical Flow Cytometry and FACS

Cells were trypsinized and suspended in DMEM for FACS analysis and sorting (BD Influx). Cells were excited with a 488-nm laser (530/40 emission) and a 561-nm laser (610/20 emission). Data analysis was performed using FlowJo_V10 (Tree Star, Ashland) software.

Live-Cell Imaging and Fluorescent Quantification

Cells were imaged with the Opera Phenix High Content Screening System in confocal mode with the ×20 water NA 1.0 objectives at 37°C and 5% CO_2 at the indicated time. The fluorophores were detected with the following excitation and emission (Ex/Em) wavelengths: Hoechst 33342 (405/435–480), GFP (488/500–550), and mOrange2 (561/570–630). Quantification analyses were performed using the Harmony software. For high-resolution imaging, cells were grown on small glass coverslips. Forty-eight hours after transfection, images were viewed using the OLYMPUS FV1200 system. All experiments were performed in triplicate.

Western Blotting

HEK 293T cells were seeded on 96-well plates with different transfection strategies and lysed by the addition of 1× SDS-PAGE loading buffer (reducing). Equal amounts of protein extracts were separated by SDS-PAGE gel and subsequently transferred to a 0.2-μm PVDF membrane for 1 h at 400 mA and blocked at room temperature for 1 h in 1× TBST (20 Mm Tris base, 0.15 M NaCl, 0.1% Tween-20, 5% milk). Proteins were analyzed using the anti-mCherry antibody, anti-HNF-4α antibody, anti-GFP antibody, and anti-GAPDH antibody. Bands were developed using ECL substrates, and band intensities were quantified by ImageJ software.

DNA Extraction and Cloning for Sanger Sequencing

Total genome DNA was extracted using phenol-chloroform DNA extraction protocol. The fully integrated HNF-4α sequences were amplified using primers (HNF-4α2-F: 5′-CCGCGGCCGCACCATGCGACTCTCCAAAAC-3′; HNF-4α2-R: 5′-TGGGATCCGGGATAACTTCCTGCTTG-3′) and cloned in the PQCXIP vector for Sanger sequencing.

RESULTS

Construction of a Dual-Fluorescence Assay Simultaneously Monitoring the Transcription Activity, Expression, and Localization of HNF-4α in Live Cell

To design a dual-fluorescence reporting system monitoring the expression level and transactivation activity of HNF-4α in live cells, we constructed a GFP reporter under the control of the HNF1A promoter (pHNF1A-GFP) and introduced the mOrange2 fluorescence protein to the C terminal of HNF-4α (HNF-4α-mOrange2) (**Figure 1A**). As HEK 293T cells have an undetectable endogenous HNF-4α expression (**Figure 1D**), the GFP reporter was expected to express only in the presence of transcript factor HNF-4α-mOrange2 (**Figure 1B**). As expected, co-transfection of the GFP reporter and wild-type HNF-4α-mOrange2 led to about 6-fold higher GFP expression compared to the cells transfected with the GFP reporter alone. In addition, confocal imaging showed the nuclear localization of HNF-4α-mOrange2 (**Figure 1C**). The correct expression was also evidenced by Western blot using a specific antibody (**Figure 1D**). This result demonstrates that exogenous HNF-4α-mOrange2 could work as that of endogenous HNF-4α does with proper expression, cellular distribution, and transactivation on the HNF-1α promoter in the HEK 293T cell line.

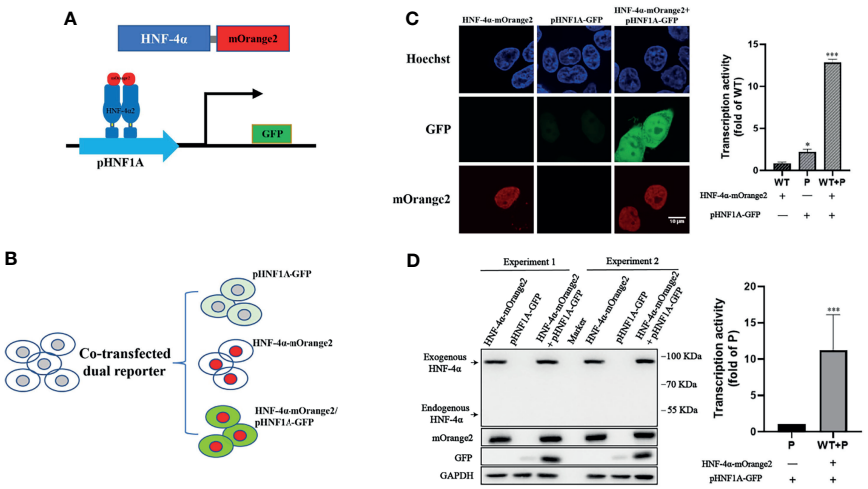

FIGURE 1 | Establishment of the dual-fluorescence assay for functional evaluation on the HNF-4α. **(A)** A schematic diagram of the dual-fluorescence reporter system. The C-terminal of HNF-4α was fused with a red fluorescent protein mOrange2 and was used to track the HNF-4α cell location and expression; pHNF1A was the GFP reporter under control of the HNF-1α promoter which was used to detect the transcription activity of the HNF-4α dimer. **(B)** Overview of the assay working in cell lines. **(C)** Representative confocal microscopy imaging of dual-fluorescence assay and quantification of the transcription activity. Nuclear staining (blue); 488-nm channel for pHNF1A-GFP (green); 561-nm channel for HNF-4α-mOrange2 (red). The GFP intensity of the three groups has also been quantified with three fields in one experiment; the data were analyzed using a Student t-test (*$p < 0.05$, ***$p < 0.001$). WT, wild-type HNF-4α-mOrange2, P, pHNF1A-GFP. **(D)** Representative Western blots and quantification of GFP intensity of cells transfected with plasmids as indicated for 48 h. The anti-mCherry antibody and anti-HNF-4α antibody were used for detection of mOrange2-conjugated HNF-4α proteins and HNF-4α proteins, respectively. The anti-GAPDH antibody was the internal reference in this experiment. The anti-GFP antibody showed the transcription activity. Data represented as mean± SD from six independent experiments.

In order to improve the performance of the dual-fluorescence reporter, we further established cell lines stably expressing the pHNF1A-GFP reporter with the lentivirus system in the HEK 293T cell line, upon which the E9 clone was selected for the highest specificity for exogenous wild-type HNF4A transactivation. Compared to the HEK293T_pHNF1AP_E9 cells without HNF-4α-mOrange2 expression, cells transiently transfected with wild-type HNF-4α-mOrange2 exhibit a significantly increased GFP expression, which was initiated from 24 h after transient transfection and reached the highest about 90 h later. The system was validated with a loss-of-function mutant identified in HH and MODY1 (11, 19), M373R, which showed the same expression pattern with reduced transactivation (**Figures 2A, B**). The transactivation activity difference between wild-type and M373R mutant was significant and distinguishable with FACS ($p < 0.0001$; **Figure 2C**). These results demonstrate that we had established a dual-fluorescence reporting system in the HEK 293T cell line for further distinguishing various unknown mutants according to the effects on the transactivate ability and expression level.

Validation of the Assay With a Library Containing Wild-Type HNF-4α and Five Previously Reported Loss-of-Function Mutations

To validate this assay, we construct a small library by equally mixing wild-type HNF-4α with five previously reported loss-of-function mutations, including three mutations (G79C, F83C, C115S) in the DBD, one mutation (L272P) in the LBD, and one mutation (M373R) in the F domain (**Figures 3A, B**). HEK293T_pHNF1AP_E9 cells (4×10^6) in a 10-cm dish were incubated with retrovirus packaged with the library at an MOI of 0.1 to ensure each cell was infected with only one virus. Selected with puromycin for 2 doubling times, cells were subsequently sorted according to the transcription activity and expression level by FACS. Three cell populations were collected which were named as Normal (same transactivation as wild type), Reduced^{exp_nor} (reduced transactivation with normal or higher expression), and Reduced^{exp_low} (reduced transactivation with lower expression) (**Figure 3C**). Integrated cDNAs were cloned into pQCXIP-mOrange2. We randomly selected five clones each group for Sanger sequencing. The results showed that two mutations (M373R and G79C) are enriched in the Reduced^{exp_nor} group, three mutations (C115S, L272P, and F83C) belong to the Reduced^{exp_low} group, while the wild type belong to the Normal group.

To verify the result, we tested the mutants individually using this dual-fluorescence assay in high content screening assay (HCS). Three mutants (F83C, C115S, and L272P) classified as Reduced^{exp_low} group with high confidence were found significantly repressing the transcription activity with lower expression, and two mutants (G79C and M373R) classified as Reduced^{exp_nor} group were found significantly disrupting the transcription activity with normal or higher expression (**Figures 4A, B**). The effects of all the missense variants on the transactivation activity and expression level were consistent with the results from FACS. In addition, we found that the localization of two mutants (G79C and M373R) was predominantly in the

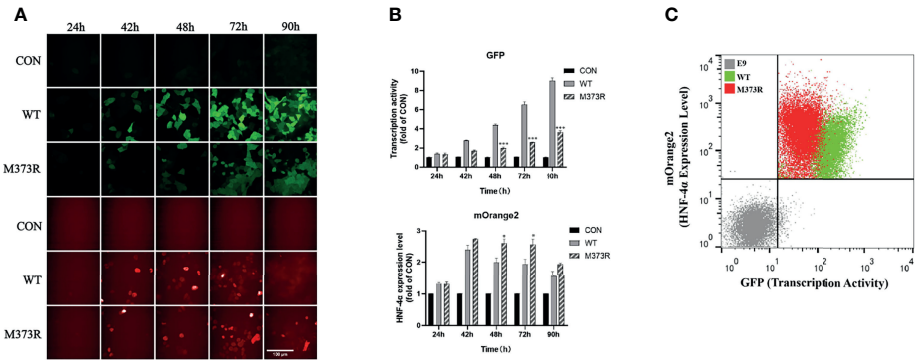

FIGURE 2 | Optimization of the assay in the single-cell clone HEK293T_pHNF1AP_E9 stably expressing the pHNF1A-GFP reporter. **(A, B)** Kinetic performance of this assay in HEK293T_pHNF1AP_E9 cells transiently transfected with HNF-4α or mutant M373R. Data were the means of triplicate fields from one experiment and were conducted twice independently; error bars show s.d. *p < 0.05, ***p < 0.001. Scale bar: 50 μm. **(C)** Sorting of HEK293T_pHNF1AP_E9 (E9) cells expressing wide-type HNF-4α (WT, green color) or M373R (M373R, red color) populations, negative control: HEK293T_pHNF1AP_E9 (gray color). The transcription activity of mutant M373R was significantly lower than that of wild type, p < 0.0001.

nucleus. By contrast, the localization of the other three mutants (F83C, C115S, and L272P) exhibited more diffusion in the cytoplasm compared to the wild-type HNF-4α (**Figure 4C**), which may partly contribute to the loss of function and lower abundance. In conclusion, our results clearly showed that this dual-fluorescence assay could be used as a simple, precise, and informative assay to evaluate the effect of mutations of HNF-4α.

DISCUSSION

In this study, we firstly developed a dual-fluorescence reporter assay that could simultaneously examine HNF-4α variants on three mechanistic aspects including the transcriptional activity, protein abundance, and cellular localization. Then the assay was validated with a small library of five established loss-of-function variants with wild-type HNF-4α to demonstrate its reliability and the potential for high-throughput functional screening of VUS in HNF-4α.

The five mutants used to validate our assay were selected to represent the wide spectrum of potential functional defects that could originate from many possible HNF-4α variants. G79C and F83C in the DNA-binding domain had been reported with reduced DNA-binding affinity (6). M373R in the F domain was reported to impair the HNF-4α function by interrupting its interactions with coactivators without affecting DNA-binding affinity (19). C115S in the DBD and L272P in the LBD were identified in HH patients with severe phenotypes but poorly characterized function (10). In addition, the other three variants were also reported with a direct role in the pathogenesis of disease outcomes (6, 19). Therefore, these five mutants from different functional domains of HNF-4α, with various functional defects and all resulting in clinical consequences, could solidly anchor the assay for the examination of other VUS within this gene.

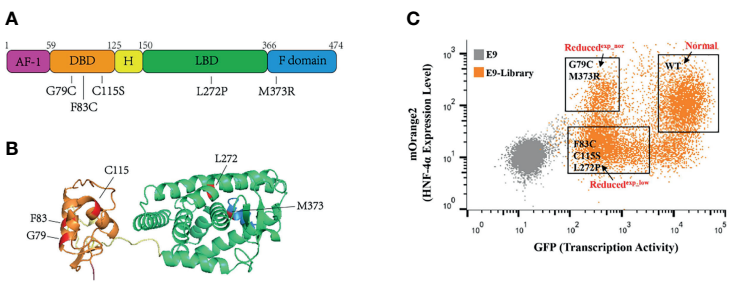

FIGURE 3 | Application of this assay in a small library containing wild-type HNF-4α and five mutants. **(A)** Schematic representation of the HNF-4α (NM_000457.6) structure, and distribution of single amino acid mutations used in this study. Five main functional domains: AF-1, activation function 1 (amino acids 1–59), purple color; DBD, DNA-binding domain (amino acids 60–125), orange color; H, hinge domain (amino acids 126–150), yellow color; LBD, ligand-binding domain (amino acids 151–366), green color; F domain (amino acids 367–474), blue color. **(B)** Three-dimensional model of human HNF-4α (4iqr) with schematic function domains of HNF-4α and distribution of five deleterious mutations used in this study. The mutations were highlighted in red. Four functional domains: the DBD, orange color; H domain, yellow color; LBD, green color and F domain, blue color. **(C)** Gating of the HEK293T_pHNF1AP_E9(E9) cells infected with library into three distinct populations based on the GFP and mOrange2 level. The mutants labeled in the gates were identified through cloning and Sanger sequence.

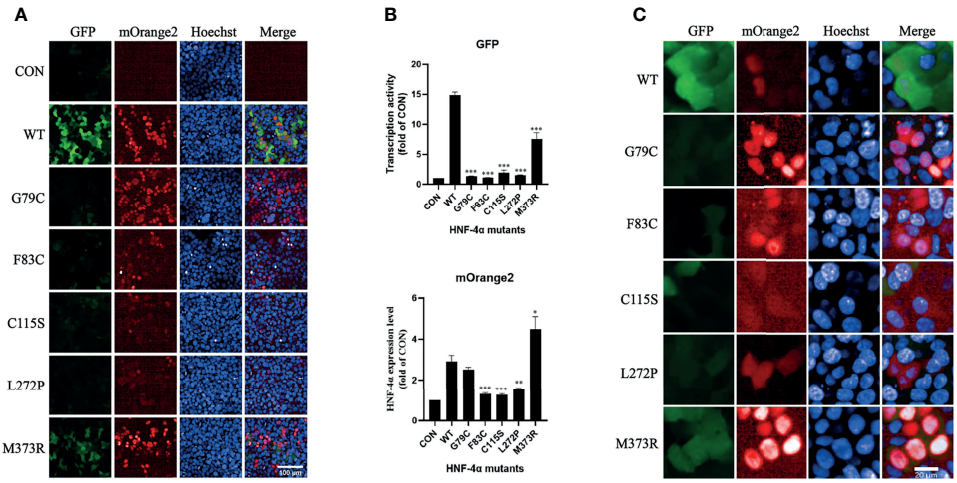

FIGURE 4 | Validation of the library mutants individually in HCS with confocal mode. **(A)** Evaluation of the transcription activity, expression level, and localization of HNF-4α wild type or mutants using the HCS image. HEK293T_pHNF1AP_E9 cells transfected with wild-type HNF-4α or different mutants as indicated for 72 h. GFP corresponds to the transactivists' ability, and mOrange2 represents the expression of HNF-4α or mutants. Scale bar: 100 μm. **(B)** Quantitative of the transcription activity and expression level of all the plasmids in the library we used. Shown is the fold change of GFP and HNF-4α-mOrange2 intensity. All data were presented as mean ± SD (n = 3 fields, and experiments were conducted twice independently. Statistical significance between WT and mutants (G79C, F83C, C115C, L272P, M373R) is indicated as asterisks: *p < 0.05, **p < 0.01, ***p < 0.001 (Student's t-test). **(C)** Cellular localization of the wild type or mutants of HNF-4α. Representative cells were shown except for three mutants (F83C, C115C, and L272P) which cells with higher mOrange2 intensity were selected for more details. Scale bar: 20 μm.

The exogenous wild-type HNF-4α-mOrange2 showed efficient regulation on the HNF-1α promoter, and our assay found that all the five established mutants had consistent and significant loss of transcriptional activity. This indicated that our *in vitro* system could mimic the action of physiological HNF-4α and provide reliable evidence of transcriptional activity on VUS.

While examining the HNF-4α protein abundance, our assay demonstrated the ability to distinguish variants with varying degrees of expression levels. Of the five loss-of-function variants, G79C and M373R were normally expressed while F83C, C115S, and L272P showed a lower expression. In regard to the cellular localization, we showed that three mutants with a lower expression exhibited more diffusion in the whole cells compared to the wild type and other two mutants. It was reported that the phosphorylation on the S87 in the DBD domain and Y286/Y288 in LBD could enhance nuclear export and cytoplasmic aggregation which induced proteasomal degradation (21, 22). Therefore, we propose that the reasons for those variants to exhibit low protein abundance in our assay might be due to enhanced degradation through posttranslational modifications such as phosphorylation (22–25). In addition, it is worth noting that the expression level of M373R was higher in our assay but was previously reported with reduced HNF-4α protein stability and in turn low abundance (19). One possible explanation for the discrepancy was that our assay was relatively simple as compared to the previous study which was complicated and might have a larger chance to generate more artificial results. Such a possibility was further strengthened as M373R showed a higher expression when tested individually (**Supplementary Figure 1**). Taken together, these results demonstrated that our assay was capable of monitoring the protein abundance and cellular localization of HNF-4α VUS.

One important feature of our assay was that it utilized FACS to examine multiple functions of HNF-4α variants simultaneously in live cells. The assay would be able to differentiate a spectrum of variants with varying levels of functional loss in either transcription activity or protein abundance. The small validation library of five variants demonstrated that after sorting the cells, sequencing could be used to classify or quantify the functional loss of each variant from a mixed pool of cells carrying different mutants. Therefore, our assay paves the way to conduct high-throughput functional screening of a saturated library of HNF-4α mutants and provide a "lookup table" for functional annotation of VUS.

One limitation of our assay was that the DNA-binding affinity was not measured directly. However, the transcription activity level test in the assay could partially capture such defect. On the other hand, our assay had a clear intention to evaluate the functional impact of HNF-4α mutants relevant to MODY1. That is why we opted to choose HNF1A expression as the reporter of HNF-4α transcriptional activity instead of other targets. Furthermore, we selected the 293T cell line to evaluate HNF-4α function because of the high expression efficiency of exogenous plasmids and undetectable endogenous HNF-4α as compared to INS-1 cells. This assay could be further improved by replacing the reporter or cell line.

In conclusion, our dual-fluorescence assay could reliably evaluate multiple functional impacts of HNF-4α variants related to MODY1. The successful validation with a small library of five loss-of-function variants demonstrated the potential of this assay to be applied in high-throughput

screening of HNF-4α variants. Systematically characterizing the functional impacts of all HNF-4α variants would arm the genetic consultants and clinicians with valuable prior knowledge when facing carriers of HNF-4α VUS.

DATA AVAILABILITY STATEMENT

The original contributions presented in the study are included in the article/**Supplementary Material**, further inquiries can be directed to the corresponding authors.

AUTHOR CONTRIBUTIONS

YG and LZ participated in the design and analysis and wrote the manuscript. JZ and RH contributed to the data measurement and analysis. TX and KZ participated in the design and revision. LZ and KZ wrote the manuscript with help from all authors. All authors read the manuscript and discussed the interpretation of results. All authors contributed to the article and approved the submitted version.

FUNDING

This work was supported by grants from the National Natural Science Foundation of China (31570765), the National Key R&D Program of China (2018YFC2001003), and the Strategic Priority Research Program of the Chinese Academy of Sciences (XDB38020100). The funding agency had no role in the design of the study; in the collection, analyses, or interpretation of data; in the writing of the manuscript; or in the decision to publish the results.

ACKNOWLEDGMENTS

The authors thank Ya Wang (Protein Science Core Facility of Institute of Biophysics) for her technical help in high-content screening determination and Junying Jia and Shu Meng (Institute of Biophysics, Chinese Academy of Science) for their help with fluorescence-activated cell sorting (FACS). We would like to thank the Center for Biological Imaging (CBI), Institute of Biophysics, Chinese Academy of Science, for our FV1200 imaging and Yan Teng, Yun Feng, and Chunliu Liu for their help. We are grateful to Zhimin Wang, Xiaoyan Wang, and Yihui Xu (CAS Key Laboratory of Infection and Immunity) for their help in FACS and confocal in this work.

SUPPLEMENTARY MATERIAL

The Supplementary Material for this article can be found online at: https://www.frontiersin.org/articles/10.3389/fendo.2022.812747/full#supplementary-material

REFERENCES

1. Chandra V, Huang P, Potluri N, Wu D, Kim Y, Rastinejad F. Multidomain Integration in the Structure of the HNF-4α Nuclear Receptor Complex. *Nature* (2013) 495:394–8. doi: 10.1038/nature11966
2. Sladek FM, Zhong WM, Lai E, Darnell JE Jr. Liver-Enriched Transcription Factor HNF-4 Is a Novel Member of the Steroid Hormone Receptor Superfamily. *Genes Dev* (1990) 4:2353–65. doi: 10.1101/gad.4.12b.2353
3. Bolotin E, Liao H, Ta TC, Yang C, Hwang-Verslues W, Evans JR, et al. Integrated Approach for the Identification of Human Hepatocyte Nuclear Factor 4alpha Target Genes Using Protein Binding Microarrays. *Hepatology* (2010) 51:642–53. doi: 10.1002/hep.23357
4. Wallerman O, Motallebipour M, Enroth S, Patra K, Bysani MS, Komorowski J, et al. Molecular Interactions Between HNF4a, FOXA2 and GABP Identified at Regulatory DNA Elements Through ChIP-Sequencing. *Nucleic Acids Res* (2009) 37:7498–508. doi: 10.1093/nar/gkp823
5. Odom DT, Zizlsperger N, Gordon DB, Bell GW, Rinaldi NJ, Murray HL, et al. Control of Pancreas and Liver Gene Expression by HNF Transcription Factors. *Science* (2004) 303:1378–81. doi: 10.1126/science.1089769
6. Taniguchi H, Fujimoto A, Kono H, Furuta M, Fujita M, Nakagawa H. Loss-Of-Function Mutations in Zn-Finger DNA-Binding Domain of HNF4A Cause Aberrant Transcriptional Regulation in Liver Cancer. *Oncotarget* (2018) 9:26144–56. doi: 10.18632/oncotarget.25456
7. Ryffel GU. Mutations in the Human Genes Encoding the Transcription Factors of the Hepatocyte Nuclear Factor (HNF)1 and HNF4 Families: Functional and Pathological Consequences. *J Mol Endocrinol* (2001) 27:11–29. doi: 10.1677/jme.0.0270011
8. Ellard S, Colclough K. Mutations in the Genes Encoding the Transcription Factors Hepatocyte Nuclear Factor 1 Alpha (HNF1A) and 4 Alpha (HNF4A) in Maturity-Onset Diabetes of the Young. *Hum Mutat* (2006) 27:854–69. doi: 10.1002/humu.20357
9. Kapoor RR, Flanagan SE, James C, Shield J, Ellard S, Hussain K. Hyperinsulinaemic Hypoglycaemia. *Arch Dis Childhood* (2009) 94:450–7. doi: 10.1136/adc.2008.148171
10. Flanagan SE, Kapoor RR, Mali G, Cody D, Murphy N, Schwahn B, et al. Diazoxide-Responsive Hyperinsulinemic Hypoglycemia Caused by HNF4A Gene Mutations. *Eur J Endocrinol* (2010) 162:987–92. doi: 10.1530/EJE-09-0861
11. Pearson ER, Boj SF, Steele AM, Barrett T, Stals K, Shield JP, et al. Macrosomia and Hyperinsulinaemic Hypoglycaemia in Patients With Heterozygous Mutations in the HNF4A Gene. *PloS Med* (2007) 4:e118. doi: 10.1371/journal.pmed.0040118
12. Delvecchio M, Pastore C, Giordano P. Treatment Options for MODY Patients: A Systematic Review of Literature. *Diabetes Ther: Res Treat Educ Diabetes Relat Disord* (2020) 11:1667–85. doi: 10.1007/s13300-020-00864-4
13. Peixoto-Barbosa R, Reis AF, Giuffrida FMA. Update on Clinical Screening of Maturity-Onset Diabetes of the Young (MODY). *Diabetol Metab Syndrome* (2020) 12:50. doi: 10.1186/s13098-020-00557-9
14. Lek M, Karczewski KJ, Minikel EV, Samocha KE, Banks E, Fennell T, et al. Analysis of Protein-Coding Genetic Variation in 60,706 Humans. *Nature* (2016) 536:285–91. doi: 10.1038/nature19057
15. Landrum MJ, Lee JM, Riley GR, Jang W, Rubinstein WS, Church DM, et al. ClinVar: Public Archive of Relationships Among Sequence Variation and Human Phenotype. *Nucleic Acids Res* (2014) 42:D980–5. doi: 10.1093/nar/gkt1113
16. Ng PC, Henikoff S. SIFT: Predicting Amino Acid Changes That Affect Protein Function. *Nucleic Acids Res* (2003) 31:3812–4. doi: 10.1093/nar/gkg509

17. Dong C, Wei P, Jian X, Gibbs R, Boerwinkle E, Wang K, et al. Comparison and Integration of Deleteriousness Prediction Methods for Nonsynonymous SNVs in Whole Exome Sequencing Studies. *Hum Mol Genet* (2015) 24:2125–37. doi: 10.1093/hmg/ddu733
18. Richards S, Aziz N, Bale S, Bick D, Das S, Gastier-Foster J, et al. Standards and Guidelines for the Interpretation of Sequence Variants: A Joint Consensus Recommendation of the American College of Medical Genetics and Genomics and the Association for Molecular Pathology. *Genet Med: Off J Am Coll Med Genet* (2015) 17:405–24. doi: 10.1038/gim.2015.30
19. Rha GB, Wu G, Chi YI. Probing the Effect of MODY Mutations Near the Co-Activator-Binding Pocket of HNF4alpha. *Biosci Rep* (2011) 31:411–9. doi: 10.1042/BSR20110013
20. Guo S, Lu H. Novel Mechanisms of Regulation of the Expression and Transcriptional Activity of Hepatocyte Nuclear Factor 4α. *J Cell Biochem* (2019) 120:519–32. doi: 10.1002/jcb.27407
21. Sun K, Montana V, Chellappa K, Brelivet Y, Moras D, Maeda Y, et al. Phosphorylation of a Conserved Serine in the Deoxyribonucleic Acid Binding Domain of Nuclear Receptors Alters Intracellular Localization. *Mol Endocrinol* (2007) 21:1297–311. doi: 10.1210/me.2006-0300
22. Chellappa K, Jankova L, Schnabl JM, Pan S, Brelivet Y, Fung CL, et al. Src Tyrosine Kinase Phosphorylation of Nuclear Receptor HNF4α Correlates With Isoform-Specific Loss of HNF4α in Human Colon Cancer. *Proc Natl Acad Sci USA* (2012) 109:2302–7. doi: 10.1073/pnas.1106799109
23. Reddy S, Yang W, Taylor DG, Shen X, Oxender D, Kust G, et al. Mitogen-Activated Protein Kinase Regulates Transcription of the ApoCIII Gene. Involvement of the Orphan Nuclear Receptor HNF4. *J Biol Chem* (1999) 274:33050–6. doi: 10.1074/jbc.274.46.33050
24. Leclerc I, Lenzner C, Gourdon L, Vaulont S, Kahn A, Viollet B. Hepatocyte Nuclear Factor-4alpha Involved in Type 1 Maturity-Onset Diabetes of the Young Is a Novel Target of AMP-Activated Protein Kinase. *Diabetes* (2001) 50:1515–21. doi: 10.2337/diabetes.50.7.1515
25. Hong YH, Varanasi US, Yang W, Leff T. AMP-Activated Protein Kinase Regulates HNF4alpha Transcriptional Activity by Inhibiting Dimer Formation and Decreasing Protein Stability. *J Biol Chem* (2003) 278:27495–501. doi: 10.1074/jbc.M304112200

Conflict of Interest: The authors declare that the research was conducted in the absence of any commercial or financial relationships that could be construed as a potential conflict of interest.

Publisher's Note: All claims expressed in this article are solely those of the authors and do not necessarily represent those of their affiliated organizations, or those of the publisher, the editors and the reviewers. Any product that may be evaluated in this article, or claim that may be made by its manufacturer, is not guaranteed or endorsed by the publisher.

frontiers in Endocrinology

ORIGINAL RESEARCH
published: 21 February 2022
doi: 10.3389/fendo.2022.835570

The Role of Lactate Exercise Test and Fasting Plasma C-Peptide Levels in the Diagnosis of Mitochondrial Diabetes: Analysis of Clinical Characteristics of 12 Patients With Mitochondrial Diabetes in a Single Center With Long-Term Follow-Up

Yuan Zhao[1†], Ying Zhang[2†], Mengya Qi[1], Fan Ping[1], Huabing Zhang[1], Lingling Xu[1], Wei Li[1] and Yuxiu Li[1*]*

[1] Key Laboratory of Endocrinology of National Health Commission, Department of Endocrinology, Peking Union Medical College Hospital, Chinese Academy of Medical Sciences & Peking Union Medical College, Beijing, China, [2] Department of Endocrinology, The Hospital of Shunyi District, Beijing, China

OPEN ACCESS

Edited by:
Ming Liu,
Tianjin Medical University General Hospital, China

Reviewed by:
Yanbing Li,
First Affiliated Hospital of Sun Yat-sen University, China
Tao Yang,
Nanjing Medical University, China

***Correspondence:**
Wei Li
weili0012@aliyun.com
Yuxiu Li
liyuxiu@medmail.com.cn

†These authors have contributed equally to this work

Specialty section:
This article was submitted to Clinical Diabetes, a section of the journal Frontiers in Endocrinology

Received: 14 December 2021
Accepted: 26 January 2022
Published: 21 February 2022

Citation:
Zhao Y, Zhang Y, Qi M, Ping F, Zhang H, Xu L, Li W and Li Y (2022) The Role of Lactate Exercise Test and Fasting Plasma C-Peptide Levels in the Diagnosis of Mitochondrial Diabetes: Analysis of Clinical Characteristics of 12 Patients With Mitochondrial Diabetes in a Single Center With Long-Term Follow-Up. Front. Endocrinol. 13:835570. doi: 10.3389/fendo.2022.835570

Objective: The aim of this study was to analyze the clinical characteristics and the pattern of long-term changes of fasting plasma C-peptide in patients with mitochondrial diabetes (MD), and to provide guidance for the diagnosis and treatment of MD.

Methods: We retrieved MD patients with long-term follow-up at Peking Union Medical College Hospital from January 2005 to July 2021 through the medical record retrieval system and retrospectively analyzed their clinical data, biochemical parameters, fasting plasma C-peptide, glycosylated hemoglobin and treatment regimens. Non-parametric receiver operating characteristic (ROC) curves were used to assess the relationship between exercise test-related plasma lactate levels and suffering from MD.

Results: A total of 12 MD patients were included, with clinical characteristics of early-onset, normal or low body weight, hearing loss, maternal inheritance, and negative islet-related autoantibodies. In addition, patients with MD exhibited significantly higher mean plasma lactate levels immediately after exercise compared to patients with type 1 diabetes mellitus (T1DM) (8.39 ± 2.75 vs. 3.53 ± 1.47 mmol/L, p=0.003) and delayed recovery time after exercise (6.02 ± 2.65 vs. 2.17 ± 1.27 mmol/L, p=0.011). The optimal cut-off points identified were 5.5 and 3.4 mmol/L for plasma lactate levels immediately after and 30 minutes after exercise, respectively. The fasting plasma C-peptide levels decreased as a

negative exponential function with disease progression ($Y= 1.343*e^{-0.07776X}$, R^2 = 0.4154). Treatment regimens in MD patients were varied, with no metformin users and a weak correlation between insulin dosage and body weight.

Conclusions: The increased level of plasma lactate during exercise or its delayed recovery after exercise would contribute to the diagnosis of MD. Changes of fasting plasma C-peptide in MD patients over the course of the disease indicated a rapid decline in the early stages, followed by a gradual slowing rate of decline.

Keywords: mitochondrial diabetes, clinical features, fasting C-peptide, lactate exercise test, monogenic diabetes

INTRODUCTION

Mitochondrial diabetes (MD) is a rare monogenic form of diabetes caused by defects in mitochondrial DNA (MtDNA) function (1), accounting for only 0.6% of adults with diabetes in China (2). van den Ouweland JM et al. (3) and Ballinger et al. (4) first reported a family of MD with elevated blood glucose and deafness caused by mutations and large segmental deletions of mitochondrial gene in 1992. Mitochondrial gene mutations are highly heterogeneous and individuals with the same mutation often exhibit different types and degrees of clinical phenotype, resulting in MD being diagnosed as type 1 or type 2 diabetes mellitus frequently.

The main pathogenesis of MD is mitochondrial gene mutation which leads to the decrease of insulin secretion by islet βcells (5). At present, the changes of islet βcell function in patients with MD have only been reported in individual cases or small families, and there is still a lack of large and long-term follow-up studies. In this study, we retrospectively analyzed and summarized the MD patients followed up in the outpatient clinic of Peking Union Medical College Hospital, in order to provide reference for understanding the changes of islet βcell function and the diagnosis and treatment of MD.

PATIENTS AND METHODS

Population

A total of 49 patients diagnosed with MD in the outpatient clinic of Peking Union Medical College Hospital from January 2005 to July 2021 were searched through the electronic medical record system. Further review of the medical records revealed 15 cases with clear mitochondrial gene mutations. To analyze the changes in pancreatic β-cell function during follow-up in these patients, the inclusion criteria were set as follows: follow-up for at least one year, and fasting plasma C-peptide test twice or more. A total of 12 patients met the criteria, and the longest follow-up period was 16 years, and a retrospective analysis of these 12 patients with MD was performed.

Data Collection

General information of patients was collected: age, sex, height, weight, time of onset, hearing status, family history. The results of islet-related autoantibodies including glutamic acid decarboxylase antibody (GADAb), protein tyrosine phosphatase antibody (IA2) and islet cell antibody (ICA), mitochondrial gene sequencing, blood biochemical parameters, plasma lactate, HbA1c, fasting plasma C-peptide and therapeutic regimen (types and doses of hypoglycemic drugs) at each visit were recorded.

Six MD patients had undergone lactate exercise testing, thus we included six patients with type 1 diabetes mellitus (T1DM) who had performed the same test as controls for comparison by matched search in the medical record retrieval system according to age and HbA1c at the time of the test.

Method of lactate exercise test: After a 30-minute rest period before the test, venous blood was taken for lactate measurement, followed by 10 minutes of stair climbing at moderate speed without stopping, and venous blood was taken immediately afterward, and the third blood sample after a 30-minute rest. The plasma lactate level was measured separately and >2 mmol/L was considered abnormal.

Statistical Analysis

Statistical analyses were performed using IBM SPSS Statistics for Windows, version 26 (IBMCorp., Armonk, N.Y., USA). Continuous data were expressed as mean ± standard deviation when normally distributed, and t-test was used for comparison of data between groups, and P values ≤ 0.05 were considered to be statistically significant. Non-parametric receiver operating characteristic (ROC) curves were constructed for plasma lactate levels immediately after and 30 minutes after exercise to assess their ability to independently discriminate between patients with and without MD. Optimal cut-off points were obtained by minimizing the distance between each point on the ROC curve and the upper left corner.

RESULTS

Analysis of Clinical Characteristics of MD Patients

Among the 12 patients with MD, the age of onset was 30.17 ± 10.57 years, 11 (92.3%) of them were younger than 45 years (**Table 1**). Their weight was normal or low with a mean BMI of 18.61 ± 4.14 kg/m2 and only one case was overweight (27.36 kg/m2) and no obese patients. Eleven cases had hearing loss. The health status of the maternal and her family was unknown in one case, and the remaining 11 cases all had a family history of maternal hereditary

TABLE 1 | Demographic and clinical characteristics of 12 patients with MD.

Patient	Diagnosis	Gender	Age at onset, y	Age at Baseline, y	Follow-Up time, y	Height, cm	Weight, kg	BMI (kg/m^2)	Resting lactate, mmol/L	Family history of	
										Diabetes	Hearing abnormalities
1	*3243 A>G*	F	38	41	14	157	39.5	16.02	–	Mother, sister, daughter	Mother, daughter, sister, niece
2	*3243 A>G*	F	15	18	14	157	54	21.91	1.67	Mother, grandmother, aunt	Mother, grandmother, aunt, aunt's daughter
3	*3243 A>G*	M	36	48	9	170	57	19.72	1.7-1.9	Mother	–
4	Mult mtDNA PM	F	11	11	16	159	57	22.55	1.7-3.1	Father, mother, uncle, grandfather, grandmother	–
5	*3243 A>G*	M	37	51	3	168	58	20.55	1.9	Aunt, brothers	Brothers
6	*m.15662 A>G*	M	23	24	3	171	80	27.36	0.76-2.7	–	–
7	*3243 A>G*	F	40	43	2	152	33	14.28	2.3-2.7	–	Sister, daughter
8	*3243 A>G*	F	37	38	4	150	45	20	1.8	Brother	Mother, brother
9	*3243 A>G*	F	27	41	3	159	39	15.43	2.6	Mother, brother, aunt	Mother, brother, uncles
10	*3243 A>G*	F	26	29	2	160	42	16.41	1.5	Father, mother, grandfather, grandmother, uncle	–
11	*m.1438 A>G*	M	26	26	1	172	47.5	16.06	0.98	Father, aunt, uncle	Sister
12	*3243 A>G*	F	46	50	6	157	32	12.98	–	Mother, sister, Niece	Mother, daughter, sister, niece

BMI, body mass index; M/F, male/female; PM, point mutation.

diabetes or hearing loss. All patients were negative for GADAb, IA2, and ICA. The details of mitochondrial gene mutations were as follows: 9 cases with *m.3243 A>G* mutation, 1 case with multi-point mutations (*m.3243 A>G, m.1438 A>G, m.3206 C>T, m.14783 T>C, m.16213 C>T, m.16319 G>A*), 1 case with *m.15662 A>G* mutation and 1 case with *m.1438 A>G* mutation.

The Level of Plasma Lactate Increased Significantly During and After Exercise in Patients With MD

In 10 of the 12 patients with MD, plasma lactate was measured at rest and its measurements ranged from 0.76 to 3.3 mmol/L (**Table 1**), with fluctuations not significantly related to the duration of the disease. P Plasma lactate at rest was detected only once in six patients, five of whom were within the normal range (0.98-1.9 mmol/L), and one was elevated (2.6 mmol/L). Four patients were tested several times for plasma lactate at rest: P#3 was tested twice, and the results were normal (1.7-1.9 mmol/L); P#7 was tested for three times, and the results were all increased (2.3-2.7 mmol/L); P#4 was tested for five times, and the results were normal (1.7-1.79 mmol/L) in two times and increased (2.31-3.3 mmol/L) in three times; P#6 was tested for three times, and the results were normal (0.76 mmol/L) in one time and increased (2.05-2.7 mmol/L) in two times.

Six MD patients and six T1DM patients underwent lactate exercise testing, with plasma lactate levels measured before, immediately after, and 30 minutes after exercise (**Table 2**). As shown in **Figure 1**, lactate was significantly higher in MD patients

TABLE 2 | Demographic characteristics of MD patients and T1DM patients.

	MD patients (n = 6)	T1DM patients[#] (n = 6)	p-value
Gender, male, n (%)	3 (66.7%)	1 (16.7%)	–
Age at onset, y	30.17 ± 10.57	40.5 ± 14.85	0.242
Age at exercise tests, y	42.58 ± 12.06	46.75 ± 16.72	0.593
Height, cm	161 ± 7.45	166.17 ± 5.6	0.155
Weight, kg	48.67 ± 13.47	64.23 ± 8.25	0.02
BMI, kg/m^2	18.61 ± 4.14	23.29 ± 2.98	0.026
Fasting C-peptide, ng/ml	0.59 ± 0.31	0.09 ± 0.02	0.007
HbA1c, %	7.93 ± 1.49	6.9 ± 1.02	0.148

MD, Mitochondrial diabetes; T1DM, Type 1 diabetes mellitus. [#]Clinical and laboratory findings of patients with T1DM were obtained from our institution's medical record retrieval system matched by age and HbA1c at the time of the test.

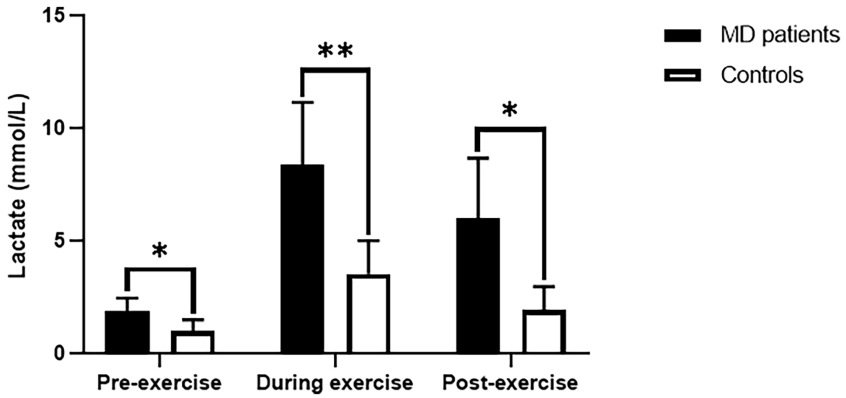

FIGURE 1 | Lactate values for exercise tests in MD patients and T1DM patients. MD, Mitochondrial diabetes; T1DM, Type 1 diabetes mellitus. *p < 0.05,**p < 0.01.

immediately after exercise compared to resting lactate and was 2-3fold higher than in T1DM patients (8.39 ± 2.75 vs. 3.53 ± 1.47 mmol/L, p=0.003). Thirty minutes after the exercise, lactate did not drop to normal levels in MD patients and was 3-4fold higher than in T1DM patients (6.02 ± 2.65 vs. 2.17 ± 1.27 mmol/L, p=0.011). Using nonparametric ROC curve, for plasma lactate levels immediately after exercise (area under the curve (AUC) 0.94, 95% confidence interval (c.i.) 0.81 to 1), the optimal cut-off was 5.5 mmol/L with a sensitivity of 83% and specificity of 100%. For plasma lactate levels 30 minutes after exercise (AUC 0.96, 95% c.i. 0.85 to 1), the optimal cut-off was 3.4 mmol/L, giving 100% sensitivity and 83% specificity (**Supplementary Figure 1**).

Changes of Fasting Plasma C-Peptide Level With Disease Duration

All 12 MD patients were tested for fasting plasma C-peptide at a median of three times (range 2-7 times) over a median of 13 years (range 2-21 years) after onset, and their C-peptide levels varied with the disease duration (**Figure 2A**). The fasting plasma C-peptide was 0.7-1.72 ng/ml with an average of 1.92 ng/ml in the first year and was 0.31-1.31 ng/ml with an average of 0.83 ng/ml in the fifth year. The fitting exponential curve of the data indicated that fasting plasma C-peptide decreased rapidly with the duration of the disease in the first 5 years ($Y= 1.343*e^{-0.07776X}$, $R^2 = 0.4154$). After 10 years of disease duration, the fasting plasma C-peptide level was maintained at a low level (0.16-0.79ng/ml) with no significant trend of further decline, except for P#9 which reached 1.21 ng/mL by the 14th year of disease duration. The fitting exponential curve reanalyzed deleting this value of P#9 showed that the decrease in fasting plasma C-peptide remained a negative exponential function with a steeper curve than in **Figure 2A** ($Y= 1.371*e^{-0.08597X}$, $R^2 = 0.4652$) (**Figure 2B**).

Comparison of Treatment Regimens Between the First and the Last Visit of 12 Patients With MD

Among the 12 patients, HbA1c of 10 patients fluctuated between 6.2 and 8.6% in 10 patients (**Table 3**), that of another 2 patients were above 10%, of which P#4 did not follow medical advice on diet control and insulin use, and P#11 only got a definite diagnosis of MD at the last visit and adjusted the glucose-lowering regimen but was not followed up later. Metformin was included in the treatment regimen of three patients at the first visit and before the diagnosis of MD was clarified. After the diagnosis of MD was confirmed and at the last follow-up visit, 11 patients used insulin, including one case combined with glucagon-like receptor agonist (GLP-1RA) and three cases combined with sodium-glucose co-transport protein 2 inhibitor (SGLT-2i), without adverse effects such as malaise, ketosis or ketoacidosis, or severe gastrointestinal reactions. One case used oral hypoglycemic agents only (glimepiride 1 mg once daily, HbA1c 6.2%). Metformin was not used. Except for P#4 and P#11, HbA1c decreased significantly at the last visit compared with the first visit.

DISCUSSION

MD is very rare, with individual cases or small families reported in China and no large long-term follow-up studies. In this study, we retrospectively analyzed the clinical data of 12 patients with MD with a maximum follow-up of 16 years and concluded that MD has the following clinical features: early age of onset, thin or normal body size, family history of maternal-inherited diabetes or hearing loss, and negative for islet-related antibodies (ICA, GAD, IA2), which is consistent with the literature (6). Patients with these characteristics need to be considered for possible MD. The diagnosis of MD currently relies on mitochondrial gene sequencing, but few hospitals are able to perform this test.

In the analysis of the clinical data of the 12 patients followed in this study, it was found that the lactate exercise test was a good indication for diagnosis, the large variation in blood lactate at rest was not significant for diagnosis. There are only a few reports on blood lactate in MD cases or families at rest (7–10), with inconsistent results, some elevated and some normal, with high variability, and no reports on lactate changes during and after exercise. Mitochondria are organelles that carry out aerobic metabolism and oxidative phosphorylation production and are responsible for 90% or more of the body's ATP supply.

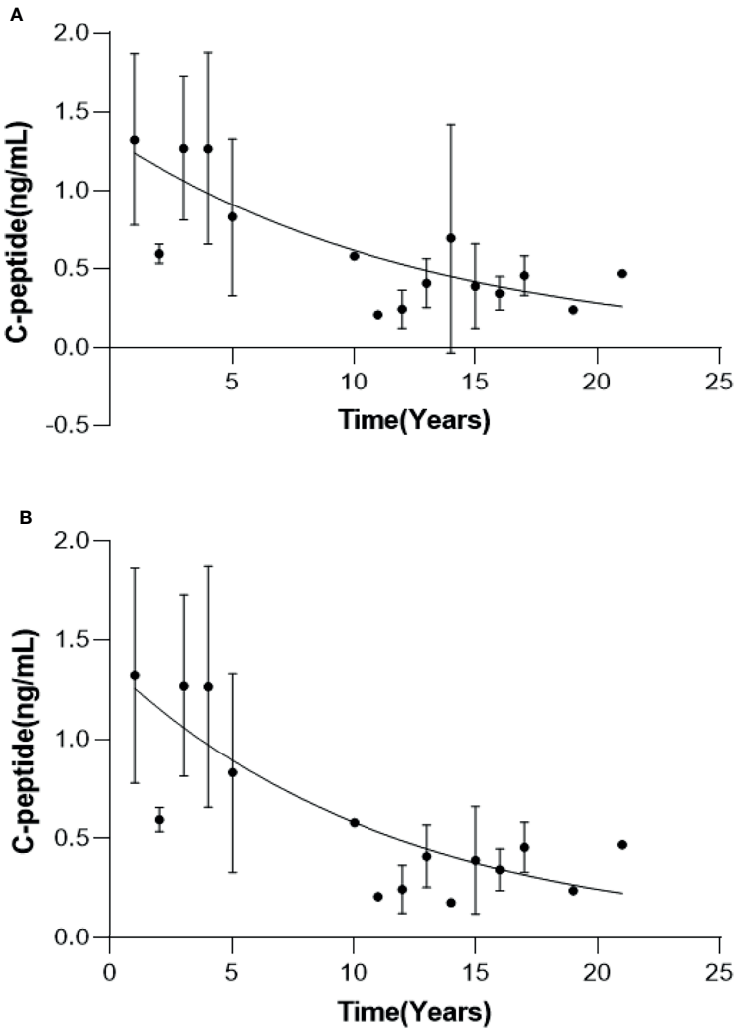

FIGURE 2 | Changes in fasting C-peptide with the duration of disease in MD patients. Curves of fasting C-peptide with disease duration for all MD patients **(A)** and MD patients except P#4 **(B)**.

Mutations in MtDNA result in oxidative phosphorylation dysfunction and reduced ATP production. This is followed by an increase in anaerobic enzyme production capacity and an increase in lactate production (11). At rest, the magnitude of blood lactate elevation depends on the degree of disease heterogeneity (12). During exercise, patients have elevated blood lactate at any given work rate compared to normal controls (13). There are no differences in serum lactate levels at rest, during and after exercise with and without clinical signs of myopathy (14). Of the 12 MD patients followed in this study, 10 patients underwent a total of 19 resting-state blood lactate tests, 10 had normal test results (0.76-1.9 mmol/L) and 9 had elevated test results (2.05-3.3 mmol/L). There was significant variability in the results of multiple measurements in the same patient with inconsistent results. This suggests that blood lactate at rest is highly variable and has limited value as a diagnostic screening indicator for patients with MD. The lactate exercise test was performed on six patients in this study, and lactate was significantly elevated during exercise, none of the blood lactate returned to resting levels after exercise. The ROC curves indicated that blood lactate during and after exercise had high diagnostic efficacy with a specificity and sensitivity of 100%, respectively, and the optimal cut-off points identified were 5.5 and 3.4 mmol/L, respectively. The lactate exercise test may be a useful screening method for MD when genetic testing is not available. To our knowledge, this is the first study to analyze the characteristics of blood lactate after exercise in MD patients and to assess its diagnostic ability. Thus, the accuracy of this test was not compared with other diagnostic tests, and further studies with larger sample sizes are needed to validate these findings.

Because of the low and rare incidence of MD, changes in islet cell function in MD have only been reported in individual cases or small family lines with short-term follow-up, and there are no large long-term follow-up studies. In this study, the first

TABLE 3 | HbA1c values and treatment regimens before and after follow-up.

Patient	First Visit			Last Visit			
	Disease Duration (y)	HbA1c (%)	Treatment	Disease Duration (y)	HbA1c (%)	Treatment	
						Insulin (Dose U/kg/d)	Other Antidiabetic Drugs (Dose)
1	3	13	Premixed human insulin 30R	17	7.4	0.35 (Premixed insulin aspart 50)	–
2	3	7.8	Intensive insulin therapy	17	8.6	1.19 (Aspart, detemir)	–
3	13	11.6	Oral drugs and insulin	21	8	0.91 (Aspart, glargine)	Linagliptin (5mg qd), dapagliflozin (10mg qd)
4	1	–	Premixed human insulin 30R	16	10.9	1.05 (Glulisine, degludec)	Sitagliptin (100mg qd), canagliflozin (100mg qd)
5	14	9.1	Metformin, vildagliptin	17	7.2	0.43 (Glulisine, degludec)	Acarbose (50mg tid), sitagliptin (100mg qd)
6	2	5.9	Metformin, glimepiride	4	7.2	0.38 (Aspart, degludec)	Dulaglutide (1.5mg qw), dapagliflozin (10mg qd)
7	3	7.9	Insulin glargine	5	6.4	0.48 (Glulisine, glargine)	–
8	1	6.3	Insulin	5	7.2	0.09 (Degludec)	Voglibose (0.3mg tid), sitagliptin (100mg qd)
9	14	9.3	Acarbose	17	8.6	1.23 (Aspart, glargine)	Pioglitazone (15mg qd), acarbose (100mg tid), sitagliptin (100mg qd)
10	3	9.3	Metformin	5	6.2	–	Glimepiride (1mg qd)
11	0	12.9	Insulin aspart, insulin glargine	1	10.5	0.53 (Premixed insulin aspart 30)	–
12	4	7.5	Acarbose	11	7	0.47 (Premixed insulin lispro 50)	–

HbA1c, hemoglobin A1c.

retrospective analysis of fasting C-peptide levels in 12 MD patients over a maximum of 16 years revealed that fasting C-peptide in MD patients decreased as a negative exponential function over the course of the disease. The decline in fasting C-peptide was faster early in the course of the disease, slowed down as the disease progressed, and remained in small amounts for more than 10 years of the disease. This is distinctly different from type 1 diabetes, which undergoes complete islet cell failure in a very short period of time. Yoshitomo Oka et al. (15) reported a similar case with similar follow-up (rapid decline in fasting C-peptide over 5 years, maintained at low levels after 11 years). The characteristics of the fasting C-peptide decline are related to the pathogenesis of MD. Mitochondria are responsible for a variety of biological functions, the most critical of which is the production of ATP and reactive oxygen species (ROS), the latter of which can cause cellular damage. Mutations in mitochondrial genes cause cellular alterations such as decreased ATP production, increased ROS, lipid peroxidation, altered membrane potential and increased apoptotic signaling, which in turn can lead to cellular damage and apoptosis. When the mutation is located in the islet, slow destruction of β-cells may occur, leading to decreased insulin secretion and the development of MD (11). MD is a highly heterogeneous disease in which each β-cell contains both mutant and wild-type mtDNA, referred to as heterogeneity, and different degrees of mutant mtDNA exist in different β-cells of the same individual (12). The ratio of mutant to wild-type mtDNA is a key factor in determining whether β-cells express biochemical abnormalities (16). Islet cells containing more mutant mtDNA develop dysfunction earlier and faster, leading to premature apoptosis (17). Our previous study also showed that individuals with high amounts of mutations had earlier onset and more severe disease (18). Islet cells containing less mutated mtDNA with wild-type mtDNA still maintain normal cellular function and can avoid initiating the apoptotic program and maintain normal β-cell function in the long term. For diabetic patients with lean body type, poor islet cell function and negative diabetes-related antibodies, and still detectable islet cell function after a longer disease course, we should be alert to the possibility of MD.

There is no evidence-based medical evidence to guide the treatment of MD. Early initiation of insulin therapy is recommended because of the rapid decline in islet cell function during the early stages of the disease. Metformin should be avoided in the treatment of MD because of the risk of lactic acidosis. Our follow-up MD patients used a variety of hypoglycemic regimens, including one case with GLP-1RA and three cases with SGLT-2i, with no significant adverse effects and all with a significant decrease in glycated hemoglobin, similar to the treatment effects reported in the literature (19, 20). It indicates that the treatment of MD patients can be diversified according to the specifics of blood glucose and islet cell function, and that the novel hypoglycemic drugs are effective without significant adverse effects. However, due to the small number of cases we observed and the limited follow-up time, whether these novel hypoglycemic drugs are safe for MD patients still needs to be observed in long-term follow-up.

In conclusion, we should consider the possibility of MD in patients with young to middle-aged onset, thin or normal body size, hearing loss, family history of maternal-inherited diabetes or hearing loss, negative antibodies (IAA, ICA, GAD), and residual islet cell function after a long course of disease. The lactate exercise test can be further completed. If there is an increase in plasma lactate level during exercise and delayed recovery after exercise, it is necessary to be highly alert to the possibility of MD. The diagnosis can be confirmed by hot spot detection of mitochondrial gene mutation. The treatment of MD should be

individualized according to the specific conditions such as blood glucose and islet cell function, as well as avoidance of metformin. However, our sample is relatively small, and a larger population-based cohort and more longitudinal studies are warranted.

DATA AVAILABILITY STATEMENT

The raw data supporting the conclusions of this article will be made available by the authors, without undue reservation.

ETHICS STATEMENT

The studies involving human participants were reviewed and approved by Ethics Committee of the Peking Union Medical College Hospital. Written informed consent for participation was not required for this study in accordance with the national legislation and the institutional requirements.

AUTHOR CONTRIBUTIONS

YAZ and YZ: data acquisition and drafting of the manuscript. MQ, FP, HZ, and LX: data acquisition and analysis and interpretation of the data. WL and YL: study concept and design, critical revision of the manuscript for important intellectual content, and study supervision. All authors contributed to the article and approved the submitted version.

FUNDING

This research is supported by the CAMS Innovation Fund for Medical Sciences (CIFMS)2021-I2M-1-002.

ACKNOWLEDGMENTS

The authors would like to thank the Chinese Academy of Medical Sciences Innovation Fund for Medical Sciences (CIFMS2021-I2M-1-002), and all of the participants in this study.

SUPPLEMENTARY MATERIAL

The Supplementary Material for this article can be found online at: https://www.frontiersin.org/articles/10.3389/fendo.2022.835570/full#supplementary-material

REFERENCES

1. Finsterer J, Frank M. Maternally Inherited Diabetes and Deafness Is a Mitochondrial Multiorgan Disorder Syndrome (MIMODS). *Acta Diabetologica* (2017) 54(10):979–80. doi: 10.1007/s00592-017-1029-3
2. Xiang K. Specific Types of Diabetes. *Nat New Books Inform* (2013) (12):99–100. doi: CNKI:SUN:QGXS.0.2013-12-015.
3. van den Ouweland JM, Lemkes HH, Ruitenbeek W, Sandkuijl LA, de Vijlder MF, Struyvenberg PA, et al. Mutation in Mitochondrial Trna(Leu)(UUR) Gene in a Large Pedigree With Maternally Transmitted Type II Diabetes Mellitus and Deafness. *Nat Genet* (1992) 1(5):368–71. doi: 10.1038/ng0892-368
4. Ballinger SW, Shoffner JM, Hedaya EV, Trounce I, Polak MA, Koontz DA, et al. Maternally Transmitted Diabetes and Deafness Associated With a 10.4 Kb Mitochondrial DNA Deletion. *Nat Genet* (1992) 1(1):11–5. doi: 10.1038/ng0492-11
5. Murphy R, Turnbull DM, Walker M, Hattersley AT. Clinical Features, Diagnosis and Management of Maternally Inherited Diabetes and Deafness (MIDD) Associated With the 3243A>G Mitochondrial Point Mutation. *Diabetic Med: J Br Diabetic Assoc* (2008) 25(4):383–99. doi: 10.1111/j.1464-5491.2008.02359.x
6. Wang S, Wu S, Zheng T, Wang L, Lu H. Analysis of Clinical Features of Diabetes Mellitus With Nt3243a→G Mutation in Mitochondrial Trna^Leu (UUR) Gene. *Chinese J Med Gen* (2009) 26(2):5. doi: 10.3760/cma.j.issn.1003-9406.2009.02.016
7. Guo J, Zhou F, Chen Y, Liu C. A Case of Mitochondrial Diabetes Mellitus With Initial Onset of Gestational Diabetes and Review of the Literature. *Chinese J Diabetes Mellitus* (2020) 12(6):415–418. doi: 10.3760/cma.j.cn115791-20191110-00416.
8. Tabebi M, Safi W, Felhi R, Alila Fersi O, Keskes L, Abid M, et al. The First Concurrent Detection of Mitochondrial DNA M.3243A>G Mutation, Deletion, and Depletion in a Family With Mitochondrial Diabetes. *Mol Genet Genomic Med* (2020) 8(7):e1292. doi: 10.1002/mgg3.1292
9. Ramakrishna MP, Pavithran PV, Bhavani N, Kumar H, Nair V, Menon AS, et al. Mitochondrial Diabetes: More Than Just Hyperglycemia. *Clin Diabetes: Publ Am Diabetes Assoc* (2019) 37(3):298–301. doi: 10.2337/cd18-0090
10. Inoue T, Murakami N, Ayabe T, Oto Y, Nishino I, Goto Y, et al. Pyruvate Improved Insulin Secretion Status in a Mitochondrial Diabetes Mellitus Patient. *J Clin Endocrinol Metab* (2016) 101(5):1924–6. doi: 10.1210/jc.2015-4293
11. Ylikallio E, Suomalainen A. Mechanisms of Mitochondrial Diseases. *Ann Med* (2012) 44(1):41–59. doi: 10.3109/07853890.2011.598547
12. Gorman GS, Chinnery PF, DiMauro S, Hirano M, Koga Y, McFarland R, et al. Mitochondrial Diseases. *Nat Rev Dis Primers* (2016) 2:16080. doi: 10.1038/nrdp.2016.80
13. Delaney NF, Sharma R, Tadvalkar L, Clish CB, Haller RG, Mootha VK. Metabolic Profiles of Exercise in Patients With Mcardle Disease or Mitochondrial Myopathy. *Proc Natl Acad Sci USA* (2017) 114(31):8402–7. doi: 10.1073/pnas.1703338114
14. Hanisch F, Müller T, Muser A, Deschauer M, Zierz S. Lactate Increase and Oxygen Desaturation in Mitochondrial Disorders–Evaluation of Two Diagnostic Screening Protocols. *J Neurol* (2006) 253(4):417–23. doi: 10.1007/s00415-006-0987-0
15. Oka Y, Katagiri H, Ishihara H, Asano T, Kikuchi M, Kobayashi T. Mitochondrial Diabetes Mellitus–Glucose-Induced Signaling Defects and Beta-Cell Loss. *Muscle Nerve Supplement* (1995) 3:S131–6. doi: 10.1002/mus.880181426
16. Finsterer J. The MELAS Phenotype may Not Only be Determined by Heteroplasmy of Causative Mtdna Variants. *Eur J Endocrinol* (2021) 184(3): L5–l6. doi: 10.1530/EJE-20-1248
17. Gerbitz DK, Gempel K, Brdiczka D. Mitochondria and Diabetes. Genetic, Biochemical, and Clinical Implications of the Cellular Energy Circuit. *Diabetes* (1996) 45(2):113–26. doi: 10.2337/diabetes.45.2.113
18. Zhou M-C, Min R, Ji J, Zhang S, Tong A, Xu J, et al. Association of Clinical Features With Mitochondriai DNA 3243 a to G Mutation Heteroplasmy Levels in Patients With Maternally Inherited Diabetes and Deafness. *Chin J Endocrinol Metab* (2016) 32(1):33–7. doi: 10.3760/cma.j.issn.1000-6699.2016.01.009
19. Lebbar M, Timsit J, Luyton C, Marchand L. Glucagon-Like Peptide-1 Receptor Agonists (GLP1-RA) in the Treatment of Mitochondrial Diabetes. *Acta Diabetol* (2021) 58(9):1281–82. doi: 10.1007/s00592-021-01729-3

20. Yeung RO, Jundi MA, Gubbi S, Bompu ME, Hannah-Shmouni FJ. Complications I. Management of Mitochondrial Diabetes in the Era of Novel Therapies. *J Diabetes Complications* (2020) 35(1):107584. doi: 10.1016/j.jdiacomp.2020.107584

Conflict of Interest: The authors declare that the research was conducted in the absence of any commercial or financial relationships that could be construed as a potential conflict of interest.

Publisher's Note: All claims expressed in this article are solely those of the authors and do not necessarily represent those of their affiliated organizations, or those of the publisher, the editors and the reviewers. Any product that may be evaluated in this article, or claim that may be made by its manufacturer, is not guaranteed or endorsed by the publisher.

frontiers in Endocrinology

REVIEW
published: 01 March 2022
doi: 10.3389/fendo.2022.829565

HNF1A:From Monogenic Diabetes to Type 2 Diabetes and Gestational Diabetes Mellitus

Li-Mei Li[1], *Bei-Ge Jiang*[2*] *and Liang-Liang Sun*[3*]

[1] Research Center for Translational Medicine, Key Laboratory of Arrhythmias of the Ministry of Education of China, Shanghai East Hospital, Tongji University School of Medicine, Shanghai, China, [2] Third Department of Hepatic Surgery, Eastern Hepatobiliary Surgery Hospital, Naval Medical University, Shanghai, China, [3] Department of Endocrinology and Metabolism, Changzheng Hospital, Naval Medical University, Shanghai, China

Diabetes, a disease characterized by hyperglycemia, has a serious impact on the lives and families of patients as well as on society. Diabetes is a group of highly heterogeneous metabolic diseases that can be classified as type 1 diabetes (T1D), type 2 diabetes (T2D), gestational diabetes mellitus (GDM), or other according to the etiology. The clinical manifestations are more or less similar among the different types of diabetes, and each type is highly heterogeneous due to different pathogenic factors. Therefore, distinguishing between various types of diabetes and defining their subtypes are major challenges hindering the precise treatment of the disease. T2D is the main type of diabetes in humans as well as the most heterogeneous. Fortunately, some studies have shown that variants of certain genes involved in monogenic diabetes also increase the risk of T2D. We hope this finding will enable breakthroughs regarding the pathogenesis of T2D and facilitate personalized treatment of the disease by exploring the function of the signal genes involved. Hepatocyte nuclear factor 1 homeobox A (HNF1α) is widely expressed in pancreatic β cells, the liver, the intestines, and other organs. HNF1α is highly polymorphic, but lacks a mutation hot spot. Mutations can be found at any site of the gene. Some single nucleotide polymorphisms (SNPs) cause maturity-onset diabetes of the young type 3 (MODY3) while some others do not cause MODY3 but increase the susceptibility to T2D or GDM. The phenotypes of MODY3 caused by different SNPs also differ. MODY3 is among the most common types of MODY, which is a form of monogenic diabetes mellitus caused by a single gene mutation. Both T2D and GDM are multifactorial diseases caused by both genetic and environmental factors. Different types of diabetes mellitus have different clinical phenotypes and treatments. This review focuses on HNF1α gene polymorphisms, HNF1A-MODY3, HNF1A-associated T2D and GDM, and the related pathogenesis and treatment methods. We hope this review will provide a valuable reference for the precise and individualized treatment of diabetes caused by abnormal HNF1α by summarizing the clinical heterogeneity of blood glucose abnormalities caused by HNF1α mutation.

Keywords: HNF1α, polymorphism, heterogeneity, MODY3, type 2 diabetes, gestational diabetes mellitus

OPEN ACCESS

Edited by:
Ming Liu,
Tianjin Medical University General Hospital, China

Reviewed by:
Michael A. Weiss,
Indiana University, United States
Juan Zheng,
Sun Yat-sen University, China

***Correspondence:**
Bei-Ge Jiang
jiang_beige@aliyun.com
Liang-Liang Sun
sun_lliang@smmu.edu.cn

Specialty section:
This article was submitted to Diabetes: Molecular Mechanisms, a section of the journal Frontiers in Endocrinology

Received: *06 December 2021*
Accepted: *03 February 2022*
Published: *01 March 2022*

Citation:
Li LM, Jiang BG and Sun LL (2022) HNF1A : From Monogenic Diabetes to Type 2 Diabetes and Gestational Diabetes Mellitus. Front. Endocrinol. 13:829565. doi: 10.3389/fendo.2022.829565

INTRODUCTION

According to the International Diabetes Federation (IDF), there were approximately 463 million adults with diabetes worldwide in 2019. The incidence is increasing, and this value will reach 700 million in 2045 (1). Diabetes has become a considerable public health problem that substantially impacts society and the families of patients (2). The disease is currently divided into four categories: type 1 diabetes (T1D), type 2 diabetes (T2D), gestational diabetes mellitus (GDM) and other special types of diabetes mellitus (3). The clinical manifestations of the different types of diabetes are similar, which greatly hinders the classification of the disease (4). Moreover, there is heterogeneity in the clinical phenotypes of the disease under the same type, which makes the clinical diagnosis of the diabetes type more difficult (4). Correctly diagnosing the type of diabetes is essential for precise treatment. The high heterogeneity of diabetes blurs the classic distinction between diabetes types. Interpreting the heterogeneity has become a major focus in diabetes research. It is necessary to establish a more accurate classification of diabetes. This will enable the precise and personalized treatment of diabetes, including the provision of more appropriate care, the development of hypoglycemic drugs, and the prevention/treatment of complications.

The most common types, i.e., T1D, T2D, and GDM, are multifactorial syndromes related to various gene effects and environmental factors (5). Two rare types, i.e., neonatal diabetes mellitus (NDM) and maturity-onset diabetes of the young (MODY), are caused by a single gene mutation (5, 6). MODY is a type of monogenic diabetes characterized by early-onset (age of diagnosis is usually before 25), autosomal dominant inheritance, no autoimmune process or insulin resistance, retention of endogenous insulin secretion, and no dependence on insulin (7). It is estimated that MODY accounts for approximately 1-2% of all diabetic cases (7). The pathogenesis of T2D and GDM is unclear. T2D is the most important type of diabetes and accounts for more than 90% of the total number of diabetic patients (3). Studies have shown that some monogenic diabetes genes are involved in T2D, with some variants significantly increasing the risk of T2D (8). T2D and GDM have solid genetic factors. Monogenic diabetes provides a good resource for elucidating the pathogenesis and developing personalized care for T2D and GDM. Substantial progress has been made in the research and development of hypoglycemic drugs targeting monogenic diabetes. This has provided the inspiration to further explore the pathogenesis and develop personalized treatments for T2D by studying the monogenic diabetes genes.

Hepatocyte nuclear factor 1α (HNF1α or HNF1A), also known as the MODY3 gene, is the pathogenic gene for MODY3 (7).Common types of HNF1α mutations cause MODY3. Other mutations do not cause MODY3 but significantly increase the risk of T2D, while others increase the risk of GDM. Hyperglycemia in MODY3 is caused by single-gene abnormalities. Unlike the pathogenesis of MODY, a large number of basic and clinical experiments show that T2D and GDM result from genetic and environmental factors. These two factors interact with each other to promote the occurrence of T2D or GDM. Why do different HNF1α mutations cause different types of diabetes? Answering these questions may improve our understanding of diabetes and advance the precise treatment of diabetes. In this review, we first summarize and discuss the relationship between HNF1α gene polymorphisms, MODY3, T2D, and GDM. We then explore the mechanism of hyperglycemia caused by HNF1α mutation by discussing the role of HNF1α in the islets and liver. Finally, we explore the reason why different HNF1α mutations can lead to different types of diabetes by analyzing the protein structure and function. We hope our review will facilitate a more comprehensive understanding of hyperglycemia caused by HNF1α mutation and will be useful for accurate diagnosis and treatment of diabetes, especially the hyperglycemia caused by HNF1α.

POLYMORPHISM OF HNF1A GENE

Human HNF1α is located at q24.31 on chromosome 12 (9) and is a widely expressed tissue-specific transcription factor (10). In the liver, HNF1α regulates numerous liver-specific genes and participates in the metabolism of glucose, fat, and other substances (11–13). In the pancreas, HNF1α controls many pancreatic-specific genes involved in β-cell maturation, growth, and insulin secretion (14–16). The HNF1α gene has a large number of polymorphisms with no specific mutation hotspots, and 894 variants are listed in the Exome Aggregation Consortium (ExAC) database. In total, 1231 variants can be queried from Genome Aggregation Database (gnomAD) (17). These variants range from the HNF1α promoter to the 3' untranslated region (UTR), including missense, translocation, nonsense, splice mutation, in-frame amino acid deletion, insertion, duplication, or partial and whole gene deletion (17).

Although mutations have been observed in all exons, they are most often detected in exons 2 and 4 (**Figures 1**, **2**). Among them, the mutation of exon 4 (p291fsinsc) is the most common (18). In a study of 414 different mutations in 1247 families carrying the HNF1α gene, the most common mutations were missense mutations (55%), frameshifts (22%), splice sites (9%), promoter region mutations (2%) and deletions (1.2%) (19). The mutations caused by these SNPs are as follows: 1) The mutation is located in the exon region and causes the substitution of an amino acid in HNF1α, resulting in a missense mutation (20). 2) The mutation is located in the exon region and causes abnormal shear in the HNF1α transcript (20). For example, although no RNA has been obtained from patients to prove this hypothesis, a synonymous mutation in HNF1α (c.1623 G > A, p.Gln541Gln) involving the last nucleotide of exon 8 was predicted to affect RNA splicing (21). 3) Mutations located in intron regions may generate new splice sites, resulting in pseudoexons (22, 23). 4) The mutation may be located in the promoter region, resulting in reduced gene expression (20).

ASSOCIATION BETWEEN HNF1A POLYMORPHISM AND MODY3

HNF1A-MODY3 is characterized as familial diabetes (9, 24). Hyperglycemia usually becomes evident and deteriorates during

puberty or early adulthood. Approximately 25% of HNF1A-MODY patients have typical polydipsia, polyuria, polyphagia, and emaciation symptoms in the initial stage, but most patients have none of the above clinical manifestations and only present elevated postprandial blood glucose, usually without ketosis (24, 25). Such patients usually show mild osmotic symptoms (polyuria and polydipsia) or asymptomatic postprandial hyperglycemia, without ketosis or ketoacidosis at age 6-25 (26). However, the clinical symptoms of HNF1A-MODY are very different. The clinical characteristics of HNF1A-MODY differ between and within families, which complicates the diagnostic process. In addition, different MODY3 patients exhibit great heterogeneity in the first-line use of sulfonylureas and the occurrence of complications. Therefore, we hope to provide some valuable information for MODY3 diagnosis, accurate treatment, and early intervention for other carriers of the same mutation in the same family before the occurrence of relevant clinical symptoms by summarizing some significant clinical features of MODY3.

Clinical Heterogeneity in MODY3

Thus far, hundreds of distinct HNF1α SNPs have been found to cause MODY3 (**Figure 1** and **Supplementary Table 1**). The genetic diversity of MODY3 leads to heterogeneity in the MODY3 clinical phenotype. However, environmental factors also contribute to the clinical heterogeneity of MODY3. The main clinical heterogeneities in MODY3 are listed below.

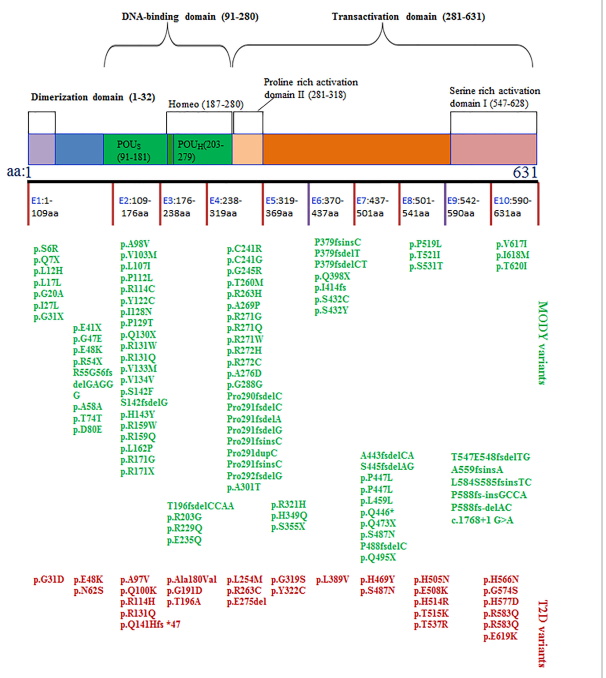

FIGURE 1 | The structure of HNF1α protein and the SNPs associated with MODY3 or T2D. The SNPs in blue often cause MODY3. The SNPs in red often cause T2D.

Family History

As a case of autosomal dominant inherited disease, MODY3 patients usually have a family history of diabetes (9, 27, 28). Some studies suggest that the probability of a family history of MODY3 is more than 20 times higher than that of T1D (29). However, some MODY patients may lack a family history of diabetes, possibly due to the following factors (1): the probability of new HNF1A-MODY mutations may be more frequent than expected, and (2) the family members of the patients were not diagnosed because of mild clinical symptoms and signs (29, 30).

Age of Onset

Comparing the age of diabetes induced by HNF1α mutation in the literature revealed the age of onset of diabetes was generally 10-16 years (**Table 1**). This finding may be attributed to the high genetic penetrance of the HNF1α mutation and is consistent with previously reported conclusions. It has been reported that 63% of carriers are younger than 25 years, 79% are younger than 35 years, and 96% are younger than 55 years (39). The average age of an HNF1A-MODY diagnosis is 14 years, and the disease is rarely diagnosed in children under 10 years old (40). This finding is consistent with our statistical data (**Table 1**).

The location of the mutation determines the age of diagnosis of abnormal blood glucose. As shown in **Supplementary Table 1** and **Table 1**, the SNPs that cause MODY3 are concentrated in exons 1, 2, and 4, with relatively few SNPs in exons 8-10. Bellanne-Chantelot C et al. reported that patients with exon 8-10 mutations were diagnosed with HNF1A-MODY3 8 years later than those with exon 1-6 mutations (41). We found that patients with mutations affecting the dimerization domain or the DNA binding domain had a lower onset age (**Table 1** and **Figure 1**). Patients with truncated mutations had a lower onset age than those with missense mutations. The above findings may indicate that the DNA binding region of HNF1α plays a more important role in regulating blood glucose, and the domain that forms a dimer plays the second most important role.

An individual's genetic background and environment may also affect the onset age of HNF1A-MODY3. For example, intrauterine exposure (mutation inherited by the mother and hyperglycemia during pregnancy) can lead to an early onset age of less than 12 years (25). There are also differences in the age of onset with the same SNP. For example, a survey of MOD3 in Britain uncovered five diabetes patients in three generations of the same family with the R54X genotype (34, 35). Among them, the proband and his brother, mother, and grandmother were diagnosed with diabetes at puberty, while their uncle carried the same SNP and was only diagnosed with T2D at the age of 29 (24). Another family from China also exhibited a difference in the onset age of diabetes with R54X SNPs (35). The daughter was diagnosed with MODY3 at the age of 19, while the mother was first diagnosed with T2D at the age of 27. Among the above six R54X carriers (**Table 2**), 50% were first diagnosed with diabetes before the age of 25 years, which conforms to the standard age of diagnosis for MODY3. However, 50% of the diagnoses occurred at an age over 25, but all occurred before the age of 30. Therefore, HNF1α may play decisive roles in the development of abnormal blood glucose, but personal living habits, including eating, daily

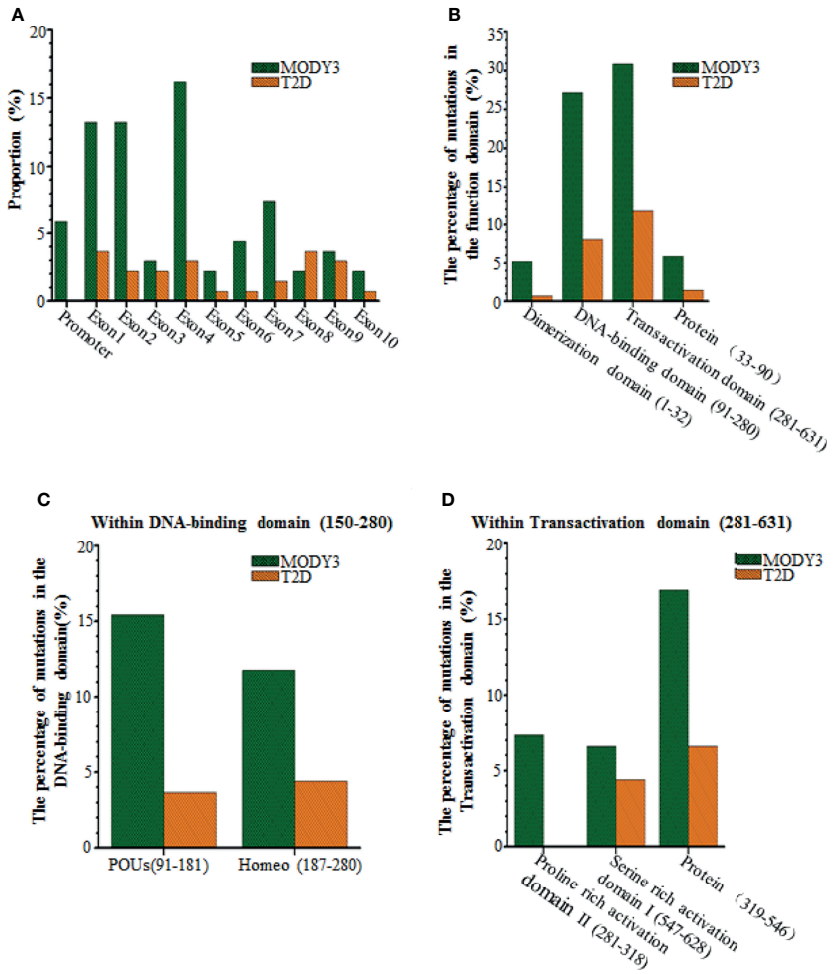

FIGURE 2 | Comparisons of the HNF1a SNPs causing MODY3 with the HNF1a SNPs causing T2D. **(A)** Location within the promoter and 10 exons, **(B)** Location within the functional domains of HNF1α protein, **(C)** Location within DNA-binding domain of HNF1α protein, **(D)** Location within transactivation domain of HNF1α protein.

life, physical exercise, and other genetic factors that can cause abnormal metabolism, also play a role. Therefore, although a single HNF1α gene mutation is the cause of MODY3, environmental factors also play a role in its pathogenesis.

Insulin

The basal insulin level and insulin response to corresponding high glucose stimulation differ among patients with HNF1A-MODY3. Byrne MM et al. found that some patients with MODY3 had normal fasting blood glucose, while others had very high fasting blood glucose (42). Compared to those with normal blood glucose, the basal insulin secretion of the MODY3 patients was lower, but their insulin secretion increased in response to high-glucose stimulation; some patients showed a limited change, while others patients showed a decrease (42). This finding may indicate that HNF1α plays a direct role in regulating insulin secretion in islet β cells in response to high glucose or other stimuli. The difference may be a result of different mutations in HNF1α.

Glycosuria

Patients with HNF1α mutations may exhibit glycosuria; however, not all HNF1A-MODY patients do. Some studies have found that diabetes accounts for approximately 30-40% of all HNF1A-MODY patients (40, 43). For example, a study involving 11 HNF1A-MODY patients in Japan found that about 36% of HNF1A-diabetic patients experienced renal dysfunction (43). Another survey by Amanda Stride et al. also showed similar results (40). These authors found that 38% of mutation carriers developed glycosuria (40) 2 hours after oral glucose. Glycosuria in MODY3 may be caused by an impaired renal tubular transport of glucose and reduced glucose reabsorption in the proximal renal tubules (40, 44, 45). The renal glucose threshold of glucose reabsorption is low.

The renal glucose threshold of HNF1A-MODY patients is lower than that of healthy individuals with positive urine glucose, likely because HNF1α regulates the expression of the glucose transporter sodium-glucose cotransporter 2 (SGLT2) in the kidney because HNF1α can bind the promoter region of

TABLE 1 | Comparison of the onset ages of diabetes caused by different MODY3 associated SNPs.

Location		Nucleotide Change at DNA Level	Mutation	Age of Onset of the Subject (Yrs, range)	BMI	Ref
Genomical DNA	Codon					
Promoter	Promoter	g.-58A>C	HNF4a binding site	22/23	NA	(31)
Exon 1	47	c.140G>A	p.G47E	12	NA	(32)
Exon 1	48	c.142C>A	p.E48K	12	NA	(33)
Exon 1	54	c.160C>T	p.R54X	14-29	21.6-29.7	(34, 35)
Exon 1	103	c.307G>A	p.V103M	25	23.6	(36)
Exon 1	107	c.319C>G	p.L107I	23.5 ± 5.8 (6/2)	25.3 ± 3.5	(37)
Exon 2	112	c.335C>T	p.P112L	9.9	20.3	(38)
Exon 2	114	c.340C>T	p.R114C	21	22.6	(36)
Exon 2	128	c.383T>C	p.I128N	16	21.2	(27)
Exon 2	131	c.392C>T	p.R131W	10-20	NA	(32)
Exon 2	143	c.427C>T	p.H143Y	7	21.5	(27)
Exon 2	171	c.511C>G	p.R171G	21	18.2	(36)
Exon 2	171	c.511C>T	p.R171X	11-26	NA	(32)
Exon 3	196	c.587_590delCCAA	T196fsdelCCAA	31	NA	(32)
Exon 3	229	c.686G>A	p.R229Q	21-36	NA	(32)
Exon 3	235	c.703G>C	p.E235Q	23	20.8	(36)
Intron 3	Intron	c.714-1G>A	IVS3–1G>A	24	NA	(32)
Exon 4	241	c.721T>G	p.C241G	12	NA	(33)
Exon 4	245	c.733G>C	p.G245R	25	25.5	(36)
Exon 4	263	c.788G>A	p.R263H	17	16.3	(36)
Exon 4	263	c.787C>T	p.R263C	13-27	NA	(32)
Exon 4	271	c.812G>A	p.R271Q	14	16.6	(36)
Exon 4	271	c.811C>T	p.R271W	16	NA	(32)
Exon 4	276	c.827C>A	p.A276D	24	NA	(32)
Exon 4	291	c.873delA	Pro291fsdelA	12	NA	(33)
Exon 4	291	c.8743elC	P291fsinsC	6-54	NA	(32)
Exon 5	349	c.1047C>G	p.H349Q	23	24.2	(36)
Exon 6	379	c.1136-1137delT	P379fsdelT	13	21.4	(27)
Exon 6	379	c.1136-1137delCT	P379fsdelCT	11-20	NA	(32)
Exon 7	445	c.1333_1334delAG	S445fsdelAG	12–13	NA	(32)
Exon 7	447	c.1340C>T	p.P447L	18	22.1	(27)
Exon 7	447	c.1340C>G	p.P447L	17	NA	(32)
Exon 7	487	c.1460G>A	p.S487N	20	18.9	(36)
Exon 8	531	c.1592G>C	p.S531T	35	NA	(32)
Exon 9	559	c.1677^1678insA	A559fsinsA	19	22.9	(27)

NA, Not available.

SGLT2 (46). In general, HNF1α needs to form a dimer to regulate the transcriptional expression of its target gene (11, 47). Both HNF1α and HNF1β are the most common transcription factors in the HNF transcription factor family and play important roles in the pancreas, liver, and kidney (10). These factors often form heterodimers (48). It has been reported by several groups that all diabetic patients with HNF1β mutations exhibit renal dysfunction (43, 49, 50). These research results imply that HNF1β plays a more dominant role in the kidney than HNF1α.

We found that HNF1α SNPs related to glycosuria were mainly concentrated in the dimer domain and DNA binding domain of HNF1α (**Table 3**), indicating that HNF1α regulates the transcription of genes that control the renal glucose threshold along with other transcription factors, likely by forming a dimer with HNF1β to regulate the genes involved in glucose transport

TABLE 2 | The clinical characteristics of two R54X variants from different countries.

Pedigree	Kindred/Generation Subject	Sex	Relation	Age at Diagnosis	BMI	Treatment	Ref
A family from U.K.	I: 2	F	Grandmather	Adolescence	NA	Insulin	(34)
	II: 1	F	Mother	18	25.2	Insulin	
	II: 2	M	Mother's brother	29	NA	NA	
	III: 1	M	Proband	14	29.7	Insulin	
	III: 2	M	Brother	17	21.6	Insulin	
B family from China	I: 1	F	Mother	27	NA	sulphonylurea (gliclazide)	(35)
	II: 1	F	Proband	19	22	insulin,glybenclamide	

NA, Not available.

TABLE 3 | The HNF1A SNPs associated glycosuria.

Location		Nucleotide Change at DNA Level	Mutation	Age of Onset of the Subject (Yrs)	Sex	IBM	Ref
Genomical DNA	Codon						
Exon 1	31	c.92G>A	p.G31D	15	Male	15.9	(51)
Exon 1	55,56	c.161-165delGAGGG	R55G56fsdelGAGGG	17	Male	24.6	(46)
Exon 1	98	c.283C>T	p.A98V	5	Male	NA	(52)
Exon 2	142	c.425C>T	p.S142F	9	Female	27.2	(46)
Exon 2	171	c.511C>T	p.R171X	14	Female	20.9	(46)
Exon 3	224	c.670C>T	p.P224S	NA	Male	NA	(44)
Exon 3	230-236	c.687_707del	p.E230_C236del	13	Female	22	(53)
Exon 4	272	c.815G>A	p.R272H	NA	Male	NA	(54)
Intron 5	Splice site	c.955+2 T>A	IVS5nt + 2T→A	20	Male	24.1	(46)
Exon 4	271	c.811C>T*	p.R271W	15	Female	NA	(55)
Intron 7	Splice site	c.1502-6G>A*	IVS7nt-6G>A	17	Female	NA	(55)

**This SNP was related to Renal malformations.*
NA, Not available.

or reabsorption in the kidney. However, this hypothesis is only our speculation and needs to be further confirmed *via* by experiments.

Cardiovascular System

HNF1A-MODY is a type of nonketotic diabetes characterized by progressive hyperglycemia in childhood, adolescence, and early adulthood and has a high risk of chronic microvascular complications (56, 57). The plasma glucose of patients deteriorates with age, and the risk of microvascular complications increases. In addition to the cardiovascular burden caused by uncontrolled blood glucose, some studies have found that some SNPs can increase the risk of vascular and cardiac diseases, such as I27L, A98V, and S487N (57). Some SNPs are closely related to dyslipidemia, a significant independent risk factor for cardiovascular abnormalities (58). This association may be related to the involvement of HNF1α in the synthesis of liver-related lipoproteins and liver lipid metabolism.

Some researchers reported that the incidence of cardiovascular and microvascular complications is similar to that in patients with T1D and T2D and is associated with poor glycemic control (25, 56, 59). However, Babaya N, et al. reported that the concentration of high-density lipoprotein cholesterol (HDL-C) in HNF1A-MODY (I27L carrier) is higher than that in normal individuals (60). HDL-C can reduce cardiovascular risk; thus, the incidence rate of coronary heart disease in HNF1A-MODY patients with I27L carrier may be lower than that in T1D patients and T2D patients.

Cancer

Recent studies showed that MODY3 is a risk factor for pancreatic cancer (61, 62). HNF1α gene mutation is related to pancreatic, liver, and kidney tumors (63–66). It has been reported that HNF1α mutations (p.E32 * and p.L214Q) are related to hepatocellular tumors (67). Somatic HNF1α mutations are found in approximately 1% to 2% of hepatocellular carcinomas and usually occur in adenomas. HNF1α mutations increase the risk of the malignant transformation of hepatocellular adenomas (67).

Treatment

HNF1A-MODY3 can cause severe diabetic retinopathy, diabetic nephropathy, diabetic peripheral neuropathy, and other complications (59). Therefore, early diagnosis and timely treatment are very important for blood glucose control, delaying the occurrence and development of complications and improving the quality of life.

The phenotype of HNF1A-MODY is characterized by mild nonprogressive hyperglycemia, progressive hyperglycemia, and hyperglycemia with extra-pancreatic characteristics (25, 26). In patients diagnosed with mild hyperglycemia, diet seems to be a reasonable and effective treatment strategy; however, in the case of progressive hyperglycemia, pharmacological methods should be attempted (68, 69). The treatment of HNF1A-MODY patients depends on their age and HbA1c level (64). Patients with HNF1α mutations are very sensitive to the oral hypoglycemic drug sulfonylurea (70, 71). It is speculated that this may be due to the decreased liver clearance of some sulfonylurea derivatives in patients with HNF1α gene mutations, resulting in an increase in serum levels (72). The increased circulating levels of these drugs could explain the enhanced efficacy. The response of HNF1A-MODY patients to sulfonylureas is five times higher than that to standard metformin (73). However, in T2D, the efficacy of the two drugs has been demonstrated to be almost the same (73). Sulfonylureas usually control blood glucose better than insulin therapy in patients with HNF1A-MODY, and the fasting hypoglycemic effect is also good (70). HNF1A-MODY patients show obvious sensitivity to oral sulfonylurea drugs. The failure of sulfonylurea treatment is rare and occurs in only a few patients with the c.618G>A mutation (74). Therefore, low-dose sulfonylurea drugs (such as 20-40 mg/day gliclazide) are preferred for long-term treatment and should be regarded as the first-line treatment for HNF1A-MODY (73).

However, studies have shown that patients with some variants no longer respond to the above treatments. Patients with p.His126Asp do not respond to sulfonylureas (low and high doses), dipeptidyl peptidase-4 inhibitors (DPP-4 inhibitors), or glucagon-like peptide-1 receptor agonists (GLP-1Raa), also known as incretin analogs (75). Low-dose sulfonylurea therapy is the first-line therapy for MODY3 but does not show special

sensitivity to HNF1α-related T2D (76). For example, Mexican carriers of the HNF1α p.E508K variant have no increased sensitivity to sulfonylureas (76).

In a word, HNF1A-MODY is a disease with genetic and clinical heterogeneity. However, MODY3 still has strong common characteristics. Patients with HNF1A-MODY usually have low high-sensitivity C-reactive protein (hsCRP) levels (77, 78). In addition, although MODY3 is a type of monogenic diabetes, the severity can differ with different genetic backgrounds and environmental factors. Previously, MODY3 patients were generally not overweight or obese and lacked other risk factors for T2D, such as hypertension or dyslipidemia (79). However, as an increasing number of people have become overweight or obese, individuals with MODY3 may also be overweight or obese. According to statistics, nearly 30% of HNF1A-MODY patients in the United States are overweight or obese, rendering the differential diagnosis between HNF1A-MODY3 and T2D more difficult (80). Therefore, although some clinical guidelines for MODY3 diagnosis exist, HNF1A-MODY3 patients often fail to meet all diagnostic criteria or are misdiagnosed with T1D or T2D.

ASSOCIATION BETWEEN HNF1A POLYMORPHISM AND T2D

Studies have found that some HNF1α SNPs do not cause MODY3 but increase the susceptibility to T2D (**Supplementary Table 1**). A large-scale association analysis of a group of people mainly of European ancestry showed that the T2D susceptibility loci existed near HNF1α (81). Moreover, SNPs related to T2D are closely related to race. The p.E508K variant was found only in T2D patients in Mexico (82). The rare p.A98V allele may be associated with T2D in the Caucasian population (83). However, the p.A98V allele does not appear to be associated with T2D in Asian populations (84). Among them, the most famous locus is G319S. The G319S polymorphism of HNF1α is positively correlated with the high prevalence of T2D in Canadian Aborigines (85, 86).

Gene sequencing revealed that the G319S mutation in HNF1α was associated with an increased incidence rate of T2D in the Oji Cree ethnic group in Canada. The specific and positive predictive values of G319S carriers suffering from T2D before the age of 50 were 97% and 95%, respectively (87). G319S is associated with a distinct form of T2D characterized by onset at an earlier age, higher postprandial plasma glucose, and lower body mass index (BMI) (85). In patients with T2D, compared to those with G319/G319, the BMIs of individuals with S319/S319 and S319/G319 were significantly lower, and postprandial blood glucose was significantly higher (85). In nondiabetic individuals, the plasma insulin of S319/G319 heterozygotes was significantly lower than that of G319/G319 homozygotes (85). A lower BMI coupled with the decrease of insulin secretion before the onset of diabetes is the pre-diabetic physiologic state of individuals with HNF1A-T2D. This group is different from those with other types of T2D caused by other genes. The latter group is often generally obese and has a high BMI with insulin resistance before obvious diabetes. Moreover, smoking appears to increase the risk of diabetes in HNF1α G319S carriers (88). G319s is located in HNF1α transactivation sites, which are rich in proline II domains (**Figure 1**), with changes in conserved glycine residues. The function of the protein carrying the G319S mutation was found to be impaired *in vitro* (87), and the transcription ability was reduced by approximately 50% (88). However, this mutation did not affect DNA binding or protein stability. There is no evidence that the mutant protein has a dominant-negative effect. The G319S mutation affected the transcriptional shear of HNF1α. Two abnormal transcripts and an alteration in the relative balance of normal splicing products were produced by the G319S variant (89). Two abnormal transcripts present only in the G319S cells included premature termination codons resulting from the inclusion of seven nucleotides from intron 4 or the deletion of exon 8. A novel isoform lacking the terminal 12 bases of exon 4 was increased compared with that in control cell lines and human pancreatic tissue. The combination of the reduced activity of the G319S protein and abnormal splicing transcripts may increase the susceptibility to diabetes.

HNF1A-SNPs associated with T2D only increase the risk of T2D. Obvious T2D requires other factors, such as genetic and/or environmental factors. An interesting example can be found in stories of a new HNF1α variant c.539C >T (p.Ala180Val) in two families in Norway (90). There was an obvious difference in the probability of T2D between these two families (90). p.Ala180Val is a mutation that affects highly conserved amino acid residues in proteins. The HNF1α mutant p. Ala180Val does not cause MODY3 but may increase the risk of T2D. This variation was found to be completely separate from diabetes in one family (family A), but the data did not support its role as a pathogenic factor of MODY3. In the other family (family B), there was no clear genotype/phenotype correlation. Two diabetic patients and one individual with normal plasma glucose levels in this family were homozygous mutation carriers. In family A, the mutation carriers had similar metabolic syndromes, including obesity, diabetes, hypertension, and dyslipidemia. Moreover, the nonmutation carriers in the family were overweight or obese, although they had normal blood glucose levels, but they were as overweight or obese as the family members carrying the mutation. Genetic factors may be related to the metabolic abnormalities in family A. Therefore, it can be speculated that HNF1α p.Ala180Val could lead to a certain degree of β cell dysfunction; however, it does not cause significant glycemic abnormalities. The genetic background of family A associated with metabolic abnormalities increased insulin resistance in the HNF1α p.Ala180Val carriers, leading to marked diabetes. In contrast, family B members did not present with obesity or metabolic syndrome, but some female mutation carriers had a history of GDM. Therefore, we can speculate that p.Ala180Val can increase the susceptibility to hyperglycemia but cannot lead to obvious diabetes. Under the influence of additional stress, such as other genetic factors responsible for obesity or pregnancy, p.Ala180Val carriers develop peripheral insulin resistance or

permanent impairment in β cellular function, resulting in marked diabetes. The difference between the two families may be due to the accumulation of the higher-risk variant for T2D in family A. Overall, lifestyle and environmental factors may also play a role in the phenotypic differences.

Low-dose sulfonylurea therapy is the first-line therapy for MODY3 but does not show special sensitivity to T2D. For carriers of HNF1α variants that may cause T2D, dietary treatment is the first recommendation.

ASSOCIATION BETWEEN HNF1A POLYMORPHISM AND GDM

GDM is a common complication of pregnancy that has adverse effects on the short-term and long-term health of women and their children (91). Approximately 2-5% of pregnant women develop GDM during pregnancy, and the incidence rate has significantly increased over the past 10 years (92). GDM is diagnosed when any degree of glucose intolerance occurs during pregnancy for the first time. GDM is also heterogeneous diabetes, with varying degrees of diabetes caused by β cell dysfunction (92). When pancreatic β cells can no longer compensate for the increased insulin resistance during pregnancy, they show varying degrees of glucose intolerance. Although the pathogenesis of the disease is still largely unknown, GDM is considered the result of an interaction between genetic and environmental risk factors. Age, obesity, and a high-fat diet are some important nongenetic factors (93).

Many studies have found that HNF1α SNP increases the risk of GDM. HNF1α is one of the pathogenic genes of GDM in Danish women. The sequencing of 354 Danish GDM patients revealed five diabetes-susceptible variants of HNF1α in seven HNF1α mutation carriers (94). Only those with the Gly288fs* variant were diagnosed with diabetes before the follow-up period and received insulin treatment. The remaining HNF1α mutation carriers were not diagnosed with diabetes before the follow-up period. p.A98V was associated with significant impairment of serum insulin and C-peptide secretion during an oral glucose tolerance test in previously GDM-free glucose-tolerant women (95). The p.I27L polymorphism of HNF1α seems to increase the risk of GDM in Scandinavian women (96). The p.I27L gene was found to increase GDM by increasing insulin resistance in Turkish women (97). In Scandinavian women, the p.I27L polymorphism of HNF1α also increased the risk of GDM (96). The p.I27L TT genotype was associated with an increased risk of preeclampsia in patients with GDM by increasing blood pressure and urinary protein (97). No difference in weight was observed compared to non-diabetic pregnant women with HNF1α mutation during the entire pregnancy.

Pregnant women with HNF1α mutation may develop GDM due to islet dysfunction. Pregnancy is a significant source of stress for women, which leads to the increase of insulin demand. If the need for insulin cannot be met, GDM will gradually develop. Dyslipidemia during pregnancy increases the risk of pregnancy complications. The lipid profile has a strong genetic determinant. In 2017, Xiaojing Wang et al. found that the total cholesterol levels of pregnant women carrying the T alleles of rs1169309 in the HNF1α gene were elevated, which could significantly increase the risk of GDM (98). Insulin resistance may also be involved in the occurrence of GDM.

Compared with other gene mutation carriers, GDM HNF1α mutation carriers exhibit a significant reduction in hsCRP expression (94). hsCRP is encoded by the CRP gene, which has an HNF1α transcription factor-specific binding site (65, 99). SNPs in HNF1α have been associated with CRP levels in different populations (100, 101). The expression of hsCRP in GDM patients is higher than that in HNF1A-MODY patients (84). This finding indicates that GDM caused by HNF1α results in the same susceptibility to diabetes as the T2D variant, but insufficient penetrance leads to clinical MODY.

Dyslipidemia in pregnancy increases the risk of pregnancy complications. Therefore, pregnant women who are HNF1α gene mutation carriers should pay special attention to their health management and consume a reasonable diet during pregnancy. If HNF1α mutation carriers have hyperglycemia during pregnancy, they should not be treated with sulfonylureas and need to be treated with insulin.

MECHANISM OF ABNORMAL BLOOD GLUCOSE ASSOCIATED WITH HNF1A GENE POLYMORPHISM

HNF1α is expressed in embryonic development, infancy, and adulthood. Moreover, the expression distribution has strong tissue specificity, mainly concentrated in the tissues responsible for metabolism, such as the pancreas and liver. Through transcriptomics and antibody-based proteomics, the analysis of human tissue-specific expression showed that the expression level of HNF1α varies in human tissue and controls the transcriptional expression of many genes in the tissue (102). According to incomplete statistics, HNF1α can bind at least 106 target genes in the pancreas (103), which may explain why the mutation location of the HNF1α gene determines the age of diabetes onset. The above results indicated that HNF1α may play varied and important roles in the tissues. Below, we focus on the possible mechanism of HNF1α for glucose homeostasis in the pancreas and liver.

Functions in Pancreas

Maintain the Mature β Cell Function

The dysfunction of mature β cells is the main reason for the hyperglycemia caused by HNF1α. Basal insulin secretion and insulin production corresponding to high glucose stimuli are the basic functions of mature β cells. MODY3 patients have insulin secretion disorder, and the islet secretion function gradually declines as the disease worsens (104). Fasting insulin and glucose-stimulated insulin secretion were found to be abnormal in 40 HNF1α mutation carries from Britain and France (105). The insulin sensitivity was elevated in these individuals as well as the proinsulin to insulin ratio. The

results indicated that HNF1α mutation directly altered basal insulin secretion, rather than glucose sensing insulin secretion. However, a recent islet study of a 33-year-old patient with MODY3, who was misdiagnosed with T1D for 17 years, found that HNF1α causes insulin deficiency diabetes by affecting glucose-stimulated insulin secretion (106). The two results were different, possibly due to different HNF1α variants. In addition, G319S carriers reportedly showed a decrease in insulin secretion before diabetes appeared (85). This indicated islet dysfunction also exists in HNF1A-T2D patients. Therefore, we think HNF1α plays very important and different roles in basal insulin secretion and insulin production corresponding to high glucose stimuli. In order to better study the role of HNF1α in β cell dysfunction, it is necessary to compare the islet function of HNF1α mutants with different degrees of clinical severity to identify the domain of HNF1α involved in the secretion of basic insulin and the domain involved in the secretion of insulin stimulated by high glucose.

HNF1α can regulate many genes involved in insulin secretion (16, 42) and directly bind to the promoter region of the insulin gene, positively regulating the transactivation of the latter. In addition to directly regulating insulin transcription, HNF1α was found to directly regulate the GLUT2 and HNF4 pyruvate kinase genes, which are the key genes involved in cellular insulin secretion (103). In addition, heterozygous HNF1α variations change the expression of key enzymes involved in mitochondrial glucose metabolism (107). In conclusion, HNF1α is an important transcription factor for the maintenance of β cell function, but the specific mechanism needs to be further studied.

Development and Maturation of Islets

HNF1α is involved in the development and maturation of islets. In normal embryonic mouse pancreas, the expression of HNF1α was detected on embryonic day 10.5 (E10.5) (108). When the dominant negative p291fsinsc HNF1α mutation is specifically expressed in β cells (driven by the rat Ins2 promoter), the islets are gradually disordered with reduced cells numbers, and the cells are dispersed in the islet (109, 110). Signs of serious cell damage can be observed, including vacuolization, immature secretory granules, swollen mitochondria, and expanded endoplasmic reticulum (109, 110). Nkx6.1 is a homologous domain transcription factor that plays a role in pancreatic development and the maintenance of mature β cellular function (111). Studies have shown that Nkx6 can directly activate the expression of HNF1α (112). HNF1α in turn directly activates the expression of MafA, which encodes transcription factors produced later in the developing pancreatic transcription program and is expressed only in differentiated insulin hormone positive cells (113).

Some studies indicated that HNF1α is not limited to β cell development and may also affect α cell development. HNF1α whole-body knockout mice died at 6 weeks after birth with small islets and a high α/β ratio (114). This phenomenon is consistent with the islet results for diabetic patients with HNF1α mutation (106). The increased α/β cell ratio may be caused by the slightly higher quality of α cells in the pancreas of these patients. The manifestations of cell hyperfunction, excessive glucagon secretion, weakened negative feedback to glucose, and decreased intestinal glucagon effect are observed in MODY3 patients (115). In 2020, Kazuya Yamagata et al. found HNF1α can inhibit glucagon secretion by regulating SGLT1 expression in α cells (116). HNF1α was found to inhibit α cell characteristics in modeling monogenic diabetes using human embryonic stem cells through mutations in HNF1α (117).

Although further research is needed, it is clear that HNF1α plays a role in pancreatic organogenesis, endocrine and exocrine cell differentiation, and growth by influencing islet specific transcription factors.

Function in Liver

In the liver, HNF1α may affect the balance of blood glucose through regulated glucose and lipid metabolism. HNF1α directly binds to the promoter region of the glucose 6-phosphate transporter (G6PT) gene, the key enzyme of the glucose-6-phosphatase (G6Pase) system, to promote the transcription of the latter (118). Compared with HNF1α (+/+) and HNF1α (+/-) littermates, hepatic G6PT mRNA levels and microsomal G6P transport activity are markedly reduced in HNF1α (-/-) mice (118). The G6Pase system is essential for the maintenance of glucose homeostasis. Thus the HNF1α variant may cause abnormal glucose homeostasis through the G6Pase system. After HNF1α deletion in the liver, the expression of genes encoding fatty acid synthetic enzymes (fatty acid synthase and acyl-CoA carboxylase) and peroxisomal β-oxidation enzymes (CYP4A3, bifunctional enzyme, and thiolase) increased (119). However, the expression of the hepatic fatty acid binding protein (L-FABP) gene decreased significantly (119). Two HNF1α binding sites were found in the 5' promoter region of L-FABP by sequence analysis. Cell experiments confirmed that HNF1α was necessary for the transactivation of L-FABP (119). We speculated that HNF1α mutation may disrupt the balance of the blood glucose through regulating glucose metabolism and adipogenesis.

HNF1α also participates in the transcription of apolipoprotein genes (120, 121). The HNF1α G319S genotype was significantly correlated with the total plasma cholesterol, low-density lipoprotein cholesterol (LDL-C), and apolipoprotein (Apo) B concentration in Oji Cree individuals with T2D (122). In Oji Cree people who did not have T2D, we found that the HNF1α G319S genotype was significantly associated with the plasma concentrations of HDL-C and apolipoprotein AI (123). The phenotype was not related to plasma triglyceride or lipoprotein (a). I27L had a protective effect on hypertriglyceridemia in these individual samples (57). The above studies all indicated that HNF1α plays a role in the lipid profile of diabetic individuals. These data enhance our understanding of the complex interactions among genes, hyperglycemia, and cardiovascular risk factors in T2D. Some studies have shown that a decreased expression of HNF1α increases the risk of fatty liver, which is closely related to insulin resistance (122, 124).

In summary, HNF1α SNPs responsible for the abnormality of blood glucose may be caused by changes in the development, promotion, and death of β cells, the maintenance of mature

pancreatic function, as well as glucose and lipid metabolism in the liver.

RELATIONSHIP BETWEEN HNF1A AND DIFFERENT TYPES OF DIABETES

HNF1A-MODY3 is characterized by not only gene heterogeneity but also phenotype heterogeneity. For example, the two human variants HNF1α (P408H) and HNF1α (P409H) can be considered different variants (125, 126). A possible reason is that these two adjacent sites regulate the promoters of two different HNF1A-targeted genes. This is not surprising and can be explained by the interactions between HNF1α and different coactivators, which are necessary for the complete activation of different HNF1α downstream target promoters (127). The above phenomena show that HNF1α plays many roles and is widely involved in the strict and fine regulation of many genes responsible for metabolism.

Some HNF1α SNPs cause obvious MODY3, while others do not cause MODY3 but increase the risk of T2D or GDM. These are very interesting phenomena. By determining the underlying mechanism of these phenomena, we may improve our ability to individualize diabetes treatment. First, what is the difference between MODY, T2D, and GDM? The biggest difference is the age/time of onset. The onset age of MODY is below 25 years old, while T2D occurs in adulthood, and the onset of GDM is obvious diabetes in the middle and later stages of pregnancy. The earlier the onset, the more dominant is the role of genetic factors in the occurrence of diseases. The impact of environmental and other physical factors is greater with later onset. In essence, pregnancy is a stressor on the female body. The second major difference is whether the family history is obvious. The more obvious the family history is, the more important is the role of genetic factors. HNF1α heterozygous mutations lead to MODY3. Since an HNF1α allele is normal in MODY patients, it can be deduced that the expression level of HNF1α is important in this group. MODY plays a vital role in cell function, especially in β cells. A lack of sufficient protein levels leads to a significant loss of function of mutant alleles (104), and dominant negative effects caused by interference between mutant products and wild-type forms lead to the formation of inactive heterodimers (128). HNF1A-MODY-related variants function through one of the above mechanisms, i.e., a simple loss of function or a dominant-negative mechanism. T2D and GDM are diabetes types caused by multiple factors. The HNF1α SNP, which triggers T2D and GDM, has a certain impact on the process of abnormal blood glucose. Therefore, we speculate that HNF1α SNPs related to T2D or GDM partially impair the function of the HNF1α protein.

The HNF1α protein contains the following three functional domains: an N-terminal dimer domain, a DNA binding region containing a nuclear localization signal, and a C-terminal transactivation domain (**Figure 1**). The N-terminal dimeric domain (residues 1-32) forms a four-helix bundle, two of which separate the α-helix in a circle to form a dimer (129, 130). Usually, two HNF1αs form a homodimer or one HNF1α associates with the HNF1β transcription factor, which has a similar structure, to form a heterodimer (47). The DNA binding domain (DBD) of HNF1α binds reverse palindrome 5'-gttaatnataac-3' and forms a helix-to-helix structure (131). The DBD includes two POU subdomains, i.e., POU-specific domain (POUs, amino acids 91-181) and POU-homologous domain (POUH, amino acids 203-279) (104). The amino acid positions of DBDs differ slightly. POUs are an integral part of HNF1α and play a vital role in maintaining protein stability (132). Comparing the common HNF1α SNPs that cause MODY3 with those that cause T2D, most of the former are concentrated in exon 1, 2, and 4, which encode the DNA binding region of the C-terminal transactivation domain of HNF1α (**Figure 1**). The HNF1α SNP leading to T2D is concentrated in exons 8 and 9. The above sites of the HNF1α SNP that lead to T2D are almost outside the proline rich activation domain II of HNF1α, which is located in the transactivation domain.

SNP mutations may affect the function of the HNF1α protein through the following mechanisms: 1) Affecting the ability of DNA to bind the transcriptional regulatory region of the target gene; 2) Affecting the transcriptional activity of HNF1α; 3) Affecting the nuclear entry ability of the HNF1α protein; 4) Affecting the stability of the HNF1α protein; and 5) Affecting the expression of the HNF1α protein, especially SNPs located in the promoter region (107, 125, 133). In 2017, Najmi et al. found that the transcriptional activity or DNA binding ability of HNF1α variants that cause T2D was between those of normal wild-type protein and the HNF1A-MODY variant (134). The above interesting study may indicate that HNF1α participates in multiple signaling pathways involved in abnormal blood glucose and that the HNF1α variants identified among T2D patients may lack sufficient penetrance to drive diabetes but still increase the susceptibility to diabetes.

In summary, the HNF1α gene is highly polymorphic, and the clinical phenotypes caused by different SNPs may vary greatly. Therefore, to better manage the abnormal blood glucose levels caused by HNF1α mutations, genotype identification should be performed to obtain detailed information concerning HNF1α.

CONCLUSION AND FUTURE PERSPECTIVES

To date, many HNF1α SNPs have been identified and are widely distributed in the HNF1α gene. HNF1α-associated diabetes mellitus has larger clinical heterogeneity. Significant differences have been found in abnormal plasma glucose caused by SNPs at different sites. Patients with some variants do not have diabetes throughout their lives, some with other variants show serious hyperglycemia in childhood, while others show hyperglycemia in their older years. HNF1α is a tissue-specific transcription factor mainly expressed in the pancreas and liver. Hundreds of target genes have been found in these tissues. In the pancreas, HNF1α not only maintains the function of mature pancreatic β cells, but also affects the development and maturation of β cells. In the liver, HNF1α abnormality inhibits hepatic glycogen decomposition

and promotes lipolysis. Uncovering the mechanism underlying why different HNF1α mutations cause different types of diabetes will provide a theoretical basis for personalized prevention and treatment of HNF1α-associated hyperglycemia and will also benefit research on T2D, which is the main type of diabetes. HNF1α may cause different forms of diabetes due to different levels of penetrance and genetic backgrounds. These differences have a certain correlation with the location of the SNPs. The SNP for HNF1A-MODY is often located in the DNA binding region, while those for T2D and GDM are located in a different region. Functional studies have shown that the transcriptional activity or DNA binding ability of the HNF1α variant of T2D is between those of the normal wild-type protein and the HNF1A-MODY variant. This finding may indicate that the HNF1α variants identified among T2D patients may lack sufficient penetrance to drive diabetes but still increase the susceptibility to diabetes. Accordingly, there must be differences in the treatment of diabetes caused by different SNPs. Low-dose sulfonylurea therapy is the first-line therapy for MODY3 but does not show special sensitivity to T2D. For carriers of the HNF1α variants that may cause T2D or GDM, dietary treatment is the first recommendation. We hope research on the pathogenesis and drug treatments for HNF1A-T2D and GDM will progress in the near future with studies on the function of HNF1α.

AUTHOR CONTRIBUTIONS

L-ML and B-GJ collected information. L-LS and L-ML wrote the manuscript. All authors contributed to the article and approved the submitted version.

FUNDING

This study was supported by grants from the National Natural Science Foundation of China (81672721), National Key Research and Development Projection (No. 2018YFC1314100), Shanghai Science Foundation (17DZ1910604 and 19ZR1456900), Diabetes Talent Research Project of China International Medical Foundation (2018-N-01-26), Key Laboratory Development Project of Minimally Invasive Techniques & Rapid Rehabilitation of Digestive System Tumor (21SZDSYS05).

SUPPLEMENTARY MATERIAL

The Supplementary Material for this article can be found online at: https://www.frontiersin.org/articles/10.3389/fendo.2022.829565/full#supplementary-material

REFERENCES

1. Saeedi P, Petersohn I, Salpea P, Malanda B, Karuranga S, Unwin N, et al. Global and Regional Diabetes Prevalence Estimates for 2019 and Projections for 2030 and 2045: Results From the International Diabetes Federation Diabetes Atlas, 9(Th) Edition. *Diabetes Res Clin Pract* (2019) 157:107843. doi: 10.1016/j.diabres.2019.107843
2. Bommer C, Heesemann E, Sagalova V, Manne-Goehler J, Atun R, Barnighausen T, et al. The Global Economic Burden of Diabetes in Adults Aged 20-79 Years: A Cost-of-Illness Study. *Lancet Diabetes Endocrinol* (2017) 5:423–30. doi: 10.1016/S2213-8587(17)30097-9
3. American Diabetes Association. Diagnosis and Classification of Diabetes Mellitus. *Diabetes Care* (2014) 37 Suppl 1:S81–90. doi: 10.2337/dc14-S081
4. Redondo MJ, Hagopian WA, Oram R, Steck AK, Vehik K, Weedon M, et al. The Clinical Consequences of Heterogeneity Within and Between Different Diabetes Types. *Diabetologia* (2020) 63:2040–8. doi: 10.1007/s00125-020-05211-7
5. Udler MS, McCarthy MI, Florez JC, Mahajan A. Genetic Risk Scores for Diabetes Diagnosis and Precision Medicine. *Endocr Rev* (2019) 40:1500–20. doi: 10.1210/er.2019-00088
6. Hattersley AT, Patel KA. Precision Diabetes: Learning From Monogenic Diabetes. *Diabetologia* (2017) 60:769–77. doi: 10.1007/s00125-017-4226-2
7. Stanik JJ, Dusatkova P, Cinek O, Valentinova L, Huckova M, Skopkova M, et al. *De Novo* Mutations of GCK, HNF1A and HNF4A may be More Frequent in MODY Than Previously Assumed. *Diabetologia* (2014) 57:480–4. doi: 10.1007/s00125-013-3119-2
8. Redondo MJ, Balasubramanyam A. Toward an Improved Classification of Type 2 Diabetes: Lessons From Research Into the Heterogeneity of a Complex Disease. *J Clin Endocrinol Metab* (2021) 106:e4822–33. doi: 10.1210/clinem/dgab545
9. Yamagata K, Oda N, Kaisaki PJ, Menzel S, Furuta H, Vaxillaire M, et al. Mutations in the Hepatocyte Nuclear Factor-1alpha Gene in Maturity-Onset Diabetes of the Young (MODY3). *Nature* (1996) 384:455–8. doi: 10.1038/384455a0
10. Harries LW, Brown JE, Gloyn AL. Species-Specific Differences in the Expression of the HNF1A, HNF1B and HNF4A Genes. *PloS One* (2009) 4:e7855. doi: 10.1371/journal.pone.0007855
11. Ktistaki E, Talianidis I. Modulation of Hepatic Gene Expression by Hepatocyte Nuclear Factor 1. *Science* (1997) 277:109–12. doi: 10.1126/science.277.5322.109
12. Shih DQ, Bussen M, Sehayek E, Ananthanarayanan M, Shneider BL, Suchy FJ, et al. Hepatocyte Nuclear Factor-1alpha is an Essential Regulator of Bile Acid and Plasma Cholesterol Metabolism. *Nat Genet* (2001) 27:375–82. doi: 10.1038/86871
13. Rufibach LE, Duncan SA, Battle M, Deeb SS. Transcriptional Regulation of the Human Hepatic Lipase (LIPC) Gene Promoter. *J Lipid Res* (2006) 47:1463–77. doi: 10.1194/jlr.M600082-JLR200
14. Boj SF, Parrizas M, Maestro MA, Ferrer J. A Transcription Factor Regulatory Circuit in Differentiated Pancreatic Cells. *Proc Natl Acad Sci USA* (2001) 98:14481–6. doi: 10.1073/pnas.241349398
15. Wang H, Antinozzi PA, Hagenfeldt KA, Maechler P, Wollheim CB. Molecular Targets of a Human HNF1 Alpha Mutation Responsible for Pancreatic Beta-Cell Dysfunction. *EMBO J* (2000) 19:4257–64. doi: 10.1093/emboj/19.16.4257
16. Malakauskas SM, Kourany WM, Zhang XY, Lu D, Stevens RD, Koves TR, et al. Increased Insulin Sensitivity in Mice Lacking Collectrin, a Downstream Target of HNF-1alpha. *Mol Endocrinol* (2009) 23:881–92. doi: 10.1210/me.2008-0274
17. Lek M, Karczewski KJ, Minikel EV, Samocha KE, Banks E, Fennell T, et al. Analysis of Protein-Coding Genetic Variation in 60,706 Humans. *Nature* (2016) 536:285–91. doi: 10.1038/nature19057
18. Ellard S, Colclough K. Mutations in the Genes Encoding the Transcription Factors Hepatocyte Nuclear Factor 1 Alpha (HNF1A) and 4 Alpha (HNF4A) in Maturity-Onset Diabetes of the Young. *Hum Mutat* (2006) 27:854–69. doi: 10.1002/humu.20357
19. Colclough K, Bellanne-Chantelot C, Saint-Martin C, Flanagan SE, Ellard S. Mutations in the Genes Encoding the Transcription Factors Hepatocyte Nuclear Factor 1 Alpha and 4 Alpha in Maturity-Onset Diabetes of the Young and Hyperinsulinemic Hypoglycemia. *Hum Mutat* (2013) 34:669–85. doi: 10.1002/humu.22279
20. Zhao Z, Fu YX, Hewett-Emmett D, Boerwinkle E. Investigating Single Nucleotide Polymorphism (SNP) Density in the Human Genome and its Implications for Molecular Evolution. *Gene* (2003) 312:207–13. doi: 10.1016/s0378-1119(03)00670-x

21. Alvelos MI, Goncalves CI, Coutinho E, Almeida JT, Bastos M, Sampaio ML, et al. Maturity-Onset Diabetes of the Young (MODY) in Portugal: Novel GCK, HNFA1 and HNFA4 Mutations. *J Clin Med* (2020) 9:288. doi: 10.3390/jcm9010288
22. Tilgner H, Nikolaou C, Althammer S, Sammeth M, Beato M, Valcarcel J, et al. Nucleosome Positioning as a Determinant of Exon Recognition. *Nat Struct Mol Biol* (2009) 16:996–1001. doi: 10.1038/nsmb.1658
23. Dhir A, Buratti E. Alternative Splicing: Role of Pseudoexons in Human Disease and Potential Therapeutic Strategies. *FEBS J* (2010) 277:841–55. doi: 10.1111/j.1742-4658.2009.07520.x
24. Peixoto-Barbosa R, Reis AF, Giuffrida FMA. Update on Clinical Screening of Maturity-Onset Diabetes of the Young (MODY). *Diabetol Metab Syndr* (2020) 12:50. doi: 10.1186/s13098-020-00557-9
25. Hattersley AT, Greeley SAW, Polak M, Rubio-Cabezas O, Njolstad PR, Mlynarski W, et al. ISPAD Clinical Practice Consensus Guidelines 2018: The Diagnosis and Management of Monogenic Diabetes in Children and Adolescents. *Pediatr Diabetes* (2018) 19(Suppl 27):47–63. doi: 10.1111/pedi.12772
26. Frayling TM, Evans JC, Bulman MP, Pearson E, Allen L, Owen K, et al. Beta-Cell Genes and Diabetes: Molecular and Clinical Characterization of Mutations in Transcription Factors. *Diabetes* (2001) 50(Suppl 1):S94–100. doi: 10.2337/diabetes.50.2007.s94
27. Hansen T, Eiberg H, Rouard M, Vaxillaire M, Moller AM, Rasmussen SK, et al. Novel MODY3 Mutations in the Hepatocyte Nuclear Factor-1alpha Gene: Evidence for a Hyperexcitability of Pancreatic Beta-Cells to Intravenous Secretagogues in a Glucose-Tolerant Carrier of a P447L Mutation. *Diabetes* (1997) 46:726–30. doi: 10.2337/diab.46.4.726
28. Vaxillaire M, Rouard M, Yamagata K, Oda N, Kaisaki PJ, Boriraj VV, et al. Identification of Nine Novel Mutations in the Hepatocyte Nuclear Factor 1 Alpha Gene Associated With Maturity-Onset Diabetes of the Young (MODY3). *Hum Mol Genet* (1997) 6:583–6. doi: 10.1093/hmg/6.4.583
29. Salzano G, Passanisi S, Mammi C, Priolo M, Pintomalli L, Caminiti L, et al. Maturity Onset Diabetes of the Young is Not Necessarily Associated With Autosomal Inheritance: Case Description of a *De Novo* HFN1A Mutation. *Diabetes Ther* (2019) 10:1543–8. doi: 10.1007/s13300-019-0633-3
30. Li M, Riviere JB, Polychronakos C. Why All MODY Variants are Dominantly Inherited: A Hypothesis. *Trends Genet* (2021) S0168-9525(21):00285–7. doi: 10.1016/j.tig.2021.10.001
31. Gragnoli C, Lindner T, Cockburn BN, Kaisaki PJ, Gragnoli F, Marozzi G, et al. Maturity-Onset Diabetes of the Young Due to a Mutation in the Hepatocyte Nuclear Factor-4 Alpha Binding Site in the Promoter of the Hepatocyte Nuclear Factor-1 Alpha Gene. *Diabetes* (1997) 46:1648–51. doi: 10.2337/diacare.46.10.1648
32. Bjørkhaug L, Sagen JV, Thorsby P, Søvik O, Molven A, Njølstad PR. Hepatocyte Nuclear Factor-1 Alpha Gene Mutations and Diabetes in Norway. *J Clin Endocrinol Metab* (2003) 88:920–31. doi: 10.1210/jc.2002-020945
33. Møller AM, Dalgaard LT, Pociot F, Nerup J, Hansen T, Pedersen O. Mutations in the Hepatocyte Nuclear Factor-1alpha Gene in Caucasian Families Originally Classified as Having Type I Diabetes. *Diabetologia* (1998) 41:1528–31. doi: 10.1007/s001250051101
34. Lambert AP, Ellard S, Allen LI, Gallen IW, Gillespie KM, Bingley PJ, et al. Identifying Hepatic Nuclear Factor 1alpha Mutations in Children and Young Adults With a Clinical Diagnosis of Type 1 Diabetes. *Diabetes Care* (2003) 26:333–7. doi: 10.2337/diacare.26.2.333
35. Fang C, Huang J, Huang Y, Chen L, Chen X, Hu J. A Novel Nonsense Mutation of the HNF1alpha in Maturity-Onset Diabetes of the Young Type 3 in Asian Population. *Diabetes Res Clin Pract* (2015) 109:e5–7. doi: 10.1016/j.diabres.2015.05.026
36. Balamurugan K, Bjørkhaug L, Mahajan S, Kanthimathi S, Njølstad PR, Srinivasan N, et al. Structure-Function Studies of HNF1A (MODY3) Gene Mutations in South Indian Patients With Monogenic Diabetes. *Clin Genet* (2016) 90:486–95. doi: 10.1111/cge.12757
37. Cervin C, Orho-Melander M, Ridderstråle M, Lehto M, Barg S, Groop L, et al. Characterization of a Naturally Occurring Mutation (L107I) in the HNF1 Alpha (MODY3) Gene. *Diabetologia* (2002) 45:1703–8. doi: 10.1007/s00125-002-0977-4
38. Hameed S, Ellard S, Woodhead HJ, Neville KA, Walker JL, Craig ME, et al. Persistently Autoantibody Negative (PAN) Type 1 Diabetes Mellitus in Children. *Pediatr Diabetes* (2011) 12:142–9. doi: 10.1111/j.1399-5448.2010.00681.x
39. Harries LW, Ellard S, Stride A, Morgan NG, Hattersley AT. Isomers of the TCF1 Gene Encoding Hepatocyte Nuclear Factor-1 Alpha Show Differential Expression in the Pancreas and Define the Relationship Between Mutation Position and Clinical Phenotype in Monogenic Diabetes. *Hum Mol Genet* (2006) 15:2216–24. doi: 10.1093/hmg/ddl147
40. Stride A, Ellard S, Clark P, Shakespeare L, Salzmann M, Shepherd M, et al. Beta-Cell Dysfunction, Insulin Sensitivity, and Glycosuria Precede Diabetes in Hepatocyte Nuclear Factor-1alpha Mutation Carriers. *Diabetes Care* (2005) 28:1751–6. doi: 10.2337/diacare.28.7.1751
41. Bellanne-Chantelot C, Carette C, Riveline JP, Valero R, Gautier JF, Larger E, et al. The Type and the Position of HNF1A Mutation Modulate Age at Diagnosis of Diabetes in Patients With Maturity-Onset Diabetes of the Young (MODY)-3. *Diabetes* (2008) 57:503–8. doi: 10.2337/db07-0859
42. Byrne MM, Sturis J, Menzel S, Yamagata K, Fajans SS, Dronsfield MJ, et al. Altered Insulin Secretory Responses to Glucose in Diabetic and Nondiabetic Subjects With Mutations in the Diabetes Susceptibility Gene MODY3 on Chromosome 12. *Diabetes* (1996) 45:1503–10. doi: 10.2337/diab.45.11.1503
43. Iwasaki N, Ogata M, Tomonaga O, Kuroki H, Kasahara T, Yano N, et al. Liver and Kidney Function in Japanese Patients With Maturity-Onset Diabetes of the Young. *Diabetes Care* (1998) 21:2144–8. doi: 10.2337/diacare.21.12.2144
44. Menzel R, Kaisaki PJ, Rjasanowski I, Heinke P, Kerner W, Menzel S. A Low Renal Threshold for Glucose in Diabetic Patients With a Mutation in the Hepatocyte Nuclear Factor-1alpha (HNF-1alpha) Gene. *Diabetes Med* (1998) 15:816–20. doi: 10.1002/(SICI)1096-9136(199810)15:10<816::AID-DIA714>3.0.CO;2-P
45. Bingham C, Ellard S, Nicholls AJ, Pennock CA, Allen J, James AJ, et al. The Generalized Aminoaciduria Seen in Patients With Hepatocyte Nuclear Factor-1alpha Mutations is a Feature of All Patients With Diabetes and is Associated With Glucosuria. *Diabetes* (2001) 50:2047–52. doi: 10.2337/diabetes.50.9.2047
46. Pontoglio M, Prie D, Cheret C, Doyen A, Leroy C, Froguel P, et al. HNF1alpha Controls Renal Glucose Reabsorption in Mouse and Man. *EMBO Rep* (2000) 1:359–65. doi: 10.1093/embo-reports/kvd071
47. Soutoglou E, Papafotiou G, Katrakili N, Talianidis I. Transcriptional Activation by Hepatocyte Nuclear Factor-1 Requires Synergism Between Multiple Coactivator Proteins. *J Biol Chem* (2000) 275:12515–20. doi: 10.1074/jbc.275.17.12515
48. Tronche F, Yaniv M. HNF1, a Homeoprotein Member of the Hepatic Transcription Regulatory Network. *Bioessays* (1992) 14:579–87. doi: 10.1002/bies.950140902
49. Horikawa Y, Iwasaki N, Hara M, Furuta H, Hinokio Y, Cockburn BN, et al. Mutation in Hepatocyte Nuclear Factor-1 Beta Gene (TCF2) Associated With MODY. *Nat Genet* (1997) 17:384–5. doi: 10.1038/ng1297-384
50. Nishigori H, Yamada S, Kohama T, Tomura H, Sho K, Horikawa Y, et al. Frameshift Mutation, A263fsinsGG, in the Hepatocyte Nuclear Factor-1beta Gene Associated With Diabetes and Renal Dysfunction. *Diabetes* (1998) 47:1354–5. doi: 10.2337/diab.47.8.1354
51. Maltoni G, Zucchini S, Scipione M, Mantovani V, Salardi S, Cicognani A. Onset of Type 1 Diabetes Mellitus in Two Patients With Maturity Onset Diabetes of the Young. *Pediatr Diabetes* (2012) 13:208–12. doi: 10.1111/j.1399-5448.2011.00788.x
52. Karaoglan M, Nacarkahya G. Clinical and Laboratory Clues of Maturity-Onset Diabetes of the Young and Determination of Association With Molecular Diagnosis. *J Diabetes* (2021) 13:154–63. doi: 10.1111/1753-0407.13097
53. Oliveira RV, Bernardo T, Martins S, Sequeira A. Monogenic Diabetes: A New Pathogenic Variant of HNF1A Gene. *BMJ Case Rep* (2021) 14:e231837. doi: 10.1136/bcr-2019-231837
54. Park HS, Kim IJ, Kim EG, Ryu CS, Lee JY, Ko EJ, et al. A Study of Associations Between CUBN, HNF1A, and LIPC Gene Polymorphisms and Coronary Artery Disease. *Sci Rep* (2020) 10:16294. doi: 10.1038/s41598-020-73048-6

55. Malecki MT, Skupien J, Gorczynska-Kosiorz S, Klupa T, Nazim J, Moczulski DK, et al. Renal Malformations may be Linked to Mutations in the Hepatocyte Nuclear Factor-1α (MODY3) Gene. *Diabetes Care* (2005) 28:2774–6. doi: 10.2337/diacare.28.11.2774
56. Steele AM, Shields BM, Shepherd M, Ellard S, Hattersley AT, Pearson ER. Increased All-Cause and Cardiovascular Mortality in Monogenic Diabetes as a Result of Mutations in the HNF1A Gene. *Diabetes Med* (2010) 27:157–61. doi: 10.1111/j.1464-5491.2009.02913.x
57. Giuffrida FM, Furuzawa GK, Kasamatsu TS, Oliveira MM, Reis AF, Dib SA. HNF1A Gene Polymorphisms and Cardiovascular Risk Factors in Individuals With Late-Onset Autosomal Dominant Diabetes: A Cross-Sectional Study. *Cardiovasc Diabetol* (2009) 8:28. doi: 10.1186/1475-2840-8-28
58. Teslovich TM, Musunuru K, Smith AV, Edmondson AC, Stylianou IM, Koseki M, et al. Biological, Clinical and Population Relevance of 95 Loci for Blood Lipids. *Nature* (2010) 466:707–13. doi: 10.1038/nature09270
59. Isomaa B, Henricsson M, Lehto M, Forsblom C, Karanko S, Sarelin L, et al. Chronic Diabetic Complications in Patients With MODY3 Diabetes. *Diabetologia* (1998) 41:467–73. doi: 10.1007/s001250050931
60. Babaya N, Ikegami H, Fujisawa T, Nojima K, Itoi-Babaya M, Inoue K, et al. Association of I27L Polymorphism of Hepatocyte Nuclear Factor-1 Alpha Gene With High-Density Lipoprotein Cholesterol Level. *J Clin Endocrinol Metab* (2003) 88:2548–51. doi: 10.1210/jc.2002-021891
61. Hoskins JW, Jia J, Flandez M, Parikh H, Xiao W, Collins I, et al. Transcriptome Analysis of Pancreatic Cancer Reveals a Tumor Suppressor Function for HNF1A. *Carcinogenesis* (2014) 35:2670–8. doi: 10.1093/carcin/bgu193
62. Lu Y, Xu D, Peng J, Luo Z, Chen C, Chen Y, et al. HNF1A Inhibition Induces the Resistance of Pancreatic Cancer Cells to Gemcitabine by Targeting ABCB1. *EBioMedicine* (2019) 44:403–18. doi: 10.1016/j.ebiom.2019.05.013
63. Willson JS, Godwin TD, Wiggins GA, Guilford PJ, McCall JL. Primary Hepatocellular Neoplasms in a MODY3 Family With a Novel HNF1A Germline Mutation. *J Hepatol* (2013) 59:904–7. doi: 10.1016/j.jhep.2013.05.024
64. Fu J, Wang T, Zhai X, Xiao X. Primary Hepatocellular Adenoma Due to Biallelic HNF1A Mutations and its Co-Occurrence With MODY 3: Case-Report and Review of the Literature. *Endocrine* (2020) 67:544–51. doi: 10.1007/s12020-019-02138-x
65. Rebouissou S, Vasiliu V, Thomas C, Bellanne-Chantelot C, Bui H, Chretien Y, et al. Germline Hepatocyte Nuclear Factor 1alpha and 1beta Mutations in Renal Cell Carcinomas. *Hum Mol Genet* (2005) 14:603–14. doi: 10.1093/hmg/ddi057
66. Zhang J, Liu Y, Xu B, Li F, Wang Y, Li M, et al. Circulating Tumor DNA Analysis of Metastatic Renal Cell Carcinoma. *Mol Clin Oncol* (2021) 14:16. doi: 10.3892/mco.2020.2178
67. Hechtman JF, Abou-Alfa GK, Stadler ZK, Mandelker DL, Roehrl MHA, Zehir A, et al. Somatic HNF1A Mutations in the Malignant Transformation of Hepatocellular Adenomas: A Retrospective Analysis of Data From MSK-IMPACT and TCGA. *Hum Pathol* (2019) 83:1–6. doi: 10.1016/j.humpath.2018.08.004
68. Tang J, Tang CY, Wang F, Guo Y, Tang HN, Zhou CL, et al. Genetic Diagnosis and Treatment of a Chinese Ketosis-Prone MODY 3 Family With Depression. *Diabetol Metab Syndr* (2017) 9:5. doi: 10.1186/s13098-016-0198-5
69. Delvecchio M, Pastore C, Giordano P. Treatment Options for MODY Patients: A Systematic Review of Literature. *Diabetes Ther* (2020) 11:1667–85. doi: 10.1007/s13300-020-00864-4
70. Pearson ER, Liddell WG, Shepherd M, Corrall RJ, Hattersley AT. Sensitivity to Sulphonylureas in Patients With Hepatocyte Nuclear Factor-1alpha Gene Mutations: Evidence for Pharmacogenetics in Diabetes. *Diabetes Med* (2000) 17:543–5. doi: 10.1046/j.1464-5491.2000.00305.x
71. Pearson ER, Starkey BJ, Powell RJ, Gribble FM, Clark PM, Hattersley AT. Genetic Cause of Hyperglycaemia and Response to Treatment in Diabetes. *Lancet* (2003) 362:1275–81. doi: 10.1016/S0140-6736(03)14571-0
72. Boileau P, Wolfrum C, Shih DQ, Yang TA, Wolkoff AW, Stoffel M. Decreased Glibenclamide Uptake in Hepatocytes of Hepatocyte Nuclear Factor-1alpha-Deficient Mice: A Mechanism for Hypersensitivity to Sulfonylurea Therapy in Patients With Maturity-Onset Diabetes of the Young, Type 3 (MODY3). *Diabetes* (2002) 51(Suppl 3):S343–8. doi: 10.2337/diabetes.51.2007.s343
73. McDonald TJ, Ellard S. Ellard. Maturity Onset Diabetes of the Young: Identification and Diagnosis. *Ann Clin Biochem* (2013) 50:403–15. doi: 10.1177/0004563213483458
74. Demol S, Lebenthal Y, Bar-Meisels M, Phillip M, Gat-Yablonski G, Gozlan Y. A Family With a Novel Termination Mutation in Hepatic Nuclear Factor 1alpha in Maturity-Onset Diabetes of the Young Type 3 Which is Unresponsive to Sulphonylurea Therapy. *Horm Res Paediatr* (2014) 81:280–4. doi: 10.1159/000356925
75. Tan C, Ang SF, Lim SC. Response to Multiple Glucose-Lowering Agents in a Sib-Pair With a Novel HNF1alpha (MODY3) Variant. *Eur J Hum Genet* (2020) 28:518–20. doi: 10.1038/s41431-019-0561-8
76. Martagon AJ, Bello-Chavolla OY, Arellano-Campos O, Almeda-Valdes P, Walford GA, Cruz-Bautista I, et al. Mexican Carriers of the HNF1A P.E508K Variant Do Not Experience an Enhanced Response to Sulfonylureas. *Diabetes Care* (2018) 41:1726–31. doi: 10.2337/dc18-0384
77. Tin A, Marten J, Halperin Kuhns VL, Li Y, Wuttke M, Kirsten H, et al. Polymorphisms of the HNF1A Gene Encoding Hepatocyte Nuclear Factor-1 Alpha are Associated With C-Reactive Protein. *Am J Hum Genet* (2008) 82:1193–201. doi: 10.1038/s41588-019-0504-x
78. Curocichin G, Wu Y, McDade TW, Kuzawa CW, Borja JB, Qin L, et al. Single-Nucleotide Polymorphisms at Five Loci are Associated With C-Reactive Protein Levels in a Cohort of Filipino Young Adults. *J Hum Genet* (2011) 56:823–7. doi: 10.1038/jhg.2011.106
79. Yahaya TO, Ufuoma SB. Genetics and Pathophysiology of Maturity-Onset Diabetes of the Young (MODY): A Review of Current Trends. *Oman Med J* (2020) 35:e126. doi: 10.5001/omj.2020.44
80. Bellanne-Chantelot C, Levy DJ, Carette C, Saint-Martin C, Riveline JP, Larger E, et al. French Monogenic Diabetes Study, Clinical Characteristics and Diagnostic Criteria of Maturity-Onset Diabetes of the Young (MODY) Due to Molecular Anomalies of the HNF1A Gene. *J Clin Endocrinol Metab* (2011) 96:E1346–1351. doi: 10.1210/jc.2011-0268
81. BellanneWiltshire S, Frayling TM, Groves CJ, Levy JC, Hitman GA, Sampson M, et al. Evidence From a Large U.K. Family Collection That Genes Influencing Age of Onset of Type 2 Diabetes Map to Chromosome 12p and to the MODY3/NIDDM2 Locus on 12q24. *Diabetes* (2004) 53:855–60. doi: 10.2337/diabetes.53.3.855
82. SIGMA Type 2 Diabetes Consortium, Estrada K, Aukrust I, Bjørkhaug L, Burtt NP, Mercader JM, et al. Association of a Low-Frequency Variant in HNF1A With Type 2 Diabetes in a Latino Population. *JAMA* (2014) 311:2305–14. doi: 10.1001/jama.2014.6511
83. Weedon MN, Owen KR, Shields B, Hitman G, Walker M, McCarthy MI, et al. A Large-Scale Association Analysis of Common Variation of the HNF1alpha Gene With Type 2 Diabetes in the U.K. Caucasian Population. *Diabetes* (2005) 54:2487–91. doi: 10.2337/diabetes.54.8.2487
84. Lee HJ, Ahn CW, Kim SJ, Song YD, Lim SK, Kim KR, et al. Mutation in Hepatocyte Nuclear Factor-1alpha is Not a Common Cause of MODY and Early-Onset Type 2 Diabetes in Korea. *Acta Diabetol* (2001) 38:123–7. doi: 10.1007/s005920170008
85. Hegele RA, Cao H, Harris SB, Hanley AJ, Zinman B. The Hepatic Nuclear Factor-1alpha G319S Variant is Associated With Early-Onset Type 2 Diabetes in Canadian Oji-Cree. *J Clin Endocrinol Metab* (1999) 84:1077–82. doi: 10.1210/jcem.84.3.5528
86. Hegele RA, Hanley AJ, Zinman B, Harris SB, Anderson CM. Disparity Between Association and Linkage Analysis for HNF1A G319S in Type 2 Diabetes in Canadian Oji-Cree. *J Hum Genet* (2000) 45:184–7. doi: 10.1007/s100380050208
87. Hegele RA, Zinman B, Hanley AJ, Harris SB, Barrett PH, Cao H. Genes, Environment and Oji-Cree Type 2 Diabetes. *Clin Biochem* (2003) 36:163–70. doi: 10.1016/s0009-9120(03)00004-3
88. Triggs-Raine BL, Kirkpatrick RD, Kelly SL, Norquay LD, Cattini PA, Yamagata K, et al. HNF-1alpha G319S, a Transactivation-Deficient Mutant, is Associated With Altered Dynamics of Diabetes Onset in an Oji-Cree Community. *Proc Natl Acad Sci USA* (2002) 99:4614–9. doi: 10.1073/pnas.062059799
89. Harries LW, Sloman MJ, Sellers EA, Hattersley AT, Ellard S. Diabetes Susceptibility in the Canadian Oji-Cree Population is Moderated by

Abnormal mRNA Processing of HNF1A G319S Transcripts. *Diabetes* (2008) 57:1978–82. doi: 10.2337/db07-1663
90. Sagen JV, Bjørkhaug L, Haukanes BI, Grevle L, Molnes J, Nedrebo BG, et al. The HNF1A Mutant Ala180Val: Clinical Challenges in Determining Causality of a Rare HNF1A Variant in Familial Diabetes. *Diabetes Res Clin Pract* (2017) 133:142–9. doi: 10.1016/j.diabres.2017.08.001
91. Słupecka-Ziemilska M, Wychowański P, Puzianowska-Kuznicka M. Gestational Diabetes Mellitus Affects Offspring's Epigenome. Is There a Way to Reduce the Negative Consequences? *Nutrients* (2020) 12:2792. doi: 10.3390/nu12092792
92. Rosik J, Szostak B, Machaj F, Pawlik A. The Role of Genetics and Epigenetics in the Pathogenesis of Gestational Diabetes Mellitus. *Ann Hum Genet* (2020) 84:114–24. doi: 10.1111/ahg.12356
93. Dalfrà MG, Burlina S, Del Vescovo GG, Lapolla A. Genetics and Epigenetics: New Insight on Gestational Diabetes Mellitus. *Front Endocrinol (Lausanne)* (2020) 11:602477. doi: 10.3389/fendo.2020.602477
94. Gjesing AP, Rui G, Lauenborg J, Have CT, Hollensted M, Andersson E, et al. High Prevalence of Diabetes-Predisposing Variants in MODY Genes Among Danish Women With Gestational Diabetes Mellitus. *J Endocr Soc* (2017) 1:681–90. doi: 10.1210/js.2017-00040
95. Bergmann A, Li J, Selisko T, Reimann M, Fischer S, Grässler J, et al. The A98V Single Nucleotide Polymorphism (SNP) in Hepatic Nuclear Factor 1 Alpha (HNF-1alpha) is Associated With Insulin Sensitivity and Beta-Cell Function. *Exp Clin Endocrinol Diabetes* (2008) 116(Suppl 1):S50–55. doi: 10.1055/s-2008-1081492
96. Shaat N, Karlsson E, Lernmark A, Ivarsson S, Lynch K, Parikh H, et al. Common Variants in MODY Genes Increase the Risk of Gestational Diabetes Mellitus. *Diabetologia* (2006) 49:1545–51. doi: 10.1007/s00125-006-0258-8
97. Beysel S, Pinarli FA, Eyerci N, Kizilgul M, Hepsen S, Alhan A, et al. HNF1A Gene P.I27L is Associated With Co-Existing Preeclampsia in Gestational Diabetes Mellitus. *Gynecol Endocrinol* (2020) 36:530–4. doi: 10.1080/09513590.2019.1698023
98. Wang X, Li W, Ma L, Ping F, Liu J, Wu X, et al. Variants in MODY Genes Associated With Maternal Lipids Profiles in Second Trimester of Pregnancy. *J Gene Med* (2017) 19:6–7. doi: 10.1002/jgm.2962
99. Wu Y, McDade TW, Kuzawa CW, Borja J, Li Y, Adair LS, et al. Genome-Wide Association With C-Reactive Protein Levels in CLHNS: Evidence for the CRP and HNF1A Loci and Their Interaction With Exposure to a Pathogenic Environment. *Inflammation* (2012) 35:574–83. doi: 10.1007/s10753-011-9348-y
100. McDonald TJ, Shields BM, Lawry J, Owen KR, Gloyn AL, Ellard S, et al. High-Sensitivity CRP Discriminates HNF1A-MODY From Other Subtypes of Diabetes. *Diabetes Care* (2011) 34:1860–2. doi: 10.2337/dc11-0323
101. Shah N, Thanabalasingham G, Owen KR, James TJ. Comparability of High-Sensitivity CRP Methods to Detect Maturity-Onset Diabetes of the Young Due to HNF1A Mutations. *Br J BioMed Sci* (2014) 71:84–5. doi: 10.1080/09674845.2014.11978288
102. Fagerberg L, Hallström BM, Oksvold P, Kampf C, Djureinovic D, Odeberg J, et al. Analysis of the Human Tissue-Specific Expression by Genome-Wide Integration of Transcriptomics and Antibody-Based Proteomics. *Mol Cell Proteomics* (2014) 13:397–406. doi: 10.1074/mcp.M113.035600
103. Odom DT, Zizlsperger N, Gordon DB, Bell GW, Rinaldi NJ, Murray HL, et al. Control of Pancreas and Liver Gene Expression by HNF Transcription Factors. *Science* (2004) 303:1378–81. doi: 10.1126/science.1089769
104. Vaxillaire M, Abderrahmani A, Boutin P, Bailleul B, Froguel P, Yaniv M, et al. Anatomy of a Homeoprotein Revealed by the Analysis of Human MODY3 Mutations. *J Biol Chem* (1999) 274:35639–46. doi: 10.1074/jbc.274.50.35639
105. Pearson ER, Velho G, Clark P, Stride A, Shepherd M, Frayling TM, et al. Beta-Cell Genes and Diabetes: Quantitative and Qualitative Differences in the Pathophysiology of Hepatic Nuclear Factor-1alpha and Glucokinase Mutations. *Diabetes* (2001) 50(Suppl 1):S101–7. doi: 10.2337/diabetes.50.2007.s101
106. Haliyur R, Tong X, Sanyoura M, Shrestha S, Lindner J, Saunders DC, et al. Human Islets Expressing HNF1A Variant Have Defective β Cell Transcriptional Regulatory Networks. *J Clin Invest* (2019) 129:246–51. doi: 10.1172/JCI121994
107. Magaña-Cerino JM, Luna-Arias JP, Labra-Barrios ML, Avendaño-Borromeo B, Boldo-León XM, Martínez-López MC. Identification and Functional Analysis of C.422_423inst, a Novel Mutation of the HNF1A Gene in a Patient With Diabetes. *Mol Genet Genomic Med* (2017) 5:50–65. doi: 10.1002/mgg3.261
108. Nammo T, Yamagata K, Hamaoka R, Zhu Q, Akiyama TE, Gonzalez FJ, et al. Expression Profile of MODY3/HNF-1alpha Protein in the Developing Mouse Pancreas. *Diabetologia* (2002) 45:1142–53. doi: 10.1007/s00125-002-0892-8
109. Hagenfeldt-Johansson KA, Herrera PL, Wang H, Gjinovci A, Ishihara H, Wollheim CB. Beta-Cell-Targeted Expression of a Dominantnegative Hepatocyte Nuclear Factor-1 Alpha Induces a Maturity-Onset Diabetes of the Young (MODY)3-Like Phenotype in Transgenic Mice. *Endocrinology* (2001) 142:5311–20. doi: 10.1210/endo.142.12.8592
110. Yamagata K, Nammo T, Moriwaki M, Ihara A, Iizuka K, Yang Q, et al. Overexpression of Dominant-Negative Mutant Hepatocyte Nuclear Fctor-1alpha in Pancreatic Beta-Cells Causes Abnormal Islet Architecture With Decreased Expression of E-Cadherin, Reduced Beta-Cell Proliferation, and Diabetes. *Diabetes* (2002) 51:114–23. doi: 10.2337/diabetes.51.1.114
111. Lyttle BM, Li J, Krishnamurthy M, Fellows F, Wheeler MB, Goodyer CG, et al. Transcription Factor Expression in the Developing Human Fetal Endocrine Pancreas. *Diabetologia* (2008) 51:1169–80. doi: 10.1007/s00125-008-1006-z
112. Donelan W, Koya V, Li SW, Yang LJ. Distinct Regulation of Hepatic Nuclear Factor 1alpha by NKX6.1 in Pancreatic Beta Cells. *J Biol Chem* (2010) 285:12181–9. doi: 10.1074/jbc.M109.064238
113. Hunter CS, Maestro MA, Raum JC, Guo M, Thompson 3FH, Ferrer J, et al. Hnf1α (MODY3) Regulates β-Cell-Enriched MafA Transcription Factor Expression. *Mol Endocrinol* (2011) 25:339–47. doi: 10.1210/me.2010-0362
114. Pontoglio M, Sreenan S, Roe M, Pugh W, Ostrega D, Doyen A, et al. Defective Insulin Secretion in Hepatocyte Nuclear Factor 1alpha-Deficient Mice. *J Clin Invest* (1998) 101:2215–22. doi: 10.1172/JCI2548
115. Østoft SH, Bagger JI, Hansen T, Pedersen O, Holst JJ, Knop FK, et al. Incretin Effect and Glucagon Responses to Oral and Intravenous Glucose in Patients With Maturity-Onset Diabetes of the Young–Type 2 and Type 3. *Diabetes* (2014) 63:2838–44. doi: 10.2337/db13-1878
116. Sato Y, Rahman MM, Haneda M, Tsuyama T, Mizumoto T, Yoshizawa T, et al. Hnf1α Controls Glucagon Secretion in Pancreatic α-Cells Through Modulation of SGLT1. *Biochim Biophys Acta Mol Basis Dis* (2020) 1866:165898. doi: 10.1016/j.bbadis.2020.165898
117. Cardenas-Diaz FL, Osorio-Quintero C, Diaz-Miranda MA, Kishore S, Leavens K, Jobaliya C, et al. Modeling Monogenic Diabetes using Human ESCs Reveals Developmental and Metabolic Deficiencies Caused by Mutations in HNF1A. *Cell Stem Cell* (2019) 25:273–89.e5. doi: 10.1016/j.stem.2019.07.007
118. Hiraiwa H, Pan CJ, Lin B, Akiyama TE, Gonzalez FJ, Chou JY. A Molecular Link Between the Common Phenotypes of Type 1 Glycogen Storage Disease and HNF1alpha-Null Mice. *J Biol Chem* (2001) 276:7963–7. doi: 10.1074/jbc.M010523200
119. Akiyama TE, Ward JM, Gonzalez FJ. Regulation of the Liver Fatty Acid-Binding Protein Gene by Hepatocyte Nuclear Factor 1alpha (HNF1alpha). Alterations in Fatty Acid Homeostasis in HNF1alpha-Deficient Mice. *J Biol Chem* (2000) 275:27117–2722. doi: 10.1074/jbc.M004388200
120. Richter S, Shih DQ, Pearson ER, Wolfrum C, Fajans SS, Hattersley AT, et al. Regulation of Apolipoprotein M Gene Expression by MODY3 Gene Hepatocyte Nuclear Factor-1alpha: Haploinsufficiency is Associated With Reduced Serum Apolipoprotein M Levels. *Diabetes* (2003) 52:2989–95. doi: 10.2337/diabetes.52.12.2989
121. Ma X, Hu YW, Zhao ZL, Zheng L, Qiu YR, Huang JL, et al. Anti-Inflammatory Effects of Propofol are Mediated by Apolipoprotein M in a Hepatocyte Nuclear Factor-1alpha-Dependent Manner. *Arch Biochem Biophys* (2013) 533:1–10. doi: 10.1016/j.abb.2013.03.002
122. Ni Q, Ding K, Wang KQ, He J, Yin C, Shi J, et al. Deletion of HNF1alpha in Hepatocytes Results in Fatty Liver-Related Hepatocellular Carcinoma in Mice. *FEBS Lett* (2017) 591:1947–57. doi: 10.1002/1873-3468.12689
123. Hegele RA, Cao H, Harris SB, Hanley AJ, Zinman B, Connelly PW. The Private Hepatocyte Nuclear Factor-1alpha G319S Variant is Associated With Plasma Lipoprotein Variation in Canadian Oji-Cree. *Arterioscler Thromb Vasc Biol* (2000) 20:217–22. doi: 10.1161/01.atv.20.1.217

124. Sakellariou S, Morgan Y, Heaton N, Portmann B, Quaglia A, Tobal K. New Monoallelic (Partial Tandem Duplication) Mutation of HNF1a Gene in Steatotic Hepatocellular Adenoma. *Eur J Gastroenterol Hepatol* (2011) 23:623–7. doi: 10.1097/MEG.0b013e328347964d
125. Nocera D, Menniti M, Belviso S, Bond HM, Lanzillotta D, Spoleti CB, et al. Functional Characterization of P.Pro409His Variant in HNF1A, a Hypomorphic Mutation Involved in Pancreatic Beta-Cell Dysfunction. *Acta Diabetol* (2019) 56:883–8. doi: 10.1007/s00592-019-01298-6
126. Kim KA, Kang K, Chi YI, Chang I, Lee MK, Kim KW, et al. Identification and Functional Characterization of a Novel Mutation of Hepatocyte Nuclear Factor-1alpha Gene in a Korean Family With MODY3. *Diabetologia* (2003) 46:721–7. doi: 10.1007/s00125-003-1079-7
127. Galán M, García-Herrero CM, Azriel S, Gargallo M, Duran M, Gorgojo JJ, et al. Differential Effects of HNF-1alpha Mutations Associated With Familial Young-Onset Diabetes on Target Gene Regulation. *Mol Med* (2011) 17:256–65. doi: 10.2119/molmed.2010.00097
128. Chi YI, Frantz JD, Oh BC, Hansen L, Dhe-Paganon S, Shoelson SE. Diabetes Mutations Delineate an Atypical POU Domain in HNF-1alpha. *Mol Cell* (2002) 10:1129–37. doi: 10.1016/s1097-2765(02)00704-9
129. Narayana N, Hua Q, Weiss MA. The Dimerization Domain of HNF-1alpha: Structure and Plasticity of an Intertwined Four-Helix Bundle With Application to Diabetes Mellitus. *J Mol Biol* (2001) 310:635–58. doi: 10.1006/jmbi.2001.4780
130. Rose RB, Endrizzi JA, Cronk JD, Holton J, Alber T. High-Resolution Structure of the HNF-1alpha Dimerization Domain. *Biochemistry* (2000) 39:15062–70. doi: 10.1021/bi001996t
131. Rose RB, Bayle JH, Endrizzi JA, Cronk JD, Crabtree GR, Alber T. Structural Basis of Dimerization, Coactivator Recognition and MODY3 Mutations in HNF-1alpha. *Nat Struct Biol* (2000) 7:744–8. doi: 10.1038/78966
132. Sneha P, Thirumal Kumar D, George Priya Doss C, Siva R, Zayed H. Determining the Role of Missense Mutations in the POU Domain of HNF1A That Reduce the DNA-Binding Affinity: A Computational Approach. *PloS One* (2017) 12:e0174953. doi: 10.1371/journal.pone.0174953
133. Malikova J, Kaci A, Dusatkova P, Aukrust I, Torsvik J, Vesela K, et al. Functional Analyses of HNF1A-MODY Variants Refine the Interpretation of Identified Sequence Variants. *J Clin Endocrinol Metab* (2020) 105:dgaa051. doi: 10.1210/clinem/dgaa051
134. Najmi LA, Aukrust I, Flannick J, Molnes J, Burtt N, Molven A, et al. Functional Investigations of HNF1A Identify Rare Variants as Risk Factors for Type 2 Diabetes in the General Population. *Diabetes* (2017) 66:335–46. doi: 10.2337/db16-0460

Conflict of Interest: The authors declare that the research was conducted in the absence of any commercial or financial relationships that could be construed as a potential conflict of interest.

Publisher's Note: All claims expressed in this article are solely those of the authors and do not necessarily represent those of their affiliated organizations, or those of the publisher, the editors and the reviewers. Any product that may be evaluated in this article, or claim that may be made by its manufacturer, is not guaranteed or endorsed by the publisher.

frontiers in Endocrinology

ORIGINAL RESEARCH
published: 01 March 2022
doi: 10.3389/fendo.2022.821091

Peptide Model of the Mutant Proinsulin Syndrome. II. Nascent Structure and Biological Implications

Yanwu Yang[1‡], Michael D. Glidden[2,3,4‡], Balamurugan Dhayalan[1‡], Alexander N. Zaykov[5†], Yen-Shan Chen[1], Nalinda P. Wickramasinghe[2], Richard D. DiMarchi[5] and Michael A. Weiss[1*]*

[1] Department of Biochemistry and Molecular Biology, Indiana University School of Medicine, Indianapolis, IN, United States, [2] Department of Biochemistry, Case Western Reserve University School of Medicine, Cleveland, OH, United States, [3] Department of Physiology & Biophysics, Case Western Reserve University School of Medicine, Cleveland, OH, United States, [4] Department of Medicine, Case Western Reserve University School of Medicine, Cleveland, OH, United States, [5] Department of Chemistry, Indiana University, Bloomington, IN, United States

Toxic misfolding of proinsulin variants in β-cells defines a monogenic diabetes syndrome, designated *mutant INS-gene induced diabetes of the young* (MIDY). In our first study (previous article in this issue), we described a one-disulfide peptide model of a proinsulin folding intermediate and its use to study such variants. The mutations (Leu^{B15}→Pro, Leu^{A16}→Pro, and Phe^{B24}→Ser) probe residues conserved among vertebrate insulins. In this companion study, we describe ^{1}H and ^{1}H-^{13}C NMR studies of the peptides; key NMR resonance assignments were verified by synthetic ^{13}C-labeling. Parent spectra retain nativelike features in the neighborhood of the single disulfide bridge (cystine B19-A20), including secondary NMR chemical shifts and nonlocal nuclear Overhauser effects. This partial fold engages wild-type side chains Leu^{B15}, Leu^{A16} and Phe^{B24} at the nexus of nativelike α-helices α_1 and α_3 (as defined in native proinsulin) and flanking β-strand (residues B24-B26). The variant peptides exhibit successive structural perturbations in order: parent (most organized) > Ser^{B24} >> Pro^{A16} > Pro^{B15} (least organized). The same order pertains to (a) overall α-helix content as probed by circular dichroism, (b) synthetic yields of corresponding three-disulfide insulin analogs, and (c) ER stress induced in cell culture by corresponding mutant proinsulins. These findings suggest that this and related peptide models will provide a general platform for classification of MIDY mutations based on molecular mechanisms by which nascent disulfide pairing is impaired. We propose that the syndrome's variable phenotypic spectrum—onsets ranging from the neonatal period to later in childhood or adolescence—reflects structural features of respective folding intermediates.

Keywords: monogenic diabetes, peptide chemistry, protein folding, folding nucleus, oxidative folding intermediate, NMR spectroscopy

OPEN ACCESS

Edited by:
Jiajun Zhao,
Shandong Provincial Hospital, China

Reviewed by:
Cheng Hu,
Shanghai Jiao Tong University, China
Pierre De Meyts,
Université Catholique de Louvain, Belgium

***Correspondence:**
Yanwu Yang
yangyanw@iu.edu
Michael A. Weiss
weissma@iu.edu

***Present address:**
Alexander N. Zaykov, Novo-Nordisk Research Center Indianapolis, Indianapolis, IN, United States

These authors have contributed equally to this work

Specialty section:
This article was submitted to Diabetes: Molecular Mechanisms, a section of the journal Frontiers in Endocrinology

Received: *23 November 2021*
Accepted: *21 January 2022*
Published: *01 March 2022*

Citation:
Yang Y, Glidden MD, Dhayalan B, Zaykov AN, Chen Y-S, Wickramasinghe NP, DiMarchi RD and Weiss MA (2022) Peptide Model of the Mutant Proinsulin Syndrome. II. Nascent Structure and Biological Implications. Front. Endocrinol. 13:821091. doi: 10.3389/fendo.2022.821091

INTRODUCTION

The mutant proinsulin syndrome (MPS) is a prototypical disease of toxic protein misfolding. Unlike toxic *extracellular* aggregation as observed among neurodegenerative diseases (1) and diverse amyloid disorders (2), in the MPS a dominant mutation impairs proinsulin folding efficiency in a critical *intracellular* organelle: the endoplasmic reticulum (ER). Impaired foldability of the variant protein of pancreatic β-cells leads to aberrant aggregation and in turn induces chronic ER stress (3–5). Although the unfolded protein response (UPR) evolved as an adaptive pathway [broadly conserved among eukaryotic cells (6, 7)], its chronic activation in β-cells impairs glucose-stimulated insulin secretion and β-cell viability [for review, see (8, 9)]. Also designated *mutant INS-gene induced diabetes of the young* (MIDY) (4), MPS encompasses a range of patient phenotypes, representing subtypes of *permanent neonatal diabetes mellitus* (PNDM) to *maturity-onset diabetes of the young* (MODY) (10–13).

Among monogenic endocrine syndromes in general [such as complete or partial androgen insensitivity (14)], a given mutation may be associated with a range of phenotypes, even in the same kindred (15). A given mutation in the androgen receptor, for example, may be associated with male development, somatic female development with Mullerian regression, or ambiguous genitalia (16). The complexity of genotype-phenotype relationships (GPR) in such syndromes presumably reflects the influence of modifier genes in multigenic regulatory pathways (17). Modifier genes have also been inferred in the genetics of Type 1 diabetes mellitus (DM). GPRs in MPS may be more straightforward: the extent of β-cell dysfunction and velocity of β-cell loss (together determining age of diabetes onset in a particular patient) may reflect mutation-specific molecular properties, i.e., whether a given amino-acid substitution is associated with a severe (PNDM) or mild (MODY) perturbation to foldability. In our initial study [preceding article in this issue (18)] we designed a 49-residue peptide model of an early on-pathway proinsulin folding intermediate and its application to three representative MIDY mutations. This single-chain model contains only one disulfide bridge and is thus designated *1SS*. This bridge (cystine B19-A20) is the first to accumulate among populated partial folds in the *in vitro* folding pathway of proinsulin and homologous factors (19, 20). The present study provides a detailed two-dimensional NMR study of the parent 1SS peptide and representative MIDY-related variants.

Native insulin contains two chains, B (30 residues) and A (21 residues) (21). Its native structure contains three α-helices stabilized by two inter-chain disulfide bridges (cystines B7-A7 and B19-A20) and one intrachain bridge (A6-A11; **Figure 1A**) (23). Whereas chain combination between the isolated chains is inefficient (24), cellular biosynthesis exploits a single-chain precursor, proinsulin, wherein disulfide pairing is intramolecular (25). Human proinsulin contains a disordered 35-residue connecting domain (C domain) between Thr^{B30} and Gly^{A1}. Efficiency of disulfide pairing in single-chain precursors can be augmented by shortening the C domain or deleting it entirely (26). The present peptide model contains a peptide bond between residues B28 and A1 (red bars in **Figure 1B**); the native Pro^{B28} is substituted by Lys to permit convenient enzymatic cleavage to a two-chain hormone (red in sequence N in **Figure 1B**) (27). The 49-residue synthetic precursor (designated "DesDi") exhibits remarkable folding efficiency, enabling preparation of certain insulin analogs refractory to classical chain combination (27). In the 1SS model cystine B7-A7 (solvent exposed in native insulin) is pairwise substituted by Ser whereas cystine A6-A11 (buried in the core of native insulin) is pairwise substituted by Ala (18). Segmental α-helical propensity and solubility were augmented by acidic surface substitutions His^{B10}→Asp (28, 29) and Thr^{A8}→Glu (30). The seven amino-acid substitutions in the parent 1SS peptide (positions B7, B10, B28, A6-A8 and A11) are highlighted in red in **Figure 1B** (entry 1SS-WT). Relative to an homologous two-chain peptide model of the corresponding 1SS IGF-I folding intermediate (**Figure 1C**) (22), we anticipated that the 1SS DesDi-based single-chain model would exhibit a conformational equilibrium biased toward a collapsed state (**Figure 1D**).

To connect our model to patient phenotypes, three MIDY mutations were introduced into the 1SS peptide model (**Figure 1B**). Two (Pro^{B15} and Pro^{A16}) are associated with neonatal-onset DM (31, 32); the third (Ser^{B24}) is associated with onset in early adulthood (33). The structural environments of these conserved side chains are shown in **Figure 2A**. Whereas the side chains of Leu^{B15} and Leu^{A16} are buried in the hydrophobic core (**Figures 2B, C, E, F**), the aromatic side chain of Phe^{B24} packs within a crevice overlying internal cystine B19-A20 such that one side of the aromatic ring is exposed to solvent (**Figures 2B–D**). Initial characterization of these peptides was described in our companion article (18). Whereas the Pro substitutions introduced marked perturbations in folding efficiency in a mini-proinsulin ["DesDi", (27)], Ser^{B24} was well tolerated. Synthetic yields mirrored residual α-helix contents (as inferred from far-UV circular dichroism; CD) in the corresponding 1SS peptides (18). A further correlation was observed between these properties and a pertinent pathogenetic process: extent of ER stress induced in a human cell line (HEK 293T) on transient expression of the corresponding mutant proinsulins. The coherence of these correlations (18) motivated this companion study wherein NMR spectroscopy provides a residue-specific view.

In this companion study we employ two-dimensional ^{1}H- and [^{1}H, ^{13}C]-NMR methods to interrogate the 1SS peptide models in relation to the native insulin. Analysis of main-chain ^{1}H and ^{13}C chemical shifts in the parent peptide (34–36) provided evidence for nativelike nascent α-helices in the B domain (residues B9-B19) and A domain (A12-A20), together in accordance with CD-defined α-helix content (18). Although chemical-shift dispersion in this and the variant partial folds is more limited than in the spectrum of a native insulin monomer (37), key side-chain resonance assignments were verified by site-specific ^{13}C (and ^{13}C, ^{15}N) labeling, using selective labeled amino-acid precursors

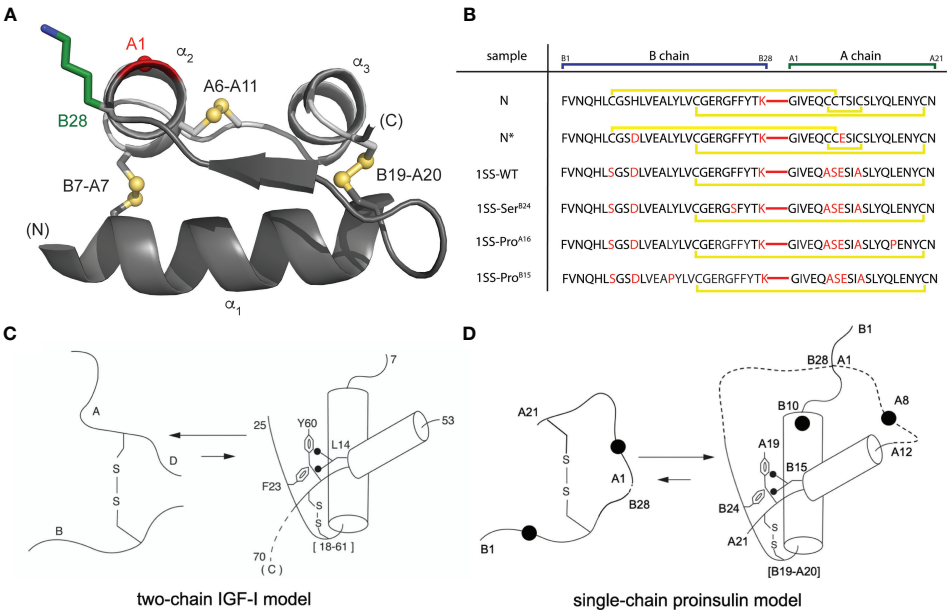

FIGURE 1 | Single-chain DesDi as a proinsulin model. **(A)** Cartoon model of single-chain DesDi molecule that connects A- and B- chains through a linkage between Lys^{B28} and Gly^{A1} (PDB entry 7JP3). Color legend: B chain, dark gray; A chain, light gray; Lys^{B28} side chain, green sticks; Gly^{A1}-C_{α}, red sphere; sulfur atoms in disulfide bonds are shown as spheres. All the spheres are set to one third Van der walls radii. N- and C- terminals are indicated. Insulin's three characteristic helices are labeled as α_1, α_2, and α_3. **(B)** DesDi protein sequences. Sample names at left report the presence of either one ([B19-A20]) or three (N and N*) disulfide bonds; yellow lines show disulfide linkages. A red line connecting the C-terminal B-domain and N-terminal A-domain sequences signifies the presence of a peptide bond between residues B28 and A1. All [B19-A20]-1SS samples and N* have additional mutations Glu^{A8} and Asp^{B10} to enhance solubility at neutral pH and the high protein concentrations needed for NMR spectroscopy. **(C)** General folding nucleus of insulin-related superfamily is shown with IGF-I as a model. **(D)** Folding nucleus of 1SS-DesDi single chain visualized as a proinsulin model. Initial pairing of B19-A20 disulfide in combination with the formation of two-helices (B9-B19 and A12-A20) are considered to be central events in the formation of folding nucleus. Dotted lines represent disordered regions. Larger circles represent the Asp^{B10} and Glu^{A8} substitutions. Key residues are highlighted by their sequence position [panel **(C, D)** modified from Hua et al. (22)].

in chemical peptide synthesis. Analysis of signature chemical shifts and framework nuclear Overhauser effects (NOEs) provides evidence for a nativelike folding nucleus in the parent 1SS peptide that is dependent on maintenance of the B19-A20 disulfide bridge. The clinical mutations perturb this nascent structure in the order Ser^{B24} (least perturbed) >> Pro^{A16} > Pro^{B15} (most perturbed). Together, these findings suggest that the DesDi-based 1SS model will provide a general platform for comparative biophysical studies of that subset of MIDY mutations that perturb initial closure of cystine B19-A20 in proinsulin biosynthesis in pancreatic β-cells.

MATERIALS AND METHODS

Solid-Phase Peptide Synthesis

Peptides were synthesized either with an ABI 433A Peptide Synthesizer (Applied Biosystems) or Tribute 2-Channel peptide synthesizer (Gyros Protein technologies) using a preprogrammed solid-phase fluorenylmethyloxycarbonyl chloride (Fmoc) protocol designed for standard 0.1mmol scale syntheses. ABI protocols consist of the following modules: cycle-1 [d], cycle-2 [aibde], cycle-3 with number of repetitions equal #aa-1 [afgbde], cycle-"#aa+2" [ffbdc], where #aa is a number of amino acids in the sequence. Automated couplings utilized diisopropylcarbodiimide (DIC)/6-Cl-hydroxybenzotriazole (6-Cl-HOBt) in *N*-methyl pyrrolidone (NMP) whereas Fmoc deprotections used 20% piperidine in NMP. α-Carboxyl-protected Asp was used in place of Asn in all syntheses of DesDi analogs to accommodate the use of ChemMatrix® Rink-Amide resin (loading = 0.46mmol/g). The Tribute peptide synthesizer used heating protocols: coupling was done at 6 min at 60°C except for Cys/His (2 min at 25°C, then 5 min at 60 °C) and Arg (20 min at 25 °C, then 5 min at 60°C); deprotection was done twice (30 sec at 50°C, then 3 min at 50°C). Reagent conditions were otherwise similar to ABI protocols except that DMF was used as solvent and choice of the resin was H-Asn (Trt)-HMPB-ChemMatrix® resin. Peptides were cleaved with a trifluoroacetic acid (TFA) cocktail (2.5% vol/vol of each: β-mercaptoethanol, triisopropylsilane, anisole, and water) followed by ether precipitation.

Folding and Purification of N and N* DesDi Analogs

Crude peptides from ether precipitation were dissolved in glycine buffer (20mM glycine and 2mM cysteine hydrochloride, pH 10.5) to a final peptide concentration of 0.1mM. The pH of this solution was readjusted to 10.5 to account for traces of residual TFA present in lyophilized peptides. This solution was

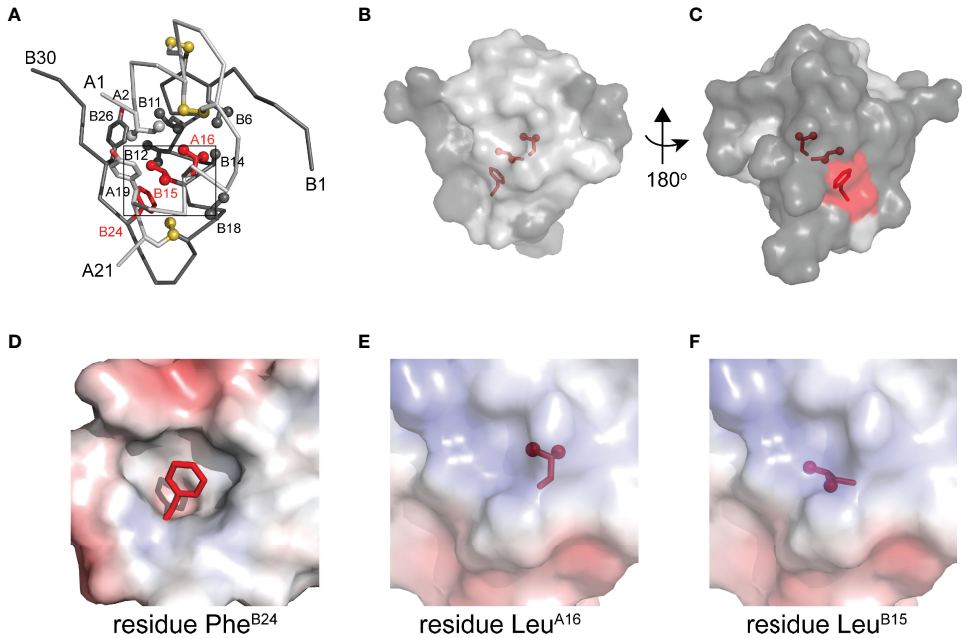

FIGURE 2 | Native structure of insulin and sites of present MIDY mutations. **(A)** ribbon diagram of insulin monomer (PDB entry 4INS). Side chains of key residues are shown as sticks with methyl groups and sulfur atoms in disulfide bonds are shown as spheres (one third van der Waals radii). Clinical mutations under the study is shown in red and all other side chains follow the color code: A chain (light gray), B chain (dark gray). **(B)** Surface representation of insulin monomer (transparency set to 40%) showing the side chains of Phe^{B24}, Leu^{B15} and Leu^{A16} (sticks shown as in panel A) within the core of the molecule. The surface of these residues is shown in red. **(C)** A view after rotating the molecule in panel B by 180° through y-axis. **(D–F)** Respective close-up views of the environments of Phe^{B24} (crevice), Leu^{A16} (core) and Leu^{B15} (core). In these panels the highlighted side chain is shown in red. These electrostatic surfaces were calculated in absence of indicated side chain.

then stirred while open to air at 4°C until reaction completion (usually overnight). The pH of the solution was then lowered to ~2.0 with 5N HCl to neutralize the folding reaction. Folded peptide was then purified by preparative rp-HPLC with a 60 min 20→40% acetonitrile elution gradient (10-15mL/min flow rate) run by a Waters rp-HPLC (Milford, MA) equipped with a Waters Model 600 Controller, Waters 2487 Dual Wavelength Detector, ProStar Model 701 Fraction Collector, Kipp & Zonen BD41 chart recorder, and a Luna 10µm C8(2) 100A AXIA (250 × 21.2mm) column. Fractions containing clean peptide were pooled and lyophilized. Purity of the materials was confirmed by LCQ Advantage Ion Trap Mass Spectrometer System coupled to an Agilent 1100 Series HPLC system utilizing a TARGA C8 5-µm (250 mm x 4.6 mm) column and a 35 min 25→50% acetonitrile elution gradient (1mL/min flow rate). See **Table S1** for LCMS retention times and mass verification.

Synthesis of Isotopically Labeled Peptides

Isotopically labeled 1SS and control peptides were prepared on 0.05 mmol scales. N* was assembled in entirety as a single batch whereas the 1SS peptides were assembled as a single batch (0.1mmol) through residue B25. At that point, half of the 1SS resin was used to complete assembly of the 1SS-Ser^{B24} analog. The remaining resin was used to complete the 1SS synthesis. Coupling of isotopically labeled amino acids (Cambridge Isotopes Inc., Tewksbury, MA) was performed manually using a single 0.3mmol mixture consisting of equivalent amounts of labeled Fmoc amino acid, 1-[Bis(dimethylamino)methylene]-1*H*-1,2,3-triazolo[4,5-*b*]pyridinium 3-oxid hexafluorophosphate (HATU), and *N,N*-diisopropylethylamine (DIEA) reacted with each individual batch of resin (2.25X overall excess). The same automated synthesis protocol used for unlabeled peptide syntheses was then used for the addition of subsequent unlabeled amino acids to the labeled peptide assembly. The following labeled amino acids were used (residual positions given in blue in **Scheme S1**): Fmoc-Gly[$^{13}C_2$, ^{15}N]-OH, Fmoc-Leu[$^{13}C_6$, ^{15}N]-OH, Fmoc-Ile[$^{13}C_6$, ^{15}N]-OH, Fmoc-Val[$^{13}C_5$, ^{15}N]-OH, and Fmoc-Tyr[$^{13}C_9$, ^{15}N]-OH. The peptides were cleaved from the resin by treatment with TFA cocktail as described above. The folding and purification of these isotope labeled 1SS peptides followed essentially same protocol as described in the companion article (18). Purity of the materials was confirmed by LC-MS with an Agilent 1260 Infinity/6120 Quadrupole instrument utilizing a Kinetex C8 2.6-µm 100A (75 mm x 2.1 mm) column and a 10 min 10-80% acetonitrile elution gradient (1mL/min flow rate) (See **Figures S1-S3**).

Purification of Clinical Analogs

Wild-type insulin and insulin *lispro* were purified from U-100 pharmaceutical formulations of Humulin® and Humalog® (Eli Lilly and Co.), respectively, using preparative RP-HPLC (C4 10µm 250×20mm Proto 300 Column; Higgins Analytical, Inc.) utilizing buffer A (0.1% TFA in H_2O) and a 10-min elution gradient of 20→70% buffer B (0.1% TFA in acetonitrile).

Following lyophilization of the collected protein fraction, purity was verified using analytical HPLC (TARGA C8 5-μm [250 mm x 4.6 mm]; Higgins Analytical, Inc.) with a 35-min elution gradient of 25→50% buffer B; molar mass was verified with an Applied Biosystems 4700 Proteomics Analyzer utilizing MALDI-TOF in reflector mode. chromatographic retention times and mass measurements for these clinical analogs are given in **Table S1**.

Proinsulin Constructs

Plasmids expressing full-length human proinsulin or variants were constructed by polymerase chain reaction (PCR). Mutations in proinsulin were introduced using QuikChange™ (Stratagene). Constructions were verified by DNA sequencing.

NMR Spectroscopy

^{1}H NMR spectra were acquired at a proton frequency of 700 MHz at pD 7.4 (direct meter reading) at 35°C. ^{1}H-^{13}C heteronuclear single-quantum coherence (HSQC) spectra were acquired at natural abundance as described. The spectra were obtained at ^{13}C frequency of 176 MHz at a constant temperature of 308 K using the "hsqcetgp" Bruker pulse sequence as described by the manufacturer. Aliphatic ^{1}H-^{13}C HSQCs were acquired with FID size 2048 x 128, 800 scans, 1.0 sec relaxation delay, sweep widths 11 ppm (^{1}H) and 70 ppm (^{13}C) with offset 4.7 and 40 ppm for the ^{1}H and ^{13}C dimension, respectively. Similar parameters were used to acquire aromatic ^{1}H-^{13}C HSQC, except with sweep widths of 40 ppm and 125 ppm offset in ^{13}C dimension. Data were processed with Topspin 4.0.6 (Bruker Biospin) and analyzed with Sparky software (38) using a 90° shifted-sine window function to a total of 2048 × 1024 data points (F2 × F1), followed by automated baseline- and phase correction. All NMR data were acquired using a BRUKER 700 MHz spectrometer equipped with quadruple [^{1}H, ^{19}F, ^{13}C, ^{15}N]-resonance liquid-helium-cooled cryoprobe.

Secondary Structure Analysis

Protein secondary structure was inferred from selected ^{1}H and ^{13}C secondary chemical shifts ($^{1}H_N$, $^{1}H_\alpha$, $^{13}C_\alpha$ and $^{13}C_\beta$) as described (35, 39, 40). In such algorithms $^{13}C_\alpha$ and $^{1}H_\alpha$ chemical shifts distinguish α-helix from β-strand or random coil (41) whereas $^{13}C_\beta$ secondary shifts are more sensitive to β-strand. These chemical shifts in the parent 1SS model were assigned on the basis of 2D ^{1}H-^{1}H NOESY, TOCSY, DQF-COSY in D_2O and H_2O (10% D_2O) and natural abundance ^{1}H-^{13}C HSQC spectra. Corresponding secondary shifts were extracted from observed chemical shifts ($\Delta = \delta_{obs} - \delta_{coil}$). Secondary structural elements were predicted by TALOSplus (34–36).

Molecular Modeling

Structural ensembles were calculated by simulated annealing using *XPLOR-NIH* (42–44). The models of the one-disulfide proinsulin and one-disulfide DesDi intermediates (containing cystine B19-A20) were generated using distance restraints pertaining to residues A16-A21 and B15-B26 as observed in an engineered proinsulin (45) or an engineered insulin monomer (46). To allow for protein flexibility in these partial folds, upper bounds on long-range distance restraints were increased by 3 Å relative to NMR-derived upper bounds obtained in prior studies of insulin and proinsulin (45, 46).

RESULTS

One-dimensional ^{1}H-NMR spectra of the 1SS peptide model and its variants were presented in our companion study (18) in relation to spectra of the native state (provided as **Figure S4** for convenience of the reader). Molecular properties of these peptides are summarized in **Table S1**. Although the 1D spectra were in overall accordance with trends in synthetic yield, CD deconvolution and redox stability (18), interpretation was limited by the small number of resolved features. To circumvent this limitation, 2D homonuclear and 2D ^{1}H-^{13}C HSQC NMR spectra were obtained at natural abundance. Analysis was undertaken in reference to baseline HSQC spectra of native DesDi (as the single-chain precursor and as cleaved two-chain hormone analog; **Figures 3A, B**). Near-complete assignment of $^{1}H_N$, $^{1}H_\alpha$, $^{13}C_\alpha$ and $^{13}C_\beta$ resonances in the parent 1SS peptide model enabled mapping of secondary structure based on pattern of secondary chemical shifts (**Figure 4**) (34–36). α-Helical segments comprise residues B9-B18 and A13-A19 (**Figure 4E**), a subset of native secondary structure. Chemical shifts (referenced below) and estimates of chemical-shift dispersion are tabulated in **Tables S2–S9**.

^{1}H-^{13}C HSQC spectra provide correlations between a ^{13}C atom and an attached proton (^{1}H) *via* a one-bond J-coupling (47, 48). Initial spectra were obtained at 35 °C. Key resonance assignments in the parent 1SS peptide and 1SS-Ser^{B24} variant were verified by site-specific ^{13}C labeling of residues Val^{B12}, Leu^{B15}, Gly^{B23}, Phe^{B24}, Tyr^{B26} and Ile^{A2} (**Scheme S1** and **Figure S5**). In each figure aromatic 2D spectra are shown at left, and aliphatic spectra at right. The spectrum of the native state is better illustrated by two-chain [Asp^{B10}, Glu^{A8}]-DesDi-insulin (**Figure 3B**; black) than its single-chain precursor (**Figure 3A**; gray) due to selected resonance broadening in the latter spectrum; such broadening may reflect partial dimerization (stronger in single-chain analogs) and/or conformational exchange intermediate on the timescale of NMR chemical shifts. The baseline 2D ^{1}H-^{13}C HSQC spectrum of two-chain [Asp^{B10}, Glu^{A8}]-DesDi-insulin is notable for its resolution of many individual spin systems; selected resonance assignments are provided in **Figures 3A, B**. Of particular interest are the aromatic resonance of Phe^{B24} and Tyr^{B26}, which pack against the central B-chain α-helix and influence the chemical shifts (via their aromatic ring currents) of the side chains of Leu^{B11} and Leu^{B15}. These respective upfield aromatic and upfield methyl resonances provide markers of the native B-chain supersecondary structure (49, 50). The upfield chemical shifts of Ile^{A2} by contrast reflects A-chain supersecondary structure (in particular the aromatic ring current of Tyr^{A19}); that of Ile^{A10} reflects inter-chain packing of His^{B5} (51, 52). The latter structural features (and their NMR signatures) are reinforced by cystines A6-A11 and B7-A7 in native insulin.

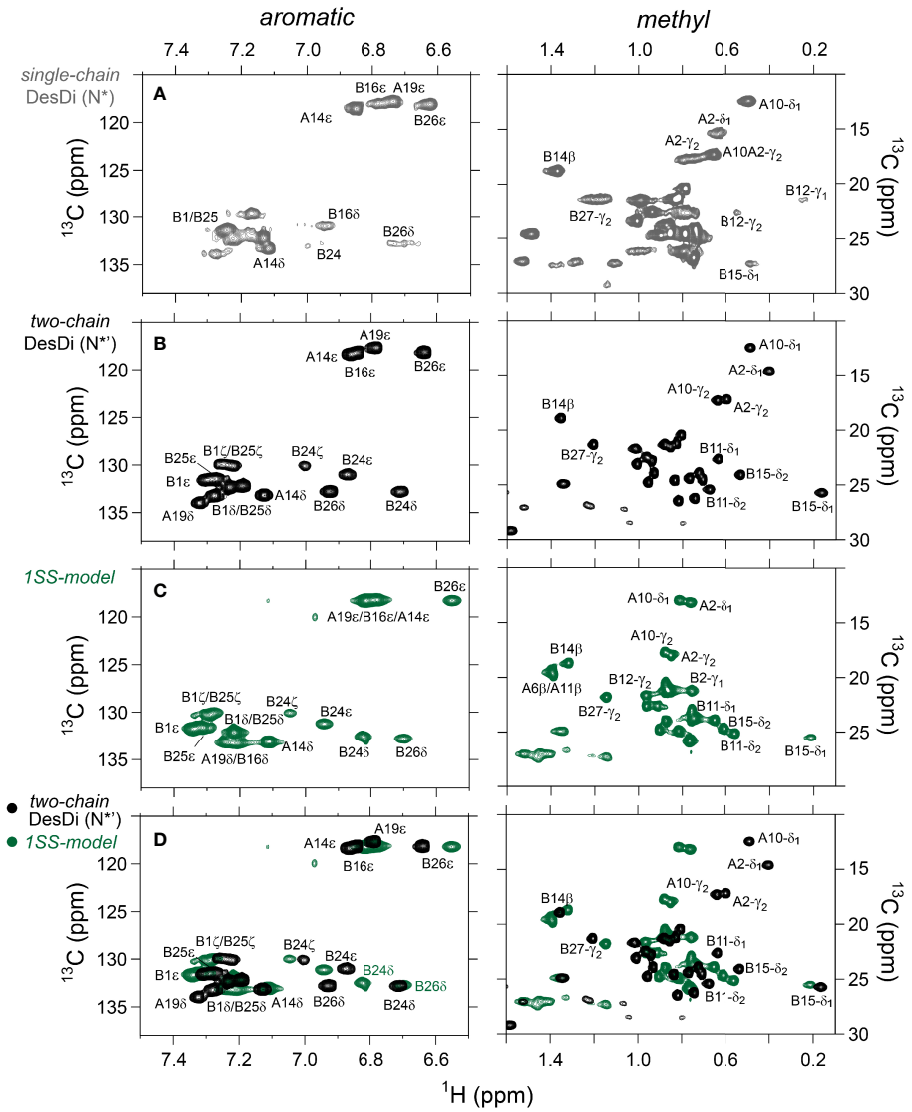

FIGURE 3 | Nature abundance ^{1}H,^{13}C HSQC NMR spectra of DesDi analogs in aromatic (*left panel*) and methyl region (*right panel*). **(A)** single-chain DesDi (N*); **(B)** two-chain DesDi (N*'); **(C)** single-chain 1SS-DesDi model (*green*) and **(D)** the ^{1}H-^{13}C HSQC spectral overlay of two-chain DesDi (N*', *black*) and 1SS-model (*green*). Spectra were acquired at a ^{1}H frequency of 700 MHz at pD 7.4 (direct meter reading) and at 35°C in D_2O. Selected resonance assignments are as indicated.

The 2D ^{1}H-^{13}C HSQC spectrum of the parent 1SS model (**Figure 3C**; green) is remarkable for preservation of some upfield shifts (Phe^{B24}, Tyr^{B26}, Leu^{B11} and Leu^{B15}) but not others (Ile^{A2} and Ile^{A10}). The former subset of nativelike chemical shifts indicates maintenance of B-chain secondary structure flanking Cys^{B19} (and therefore the B19-A20 disulfide bridge) whereas the latter attenuation of structure-dependent secondary shifts indicates destabilization of long-range structure involved the A2-A10 segment in accordance with removal of the B7-A7 and A6-A11 disulfide bridges (50, 53, 54). This combination of preserved and attenuated chemical shifts in the spectrum of the parent 1SS model is illustrated by overlay of its spectrum (green) and that of two-chain [Asp^{B10}, Glu^{A8}]-DesDi-insulin (black) in **Figure 3D**. The spectrum of the parent 1SS peptide in turn provides a baseline for comparative analysis of the MIDY-derived variants (**Figure 5**). Chemical-shift dispersion is markedly attenuated in each of the variants (**Figures 5B–D**), most markedly in 1SS-Pro^{B15} (**Figure 5D**). In the case of 1SS-Ser^{B24} (**Figure 5B**) such attenuation may reflect both loss of ordered structure and removal of the Phe^{B24} aromatic ring current (52), potentially a confounding issue (the same issue pertains to Ser^{B24}-insulin analogs with native pairing; **Figure S6**). A subtle trend is observed in the $^{1}H_{\epsilon}$ chemical shift of Tyr^{B26} (arrows in **Figures 5B–D**) in which slight upfield shifts are observed in two case (1SS-Ser^{B24} > 1SS-Pro^{A16}), but not observed in 1SS-Pro^{B15}. This trend is shown in an enlargement of spectra in **Figure S7**.

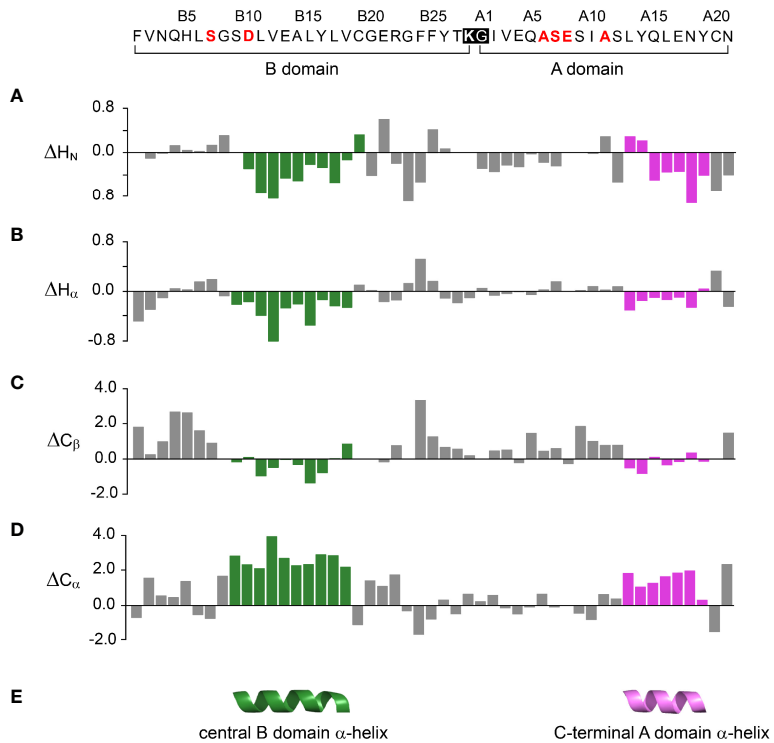

FIGURE 4 | Chemical shift index (CSI) and inferred secondary structure of parent peptide model. *Top*, 49-residue polypeptide sequence with six amino-acid substitutions in red. DesDi's engineered junction between Lys^{B28} (bold) and Gly^{A1} (27) is highlighted within black box. The secondary shift was defined as the difference of observed chemical shift and random coil shift ($\Delta = \delta_{obs} - \delta_{coil}$). Positive (negative) values indicate that the observed chemical shift is downfield (upfield) of expected random-coil frequency (34, 35). **(A–D)** CSI-related secondary chemical shifts by residue: **(A)** amide protons (ΔH_N); **(B)** α-protons (ΔH_α); **(C)** β-carbons (ΔC_β); **(D)** α-carbons (ΔC_α). **(E)** Inferred elements of secondary structure as predicted by *TALOSplus* (34–36): central B-domain α-helix (residues B9-B18) and C-terminal A-domain α-helix (residues A13-A19). Corresponding residue-specific secondary shifts are given in **Table S9**.

Analysis of ^{1}H-^{13}C chemical shifts was extended by 2D ^{1}H-^{1}H NOE spectroscopy (NOESY). Of particular interest are inter-proton NOEs (reflecting distances < 5 Å) between aromatic and aliphatic side chains. Such NOEs are prominent in the spectrum of native insulin (upper panel of **Figures 6A, B**), shown in relation to the corresponding TOCSY (total correlation spectroscopy) spectra of aromatic spin systems (lower panel). These inter-residue NOEs in part retained in the NOESY spectrum of the parent 1SS peptide (upper panel in **Figure 6C**). Particularly notable is the retention of close contacts between Phe^{B24} and Tyr^{B26} and the methyl groups of Leu^{B15}, resolved due to native-like chemical-shift dispersion. A subtle feature is observed in the aromatic TOCSY spectra: the spin systems of Tyr^{B16} and Tyr^{A19}, downfield of the mobile and solvent-exposed side chain of Tyr^{A14} in native insulin (lower panels of **Figures 6A, B**), is retained in attenuated form in the TOCSY spectrum of 1SS peptide (lower panel of **Figure 6C**). NOEs between aromatic and aliphatic protons are observed in the spectra of the variants, but with decreased dispersion (inset boxes in **Figures 6D–F**); in the case of 1SS-Pro^{B15}, the overall integrated cross-peak envelope intensity is reduced (**Figure 6F**). Although as expected the aromatic spin system of Phe^{B24} is absent in the TOCSY spectrum of 1SS-Ser^{B24} (lower panel of **Figure 6D**), subtle upfield shifts of Phe^{B24} are retained in 1SS-Pro^{A16} and 1SS-Pro^{B15}. These trends are shown in expanded form in **Figure S8**. We imagine that the latter conformational ensembles contain a minor fraction of compact substates with long-range contacts, which nonetheless are less populated than in the parent 1SS peptide. This interpretation is supported by more detailed examination of these NOESY regions (**Figures 7C–F**) in relation to the structural relationships in native insulin (**Figures 7A, B**). Aromatic-methyl NOEs in the parent 1SS model are shown in expanded form in **Figure 7C**; long-range contacts are prominent in the neighborhood of cystine B19-A20, proposed to constitute the specific folding nucleus of proinsulin (green side chains in **Figure 7A**) (22). Also observed are long-range NOEs from Tyr^{B26} to the methyl groups of Ile^{A2} and Val^{A3}, presumably reinforced by the B28-A1 peptide bond in the DesDi framework and foreshadowing subsequent steps in A-domain segmental folding associated with pairing of the remaining two cystines. This subset of these nativelike long-range NOEs can be resolved in the variants despite their attenuated chemical-shift dispersion (**Figures 7D–F**).

The above degree of organization in the nascent structure of the parent 1SS model is dependent on pairing of Cys^{B19} and

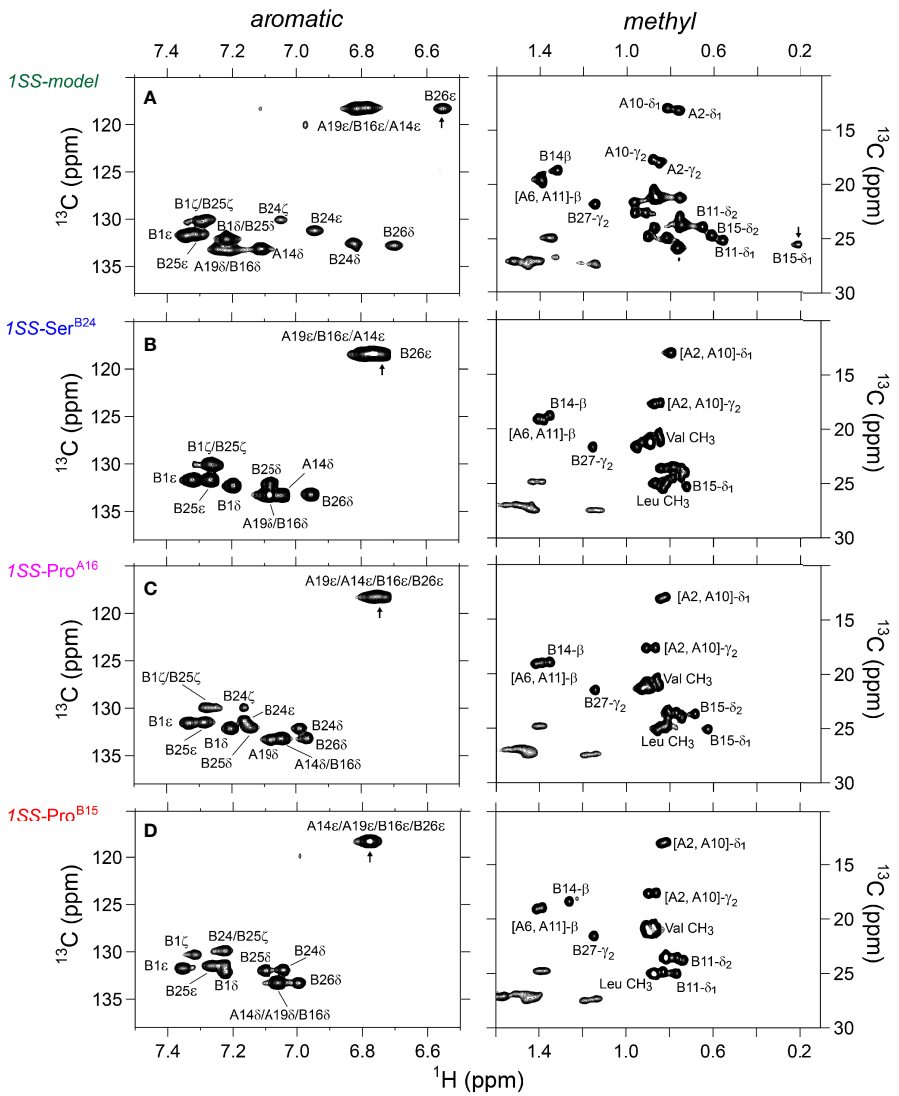

FIGURE 5 | Nature abundance ^{1}H-^{13}C HSQC NMR spectra of single-chain 1SS-DesDi analogs in aromatic (*left panel*) and methyl region (*right panel*). **(A)** single-chain 1SS model; **(B)** single-chain 1SS-Ser^{B24} analog. **(C)** single-chain 1SS-Pro^{A16} analog and **(D)** single-chain 1SS-Pro^{B15} analog. Spectra were acquired at a ^{1}H NMR frequency of 700 MHz at pD 7.4 (direct meter reading) and 35°C in D_2O. Selected resonance assignments are as indicated.

Cys^{A20}. Whereas overlay of the ^{1}H-^{13}C HSQC spectra of the parent 1SS peptide and two-chain [Asp^{B10}, Glu^{A8}]-DesDi-insulin reveals similar limits of dispersion (green versus black in **Figure 8A**; inset vertical and horizontal arrows), reduction of the 1SS disulfide bridge by deuterated dithiothreitol (to yield a linear peptide) led to loss of ^{1}H-^{13}C chemical-shift dispersion (green versus brown in **Figure 8B**). The reduced 1SS peptide exhibits limited dispersion, with pattern that is similar in detail to that of 1SS-Pro^{B15} (brown versus red in **Figure 8C**). Possible transient or nascent long-range interactions in the linear 1SS peptide have not been investigated. ^{1}H-^{13}C HSQC spectra of the four 1SS peptides are overlaid in **Figure 8D**; relative main-chain dispersions exhibit the qualitative trend: parent > Ser^{B24} > Pro^{A16} > Pro^{B15} in accordance with the findings above. This trend was made quantitative by detailed analysis of respective secondary shifts [in reference to tabulated random-coil values (55)] as shown in the four histograms in **Figure S11**. Reliance of $^{1}H_{\alpha}/^{13}C_{\alpha}$ chemical shifts circumvents the confounding absence of the B24 ring current in 1SS-Ser^{B24} as these resonances are less influenced by aromatic ring currents (52, 56). The greater main-chain chemical-shift dispersion in 1SS-Ser^{B24} and 1SS-Pro^{A16} relative to 1SS-Pro^{B15} was accentuated by lowering the temperature from 35 to 10°C. Stacked plots of 1D ^{1}H-NMR spectra are shown for each 1SS peptide as a function of temperature in the range 5-35°C (in steps of 5°C) in **Figure S9**. At lower temperatures spectra of the parent 1SS peptide, 1SS-Ser^{B24} and 1SS-Pro^{A16} exhibit conformational broadening of upfield aromatic and aliphatic features, suggesting slowing of conformational fluctuations into the millisecond

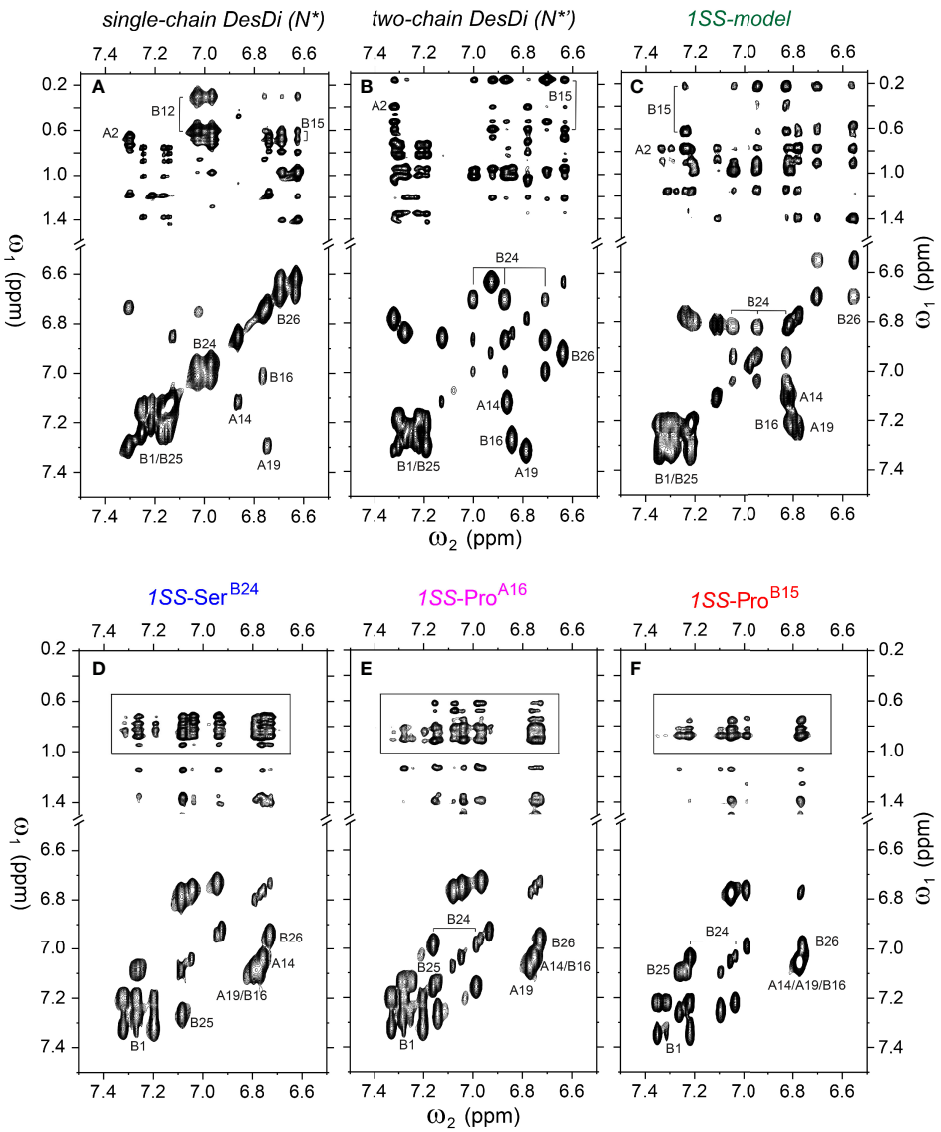

FIGURE 6 | Homonuclear 2D-NMR spectra: NOESY spectra (mixing time 150 ms) showing NOEs from aromatic protons to methyl protons (*top panel*) and TOCSY spectra (mixing time 55 ms) showing aromatic resonance correlation (*bottom panel*). **(A)** single-chain DesDi (N*); **(B)** two-chain DesDi (N*'); **(C)** single-chain DesDi 1SS model; **(D)** single-chain 1SS-Ser^{B24} analog; **(E)** single-chain 1SS-Pro^{A16} analog and **(F)** single-chain 1SS-Pro^{B15} analog. The boxes in panel D-F indicate spectral expansion for detailed analysis. Spectra were acquired at pD 7.4 (direct meter reading) and 35°C in D_2O.

regime characteristic of intermediate exchange on the time scale of ^{1}H-NMR chemical shifts. This phenomenon is not observed in the spectrum of 1SS-Pro^{B15}. Comparison of $^1H_\alpha$-$^{13}C_\alpha$ cross peaks in respective HSQC spectra likewise highlights the anomalous temperature-independence of the 1SS-Pro^{B15} spectrum (**Figure S10**). This trend extends to the aromatic and methyl regions of the HSQC spectra (**Figure S12**). The chemical shift of Tyr^{B26} H_ϵ and a resolved methyl resonance in the reduced 1SS peptide are likewise independent of temperature (**Figures S12**, **S13**). We speculate that the anomalous NMR properties of 1SS-Pro^{B15}, indicating loss of nascent structure relative to the other 1SS peptides, rationalizes this mutation's essentially complete block to the folding of Pro^{B15}-DesDi, even in the presence of stabilizing substitutions Asp^{B10} and Glu^{A8} [preceding article in this issue (18)].

DISCUSSION

The discovery of proinsulin by Steiner and colleagues in 1967 [(25, 57); for review, see (58)] solved a problem encountered in the chemical synthesis of insulin: inefficient specific disulfide pairing encountered in chain combination (24). Although the isolated A- and B chains of insulin contain sufficient information to specify the native structure (59), yield is reduced by competing

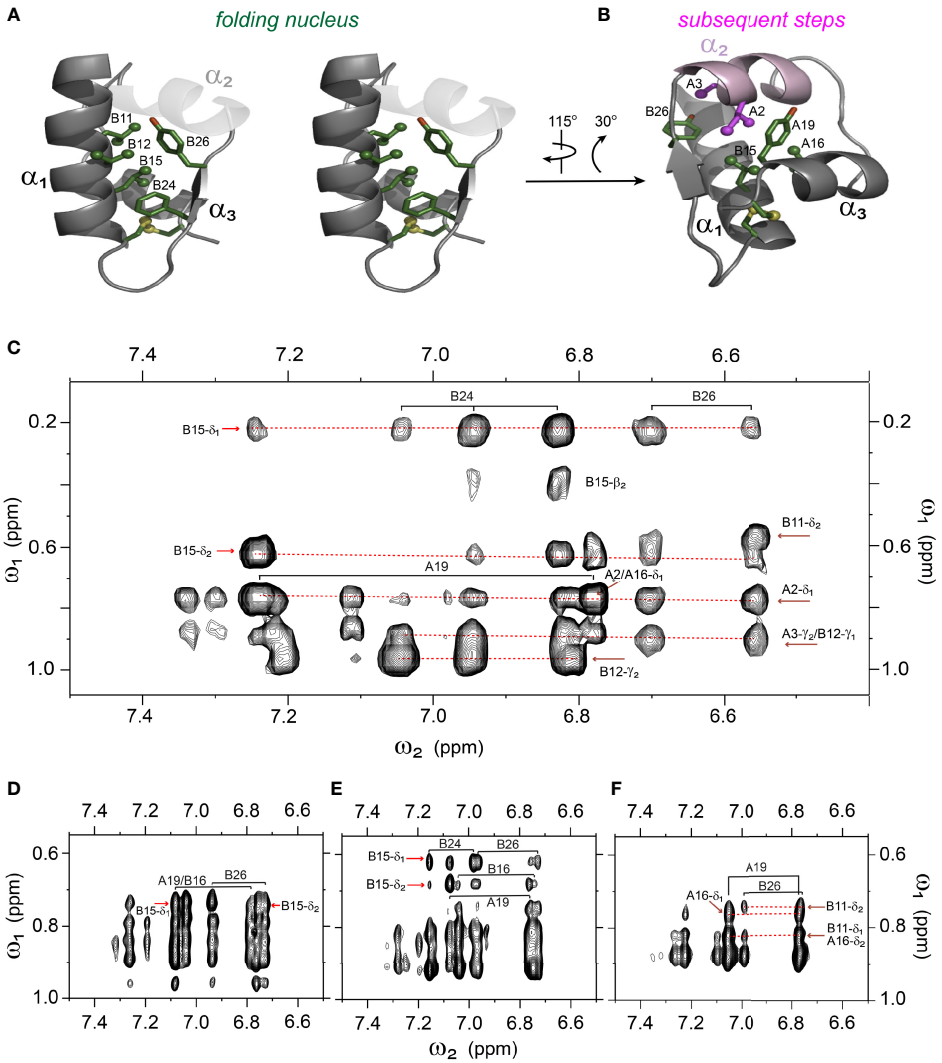

FIGURE 7 | Spectral expansion of 2D-NOESY revealing signature long-range NOEs in the variants of single-chain 1SS-DesDi. **(A)** stereo view of the ribbon structure of single-chain DesDi (PDB entry 7JP3). The side-chains of indicated residues assembled a hydrophobic cluster that functions as a folding nucleus. **(B)** the ribbon structure of single-chain DesDi showing subsequent steps of insulin folding. **(C)** NOESY expansion of single-chain DesDi 1SS model. **(D)** single-chain 1SS-Ser^{B24} analog. **(E)** single-chain 1SS-Pro^{A16} analog and **(F)** single-chain 1SS-Pro^{B15} analog. All spectra were acquired at pD 7.4 (direct meter reading) and at 35°C in D_2O.

off-pathway reactions, including formation of cyclic peptides and amyloid. Proinsulin is nonetheless itself difficult to fold. The majority of human cell lines in routine laboratory use do not efficiency fold proinsulin (4), leading to detectable disulfide isomers (3). The specialized folding environment of the β-cell ER is adapted to the biochemical demands of proinsulin biosynthesis, and yet even so physiological overexpression of the *INS* gene—as a compensatory response to peripheral insulin resistance (60)—can induce chronic ER stress and contribute to the progression of prediabetes and Type 2 DM (8). The growing collection of MIDY mutations in proinsulin associated with toxic misfolding leading to β-cell dysfunction (9) has motivated the hypothesis that insulin sequences, well conserved among vertebrates (23, 61), are entrenched at the edge of foldability (46). The marginal stability of insulin and proinsulin, relative to such classical model proteins as bovine pancreatic trypsin inhibitor and hen egg white lysozyme, is associated with qualitative differences in their respective refolding properties (62–67) (see also Supplemental Discussion).

In this and our companion study (18) we have introduced a single-chain peptide model of an early proinsulin folding intermediate. A framework ("DesDi") was provided by an innovative mini-proinsulin containing a peptide bond between residues B28 and A1, with Pro^{B28} substituted by Lys to enable facile enzymatic cleavage to liberate an active insulin analog (27). The B28-A1 peptide bond enables successful oxidative folding of the 49-residue synthetic precursor even in the presence of mutations (such as Val^{A16}) that otherwise block classical chain

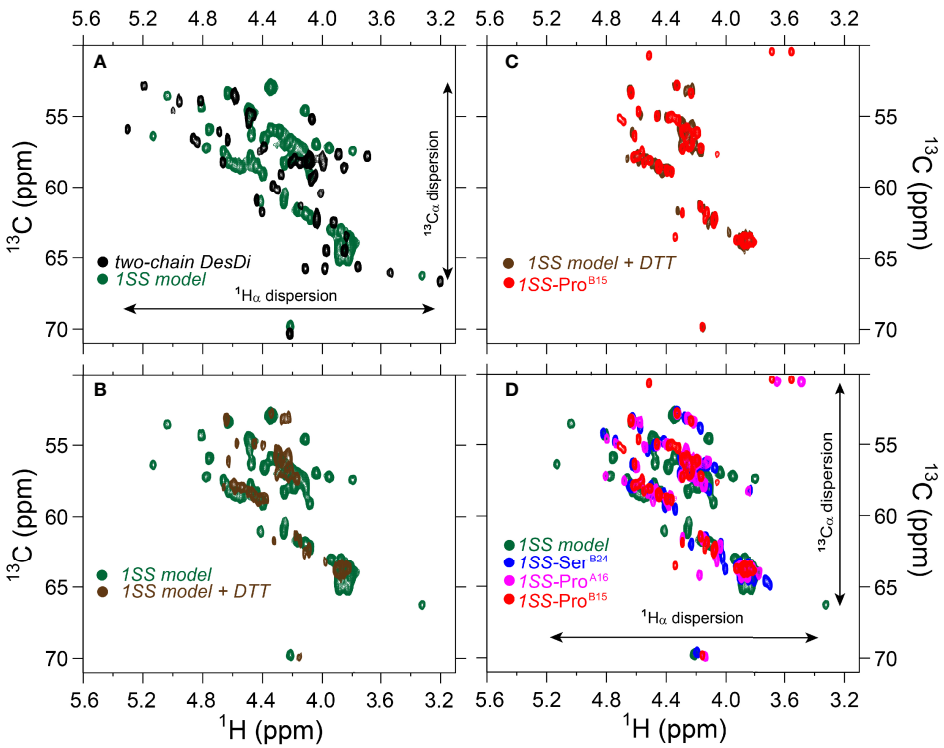

FIGURE 8 | Comparison of nature abundance ^{1}H-^{13}C HSQC spectra of single-chain DesDi analogs in $^{1}H_{\alpha}/^{13}C_{\alpha}$ region. **(A)** ^{1}H-^{13}C HSQC spectral overlay of two-chain DesDi (N*', *black*) and single-chain DesDi 1SS model (*green*); **(B)** ^{1}H-^{13}C HSQC spectral overlay of single-chain DesDi 1SS model (*green*) and 1SS model in 70 mM deuterated dithiothreitol (DTT) (*brown*); **(C)** spectral overlay of single-chain 1SS-Pro^{B15} analog (*red*) and *1SS-model* in 70 mM deuterated dithiothreitol (*brown*); **(D)** spectral overlay of single-chain DesDi 1SS model (*green*), single-chain 1SS-Ser^{B24} analog (*blue*), single-chain 1SS-Pro^{A16} analog (*magenta*) and single-chain 1SS-Pro^{B15} analog (*red*). Spectra were acquired at a ^{1}H frequency of 700 MHz at pD 7.4 (direct meter reading) and at 35°C in D_2O.

combination (68). The B28-A1 inter-chain tether in DesDi presumably favors a productive orientation between A- and B-domain folding determinants and limits off-pathway events. We further stabilized DesDi by enhancing the α-helical propensity of the central B-domain segment [His^{B10}→Asp (29)] and N-terminal A-domain segment [Thr^{A8} →Glu (30)]. Increasing the net negative charge through these acidic substitutions would also be expected to enhance solubility and retard competing formation of amyloid (69). A one-disulfide model of an initial proinsulin folding intermediate was thus obtained by pairwise substitution of exposed cystine B7-A7 by Ser and internal cystine A6-A11 by Ala (18).

The present study builds on our foundational characterization of the 1SS peptide model to interrogate nascent structure by two-dimensional ^{1}H and ^{1}H-^{13}C NMR spectroscopy. In accordance with prior NMR studies of a two-chain peptide model of a one-disulfide IGF-I folding intermediate (22), the parent 1SS model contains a subset of native secondary structure: central B-domain α-helix (residues B9-B19), C-terminal A-domain α-helix (A12-A20) and nascent β-strand (B24-B26). Molecular models of the parent model and the corresponding proinsulin intermediate are shown in **Figure 9A** in relation to the solution structure of an engineered proinsulin monomer (45). In these models cystine B19-A20 is integral to the hydrophobic mini-core formed at the confluence of the nascent elements of secondary structure. We envision that this nativelike subdomain represents the first organized nucleus in a series of successive folding landscapes (**Figure 9B**). Although disulfide chemistry in polypeptides can exhibit (especially at basic pH) complex patterns of native and non-native disulfide exchange and rearrangement, this structural perspective offers a simplified view of the predominant proinsulin folding scheme at neutral pH (**Figure 9C**). This scheme in principle provides a framework for interpreting clinical mutations that impair folding efficiency.

Comparative NMR studies of the variant 1SS peptides suggest structural mechanisms of impaired foldability. In particular, patterns of chemical shifts and NOEs provide evidence of native-like tertiary structure in the neighborhood of cystine B19-A20 and its destabilization in the variant peptides in rank order Ser^{B24} >> Pro^{A16} > Pro^{B15} (least organized). Their respective ensembles of partial folds each exhibit a subset of nativelike long-range NOEs—presumably reflecting fractional occupancies of analogous molten-globule states that foreshadow native structural relationships—but with progressively more complete averaging of chemical shifts in this series (**Figure S14**). Among these 1SS peptides and native insulin, striking correlations are observed between CD-defined α-helix contents [in the same rank order (18)] and NMR

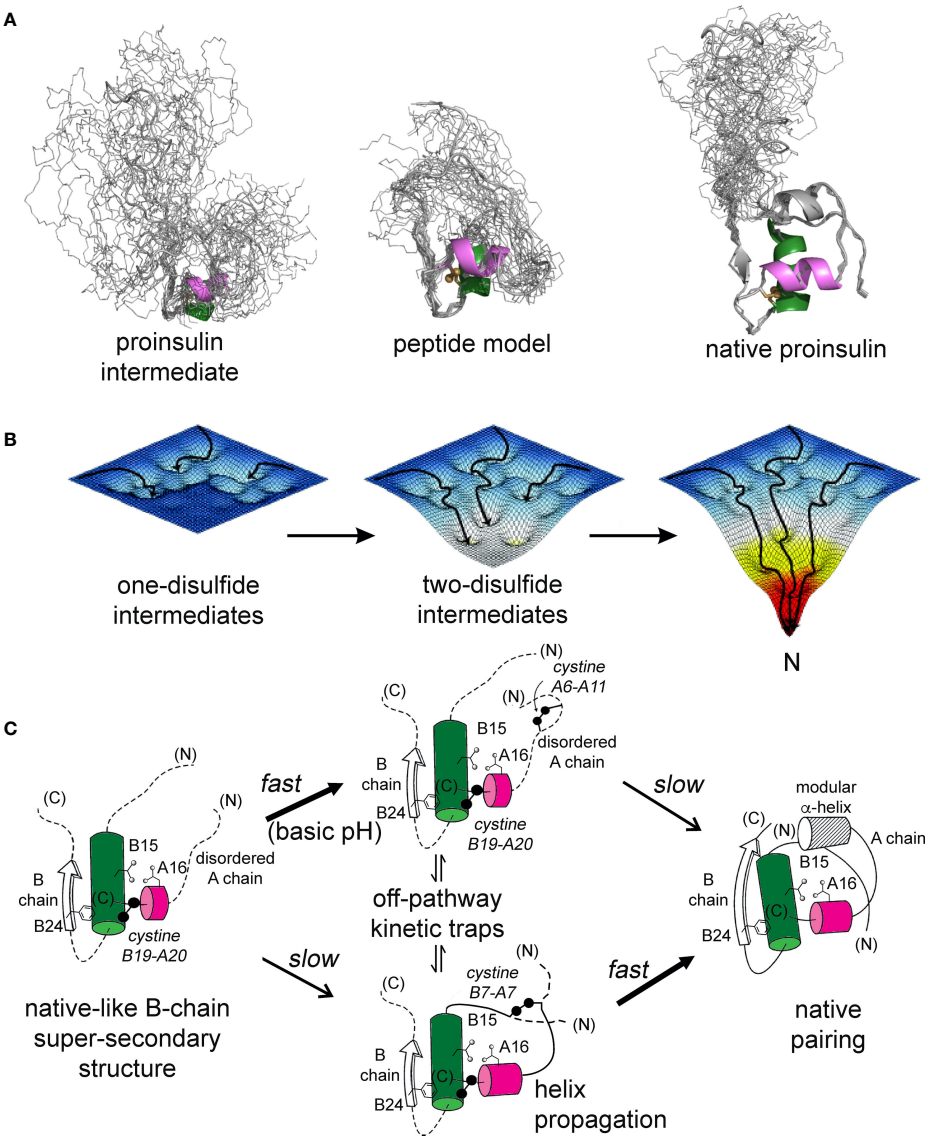

FIGURE 9 | Proinsulin peptide models and hierarchical disulfide pathway. **(A)** Predicted structural ensembles for one-disulfide 86-residue proinsulin intermediate containing cystine B19-A20 (left) and corresponding 49-residue one-disulfide model (middle) relative to the solution structure of an engineered proinsulin monomer [PDB entry 2KQP; (45)] (right). In each ensemble α-helices are shown in green (central B domain) and magenta (C-terminal A domain). The simulated ensembles were generated by restrained molecular dynamics using XPLOR-NIH software (43, 44) and visualized by PyMol (https://sourceforge.net/projects/pymol/). **(B)** Free-energy landscapes as envisioned to govern proinsulin folding: disulfide pairing follows a sequence of folding trajectories on successively steeper landscapes. **(C)** Preferred pathway of disulfide pairing begins with cystine B19-A20 (left), directed by a nascent hydrophobic core formed by the central B-domain α-helix (residues B9–B19), part of the C-terminal B-chain β-strand (B24-B26) and part of the C-terminal A-domain α-helix (A16–A20). Alternative pathways mediate formation of successive disulfide bridges (middle panel) en route to the native state (right panel). This pathway is perturbed by diverse MIDY mutations. Nascent α-helices are color-coded as in **(A)**. Panel **(B)** is adapted from an image kindly provided by J. Williamson; Panel **(C)** is adapted from reference (70).

parameters: mean $^{1}H_{\alpha}$ chemical-shift dispersion (**Figure 10A**) and average $^{1}H_{\alpha}/^{13}C_{\alpha}$ main-chain secondary shifts (**Figure 10B**). The biological importance of these CD- and NMR-derived biophysical parameters is demonstrated by their further correlation with levels of ER stress induced by expression of the corresponding mutant proinsulin (**Figures 10C, D**) (18). Although each MIDY mutation alters an invariant framework residue—conserved among both vertebrate insulins and vertebrate insulin-like growth factors (23, 61, 71) —the less severe biophysical consequences of Phe^{B24}→Ser in consistent with the delayed onset of DM in patients with this mutation (4, 33). Although Pro^{B15} is more profoundly perturbing than is Pro^{A16}, each is associated with neonatal-onset DM (31, 32) and so must surpass the threshold for post-natal β-cell ER stress leading to the rapid progression of β-cell dysfunction and death (8).

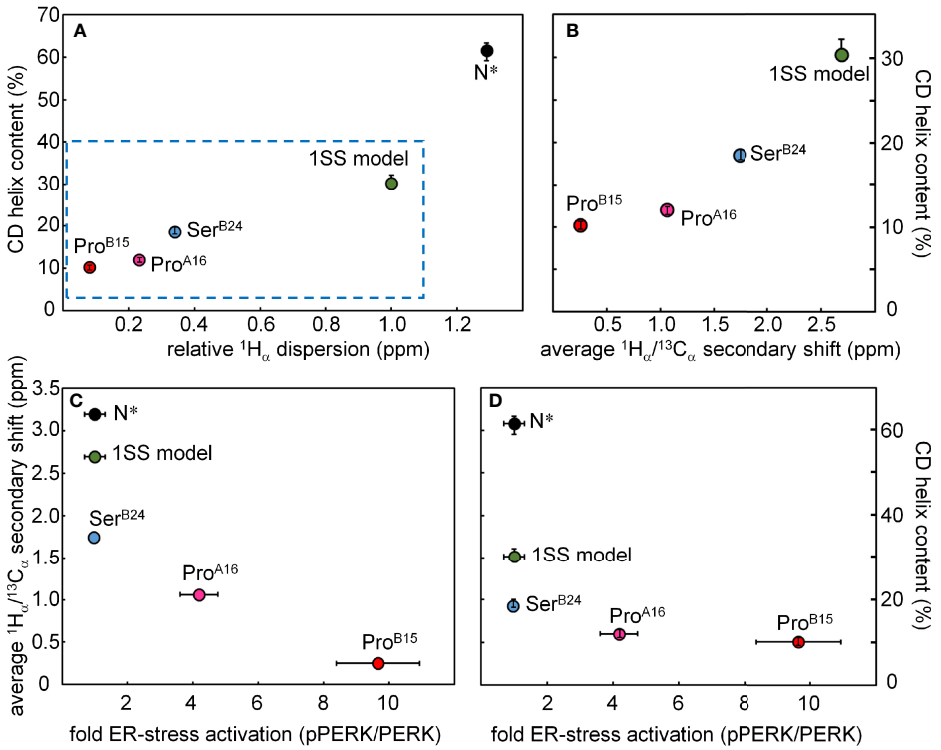

FIGURE 10 | Plots showing correlations among biophysical features, NMR parameters and cellular ER-stress activation. **(A)** The plot shows the relationship between the relative $^1H_\alpha$ dispersion (X axis; ppm) CD-derived helix contents of DesDi variants (Y axis; %). N* analogs provide control data pertaining to the single-chain ground state stabilized by the three native disulfide bridges; sequences contain the same favorable substitutions at B10 and A8 as in the 1SS analogs. Relative $^1H_\alpha$ dispersion was defined by the difference of $^1H_\alpha$ chemical-shift dispersion of DesDi analogs and base line control (1SS model in 70 mM deuterated dithiothreitol). **(B)** Correlation between CD-derived helix contents (Y axis) with the average $^1H_\alpha/^{13}C_\alpha$ secondary shift (X-axis). Average $^1H_\alpha/^{13}C_\alpha$ secondary shift ($\bar{\Delta}$) was calculated using equation $\bar{\Delta} = \sqrt{(\Delta^2_{B12} + \Delta^2_{B14} + \Delta^2_{B18})/3}$. Δ_{B12}, Δ_{B14} and Δ_{B18} are $^1H_\alpha/^{13}C_\alpha$ secondary shift of residues Val^{B12}, Ala^{B14} and Val^{B18}, respectively. **(C, D)** Relationship between ER stress in cell-based assay and NMR/biophysical parameters. **(C)** Relationship between fold-change in ER stress (X axis; pPERK/PERK ratio) and $^1H_\alpha/^{13}C_\alpha$ secondary shift (Y axis; ppm) among DesDi variants. **(D)** Relationship between ER stress and α-helix content of related DesDi variants (Y-axis; %).

A surprising aspect of the present NMR studies is extent to which the parent 1SS peptide retains native-like spectroscopic features. Such structure is lost on reduction of cystine B19-A20. We ascribe the nascent organization of the parent 1SS peptide to (a) the B28-A1 peptide bond, which orients flanking B- and A-domain segments, and (b) stabilizing α-helical substitutions Asp^{B10} and Glu^{A8}. Although such extensive nascent structure would not be expected in a one-disulfide analog of proinsulin (86 residues), the richness of the 1SS NMR spectrum suggests that it would be of future interest to develop a biosynthetic expression system, so that uniform ^{13}C and ^{15}N isotopic labeling would enable application of powerful 3D/4D heteronuclear NMR methods (72, 73), including residual dipolar couplings (74). We foresee that such high-resolution analysis would enable comparison between the nascent structure and dynamics of the 1SS peptide and the classic globular structure of native insulin (23). Further, such complete ^1H, ^{13}C and ^{15}N characterization would provide a rigorous platform for comparative studies of those MIDY mutations that perturb pairing of Cys^{B19} and Cys^{A20}.

CONCLUDING REMARKS

The spectrum of diabetes-associated mutations in the insulin gene implicates diverse genotype-phenotype relationships (9, 75). These include not only mutations toxic misfolding of proinsulin with the ER (the present focus), but also those affecting upstream translocation of nascent preproinsulin (76, 77) and downstream trafficking, prohormone processing, and receptor binding (75). Each class of clinical mutations promises an opportunity to dissect respective molecular mechanisms critical to wild-type hormone biosynthesis and function. Because mutations may introduce mild, intermediate or severe biochemical perturbations, their comparative study may reveal quantitative thresholds of dysfunction associated with clinical features, such as age of diabetes onset or degree of genetic penetrance. Adult-onset Ser^{B24} represents a mild perturbation of folding efficiency whereas both neonatal-onset Pro^{A16} and Pro^{B15} mutations—albeit distinct in location and degree of structural perturbation—must be below the threshold of foldability required for β-cell viability. Extending the present approach to additional MIDY mutations may define molecular

determinants of this threshold. The mutant proinsulin syndrome thus promises to provide an intriguing model to relate chemistry to biology in a prototypical disease of intracellular protein misfolding.

DATA AVAILABILITY STATEMENT

The original contributions presented in the study are included in the article/**Supplementary Material**. Further inquiries can be directed to the corresponding authors.

AUTHOR CONTRIBUTIONS

Chemical peptide syntheses were performed by BD, AZ, and RD. NMR studies were performed and interpreted by YY, MG, NW, and MW. Figures were prepared by YY, BD, MG, AZ, Y-SC and MW. The Supplementary Material was prepared by YY, BD, AZ and MW. All authors contributed to editing the manuscript with first draft prepared by MG and MW. Overall experimental design and oversight were provided by MW. All authors contributed to the article and approved the submitted version.

FUNDING

This work was supported in part by grants to MW from the National Institutes of Health (R01 DK040949 and R01 DK069764). AZ was supported in part by Callibrium, LLC; the authors declare that this funder was not involved in the study design, collection, analysis, interpretation of data, the writing of this article or the decision to submit it for publication. MG was a Pre-doctoral Fellow of the National Institutes of Health (Medical Scientist Training Program 5T32GM007250-38 and Fellowship 1F30DK104618-01).

ACKNOWLEDGMENTS

We thank Prof. Peter Arvan (University of Michigan), G.I. Bell (University of Chicago) and L. Philipson (University of Chicago) for helpful discussion and communication of genetic results prior to publication; Drs. M. Jarosinski (IUSM) and J.P. Mayer (Indiana University) for advice on peptide synthesis; and Prof. P. Arvan, M. Liu (Tianjin Research Institute of Endocrinology, Tianjin, China) and R. Wek (IUSM) for advice regarding ER stress assays. We dedicate this article to the memory of the late Prof. C.M. Dobson (Cambridge University, UK), to whom the senior author (MW) is grateful for ever-kind encouragement since his years as a graduate student.

SUPPLEMENTARY MATERIAL

The Supplementary Material for this article can be found online at: https://www.frontiersin.org/articles/10.3389/fendo.2022.821091/full#supplementary-material

REFERENCES

1. Dobson CM. Protein Folding and Misfolding. *Nature* (2003) 426(6968):884–90. doi: 10.1038/nature02261
2. Chiti F, Dobson CM. Protein Misfolding, Amyloid Formation, and Human Disease: A Summary of Progress Over the Last Decade. *Annu Rev Biochem* (2017) 86:27–68. doi: 10.1146/annurev-biochem-061516-045115
3. Liu M, Hodish I, Rhodes CJ, Arvan P. Proinsulin Maturation, Misfolding, and Proteotoxicity. *Proc Natl Acad Sci USA* (2007) 104(40):15841–6. doi: 10.1073/pnas.0702697104
4. Liu M, Haataja L, Wright J, Wickramasinghe NP, Hua Q-X, Phillips NF, et al. Mutant INS-Gene Induced Diabetes of Youth: Proinsulin Cysteine Residues Impose Dominant-Negative Inhibition on Wild-Type Proinsulin Transport. *PloS One* (2010) 5(10):e13333. doi: 10.1371/journal.pone.0013333
5. Sun J, Cui J, He Q, Chen Z, Arvan P, Liu M. Proinsulin Misfolding and Endoplasmic Reticulum Stress During the Development and Progression of Diabetes. *Mol Aspects Med* (2015) 42:105–18. doi: 10.1016/j.mam.2015.01.001
6. Walter P, Ron D. The Unfolded Protein Response: From Stress Pathway to Homeostatic Regulation. *Science* (2011) 334(6059):1081–6. doi: 10.1126/science.1209038
7. Wek RC, Cavener DR. Translational Control and the Unfolded Protein Response. *Antioxid Redox Signal* (2007) 9(12):2357–72. doi: 10.1089/ars.2007.1764
8. Liu M, Weiss MA, Arunagiri A, Yong J, Rege N, Sun J, et al. Biosynthesis, Structure, and Folding of the Insulin Precursor Protein. *Diabetes Obes Metab* (2018) 20:28–50. doi: 10.1111/dom.13378
9. Støy J, De Franco E, Ye H, Park S-Y, Bell GI, Hattersley AT. In Celebration of a Century With Insulin–Update of Insulin Gene Mutations in Diabetes. *Mol Metab* (2021) 52:101280. doi: 10.1016/j.molmet.2021.101280
10. Støy J, Edghill EL, Flanagan SE, Ye H, Paz VP, Pluzhnikov A, et al. Insulin Gene Mutations as a Cause of Permanent Neonatal Diabetes. *Proc Natl Acad Sci USA* (2007) 104(38):15040–4. doi: 10.1073/pnas.0707291104
11. Colombo C, Porzio O, Liu M, Massa O, Vasta M, Salardi S, et al. Seven Mutations in the Human Insulin Gene Linked to Permanent Neonatal/Infancy-Onset Diabetes Mellitus. *J Clin Investig* (2008) 118(6):2148–56. doi: 10.1172/JCI33777
12. Aguilar-Bryan L, Bryan J. Neonatal Diabetes Mellitus. *Endocr Rev* (2008) 29(3):265–91. doi: 10.1210/er.2007-0029
13. Edghill EL, Flanagan SE, Patch A-M, Boustred C, Parrish A, Shields B, et al. Insulin Mutation Screening in 1,044 Patients With Diabetes: Mutations in the INS Gene Are a Common Cause of Neonatal Diabetes But a Rare Cause of Diabetes Diagnosed in Childhood or Adulthood. *Diabetes* (2008) 57(4):1034–42. doi: 10.2337/db07-1405
14. Hughes IA, Davies JD, Bunch TI, Pasterski V, Mastroyannopoulou K, MacDougall J. Androgen Insensitivity Syndrome. *Lancet* (2012) 380(9851):1419–28. doi: 10.1016/S0140-6736(12)60071-3
15. Boehmer AL, Brggenwirth H, van Assendelft C, Otten BJ, Verleun-Mooijman MC, Niermeijer MF, et al. Genotype Versus Phenotype in Families With Androgen Insensitivity Syndrome. *J Clin Endocrinol Metab* (2001) 86(9):4151–60. doi: 10.1210/jcem.86.9.7825
16. Galani A, Kitsiou-Tzeli S, Sofokleous C, Kanavakis E, Kalpini-Mavrou A. Androgen Insensitivity Syndrome: Clinical Features and Molecular Defects. *Hormones* (2008) 7(3):217–29. doi: 10.14310/horm.2002.1201
17. Chakravorty S, Hegde M. Inferring the Effect of Genomic Variation in the New Era of Genomics. *Hum Mutat* (2018) 39(6):756–73. doi: 10.1002/humu.23427
18. Dhayalan B, Glidden MD, Zaykov A, Chen Y-S, Yang Y, Phillips NB, et al. Peptide Model of the Mutant Proinsulin Syndrome. I. Design and Clinical Correlation. (2022). *Front Endocrinol* (2022) 13:821069. doi: 10.3389/fendo.2022.821069
19. Miller JA, Narhi LO, Hua QX, Rosenfeld R, Arakawa T, Rohde M, et al. Oxidative Refolding of Insulin-Like Growth Factor 1 Yields Two Products of Similar Thermodynamic Stability: A Bifurcating Protein-Folding Pathway. *Biochemistry* (1993) 32:5203–13. doi: 10.1021/bi00070a032

20. Qiao Z-S, Min C-Y, Hua Q-X, Weiss MA, Feng Y-M. *In Vitro* Refolding of Human Proinsulin Kinetic Intermediates, Putative Disulfide-Forming Pathway, Folding Initiation Site, and Potential Role of C-Peptide in Folding Process. *J Biol Chem* (2003) 278(20):17800–9. doi: 10.1074/jbc.M300906200
21. Ryle A, Sanger F, Smith L, Kitai R. The Disulphide Bonds of Insulin. *Biochem J* (1955) 60(4):541–56. doi: 10.1042/bj0600541
22. Hua QX, Mayer J, Jia W, Zhang J, Weiss MA. The Folding Nucleus of the Insulin Superfamily: A Flexible Peptide Model Foreshadows the Native State. *J Biol Chem* (2006) 281:28131–42. doi: 10.1074/jbc.M602616200
23. Baker EN, Blundell TL, Cutfield JF, Dodson EJ, Dodson GG, Hodgkin DMC, et al. The Structure of 2Zn Pig Insulin Crystals at 1.5 Å Resolution. *Philos Trans R Soc Lond B Biol Sci* (1988) 319(1195):369–456. doi: 10.1098/rstb.1988.0058
24. Katsoyannis P. Synthesis of Insulin. *Science* (1966) 154:1509–14. doi: 10.1126/science.154.3756.1509
25. Steiner DF, Cunningham D, Spigelman L, Aten B. Insulin Biosynthesis: Evidence for a Precursor. *Science* (1967) 157(3789):697–700. doi: 10.1126/science.157.3789.697
26. Markussen J. Comparative Reduction/Oxidation Studies With Single Chain Des-(B30) Insulin and Porcine Proinsulin. *Int J Pept Protein Res* (1985) 25:431–4. doi: 10.1111/j.1399-3011.1985.tb02197.x
27. Zaykov AN, Mayer JP, Gelfanov VM, DiMarchi RD. Chemical Synthesis of Insulin Analogs Through a Novel Precursor. *ACS Chem Biol* (2014) 9(3):683–91. doi: 10.1021/cb400792s
28. Schwartz GP, Burke GT, Katsoyannis PG. A Superactive Insulin: [B10-Aspartic Acid]Insulin(Human). *Proc Natl Acad Sci USA* (1987) 84:6408–11. doi: 10.1073/pnas.84.18.6408
29. Kaarsholm NC, Norris K, Jorgensen RJ, Mikkelsen J, Ludvigsen S, Olsen OH, et al. Engineering Stability of the Insulin Monomer Fold With Application to Structure-Activity Relationships. *Biochemistry* (1993) 32:10773–8. doi: 10.1021/bi00091a031
30. Weiss MA, Hua Q-X, Jia W, Nakagawa SH, Chu Y-C, Hu S-Q, et al. Activities of Monomeric Insulin Analogs at Position A8 Are Uncorrelated With Their Thermodynamic Stabilities. *J Biol Chem* (2001) 276(43):40018–24. doi: 10.1074/jbc.M104634200
31. Ortolani F, Piccinno E, Grasso V, Papadia F, Panzeca R, Cortese C, et al. Diabetes Associated With Dominant Insulin Gene Mutations: Outcome of 24-Month, Sensor-Augmented Insulin Pump Treatment. *Acta Diabetol* (2016) 53 (3):499–501. doi: 10.1007/s00592-015-0793-1
32. Flanagan SE, De Franco E, Allen HL, Zerah M, Abdul-Rasoul MM, Edge JA, et al. Analysis of Transcription Factors Key for Mouse Pancreatic Development Establishes NKX2-2 and MNX1 Mutations as Causes of Neonatal Diabetes in Man. *Cell Metab* (2014) 19(1):146–54. doi: 10.1016/j.cmet.2013.11.021
33. Shoelson S, Polonsky K, Zeidler A, Rubenstein A, Tager H. Human Insulin B24 (Phe→Ser). Secretion and Metabolic Clearance of the Abnormal Insulin in Man and in a Dog Model. *J Clin Invest* (1984) 73(5):1351–8. doi: 10.1172/JCI111338
34. Wishart DS, Sykes BD, Richards FM. The Chemical Shift Index: A Fast and Simple Method for the Assignment of Protein Secondary Structure Through NMR Spectroscopy. *Biochemistry* (1992) 31(6):1647–51. doi: 10.1021/bi00121a010
35. Wishart DS, Sykes BD. The ^{13}C Chemical-Shift Index: A Simple Method for the Identification of Protein Secondary Structure Using ^{13}C Chemical-Shift Data. *J Biomol NMR* (1994) 4(2):171–80. doi: 10.1007/BF00175245
36. Shen Y, Delaglio F, Cornilescu G, Bax A. TALOS+: A Hybrid Method for Predicting Protein Backbone Torsion Angles From NMR Chemical Shifts. *J Biomol NMR* (2009) 44(4):213–23. doi: 10.1007/s10858-009-9333-z
37. Hua Q-X, Jai W, Weiss MA. Conformational Dynamics of Insulin. *Front Endocrinol* (2011) 2:48. doi: 10.3389/fendo.2011.00048
38. Lee W, Tonelli M, Markley JL. NMRFAM-SPARKY: Enhanced Software for Biomolecular NMR Spectroscopy. *Bioinformatics* (2015) 31(8):1325–7. doi: 10.1093/bioinformatics/btu830
39. Szilágyi L, Jardetzky O. α-Proton Chemical Shifts and Secondary Structure in Proteins. *J Magn Reson* (1989) 83(3):441–9. doi: 10.1016/0022-2364(89)90341-7
40. Wüthrich K. NMR With Proteins and Nucleic Acids. *Europhys News* (1986) 17(1):11–3. doi: 10.1051/epn/19861701011
41. Wang Y, Jardetzky O. Probability-Based Protein Secondary Structure Identification Using Combined NMR Chemical-Shift Data. *Protein Sci* (2002) 11(4):852–61. doi: 10.1110/ps.3180102
42. Nilges M, Clore GM, Gronenborn AM. Determination of Three-Dimensional Structures of Proteins From Interproton Distance Data by Hybrid Distance Geometry-Dynamical Simulated Annealing Calculations. *FEBS Lett* (1988) 229(2):317–24. doi: 10.1016/0014-5793(88)81148-7
43. Schwieters CD, Kuszewski JJ, Tjandra N, Clore GM. The Xplor-NIH NMR Molecular Structure Determination Package. *J Magn Reson* (2003) 160(1):65–73. doi: 10.1016/S1090-7807(02)00014-9
44. Schwieters CD, Kuszewski JJ, Clore GM. Using Xplor–NIH for NMR Molecular Structure Determination. *Prog Nucl Magn Reson Spectrosc* (2006) 48(1):47–62. doi: 10.1016/j.pnmrs.2005.10.001
45. Yang Y, Hua QX, Liu J, Shimizu EH, Choquette MH, Mackin RB, et al. Solution Structure of Proinsulin: Connecting Domain Flexibility and Prohormone Processing. *J Biol Chem* (2010) 285:7847–51. doi: 10.1074/jbc.C109.084921
46. Rege NK, Liu M, Yang Y, Dhayalan B, Wickramasinghe NP, Chen Y-S, et al. Evolution of Insulin at the Edge of Foldability and its Medical Implications. *Proc Natl Acad Sci USA* (2020) 117(47):29618–28. doi: 10.1073/pnas.2010908117
47. Bodenhausen G, Ruben DJ. Natural Abundance Nitrogen-15 NMR by Enhanced Heteronuclear Spectroscopy. *Chem Phys Lett* (1980) 69(1):185–9. doi: 10.1016/0009-2614(80)80041-8
48. Vuister GW, Bax A. Resolution Enhancement and Spectral Editing of Uniformly ^{13}C-Enriched Proteins by Homonuclear Broadband ^{13}C Decoupling. *J Magn Reson* (1992) 98(2):428–35. doi: 10.1016/0022-2364(92)90144-V
49. Hua QX, Shoelson SE, Weiss MA. Nonlocal Structural Perturbations in a Mutant Human Insulin: Sequential Resonance Assignment and ^{13}C-Isotope-Aided 2D-NMR Studies of [Phe^{B24}→Gly]insulin With Implications for Receptor Recognition. *Biochemistry* (1992) 31(47):11940–51. doi: 10.1021/bi00162a037
50. Hua Q-X, Hu S-Q, Frank BH, Jia W, Chu Y-C, Wang S-H, et al. Mapping the Functional Surface of Insulin by Design: Structure and Function of a Novel A-Chain Analogue. *J Mol Biol* (1996) 264(2):390–403. doi: 10.1006/jmbi.1996.0648
51. Hua Q-X, Liu M, Hu S-Q, Jia W, Arvan P, Weiss MA. A Conserved Histidine in Insulin Is Required for the Foldability of Human Proinsulin: Structure and Function of an Ala^{B5} Analog. *J Biol Chem* (2006) 281(34):24889–99. doi: 10.1074/jbc.M602617200
52. Jacoby E, Hua QX, Stern AS, Frank BH, Weiss MA. Structure and Dynamics of a Protein Assembly. ^{1}H-NMR Studies of the 36 kDa R_6 Insulin Hexamer. *J Mol Biol* (1996) 258(1):136–57. doi: 10.1006/jmbi.1996.0239
53. Weiss MA, Hua QX, Jia W, Chu YC, Wang RY, Katsoyannis PG. Hierarchiacal Protein "Un-Design": Insulin's Intrachain Disulfide Bridge Tethers a Recognition α-Helix. *Biochemistry* (2000) 39:15429–40. doi: 10.1021/bi001905s
54. Hua QX, Nakagawa SH, Jia W, Hu SQ, Chu YC, Katsoyannis PG, et al. Hierarchical Protein Folding: Asymmetric Unfolding of an Insulin Analogue Lacking the A7-B7 Interchain Disulfide Bridge. *Biochemistry* (2001) 40:12299–311. doi: 10.1021/bi011021o
55. Schwarzinger S, Kroon GJ, Foss TR, Wright PE, Dyson HJ. Random Coil Chemical Shifts in Acidic 8 M Urea: Implementation of Random Coil Shift Data in NMRView. *J Biomol NMR* (2000) 18(1):43–8. doi: 10.1023/A:1008386816521
56. Hoch JC, Dobson CM, Karplus M. Fluctuations and Averaging of Proton Chemical Shifts in the Bovine Pancreatic Trypsin Inhibitor. *Biochemistry* (1982) 21(6):1118–25. doi: 10.1021/bi00535a002
57. Steiner DF, Oyer PE. The Biosynthesis of Insulin and a Probable Precursor of Insulin by a Human Islet Cell Adenoma. *Proc Natl Acad Sci USA* (1967) 57 (2):473–80. doi: 10.1073/pnas.57.2.473
58. Steiner DF. On the Discovery of Precursor Processing. In: Mbikay M, Seidah N, editors. *Proprotein Convertases. Methods Mol Biol (Methods and Protocols)*. Humana Press (2011). vol 768. doi: 10.1007/978-1-61779-204-5_1
59. Wei J, Xie L, Lin Y-Z, Tsou C-L. The Pairing of the Separated A and B Chains of Insulin and Its Derivatives, FTIR Studies. *Biochim Biophys Acta* (1992) 1120 (1):69–74. doi: 10.1016/0167-4838(92)90425-D

60. Johnson JD. On the Causal Relationships Between Hyperinsulinaemia, Insulin Resistance, Obesity and Dysglycaemia in Type 2 Diabetes. *Diabetologia* (2021) 64(10):2138–46. doi: 10.1007/s00125-021-05505-4
61. Conlon JM. Molecular Evolution of Insulin in Non-Mammalian Vertebrates. *Am Zool* (2000) 40(2):200–12. doi: 10.1093/icb/40.2.200
62. van Mierlo CP, Darby NJ, Keeler J, Neuhaus D, Creighton TE. Partially Folded Conformation of the (30-51) Intermediate in the Disulphide Folding Pathway of Bovine Pancreatic Trypsin Inhibitor: 1H and 15N Resonance Assignments and Determination of Backbone Dynamics From 15N Relaxation Measurements. *J Mol Biol* (1993) 229(4):1125–46. doi: 10.1006/jmbi.1993.1108
63. Miranker A, Radford SE, Karplus M, Dobson CM. Demonstration by NMR of Folding Domains in Lysozyme. *Nature* (1991) 349(6310):633–6. doi: 10.1038/349633a0
64. Staley JP, Kim PS. Formation of a Native-Like Subdomain in a Partially Folded Intermediate of Bovine Pancreatic Trypsin Inhibitor. *Protein Sci* (1994) 3 (10):1822–32. doi: 10.1002/pro.5560031021
65. Barbar E, Barany G, Woodward C. Dynamic Structure of a Highly Ordered. β-Sheet Molten Globule: Multiple Conformations With a Stable Core. *Biochemistry* (1995) 34(36):11423–34. doi: 10.1021/bi00036a015
66. Ittah V, Haas E. Nonlocal Interactions Stabilize Long Range Loops in the Initial Folding Intermediates of Reduced Bovine Pancreatic Trypsin Inhibitor. *Biochemistry* (1995) 34(13):4493–506. doi: 10.1021/bi00013a042
67. Barbar E, Hare M, Daragan V, Barany G, Woodward C. Dynamics of the Conformational Ensemble of Partially Folded Bovine Pancreatic Trypsin Inhibitor. *Biochemistry* (1998) 37(21):7822–33. doi: 10.1021/bi973102j
68. Liu M, Wan Z-l, Chu Y-C, Aladdin H, Klaproth B, Choquette M, et al. Crystal Structure of a "Nonfoldable" Insulin: Impaired Folding Efficiency Despite Native Activity. *J Biol Chem* (2009) 284(50):35259–72. doi: 10.1074/jbc.M109.046888
69. DuBay KF, Pawar AP, Chiti F, Zurdo J, Dobson CM, Vendruscolo M. Prediction of the Absolute Aggregation Rates of Amyloidogenic Polypeptide Chains. *J Mol Biol* (2004) 341(5):1317–26. doi: 10.1016/j.jmb.2004.06.043
70. Weiss MA. Diabetes Mellitus Due to the Toxic Misfolding of Proinsulin Variants. *FEBS Lett* (2013) 587(13):1942–50. doi: 10.1016/j.febslet.2013.04.044
71. Conlon JM. Evolution of the Insulin Molecule: Insights Into Structure-Activity and Phylogenetic Relationships. *Peptides* (2001) 22(7):1183–93. doi: 10.1016/S0196-9781(01)00423-5
72. Bax A. Multidimensional Nuclear Magnetic Resonance Methods for Protein Studies. *Curr Opin Struct Biol* (1994) 4(5):738–44. doi: 10.1016/S0959-440X(94)90173-2
73. Clore GM, Gronenborn AM. Applications of Three-and Four-Dimensional Heteronuclear NMR Spectroscopy to Protein Structure Determination. *Prog Nucl Magn Reson Spectrosc* (1991) 23(1):43–92. doi: 10.1016/0079-6565(91)80002-J
74. Bax A, Grishaev A. Weak Alignment NMR: A Hawk-Eyed View of Biomolecular Structure. *Curr Opin Struct Biol* (2005) 15(5):563–70. doi: 10.1016/j.sbi.2005.08.006
75. Steiner DF, Tager HS, Chan SJ, Nanjo K, Sanke T, Rubenstein AH. Lessons Learned From Molecular Biology of Insulin-Gene Mutations. *Diabetes Care* (1990) 13:600–9. doi: 10.2337/diacare.13.6.600
76. Liu M, Lara-Lemus R, Shan S-o, Wright J, Haataja L, Barbetti F, et al. Impaired Cleavage of Preproinsulin Signal Peptide Linked to Autosomal-Dominant Diabetes. *Diabetes* (2012) 61(4):828–37. doi: 10.2337/db11-0878
77. Guo H, Xiong Y, Witkowski P, Cui J, Wang L-j, Sun J, et al. Inefficient Translocation of Preproinsulin Contributes to Pancreatic β Cell Failure and Late-Onset Diabetes. *J Biol Chem* (2014) 289(23):16290–302. doi: 10.1074/jbc.M114.562355

Conflict of Interest: The authors declare that the research was conducted in the absence of any commercial or financial relationships that could be construed as a potential conflict of interest.

Publisher's Note: All claims expressed in this article are solely those of the authors and do not necessarily represent those of their affiliated organizations, or those of the publisher, the editors and the reviewers. Any product that may be evaluated in this article, or claim that may be made by its manufacturer, is not guaranteed or endorsed by the publisher.

GLOSSARY

MIDY	mutant *INS*-induced diabetes of the young
MODY	maturity-onset diabetes of the young
MPS	mutant proinsulin syndrome
PNDM	permanent neonatal diabetes mellitus
DesDi	single-chain insulin analog containing Lys^{B28} and lacking residues B29 and B30
N	DesDi insulin template with all three native disulfide bonds
N*	DesDi insulin control with solubility enhancements
[B19-A20]	DesDi variant based on N* retaining only the B19-A20 disulfide linkage
ER	endoplasmic reticulum
SCI	single-chain insulin
CD	circular dichroism
NMR	nuclear magnetic resonance
rp-HPLC	reverse-phase high-performance liquid chromatography
LC-MS	liquid chromatography-mass spectrometry
MALDI-TOF	matrix-assisted laser desorption ionization - time of flight
IGF	insulin-like growth factor
NOE	nuclear Overhauser enhancement
NOESY	nuclear Overhauser enhancement spectroscopy
TOCSY	total correlation spectroscopy
HSQC	heteronuclear single-quantum coherence. Insulin residues are denoted by residue type (in standard three-letter code) followed by the chain and position (e.g., Phe^{B24} designates a phenylalanine at the 24^{th} position of the B chain)

frontiers in Endocrinology

ORIGINAL RESEARCH
published: 01 March 2022
doi: 10.3389/fendo.2022.821069

Peptide Model of the Mutant Proinsulin Syndrome. I. Design and Clinical Correlation

Balamurugan Dhayalan[1‡], Michael D. Glidden[2,3,4‡], Alexander N. Zaykov[5†‡], Yen-Shan Chen[1], Yanwu Yang[1], Nelson B. Phillips[2], Faramarz Ismail-Beigi[2,3,4], Mark A. Jarosinski[1], Richard D. DiMarchi[5] and Michael A. Weiss[1*]*

[1] Department of Biochemistry and Molecular Biology, Indiana University School of Medicine, Indianapolis, IN, United States, [2] Department of Biochemistry, Case Western Reserve University School of Medicine, Cleveland, OH, United States, [3] Department of Physiology & Biophysics, Case Western Reserve University School of Medicine, Cleveland, OH, United States, [4] Department of Medicine, Case Western Reserve University School of Medicine, Cleveland, OH, United States, [5] Department of Chemistry, Indiana University, Bloomington, IN, United States

The mutant proinsulin syndrome is a monogenic cause of diabetes mellitus due to toxic misfolding of insulin's biosynthetic precursor. Also designated *mutant INS-gene induced diabetes of the young* (MIDY), this syndrome defines molecular determinants of foldability in the endoplasmic reticulum (ER) of β-cells. Here, we describe a peptide model of a key proinsulin folding intermediate and variants containing representative clinical mutations; the latter perturb invariant core sites in native proinsulin (Leu^{B15}→Pro, Leu^{A16}→Pro, and Phe^{B24}→Ser). The studies exploited a 49-residue single-chain synthetic precursor (designated DesDi), previously shown to optimize *in vitro* efficiency of disulfide pairing. Parent and variant peptides contain a single disulfide bridge (cystine B19-A20) to provide a model of proinsulin's first oxidative folding intermediate. The peptides were characterized by circular dichroism and redox stability in relation to effects of the mutations on (a) *in vitro* foldability of the corresponding insulin analogs and (b) ER stress induced in cell culture on expression of the corresponding variant proinsulins. Striking correlations were observed between peptide biophysical properties, degree of ER stress and age of diabetes onset (neonatal or adolescent). Our findings suggest that age of onset reflects the extent to which nascent structure is destabilized in proinsulin's putative folding nucleus. We envisage that such peptide models will enable high-resolution structural studies of key folding determinants and in turn permit molecular dissection of phenotype-genotype relationships in this monogenic diabetes syndrome. Our companion study (next article in this issue) employs two-dimensional heteronuclear NMR spectroscopy to define site-specific perturbations in the variant peptides.

Keywords: monogenic diabetes, endoplasmic reticular stress, peptide chemistry, protein folding, oxidative folding intermediate

OPEN ACCESS

Edited by:
Jiajun Zhao,
Shandong Provincial Hospital, China

Reviewed by:
Ya-Xiong Tao,
Auburn University, United States
Pierre De Meyts,
Université Catholique de Louvain, Belgium

***Correspondence:**
Balamurugan Dhayalan
bdhayal@iu.edu
Michael A. Weiss
weissma@iu.edu

†Present address:
Alexander N. Zaykov,
Novo-Nordisk Research Center, Seattle, WA, United States

‡These authors have contributed equally to this work

Specialty section:
This article was submitted to Diabetes: Molecular Mechanisms, a section of the journal Frontiers in Endocrinology

Received: *23 November 2021*
Accepted: *17 January 2022*
Published: *01 March 2022*

Citation:
Dhayalan B, Glidden MD, Zaykov AN, Chen Y-S, Yang Y, Phillips NB, Ismail-Beigi F, Jarosinski MA, DiMarchi RD and Weiss MA (2022) Peptide Model of the Mutant Proinsulin Syndrome. I. Design and Clinical Correlation. Front. Endocrinol. 13:821069. doi: 10.3389/fendo.2022.821069

INTRODUCTION

The mutant proinsulin syndrome (MPS) is a monogenic cause of diabetes mellitus (DM) presenting at a broad range of ages: onset can occur either in the neonatal period, childhood, adolescence or early adulthood (1–4). Characterization of this syndrome and related mouse models (5, 6) has established the paradigm that DM may arise as a proteotoxic disorder of insulin biosynthesis (**Figure 1A**). Also designated *Mutant INS-gene Induced Diabetes of the Young* (MIDY) (11), MPS thus pertains to patients traditionally classified, on the basis of age at presentation, as either *Permanent Neonatal Diabetes Mellitus* (PNDM) or *Maturity Onset Diabetes of the Young* (MODY) (12). This phenotypic spectrum may reflect polygenic differences in β-cell biology (13) or intrinsic mutation-dependent biophysical properties of the variant proinsulins (11, 14, 15).

MIDY mutations are ordinarily dominant and associated with misfolding of the proinsulin variant in the endoplasmic reticulum (ER), leading to β-cell dysfunction and eventual death [(16); for reviews, see (17, 18)]. Whereas the majority of MIDY mutations introduce or remove a Cys residue—in either case leading to an odd number of thiol groups and hence risk of aberrant intermolecular disulfide pairing (19)—PNDM- and MODY phenotypes are also associated with non-cysteine-related mutations (20). The latter amino-acid substitutions generally occur at sites conserved among vertebrate insulins [and in most cases also shared by vertebrate insulin-like growth factors (IGFs) (21)]. These mutational "hot spots" define the structural framework of native insulin (**Figure 1B**) and are of mechanistic interest as putative molecular determinants of protein folding efficiency (20, 22, 23). The present study, based on the oxidative refolding pathway of native proinsulin (**Figure 1C**), describes the design and chemical synthesis of a single-chain peptide model of a key on-pathway proinsulin folding intermediate (8, 24). This model enables comparative biophysical studies of representative MIDY "hot-spot" mutations with neonatal or delayed disease onset (**Figure 1D**). First introduced in studies of bovine pancreatic trypsin inhibitor (25), peptide models of protein-folding intermediates have provided a general approach toward dissecting critical molecular interactions guiding the conformational search of a nascent polypeptide (see **Box 1** and **Figure 2**) (31, 32).

Abbreviations: MIDY, mutant *INS*-induced diabetes of the young; MODY, maturity-onset diabetes of the young; MPS, mutant proinsulin syndrome; PNDM, permanent neonatal diabetes mellitus; DesDi, single-chain insulin analog insulin containing Lys^{B28} and lacking residues B29 and B30; N, DesDi insulin template with all three native disulfide bonds; N*, DesDi insulin control with solubility enhancements; [B19-A20], DesDi variant based on N* retaining only the B19-A20 disulfide linkage; ER, endoplasmic reticulum; SCI, single-chain insulin; CD, circular dichroism; NMR, nuclear magnetic resonance; rp-HPLC, reverse-phase high-performance liquid chromatography; LC-MS, liquid chromatography-mass spectrometry; MALDI-TOF, matrix-assisted laser desorption ionization - time of flight; and IGF, insulin-like growth factor. Insulin residues are denoted by residue type (in standard three-letter code) followed by the chain and position (e.g., Phe^{B24} designates a phenylalanine at the 24^{th} position of the B chain).

The present peptide model contains a single disulfide bridge, internal cystine B19-A20, the first partial fold to accumulate in chemical-trapping studies of proinsulin (or homologous IGF-I) refolding *in vitro* (8, 9, 24) (see Supplemental Discussion regarding effects of pH in such refolding assays). Its framework derives from a foreshortened single-chain synthetic precursor of insulin optimized for efficiency of disulfide pairing (50). Designated "DesDi", the parent analog comprises 49 residues (**Figure 3A**): B-chain residues B1-B28 followed by A-chain residues A1-A21. Substitution of Pro^{B28} by Lys enables enzymatic cleavage to liberate an active two-chain insulin analog (50). Our one-disulfide model contains pairwise substitution of cystine B7-A7 by Ser and pairwise substitution of cystine A6-A11 by Ala (**Figure 3B**). Segmental α-helical propensity and solubility were augmented by substitutions His^{B10}→Asp (native α-helix α_1 spanning residues B9-B19) and Thr^{A8}→Glu (native α-helix α_2; A1-A8) (58, 59). Representative MIDY mutations (Leu^{B15}→Pro, Leu^{A16}→Pro, and Phe^{B24}→Ser) were introduced into the parent DesDi framework with six cysteines ("native state") and the peptide model ("1SS"). These amino-acid substitutions were chosen based on phenotype and structural interest: the proline variants (each neonatal in onset) are predicted to perturb nascent α-helical folding and native packing of the hydrophobic core (20, 60) whereas Ser^{B24} [with onset in adolescence or early adulthood (61)] perturbs the "aromatic anchor" of the B-chain β-strand (B24-B28) (60, 62, 63). Each of these conserved side chains contributes to core packing near internal cystine B19-A20 (**Figure 3C**). A related two-chain one-disulfide model of the homologous IGF-I folding nucleus has previously been described (51); the corresponding three side chains (IGF-I residues Leu14, Phe23 and Leu57) were observed to participate in its molten native-like structure at low temperatures.

The present study (the first of two in this issue) describes the synthesis and respective foldabilities of the above set of native state and 1SS 49-residue peptides. Circular dichroism (CD) is employed to probe α-helix contents, thermal unfolding profiles and thermodynamic stabilities. Characterization of such chemical and biophysical properties were extended through cell-biological assays of ER stress induced in human cells on transient expression of the corresponding mutant proinsulins. Striking correlations were observed among foldability, nascent α-helical folding and extent of ER stress in human cell culture. Our companion study further interrogates the nascent structures of these peptide models and their mutational perturbation by ^{1}H and ^{1}H-^{13}C NMR spectroscopy [(64); following article in this issue]. Together, our findings establish a general platform for biophysical studies of a subset of MIDY mutations in relation to molecular mechanisms of proinsulin biosynthesis in pancreatic β-cells.

MATERIALS AND METHODS

Automated DesDi Peptide Synthesis

Peptides were synthesized either with an ABI 433A Peptide Synthesizer (Applied Biosystems) or Tribute 2-Channel peptide synthesizer (Gyros Protein technologies) using a preprogrammed

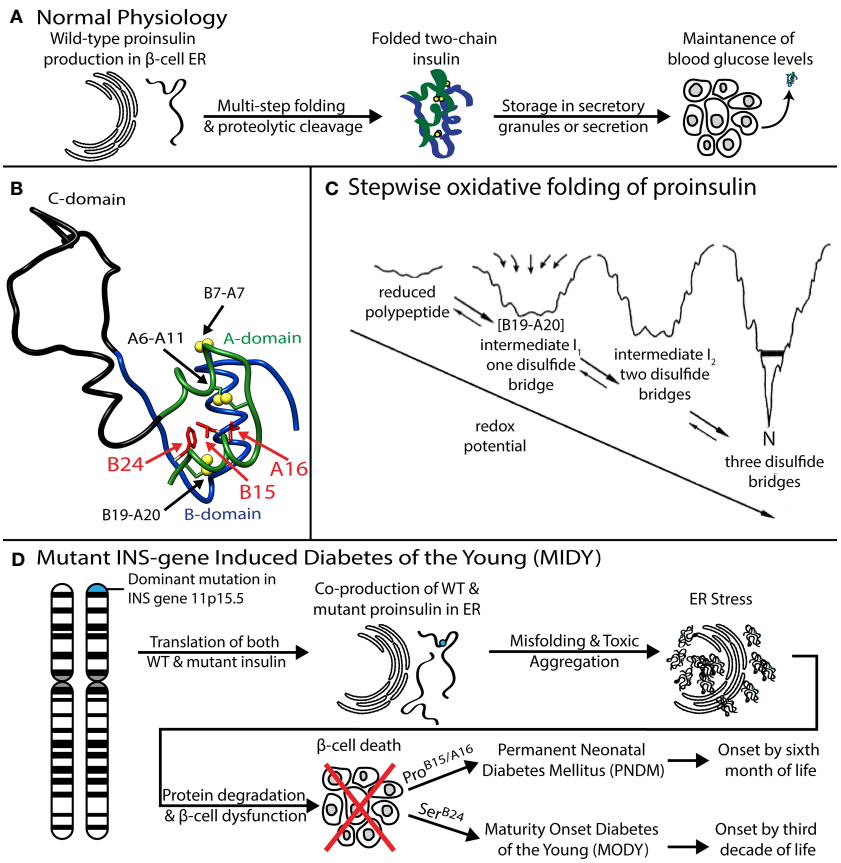

FIGURE 1 | Genetic etiology, pathophysiology, and structural basis of Mutant Proinsulin Syndrome. **(A)** Overview of normal proinsulin production and maintenance of glucose homeostasis. **(B)** Solution structure of WT proinsulin (7) showing the A- (*green*), B- (*blue*), and C (*black*) domains and three native disulfide bridges (*yellow spheres*). Wild-type residues Phe^{B24}, Leu^{B15} and Leu^{A16}, which are examined in this study as sites of mutation, are shown as red side chains. **(C)** Folding of proinsulin proceeds *via* sequential disulfide linkage steps from the fully unfolded state through one (1SS), two (2SS), and three disulfide bonded (3SS) conformational ensembles before reaching the native state (N). Chemical trapping experiments showed that the formation of B19-A20 disulfide as the predominant key first step in the hierarchical disulfide pathway (8–10). Reprinted with permission from Hua QX, et al. Biochemistry. 2001;40:12299-311. Copyright (2001) American Chemical Society. **(D)** Dominant mutations in the *INS* gene causing co-production of both WT and mutant proinsulin, leading to ER stress, β-cell dysfunction, and, ultimately, diabetes. Clinically identified mutations Ser^{B24}, Pro^{B15} and Pro^{A16} present with a spectrum of disease severity and age of diabetes onset.

BOX 1 | Peptide models of protein-folding intermediates.

Studies of the mutant proinsulin syndrome (17) have built on general principles of cell biology and protein chemistry established over the past sixty years (26–28). This deep interdisciplinary background highlights mechanisms underlying the biosynthesis of disulfide-stabilized secretory proteins from the scale of organelles and macromolecular complexes (29, 30) to the molecular biophysics of a nascent polypeptide chain's conformational search (31–34).

Ribosomal translation at the outer surface of the rough ER is coupled to cleavage of the signal peptide and associated translocation into the ER [**Figure 2A**; for review, see (37)]; the latter environment provides chaperones and oxidative machinery for disulfide bond formation, rearrangement, and quality control (38–42). These general processes pertain to β-cell physiology and dysfunction in DM (17, 35, 36). Although initial steps of protein folding can in some cases be co-translational (30), the nascent proinsulin chain is likely to form an unfolded-state ensemble (at right in **Figure 2A**) to enable initial pairing of two cysteines distant in the sequence (Cys^{B19} and Cys^{A20}; residues 43 and 109 in preproinsulin) (9, 24, 43). The present study has exploited a subset of diabetes-associated mutations to investigate such long-range pairing.

Analysis of atomic-scale events in the *in vitro* refolding of polypeptide chains and their computational simulation (44, 45) provide insight into the challenges faced in cellular protein biosynthesis (27, 46). Folding is visualized as proceeding through funnel-shaped free-energy landscapes (**Figure 2B**), in general *via* multiple trajectories (*e.g.*, yellow or magenta lines) (31). Dissection of globular proteins into peptide models, pioneered by Oas and Kim in 1988 (25) has been broadly influential in enabling key steps to be identified (47). Applications have been described to both oxidative folding intermediates (25), the rapid autonomous folding of disulfide-free subdomains (48) and fragments containing engineered disulfide bridges (49). Use of peptide models may circumvent the usual cooperativity of globular protein folding, which can obscure discrete steps (25). The latter perspective has been reinforced by studies of intact proteins by native-state amide-proton exchange kinetics (34).

The present studies have exploited a peptide model of a key one-disulfide proinsulin folding intermediate (simulated ensemble in **Figure 2C**); its features favor formation of on-pathway nascent structure [see also **Figure 9** and Discussion (50)]. Peptide design builds on prior studies of insulin-related polypeptides lacking specific disulfide bridges (10, 51–55). To our knowledge, this is the first investigation of clinical mutations in a peptide model of a proinsulin folding intermediate.

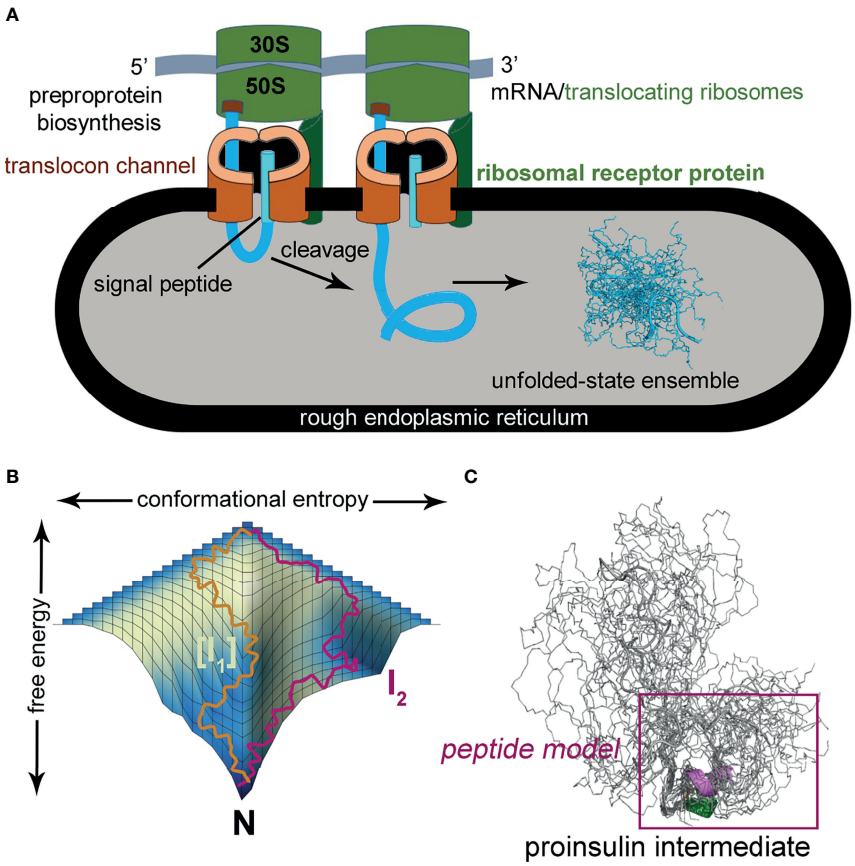

FIGURE 2 | Peptide models of protein-folding intermediates probe critical biosynthetic steps. **(A)** Preproprotein biosynthesis in rough endoplasmic reticulum: nascent polypeptide chain (blue ribbon) enters ER (gray) with cleavage of signal peptide (cyan ribbon) *via* translocon channel (brown). Protein folding may in part be co-translational or begin from an unfolded-state ensemble (blue chains at right); this model was calculated by Xplor-NIH software and ensemble generated by PyMOL (ribbon and sticks). The cartoon was otherwise adapted from (56). **(B)** Energy folding landscape. Yellow and magenta lines indicate alternative paths to the native state (N): $[I_1]$, set of unobserved intermediate species; I_2, observed intermediate that can accumulate in a kinetic trap. Panel adapted from reference (57). **(C)** Conformational ensemble of a one-disulfide proinsulin intermediate containing cystine B19-A20. A minimal model (magenta box) was designed based on a 49-residue peptide (50) as described in the main text. The present CD studies suggest formation of nascent α-helices in the central B domain and C-terminal A domain (dark green and magenta, respectively).

solid-phase fluorenylmethyloxycarbonyl (Fmoc) protocol designed for standard 0.1 mmol scale syntheses. ABI protocols consist of the following modules: cycle-1 [d], cycle-2 [aibde], cycle-3 with number of repetitions equal #aa-1 [afgbde], cycle"#aa+2" [ffbdc], where #aa is a number of amino acids in the sequence. Automated couplings utilized diisopropylcarbodiimide (DIC)/6-Cl-hydroxybenzotriazole (6-Cl-HOBt) in *N*-Methyl pyrrolidone (NMP) whereas Fmoc deprotections used 20% piperidine in NMP. α-carboxyl-protected Asp was used in place of Asn in all syntheses of DesDi analogs to accommodate the use of ChemMatrix® Rink-Amide resin (loading = 0.46 mmol/g). The Tribute peptide synthesizer used heating protocols: couplings were done for 6 min at 60°C except for Cys/His (2 min at 25°C, then 5 min at 60°C) and Arg (20 min at 25°C, then 5 min at 60°C); deprotection was done twice (30 sec at 50°C, then 3 min at 50°C). Reagent conditions were otherwise similar to ABI protocols except that DMF was used as solvent and choice of the resin was H-Asn(Trt)-HMPB-ChemMatrix® resin. Peptides were cleaved with TFA cocktail (2.5% vol/vol of each: β-mercaptoethanol, triisopropylsilane, anisole, and water) followed by ether precipitation.

Folding and Purification of N and N* DesDi Analogs

Crude peptides from ether precipitation were dissolved in glycine buffer (20 mM glycine and 2 mM cysteine hydrochloride, pH 10.5) to a final peptide concentration of 0.1 mM. The pH of this solution was readjusted to 10.5 to account for traces of residual TFA present in lyophilized peptides. This solution was then stirred while open to air at 4°C until reaction completion (usually overnight). After monitoring of the folding reaction by analytical HPLC to determine the extent of conversion, the pH of the solution was then lowered to ~2.0 with 5N HCl to neutralize the folding reaction. Folded peptide was then purified by preparative rp-HPLC using Waters 2545 Quaternary pumping system equipped with FlexInject. Chromatographic separations were

performed on a C4 Proto (20x250 mm) 300 Å, 10 µm, Higgins Analytical Inc. column, using 25-50% solvent B (0.1% TFA in acetonitrile) in solvent A (0.1% TFA in H_2O) over 35 minutes (min) at a flow rate of 20 ml/min with detection by UV absorption at 215 nm. Fractions containing clean peptide were pooled and lyophilized. Purity of the materials was confirmed by LCQ Advantage Ion Trap Mass Spectrometer System coupled to an Agilent 1100 Series HPLC system. Masses were obtained by online electrospray mass spectrometry. MS data shown were collected across the entire principal UV-absorbing peak in each chromatogram; LC-MS retention times and mass verification are given in **Table S1**.

Folding and Purification of [B19-A20]-SS DesDi Analogs

Purification of single-disulfide analogs was performed in a two-step process. First, the crude peptide was fully dissolved in pH 11 buffer in presence of excess DTT. The pH was then lowered to 8.0 before purification by semi-preparative rp-HPLC under alkaline conditions using 25 mM ammonium bicarbonate buffer (pH 8.0) and acetonitrile (60 min gradient of 20→50%) as eluents on a TRIART C18, 250 x 10mm 5µm, 120Å column. Fractions containing linear, fully reduced peptides were pooled and lyophilized. Folding was performed either using room air oxidation as described for N and N* analogs or utilizing cysteine-cystine redox pair. For the latter, peptides were dissolved in 20 mM glycine buffer (pH 10.5) at a final 0.1 mM peptide concentration followed by addition of 1:1 cystine/cysteine (2 mM each). Folding was allowed to proceed for 1 hour (hr), followed by purification by rp-HPLC using the same 20→50% acetonitrile elution gradient as described above. Collected fractions were pooled and lyophilized. When necessary, an additional purification using acidic RP-HPLC conditions was performed. Peptide purity was confirmed by analytical LC-MS as described for N and N* DesDi analogs above (LC-MS retention times and mass measurements are given in **Table S1**).

Two-Chain DesDi Conversion

In cases of three disulfide containing DesDi analogs, single-chain insulins were converted to two-chain version by Lys-specific enzyme. In a typical experiment, single-chain DesDi analog was treated with Endo Lys-C enzyme (65) in 25 mM Tris base, 100 mM urea buffer (pH 8.5) at 12°C water bath for 24 h. After analytical rp-HPLC indicated two-chain conversion (typically 60-80%), the reaction mixture was acidified and purified on semi-preparative rp-HPLC. Fractions containing clean protein were pooled, lyophilized and masses were confirmed by LC-MS.

Purification of Insulin Analogs

Wild-type human insulin and insulin *lispro* were purified from U-100 pharmaceutical formulations of Humulin® and Humalog® (Eli Lilly and Co.), respectively, using preparative rp-HPLC (C4 10µm 250×20mm Proto 300 Column; Higgins Analytical, Inc.) utilizing Buffer A (0.1% TFA in H_2O) and a 10-min elution gradient of 20→70% Buffer B (0.1% TFA in acetonitrile). Following lyophilization of the collected protein fraction, purity was verified using analytical rp-HPLC (C4 5µm 250×4.6mm Proto 300 Column; Higgins Analytical, Inc.) with a 35-min elution gradient of 25→50% Buffer B; molar mass was verified with an Applied Biosystems 4700 Proteomics Analyzer utilizing MALDI-TOF in reflector mode; chromatographic retention times and mass measurements for these clinical analogs are given in **Table S1**.

Nuclear Magnetic Resonance (NMR) Spectroscopy

All spectra were acquired at a protein concentration of ~0.2 mM in 100% D_2O (pD 7.4) at 35°C with a Bruker AVANCE 700-MHz spectrometer, as described (23). All chemical shifts were calibrated in parts per million (ppm) relative to 4,4-dimethyl-4-silapentane-1-sulfonic acid (DSS) as an internal standard. The spectrometer was equipped with ^{1}H, ^{19}F, ^{13}C, ^{15}N quadruple resonance cryoprobe.

CD Spectropolarimetry

Far ultraviolet (255-190 nm) CD spectra were obtained at high signal-to-noise for WT insulin, insulin *lispro*, and all [B19-A20], N and N* DesDi peptides (summarized in **Figure 4**) using a CD spectropolarimeter (Aviv-400 or Jasco J-1500) equipped with temperature control and an automated titration unit. Samples were prepared at a concentration of 20-70 µM protein in degassed potassium phosphate (10 mM KH_2PO_4/K_2HPO_4 with 50 mM KCl), brought to pH 7.4 with KOH, and placed in a parafilm-sealed 1-mm pathlength quartz cuvette. Automated macros were utilized that acquired full far-UV CD spectra (255-190 nm) in 2°C steps from 4°C to 40°C (plus 25°C and 37°C) with a wavelength resolution of 0.5 nm and 30 sec. photocount averaging time. Following this, spectra were acquired from 4-88°C in 4°C steps. To reduce acquisition time at high temperatures, ellipticity measurements made above 40°C included only wavelength sets of 254(± 1), 222(± 1) and 208(± 1) nm using a 0.5-nm wavelength resolution and 30-sec. detector averaging time. Buffer-only CD spectra were obtained using degassed buffer with no protein at temperatures of 4, 25 and 37°C using a 0.5-nm wavelength resolution and 90 sec. averaging time. The linear temperature dependence at all wavelengths of buffer-only spectra allowed interpolation and extrapolation of buffer-only spectra at any temperature. Extrapolated reference spectra were then subtracted from all CD spectra acquired at the same temperature. Estimates of secondary-structure content were obtained from normalized spectra acquired at 4, 25 and 37°C using the SELCON-3 algorithm packaged with the CDPro spectral analysis software (66–68).

The temperature dependence of protein folds was assessed by plotting the average of molar ellipticity values at wavelengths straddling the α-helix sensitive wavelength of 222 nm (i.e., 221-223 nm with 0.5-nm resolution) against temperature. The quantity resulting from averaging wavelengths 221-223 nm, $\langle [\theta]_{222\pm1nm} \rangle$, enhances signal-to-noise while ensuring that any difference in ellipticity that may be observed between sequential temperature steps is not confounded by random error.

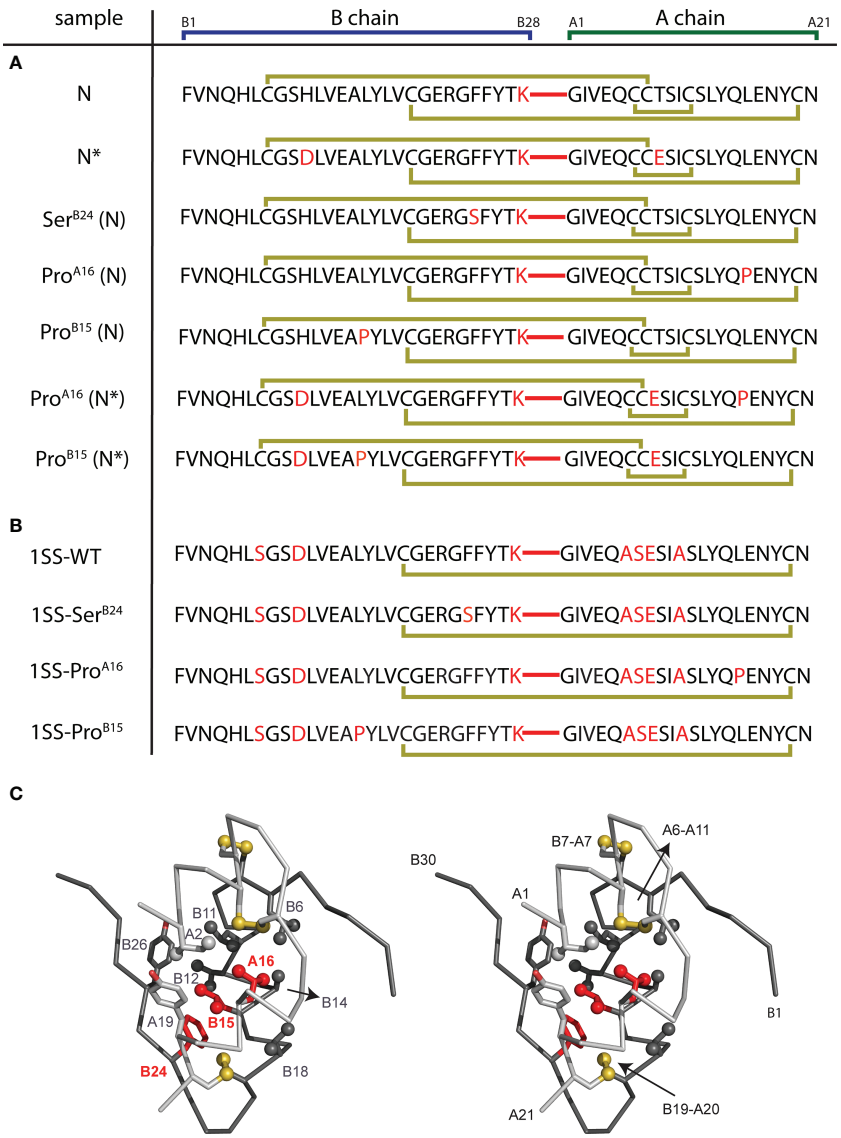

FIGURE 3 | DesDi variant protein sequences. **(A)** Sample names and sequences of three disulfide bond containing analogs (N and N*). **(B)** Sample names and sequences of one disulfide-bond-containing analogs ([B19-A20]; abbreviated as 1SS). Yellow lines show disulfide linkages. A red line connecting the C-terminal B-domain and N-terminal A-domain sequences signifies the presence of a peptide bond between residues B28 and A1. All 1SS samples and N* have additional mutations Glu^{A8} and Asp^{B10} to enhance solubility at neutral pH (e.g., to enable the high protein concentrations needed for NMR spectroscopy). Residues in *red* highlight mutations to the WT insulin sequence. **(C)** Stereo view showing ribbon model of an insulin monomer [as extracted from the T_6 Zn hexamer; PDB entry 4INS (60)]. Sites of clinical mutation investigated here [B15, B24 and A16; highlighted in red] and neighboring residues are shown as sticks. Sulfur atoms in disulfide bridges are shown as gold spheres, and selected side-chain methyl groups as spheres (one-third van der Waals radius). A- and B chains are otherwise shown in light and dark gray, respectively.

Quantitation of Samples and Normalization of CD Spectra

CD samples were quantitated *via* reference-subtracted UV-Vis spectra acquired in 10 mM potassium phosphate (pH 7.4) with a UV-Vis spectrometer (Aviv Biomedical Inc., Lakewood, NJ) and a 3-mm quartz cuvette. Protein concentrations in potassium phosphate, $[C]_{KPi}$, were calculated using absorbance at λ=280 nm and estimated extinction coefficients predicted by the online ExPASy ProtParam tool (69), which estimates molar absorptivity using the amino-acid sequence and cysteine sulfur oxidation states of each peptide. Calibration of these estimated extinction coefficients, which do not anticipate the effects of intramolecular dipole-dipole interactions in a folded protein, was achieved by quantifying $[C]_{GuCl}$, the concentration of the same amount of protein in a buffer containing 8M guanidine hydrochloride, 10 mM potassium phosphate (pH 7.4) and 50 mM KCl; and then calculating a unique correction factor $M_G = [C]_{KPi}/[C]_{GuCl}$ for each sample. As DesDi protein samples containing all three

native disulfide bridges do not fully unfold in 8M guanidine, extinction coefficients for N, N* and WT insulin were calibrated by determining amino-acid compositions of the samples from three cycles of N-terminal Edman degradation sequencing using an Applied Biosystems Procise 494 Sequencer. This approach was validated by the fact that calibration *via* UV-Vis spectroscopy with potassium phosphate buffer containing guanidine hydrochloride yielded the same correction factors for wildtype insulin. Percent error in the estimated extinction coefficient of WT insulin and insulin *lispro* was ~4% whereas that of N* and N was 9% and 24%, respectively. The predicted extinction coefficients of all 1SS peptides, which are mostly unfolded in zero denaturant (see **Figure 4**), had <0.5% deviation from the experimental value. CD spectra reporting molar ellipticity per residue, [Θ], were calculated by dividing raw ellipticities by the corrected protein concentration ($[C]_{cal} = [C]_{KPi}/M_G$) and the number of amino acids, *N*, for each protein.

CD-Monitored Guanidine-Induced Unfolding Studies

Thermodynamic stabilities of all insulin peptides in 10 mM potassium phosphate buffer (pH 7.4) at 25°C were determined using guanidine hydrochloride titrations monitored by CD at the α-helix-sensitive wavelength 222 nm as described (23). Using non-linear least squares regression, plots of ellipticity vs. guanidine concentration were fit to a two-state unfolding model (70):

$$\Theta(c) = \frac{\Theta_A + \Theta_B e^{(-\Delta G - mc)/RT}}{1 + e^{(-\Delta G - mc)/RT}}. \quad [1]$$

where ΔG is the Gibbs free energy of unfolding, *C* is guanidine concentration, *R* is the ideal gas law constant, *T* is temperature, and Θ_A and Θ_B are baseline ellipticity values reflecting the folded and unfolded state. Baseline ellipticities were calculated *via* simultaneous fitting of linear equations $\Theta_A(c) = \Theta_A + m_A c$ and $\Theta_B(c) = \Theta_B + m_B c$ as described (71).

GSH-GSSH Assay

1SS-peptides (50 μg, 45 μM final concentration) were treated with 25 mM reduced glutathione (GSH) and 5 mM oxidized glutathione (GSSH) in 200 μL buffer (20 mM sodium phosphate [pH 8.2] and 100 mM NaCl) and allowed to attain equilibrium at 25°C. After 3 hrs, an aliquot was acidified with 6 M guanidine hydrochloride in 0.1% trifluoroacetic acid and analyzed by analytical rp-HPLC using 5-65% solvent B (0.1% TFA in acetonitrile) in solvent A (0.1% TFA in water) over 23 min.

Proinsulin Constructs

Plasmids expressing full-length human proinsulin or variants were constructed by polymerase chain reaction (PCR). Mutations in proinsulin were introduced using QuikChange™ (Stratagene). Constructions were verified by DNA sequencing.

Mammalian Cell Culture and ER Stress Assays

Human embryonic kidney 293T cells were purchased from American Type Culture Collection and cultured in Dulbecco's Modified Eagle Medium (DMEM), supplemented with 10% fetal bovine serum (FBS), 1% penicillin/streptomycin as recommended. Transfections were performed using Lipofectamine 3000 as described by the vendor (Invitrogen). Transfected HEK 293T cells were subjected to the Bio-Rad one-step real-time qPCR protocol. Readouts were provided by the up-regulation of ER stress markers CHOP and BiP. The gene expression values were normalized by the expression of the gene encoding glyceraldehyde 3-phosphate dehydrogenase (GAPDH) as internal control. The mRNA abundances were measured in triplicate. In Western blot assay probing ER stress markers (72, 73), after 24 hr post transient transfection, cells were lysed by RIPA buffer (Cell Signaling Technology; CST). Protein concentrations in lysates were measured by BCA assay (Thermo) and subjected to 4-20% SDS-PAGE and WB using anti-pPERK. Anti-PERK, anti-BiP and anti-CHOP antibodies (CST) at a dilution ratio of 1:1000; GAPDH provided a loading control.

Rat Experiments

Animals were maintained in accredited facility of Case Western Reserve University School of Medicine. All procedures were approved by the Institutional Animal Care and Use Committee (IACUC) office of the University. Animal care and use was monitored by the University's Veterinary Services.

Measurement of the Glucose-Lowering Effect of Insulins in Diabetic Rats

Male Lewis rats (average body mass of ~300 g) were rendered diabetic by streptozotocin (STZ) as described (23). Insulin analogs were dissolved in Lilly® Diluent buffer with the specified dose and injected in 100 μL/300 g rat. Lispro insulin (KP) was diluted as appropriate in Lilly® Diluent buffer. Control rats received the appropriate volume of the Lilly buffer. For intravenous (IV) injection, rats were anesthetized in a chamber for 5 min using a mixture of 5% isoflurane and 95% oxygen. Following cleaning of the tail, rats were injected while under anesthesia using the lateral tail vein. For subcutaneous (SQ) experiments, rats were injected under the skin into the soft tissue in the posterior aspect of the neck. Following injection, blood glucose was measured using a small drop of blood obtained from the clipped tip of the rat's tail using a clinical glucometer (EasyMax® V Glucose Meter, Oak Tree Health, Las Vegas, NV). Blood-glucose concentrations were measured at time t=0, and every 10 min for the first hr, every 20 min for the second hr, every 30 min for the third hr, and then each hr for the rest of the experiment.

Molecular Modeling

Structural ensembles were calculated by simulated annealing using *XPLOR-NIH* (74–76). A model of the one-disulfide proinsulin intermediate (containing cystine B19-A20; see **Box 1**) was generated using distance restraints pertaining to residues A16-A21 and B15-B26 as observed in an engineered proinsulin monomer (7). A similar modeling protocol was employed to generate ensembles for 1SS-DesDi variants; selected distance restraints were extracted from NOESY spectrum of an engineered insulin monomer (23). For the parent 1SS DesDi

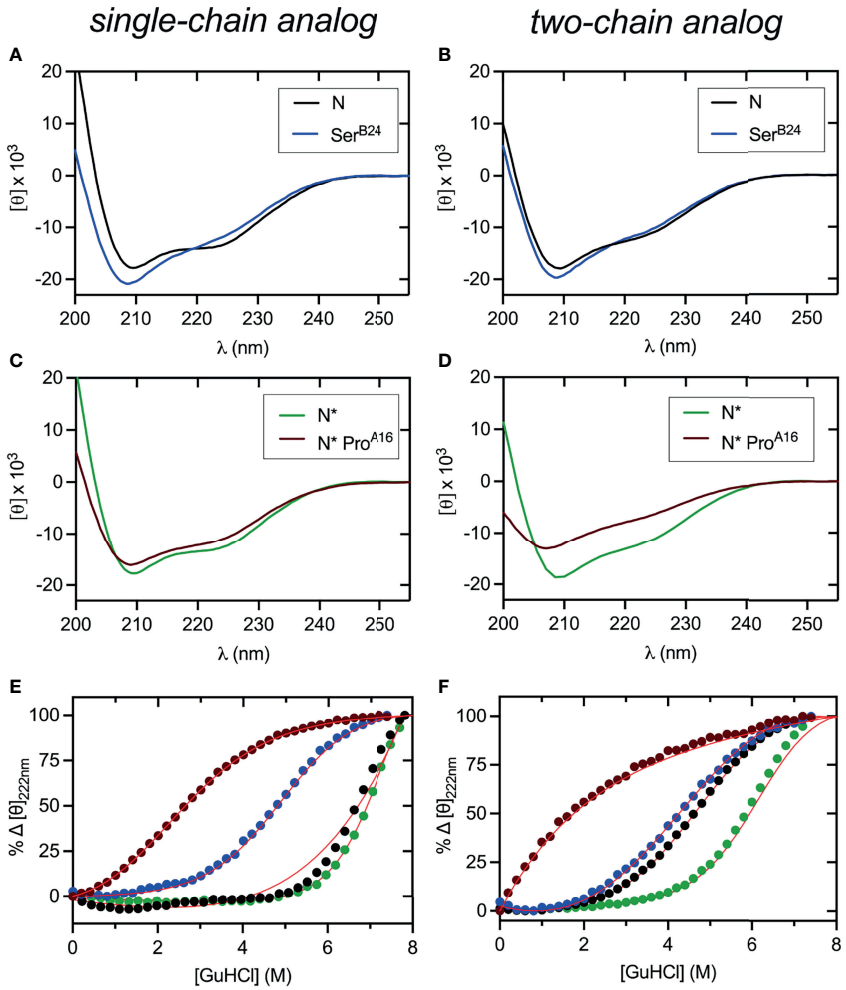

FIGURE 4 | Far UV-CD and stability studies of three disulfide containing DesDi variants. **(A, B)** CD wavelength scans of samples (N) acquired at 25°C. **(C, D)** CD wavelength scans of N*-samples acquired at 25°C. In panels **(A–D)**, left hand side represent single-chain data and right-hand side two-chain data. **(E, F)** Comparative CD-guanidine titrations of all three disulfide samples (solid lines are fits). Color legend: N (black), N* (green), Ser^{B24} (blue) and N* Pro^{A16} (maroon). ΔG_u values obtained by titration curve fitting are presented in **Table 1**. All titrations were performed at 25°C, except for N (37°C), Ser^{B24} (37°C) and N* (50°C) single-chain samples where higher temperature was used to enhance their unfolding transition.

model, helix-related distance restraints were corroborated by NMR [see companion study (64)]. To allow for protein flexibility in these partial folds, upper bounds on long-range distance restraints were increased by 3 Å relative to NMR-derived bounds obtained in prior studies of insulin and proinsulin (7, 23).

RESULTS

Eleven 49-residue peptides were prepared by solid-phase peptide chemistry (**Figure 3**); the red segments represent a peptide bond between residues B28 and A1. Seven peptides contained insulin's canonical six cysteines with intended disulfide pairing indicated in gold (**Figure 3A**). As expected (50), peptide N and N* (DesDi and [Asp^{B10}, Glu^{A8}]-DesDi, respectively) underwent oxidative folding with high efficiency to yield a single predominant product (**Table 1**). DesDi's foldability was decreased or blocked by the MIDY substitutions in order Ser^{B24} (least perturbed relative to the N parent peptide) >> Pro^{A16} = Pro^{B15} (no folded product detected). Introduction of N* substitutions Asp^{B10} and Glu^{A8} rescued inefficient but detectable folding of Pro^{A16}-N* but not Pro^{B15}-N* (**Table 1**). Four 1SS model peptides were also synthesized (**Figure 3B**). Because these contain only two cysteines, disulfide pairing was efficient in each case, including in the presence of Pro^{A16} and Pro^{B15}. Reverse-phase HPLC retention times and molecular masses are given in **Table S1**. Two-chain versions of N/N* analogs and the parent 1SS model peptide were obtained following enzymatic cleavage with Lys-C protease (50). Analytical rp-HPLC chromatograms and LC-MS profiles are provided as **Figures S1–S15**.

CD studies were conducted of the native-state analogs as single chains (left-hand panels in **Figure 4**) and on cleavage of

TABLE 1 | Folding yields of DesDi synthetic precursors and thermodynamic stabilities.

native state peptide domain	isolated yield (mg)[a]	ΔG_u(kcal/mol)[b]	*m* value(kcal/mol/M)	C_{mid}(M)
single-chain (N)[c]	21.7 mg	>4[c]	N.D.[c]	N.D.[c]
single-chain (N*)[c]	21.2 mg	7.6 ± 0.4[c]	0.99 ± 0.02	7.68 ± 0.1
Ser^{B24} single-chain (N)[c]	12.0 mg	3.4 ± 0.1[c]	0.69 ± 0.02	4.93 ± 0.1
Pro^{A16} single-chain (N)[d]	0	–	–	–
Pro^{A16} single-chain (N*)[d]	2.1 mg	0.9 ± 0.1	0.51 ± 0.02	1.76 ± 0.1
Pro^{B15} single-chain (N)[e]	0	–	–	–
Pro^{B15} single-chain (N*)[e]	0	–	–	–

[a]*Isolated yield represents amounts after rp-HPLC purification from a folding reaction of 100 mg reduced polypeptide.*

[b]*ΔG_u values provided were obtained from curve fitting of CD-guanidine titrations to a two-state unfolding transition model as described in Methods (23).*

[c]*CD-guanidine titrations performed at 37°C for N and 50°C N* (see **Figure 4**) yielded partially folded peptides at the maximum guanidine concentration. Fitting of the N* titration was successful (R^2 = 0.9994), but analysis of the N titration curve could only place a lower limit on thermodynamic stability of 4 kcal/mol.*

[d]*No product obtained. Folding was nonetheless rescued in part by Asp^{B10} and Glu^{A8} substitutions (N*).*

[e]*No isolable product obtained. In the case of Pro^{B15}, inclusion of stabilizing substitutions Asp^{B10} and Glu^{A8} (N*) did not rescue foldability: only disulfide isomers were observed.*

the Lys^{B28}-Gly^{A1} peptide bond (right-hand panels in **Figure 4**).[1] MIDY mutations Ser^{B24} and Pro^{A16} are each associated with reduced α-helix content (**Table 2**).[2] The extent of perturbation was more marked in the case of Pro^{A16}, especially in the two-chain context (**Figure 4D** and **Table 2**, row 8 *versus* row 10). Thermodynamic stabilities were inferred from CD-detected guanidine denaturation studies (**Figures 4E, F**). Application of a two-state model provided estimates of free energies of unfolding (ΔG_u; **Table S1**, column 3). In accordance with their relative susceptibilities to guanidine-induced unfolding, apparent by qualitative inspection of the denaturation data, Pro^{A16} is more profoundly destabilizing than is Ser^{B24}. In each case imposition of the B28-A1 peptide bond enhances stability [which may rationalize its utility as a vehicle for oxidative folding (50)]. The two-chain Pro^{A16} N* analog did not exhibit a cooperative unfolding transition, and so its stability could not be estimated by this method. The stabilities of corresponding Pro^{B15} native state analogs could not be assessed due to absence of folded product. Functional studies of two-chain versions of Ser^{B24}-N demonstrated reduced but substantial activity in a rodent model of DM (**Figure S16**) in accordance with past studies (23, 61, 78). The two-chain derivative of Pro^{A16}-N* was inactive as was the two-chain derivative of the 1SS parent peptide.

CD studies of 1SS analogs are shown in **Figure 5** in relation to the parent 1SS model (labeled *d* in panel B), insulin lispro (labeled *e* in panel B) and native-state domains N and N* (respectively labeled *f* and *g* in panel B); for clarity, a color code is shown at bottom. Qualitative inspection of the far-UV spectra at 4, 25 and 37°C (**Figures 5A–C**) suggest rank order N* (most structured) > N > insulin *lispro* >> parent 1SS model > 1SS-Ser^{B24} > 1SS-Pro^{A16} > 1SS Pro^{B15} (least structured). These inferences are in accordance with CD deconvolution (**Tables 2A, B**) and two-state thermodynamic modeling (**Table 1** and **Table S1**). Of the 1SS analogs, only the parent model peptide exhibits, to a small extent, a cooperative thermal unfolding curve at low

[1] Normalized CD spectra are unaffected by changes in peptide concentration in the 20-90 μM range.

[2] CD -based estimates of secondary structure content are in good agreement with published values based on SELCON-3 deconvolution (77).

TABLE 2 | CD-derived secondary-structure contents[a].

sample Name	α-helix	β-sheet	disordered
A)			
insulin *lispro*	38 – 40%	9 – 10%	32 – 33%
wild-type insulin[b]	47 – 56%	3 – 10%	24 – 29%
single-chain (N)	49 – 64%	2 – 10%	24 – 27%
single-chain (N*)	49 – 58%	4 – 10%	24 – 26%
Ser^{B24} single-chain (N)	55 – 61%	3 – 7%	27 – 28%
Pro^{A16} single-chain (N*)	43 – 48%	11 – 14%	27 – 28%
two-chain DesDi (N)	47 – 53%	10 – 12%	26 – 28%
two-chain DesDi (N*)	56 – 61%	7 – 10%	24 – 26%
two-chain Ser^{B24} (N)	50 – 58%	5 – 6%	27 – 29%
two-chain Pro^{A16} (N*)	25 – 26%	22 – 23%	31 – 32%
B)			
1SS-WT	27 – 30%	18 – 20%	30 – 31%
1SS-Ser^{B24}	19 – 20%	26 – 27%	31 – 32%
1SS-Pro^{A16}	12 – 14%	32 – 33%	30 – 31%
1SS-Pro^{B15}	10 – 11%	29 – 32%	32 – 34%

[a]*Total percent α-helix, β-sheet, and disordered coil were obtained from spectra acquired at discreet temperatures of 4°C, 25°C, and 37°C using the SELCON-3 algorithm (66–68). Estimated percentages are presented as the minimum to maximum content calculated across the three sampled temperatures.*

[b]*Estimates were calculated from WT insulin spectra to confirm that SELCON-3 processing of our own CD data gives values that match those published in the literature (77).*

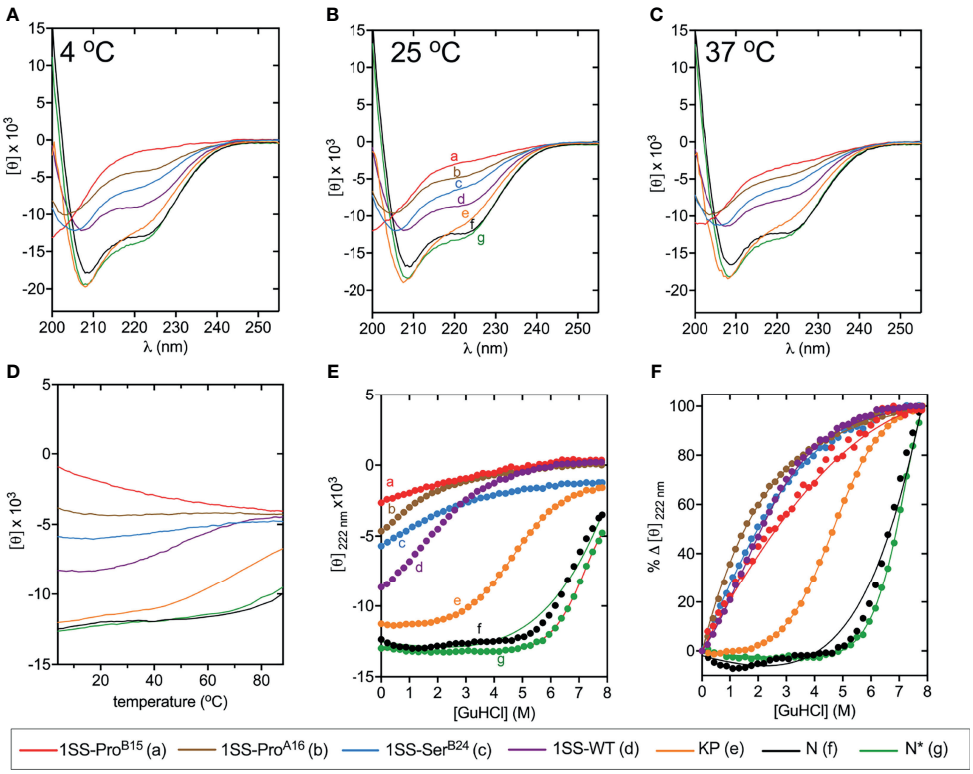

FIGURE 5 | Folding and thermodynamic stability of 1SS variants and controls. **(A–C)** CD wavelength scans of all 1SS variants, N, and N* acquired at **(A)** 4°C, **(B)** 25°C, and **(C)** 37°C. The weak temperature dependence of each secondary structure is visualized with **(D)** a plot of $\langle[\theta]_{222\pm1nm}\rangle$ versus temperature. **(E, F)** Comparative CD-guanidine titrations of insulin *lispro* and all 1SS samples (solid lines are fits). Color legend: insulin lispro (orange), N* (green), N (black), 1SS-WT (purple), 1SS-Ser^{B24} (blue), 1SS-Pro^{A16} (brown) and 1SS-Pro^{B15} (red). ΔG_u values obtained by titration curve fitting are presented in **Table 1** and **Table S1**. To enhance their unfolding transition, N and N* titrations were performed at 37°C and 50°C, respectively; all other titrations were performed at 25°C.

temperatures[3] (**Figure 5D**) and possibly a cooperative guanidine-denaturation transition with ΔG_u < 1 kcal/mole (**Figures 5E, F** and **Table S1**).

We imagine that the 1SS peptides exist as a conformational equilibrium between a disulfide-tethered random coil (at left in **Figure 6A**) and a collapsed conformation in which nascent α-helical structure occurs in the B domain (residues B9-B19; helix α_1 in insulin and proinsulin) and A domain (A12-A18; helix α_3 in insulin and proinsulin). Diffusion-collision of these nascent helices creates a molten proto-core engaging (in the parent model) Leu^{B11}, Val^{B12}, Leu^{B15}, Val^{B18}, Phe^{B24}, Tyr^{B26}, Leu^{A16} and Tyr^{A19} in the neighborhood of internal cystine B19-A20. This scheme envisions that this molten-core functions as proinsulin's specific folding nucleus (51) and is destabilized by the MIDY mutations but to different extents. Evidence supporting this hypothesis was provided by one-dimensional ^{1}H-NMR spectroscopy (**Figure 6B**). Whereas native state analogs (single-chain N* and two-chain N*) exhibit marked chemical-shift dispersion as expected of native globular domains, such dispersion is attenuated among the 1SS analogs in order N* > parent 1SS model > 1SS-Pro^{A16} > 1SS-Pro^{B15}. Preservation of chemical-shift dispersion in the proto-core of the parent 1SS peptide is remarkable, as evident by the upfield chemical shifts of aromatic resonances (Phe^{B24}, Tyr^{B26} and Tyr^{A19}) and aliphatic resonances (Leu^{B11} and Leu^{B15}). Qualitative interpretation of the NMR spectrum of Ser^{B24} native state and 1SS analogs was confounded by the absence of the diamagnetic ring-current field of Phe^{B24}, a major source of chemical-shift dispersion in native insulin (79). These NMR features are investigated further by two-dimensional heteronuclear NMR in our companion study with focus on $^{13}C_\alpha$ and $^1H_\alpha$ secondary NMR shifts (64).

The relative stabilities of the 1SS proto-cores, although inaccessible to guanidine denaturation studies (above), were instead probed by resistance to reduction at equilibrium in a defined redox buffer (25 mM reduced glutathione and 5 mM oxidized glutathione). Initial solutions contained only the disulfide-constrained peptides and were allowed to come to equilibrium as monitored by serial rp-HPLC chromatograms; representative steady-state chromatograms are shown in **Figure 7A**. Quantitation of the surviving disulfide-constrained elution peaks (arrows in **Figure 7A**) indicates a rank order of

[3]For single-chain N and N* parent domains, their limited temperature dependence of in the range 4-40°C correlates with enhanced folding efficiency and increased thermodynamic stability.

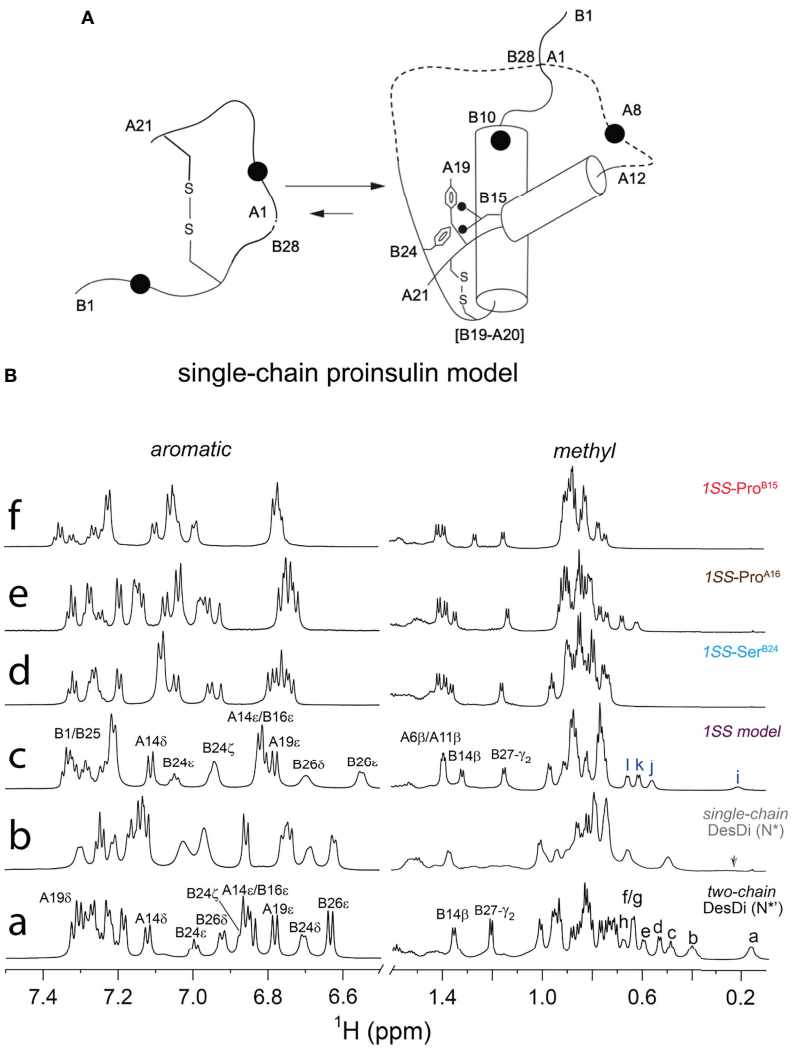

FIGURE 6 | Folding pathway of proinsulin model and NMR spectroscopy. **(A)** Model of proinsulin's specific folding nucleus based on single-chain 1SS-DesDi analog. Initial pairing of B19-A20 disulfide in combination with the formation of two-helices (B9-B19 and A12-A20) are considered to be central events in the formation of folding nucleus. Dotted lines represent disordered regions. Larger circles represent the Asp^{B10} and Glu^{A8} substitutions. Key residues are highlighted by their sequence position [panel modified from reference (51)] **(B)** Stack plot of 1D ^{1}H-NMR spectra of DesDi insulin analogs: aromatic (*left panel*) and methyl (*right panel*) region. (a) two-chain DesDi (N*'). Selected resonance assignments are as indicated in the top of signals. The well-resolved methyl resonances are indicated as a: Leu^{B15} δ_1-CH_3; b: Ile^{A2} δ_1-CH_3; c: Ile^{A10} δ_1-CH_3; d: Leu^{B15} δ_2-CH_3; e: Ile^{A2} γ_2-CH_3; f/g: Ile^{A2} γ_2-CH_3 and Leu^{B11} δ_1-CH_3; h: Leu^{B11} δ_2-CH_3; (b) single-chain DesDi (N*). The arrow indicates broadening signal of Leu^{B15} δ_1-CH_3. (c) single-chain DesDi model with one disulfide bond at [B19-A20]. Cys^{A6} and Cys^{A11} were replaced by alanine, and Cys^{A7} and Cys^{B7} were mutated by serine. The 1SS model exhibits a spectral property of native-like insulin as observed in the aromatic region and in the upfield-shifted methyl region (*far right*). Selected resonance assignments are as indicated in the top of signals. The well-resolved methyl resonances are indicated as i: Leu^{B15} δ_1-CH_3; j: Leu^{B11} δ_1-CH_3; k: Leu^{B15} δ_2-CH_3 and l: Leu^{B11} δ_2-CH_3. (d) single-chain 1SS-Ser^{B24} analog. (e) single-chain 1SS-Pro^{A16} analog and (f) single-chain 1SS-Pro^{B15} analog. Aromatic and methyl resonances of signature residues for three 1SS variants shifted to downfield, as well as exhibited a reduction in chemical-shift dispersion. Spectra were acquired at pD 7.4 (direct meter reading) at 35°C in D_2O.

redox stability parent 1SS model (most stable) > 1SS-Ser^{B24} > 1SS-Pro^{A16} >> 1SS-Pro^{B15} (least stable; histogram in **Figure 7B**). This trend is in accordance with effects of these mutations on native state DesDi folding yields (**Table 1**) and relative α-helix contents of the 1SS models (**Figure 7C**). Encouraged by this coherence, we speculate that the relative native state folding yields mirror the efficiency of initial closure of cystine B19-A20, in turn dependent on diffusion-collision of the proposed α-helical proto-core.

In an effort to connect the above chemical and biophysical properties to cell biology—and ultimately to the pathophysiology of the MPS in patients—we undertook studies of ER stress induced by transient expression of wild-type or mutant proinsulins in a human kidney-derived embryonic cell line readily grown in culture and amenable to transient transfection (HEK 293T cells). Although not related to β-cell lineages, Arvan and colleagues have shown the utility of these cells in studies of proinsulin biosynthesis (**Figure 8A**) (11). ER stress was probed through Western-blot

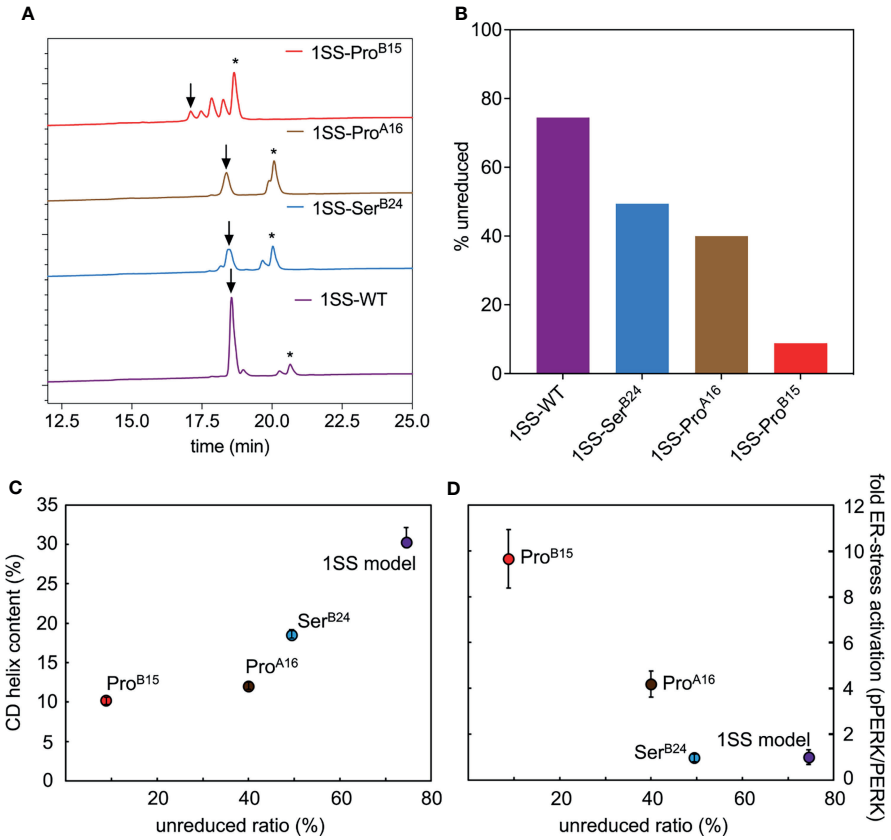

FIGURE 7 | Determination of equilibrium ratios of 1SS analogs in redox buffer containing glutathione reduced (GSH) and glutathione oxidized (GSSH) in 5:1 ratio. **(A)** Reverse-phase HPLC profiles of the equilibrium reaction mixtures after 3 h at 25 °C. Downward arrow indicates the remaining amount of polypeptide (in oxidized state) and asterisk (*) indicates the fully reduced polypeptide. Glutathione adducts were seen intermediate of the oxidized and reduced peaks. **(B)** Bar graph showing percentage remaining unreduced 1SS-polypeptides in the GSH-GSSH redox equilibrium buffer. **(C, D)** Correlations between the stability of 1SS-peptides in redox buffer with other biophysical and biological parameters reflects the same trend as the clinical severity of these mutants. Plots showing the amount of remaining unreduced 1SS-peptides correlates with their CD α-helical content **(C)** and ER-stress levels in a cell-based assay **(D)**.

studies of the pPERK/PERK ratio, induction of ER chaperone BiP (a member of the HSP70 family), and ER-stress-responsive transcription factor CHOP (**Figure 8B**). Changes in these markers (relative to the wild-type proinsulin baseline; horizontal dashed line in **Figure 8B**) are shown in **Figures 8C** (BiP on left and CHOP on right). The rank order of ER stress was Pro^{B15} (highest ER stress) > Pro^{A16} > Ser^{B24} > WT > empty vector control. This pattern parallels the sensitivity of the 1SS models to reduction in a defined redox buffer (**Figure 7D**), 1SS α-helix contents (**Figure 8D**) and native-state DesDi folding yields (**Figure 8E**). Such extensive correlations provide evidence that the biophysical and biochemical properties of DesDi 1SS and native-state peptides relate to the pathophysiology of proinsulin biosynthesis in the ER of a human cell.

DISCUSSION

How proteins fold and misfold define key problems at the intersection of biophysics, cell biology and medicine (80). The mutant proinsulin syndrome highlights the importance of foldability in the process of insulin biosynthesis (81). Mutational impairment of native disulfide pairing in the ER of pancreatic β-cells leads to ER stress, β-cell dysfunction and eventual death (17, 18). This syndrome ordinarily exhibits genetic dominance, implying that misfolding of a variant proinsulin impairs bystander biosynthesis of wild-type proinsulin (19). This monogenic diabetes syndrome thus illuminates structural determinants of specific disulfide pairing (20) and folding efficiency as an implicit evolutionary constraint (23). The present study sought to develop a peptide model of a one-disulfide proinsulin folding intermediate as a general platform for studies of a mechanistic subclass of MIDY mutations: those that impair the nascent conformational search leading to initial pairing of Cys^{B19} and Cys^{A20}, an early step in biosynthesis (8, 24). We exploited this platform to investigate three clinical mutations, two with neonatal onset [Pro^{B15} and Pro^{A16} (82, 83)] and one with onset in early adulthood [Ser^{B24} (11, 61, 62)]. The present study extends the use of peptide models of protein-folding intermediates (see **Box 1** (25)] to investigate the molecular pathogenesis of a monogenic syndrome of toxic protein misfolding.

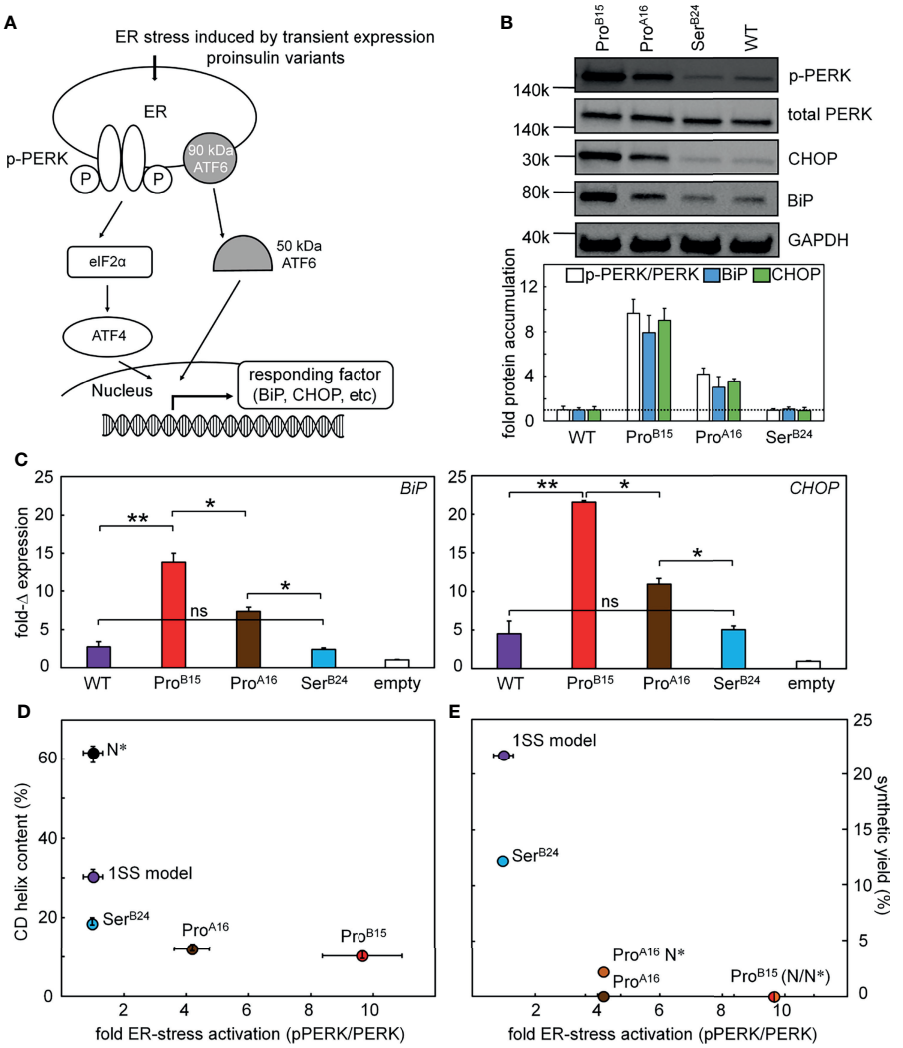

FIGURE 8 | Proinsulin mutants induce ER stress. **(A)** Schematic picture shows that the induced ER stress would be regulated by the expression of different proinsulin variants. Proinsulin variants give rise to accumulation of unfolded protein in the ER resulting in the phosphorylation of PERK and induction of ISR. As common markers, CHOP is a downstream response of the ISR and BiP is a chaperon, which would exhibit increased expression. Western blot was applied to test the protein levels of p-PERK and the accumulations of BiP and CHOP in panel **(B)** The transcription responses of these two ER stress markers were monitored by qPCR assay in panel **(C)**. **(B)** Western-blot assays probing the ER stress markers including p-PERK/PERK, CHOP, and BiP. A total of 3 blots provided ER stress markers: (i) p-PERK alone (due to a specific protocol requirement for antibody), (ii) PERK and GAPDH and (iii) BiP and CHOP. Samples were obtained from the same lysate. WT proinsulin induces low ER stress. Representative gel images (above) shows the WB results and the histogram (bottom) presents the quantification of the WB signals (n=3, biological replicates). **(C)** Real-time qPCR assay probing the transcription responses of *BiP* and *CHOP* genes induced by WT (purple) and variants of proinsulin. Gene markers for ER stress were significantly activated by the expressions of Pro^{B15} (red) and Pro^{A16} (brown) variants but not the Ser^{B24} (blue) proinsulin. Endogenous extent of GAPDH mRNA is applied as internal control to normalize the quantitative analysis of PCR gene expression. Asterisks (*) and (**) indicate p-value < 0.05 and < 0.01. The "ns" indicates p-value > 0.05 (ns - not significant). **(D, E)** Plots show the relationship between cellular ER stress activation and biophysics phenomena. **(D)** The plot shows the relationship between extents of fold of activated ER stress associated with different proinsulin variants (X-axis; using the representative ER stress marker pPERK/PERK ratio) and their percentage of helix contents evaluated by CD (Y-axis). **(E)** Plot showing the result of activated cellular ER stress correlating to the synthetic yield of these analogs in a three-disulfide containing DesDi model. N* indicates Asp^{B10} and Glu^{A8} substitutions that are used to rescue the folding in those cases.

Our peptide model is a 49-residue "mini-proinsulin" based on the DesDi framework as developed by DiMarchi and colleagues to optimize the efficiency of disulfide pairing in an enzyme-cleavable synthetic precursor (50). This framework contains B-chain residues B1-B28 followed by A-chain residues A1-A21. Its Lys^{B28}-Gly^{A1} peptide bond (cleavable by protease Lys-C) enables productive folding even of mutant insulins otherwise refractory to classical insulin chain combination (50), presumably by constraining the orientation of A- and B-chain residues to stabilize a specific folding nucleus. We obtained a one-disulfide model through pairwise substitutions of cystines B7-A7 (by serine) and A6-A11 (by alanine). Choice of Ser or Ala was

determined by solvent exposure of these disulfide bridges in native insulin (60). Nascent structure in the 1SS model, presumably stabilized by the B28-A1 peptide bond, was further favored by helicogenic substitutions His^{B10}→Asp (58) and Thr^{A8}→Glu (59). Their additional negative charges were also intended to enhance solubility and mitigate the propensity of partial folds to aggregate *via* exposed nonpolar surfaces. In native state DesDi analogs introduction of these acidic side chains rescues the folding of a Pro^{A16} analog, albeit in small yield. Pro^{B15} blocks folding of DesDi even in the presence of Asp^{B10} and Glu^{A8}. Insight into even such deleterious mutations can nonetheless be obtained through studies of corresponding 1SS peptide models.

We have characterized the above three clinical mutations in both native state and 1SS contexts. Physico-chemical properties included oxidative folding yield, nascent structure (including CD-defined α-helix contents), stability to chemical denaturation, and stability to reduction under defined redox conditions. A consistent trend in rank order of perturbations was observed: wild-type > Ser^{B24} >> Pro^{A16} > Pro^{B15} (grossly perturbed). Although CD provides only a low-resolution structural probe, the wealth of prior information (including NMR studies of insulin, proinsulin and homologous growth factors) enables construction of molecular models (**Figure 9**). Intended as working hypotheses, these models highlight the following predicted features:

i. *Parent ensemble*. The overall conformation is globular as a partial fold, stabilized by the confluence of a central B-domain α-helix (green ribbon in **Figure 9A**) and C-terminal A-domain α-helix (magenta ribbon). The mini-core contains a native-like cluster of nonpolar and aliphatic

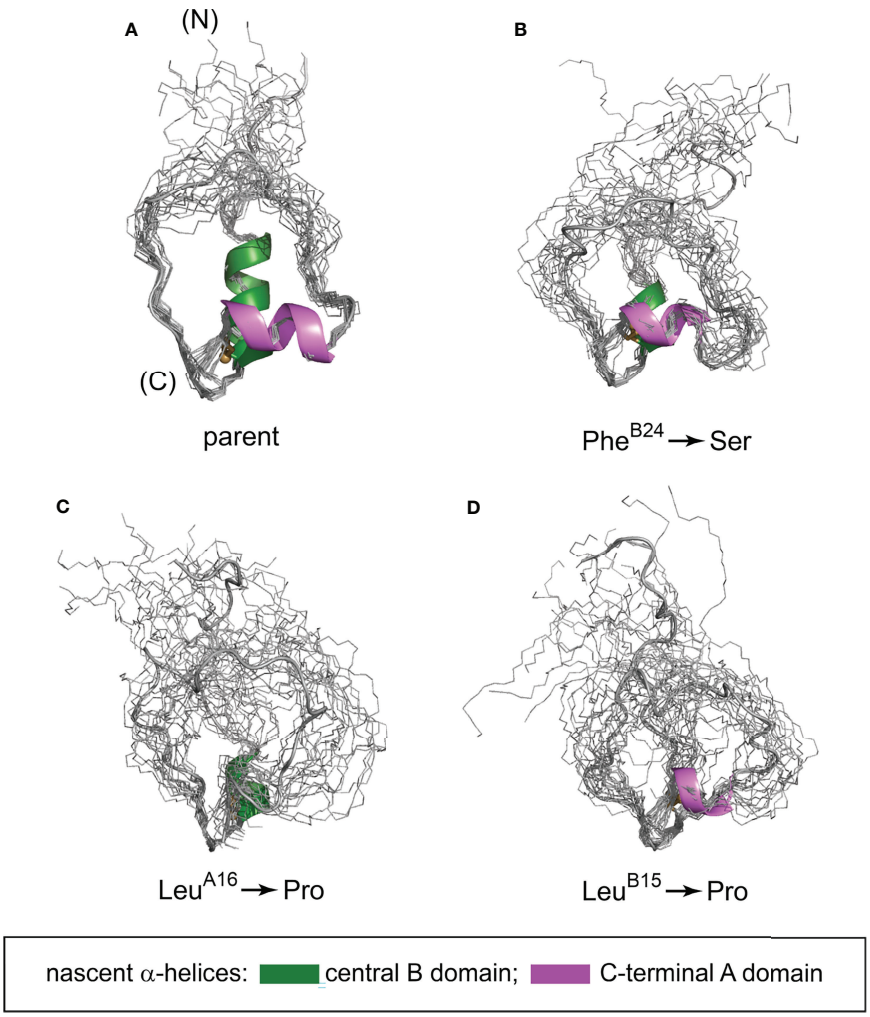

FIGURE 9 | Predicted conformational ensembles of one-disulfide peptide analogs. **(A)** parent model; **(B)** Ser^{B24} variant; **(C)** Pro^{A16} variant and **(D)** Pro^{B15} variant. The ensembles were generated by restrained molecular dynamics using the XPLOR-NIH software (75, 76) and visualized by PyMol (https://sourceforge.net/projects/pymol/). Nascent α-helices in the central segment of the B domain and C-terminal segment of the A domain are respectively shown in green and magenta (box at bottom); predicted helix lengths differ depending on the mutation in accordance with corresponding CD spectra (see **Figure 5** and **Table 2B**).

side chains (Leu^{B11}, Val^{B12}, Leu^{B15}, Val^{B18} and Leu^{A16}) near cystine B19-A20, extended by packing of a nascent C-terminal B-domain β-strand (Phe^{B24} and Tyr^{B26}).

ii. *Ser^{B24} ensemble*. Substitution of Phe^{B24} by Ser would replace aromatic packing against Val^{B12}, Leu^{B15} and Cys^{B19} by a small hydrophilic side chain. Our model posits substantial retention of the parent α-helices but with increased flexibility in the N-terminal portion of the B-chain α-helix due to loss of stabilizing Phe^{B24}-Val^{B12} and Phe^{B24}-Leu^{B15} as well as transmitted destabilization of corresponding long-range Tyr^{B26} contacts.

iii. *Pro^{A16} ensemble*. Proline has low intrinsic helical propensity (84). Accordingly, substitution of Leu^{A16} by Pro would be expected to destabilize the nascent A-domain α-helix and perturb its packing against the B domain. Our model posits substantial retention of the parent B-domain super-secondary structure but with increased flexibility in these elements and as broadly transmitted in the globule.

iv. *Pro^{B15} ensemble*. Substitution of Leu^{B15} by Pro would likewise be predicted to destabilize the nascent B-domain α-helix and also introduce multiple long-range perturbations, both to the C-terminal B-domain β-strand (Phe^{B24} and Tyr^{B26}) and within the mini-core. Our model posits N-terminal shortening of both B- and A-domain α-helices in accordance with CD spectra (**Figure 5** and **Table 2B**). These segmental and long-range perturbations would be associated with a global enhancement of conformational fluctuations.

Together, our experimental findings and molecular modeling are in accordance with genotype-phenotype relationships as Ser^{B24} (only mildly perturbed in the peptide model) is associated with adult-onset disease (MODY) whereas the more severe Pro substitutions are associated with neonatal onset (PNDM). A direct connection between chemistry and biology was further suggested by correlations between our synthetic and biophysical findings and assays of ER stress induced by the corresponding proinsulin variants in a human cell line. Such coherence among diverse probes validates the present peptide model as a general platform for mechanism-based studies of MIDY mutations mapping near cystine B19-A20. In our companion study in this issue (64), we describe more detailed two-dimensional NMR studies in an effort to deepen the biophysical characterization of this platform. These findings validate major features of the parent model depicted in **Figure 9A**.

Pairing of Cys^{B19} and Cys^{A20} represents only a first step in a complex choreography of disulfide pairing leading to the native state (**Figure 1C**). Indeed, many MIDY mutations map outside of the present folding nucleus as exemplified by substitutions at positions B5, B8 and A4 (18, 20). We envisage that in the future peptide-based strategies can be extended to two-disulfide models that encompass such additional MIDY mutations. Together, reductionist approaches promise to dissect molecular events that underlie aberrant disulfide pairing in a monogenic disease of toxic protein misfolding (17, 18). The evolution of wildtype insulin at the edge of foldability (23) suggests that such studies may inform baseline mechanisms of β-cell ER stress in the natural history of *non-syndromic* Type 2 DM. Structural lessons of the mutant proinsulin syndrome (20) thus promise to uncover a new layer of understanding in deciphering the informational content of insulin sequences (60). This layer, although of only fleeting importance in biosynthesis and hidden once the native state is reached, may nonetheless underlie the phenomenon of β-cell "exhaustion" in Type 2 DM.

Peptide models can facilitate analysis of protein folding by reducing to a minimum the complexity of a globular protein architecture. In favorable cases such simplification can enable critical determinants of folding efficiency to be dissected. We nonetheless caution that such models can be a double-edged sword: the same simplification can lead other structural contributions to foldability (or kinetic obstacles) to be overlooked. In the present case omission of proinsulin's C domain is likely to introduce offsetting advantages and disadvantages. On the one hand, 1SS DesDi exhibits a surprising richness of structure amenable to high-resolution NMR study (64). On the other hand, insertion of the long and flexible C domain, which impairs the *in vitro* refolding efficiency of single-chain insulin analogs, may allow a broader set of native and non-native disulfide bridges to be formed (8), some as off-pathway kinetic traps (43, 85, 86). Further, the present model pertains to only a subset of clinical mutations; other models may be required to investigate mutations distant from cystine B19-A20. These caveats notwithstanding, the complex biophysical chemistry of disulfide pairing in proinsulin, considered in its entirety, poses a foundational problem in protein science, central to the pathogenesis of β-cell dysfunction as a pandemic disease of civilization.

DATA AVAILABILITY STATEMENT

The original contributions presented in the study are included in the article/**Supplementary Material**. Further inquiries can be directed to the corresponding authors.

ETHICS STATEMENT

The animal study was reviewed and approved by Institutional Animal Care and Use Committee.

AUTHOR CONTRIBUTIONS

Chemical peptide syntheses were performed by BD, AZ, MJ, and RD. CD studies were performed by BD, MG, and NP. ER stress assays were conducted by Y-SC. NMR studies were performed and interpreted by YY, and MW. Figures were prepared by BD, MG, AZ, Y-SC, and MW. Supplemental rat studies were overseen by NP and FI-B. The Supplement was prepared by BD, AZ, YY, and MW. All authors contributed to editing the manuscript with first draft prepared by BD, MG, and MW. Overall experimental design and oversight were provided by MW. All authors contributed to the article and approved the submitted version.

FUNDING

This work was supported in part by grants to MW from the National Institutes of Health (R01 DK040949 and R01 DK069764). AZ were supported in part by Calibrium, LLC. NP was supported in part by the American Diabetes Association (grant no. Grants 7-13-IN-31 and 1-08-RA-149). MG was a Pre-doctoral Fellow of the National Institutes of Health (Medical Scientist Training Program 5T32GM007250-38 and Fellowship 1F30DK104618-01).

ACKNOWLEDGMENTS

We thank Prof. T. Gerken (CWRU) for N-terminal peptide sequencing, members of the Ismail-Beigi laboratory (A. Tustan, K. Carr, S. Poordian, R. Grabowski and K. Mackenzie; CWRU) for assistance with supplemental rat studies, and Dr. J.P. Mayer (Indiana University) for advice on peptide synthesis. We also thank Prof. P. Arvan (University of Michigan), M. Liu (Tianjin Research Institute of Endocrinology, Tianjin, China) and R. Wek (IUSM) for advice regarding ER stress assays. We dedicate this article to the memory of our late colleagues, Prof. D.F. Steiner (University of Chicago) and Prof. G.G. Dodson (University of York, U.K.), to whom the senior author (MW) is grateful for their advice and collaboration in the early stages of this work.

SUPPLEMENTARY MATERIAL

The Supplementary Material for this article can be found online at: https://www.frontiersin.org/articles/10.3389/fendo.2022.821069/full#supplementary-material

REFERENCES

1. Støy J, Edghill EL, Flanagan SE, Ye H, Paz VP, Pluzhnikov A, et al. Insulin Gene Mutations as a Cause of Permanent Neonatal Diabetes. *Proc Natl Acad Sci USA* (2007) 104(38):15040–4. doi: 10.1073/pnas.0707291104
2. Colombo C, Porzio O, Liu M, Massa O, Vasta M, Salardi S, et al. Seven Mutations in the Human Insulin Gene Linked to Permanent Neonatal/Infancy-Onset Diabetes Mellitus. *J Clin Investig* (2008) 118(6):2148–56. doi: 10.1172/JCI33777
3. Aguilar-Bryan L, Bryan J. Neonatal Diabetes Mellitus. *Endocr Rev* (2008) 29 (3):265–91. doi: 10.1210/er.2007-0029
4. Edghill EL, Flanagan SE, Patch A-M, Boustred C, Parrish A, Shields B, et al. Insulin Mutation Screening in 1,044 Patients With Diabetes: Mutations in the INS Gene Are a Common Cause of Neonatal Diabetes But a Rare Cause of Diabetes Diagnosed in Childhood or Adulthood. *Diabetes* (2008) 57(4):1034–42. doi: 10.2337/db07-1405
5. Ron D. Proteotoxicity in the Endoplasmic Reticulum: Lessons From the Akita Diabetic Mouse. *J Clin Invest* (2002) 109:443–5. doi: 10.1172/JCI0215020
6. Araki E, Oyadomari S, Mori M. Impact of Endoplasmic Reticulum Stress Pathway on Pancreatic β-Cells and Diabetes Mellitus. *Exp Biol Med* (2003) 228(10):1213–7. doi: 10.1177/153537020322801018
7. Yang Y, Hua QX, Liu J, Shimizu EH, Choquette MH, Mackin RB, et al. Solution Structure of Proinsulin: Connecting Domain Flexibility and Prohormone Processing. *J Biol Chem* (2010) 285:7847–51. doi: 10.1074/jbc.C109.084921
8. Qiao Z-S, Min C-Y, Hua Q-X, Weiss MA, Feng Y-M. *In Vitro* Refolding of Human Proinsulin Kinetic Intermediates, Putative Disulfide-Forming Pathway, Folding Initiation Site, and Potential Role of C-Peptide in Folding Process. *J Biol Chem* (2003) 278(20):17800–9. doi: 10.1074/jbc.M300906200
9. Qiao ZS, Guo ZY, Feng YM. Putative Disulfide-Forming Pathway of Porcine Insulin Precursor During Its Refolding *In Vitro*. *Biochemistry* (2001) 40:2662–8. doi: 10.1021/bi001613r
10. Yan H, Guo ZY, Gong XW, Xi D, Feng YM. A Peptide Model of Insulin Folding Intermediate With One Disulfide. *Protein Sci* (2003) 12:768–75. doi: 10.1110/ps.0237203
11. Liu M, Haataja L, Wright J, Wickramasinghe NP, Hua Q-X, Phillips NF, et al. Mutant INS-Gene Induced Diabetes of Youth: Proinsulin Cysteine Residues Impose Dominant-Negative Inhibition on Wild-Type Proinsulin Transport. *PloS One* (2010) 5(10):e13333. doi: 10.1371/journal.pone.0013333
12. Liu M, Hodish I, Haataja L, Lara-Lemus R, Rajpal G, Wright J, et al. Proinsulin Misfolding and Diabetes: Mutant INS Gene-Induced Diabetes of Youth. *Trends Endrocrinol Metab* (2010) 21(11):652–9. doi: 10.1016/j.tem.2010.07.001
13. Weiss MA. Proinsulin and the Genetics of Diabetes Mellitus. *J Biol Chem* (2009) 284(29):19159–63. doi: 10.1074/jbc.R109.009936
14. Meur G, Simon A, Harun N, Virally M, Dechaume A, Bonnefond A, et al. Insulin Gene Mutations Resulting in Early-Onset Diabetes: Marked Differences in Clinical Presentation, Metabolic Status, and Pathogenic Effect Through Endoplasmic Reticulum Retention. *Diabetes* (2010) 59(3):653–61. doi: 10.2337/db09-1091
15. Weiss MA. Diabetes Mellitus Due to the Toxic Misfolding of Proinsulin Variants. *FEBS Lett* (2013) 587(13):1942–50. doi: 10.1016/j.febslet.2013.04.044
16. Liu M, Hodish I, Rhodes CJ, Arvan P. Proinsulin Maturation, Misfolding, and Proteotoxicity. *Proc Natl Acad Sci USA* (2007) 104(40):15841–6. doi: 10.1073/pnas.0702697104
17. Liu M, Weiss MA, Arunagiri A, Yong J, Rege N, Sun J, et al. Biosynthesis, Structure, and Folding of the Insulin Precursor Protein. *Diabetes Obes Metab* (2018) 20:28–50. doi: 10.1111/dom.13378
18. Støy J, De Franco E, Ye H, Park S-Y, Bell GI, Hattersley AT. In Celebration of a Century With Insulin–Update of Insulin Gene Mutations in Diabetes. *Mol Metab* (2021) 52:101280. doi: 10.1016/j.molmet.2021.101280
19. Haataja L, Snapp E, Wright J, Liu M, Hardy AB, Wheeler MB, et al. Proinsulin Intermolecular Interactions During Secretory Trafficking in Pancreatic β Cells. *J Biol Chem* (2013) 288(3):1896–906. doi: 10.1074/jbc.M112.420018
20. Dhayalan B, Chatterjee D, Chen Y-S, Weiss MA. Structural Lessons From the Mutant Proinsulin Syndrome. *Front Endocrinol* (2021) 12:754693. doi: 10.3389/fendo.2021.754693
21. Blundell T, Humbel R. Hormone Families: Pancreatic Hormones and Homologous Growth Factors. *Nature* (1980) 287(5785):781–7. doi: 10.1038/287781a0
22. Nakagawa SH, Zhao M, Hua Q-x, Hu S-Q, Wan Z-l, Jia W, et al. Chiral Mutagenesis of Insulin. Foldability and Function Are Inversely Regulated by a Stereospecific Switch in the B Chain. *Biochemistry* (2005) 44(13):4984–99. doi: 10.1021/bi048025o
23. Rege NK, Liu M, Yang Y, Dhayalan B, Wickramasinghe NP, Chen Y-S, et al. Evolution of Insulin at the Edge of Foldability and Its Medical Implications. *Proc Natl Acad Sci USA* (2020) 117(47):29618–28. doi: 10.1073/pnas.2010908117
24. Miller JA, Narhi LO, Hua QX, Rosenfeld R, Arakawa T, Rohde M, et al. Oxidative Refolding of Insulin-Like Growth Factor 1 Yields Two Products of Similar Thermodynamic Stability: A Bifurcating Protein-Folding Pathway. *Biochemistry* (1993) 32:5203–13. doi: 10.1021/bi00070a032
25. Oas TG, Kim PS. A Peptide Model of a Protein Folding Intermediate. *Nature* (1988) 336(6194):42–8. doi: 10.1038/336042a0
26. Rheinberger H-J. *A History of Protein Biosynthesis and Ribosome Research. Protein Synthesis and Ribosome Structure*. Weinheim, Germany: Wiley-VCH Verlag (2004). p. 1–51.
27. Baldwin RL. Early Days of Studying the Mechanism of Protein Folding. *Protein Folding Handbook* (2005) 1:3–21. doi: 10.1002/9783527619498.ch1

28. Hartl FU, Hayer-Hartl M. Converging Concepts of Protein Folding *In Vitro* and *In Vivo*. *Nat Struct Mol Biol* (2009) 16(6):574. doi: 10.1038/nsmb.1591
29. Pederson T. The Ribosome: A Structural Biology Triumph Offering New Horizons. *FASEB J* (2019) 33(4):4655–56. doi: 10.1096/fj.190401ufm
30. Cassaignau AM, Cabrita LD, Christodoulou J. How Does the Ribosome Fold the Proteome? *Annu Rev Biochem* (2020) 89:389–415. doi: 10.1146/annurev-biochem-062917-012226
31. Onuchic JN, Nymeyer H, García AE, Chahine J, Socci ND. The Energy Landscape Theory of Protein Folding: Insights Into Folding Mechanisms and Scenarios. *Adv Protein Chem* (2000) 53:87–152. doi: 10.1016/S0065-3233(00)53003-4
32. Baker D. A Surprising Simplicity to Protein Folding. *Nature* (2000) 405 (6782):39–42. doi: 10.1038/35011000
33. Baldwin RL. The Nature of Protein Folding Pathways: The Classical Versus the New View. *J Biomol NMR* (1995) 5(2):103–9. doi: 10.1007/BF00208801
34. Englander SW, Mayne L. The Nature of Protein Folding Pathways. *Proc Natl Acad Sci USA* (2014) 111(45):15873–80. doi: 10.1073/pnas.1411798111
35. Arunagiri A, Haataja L, Cunningham CN, Shrestha N, Tsai B, Qi L, et al. Misfolded Proinsulin in the Endoplasmic Reticulum During Development of Beta Cell Failure in Diabetes. *Ann NY Acad Sci* (2018) 1418(1):5. doi: 10.1111/nyas.13531
36. Ghosh R, Colon-Negron K, Papa FR. Endoplasmic Reticulum Stress, Degeneration of Pancreatic Islet β-Cells, and Therapeutic Modulation of the Unfolded Protein Response in Diabetes. *Mol Metab* (2019) 27:S60–8. doi: 10.1016/j.molmet.2019.06.012
37. Gemmer M, Förster F. A Clearer Picture of the ER Translocon Complex. *J Cell Sci* (2020) 133(3):jcs231340. doi: 10.1242/jcs.231340
38. Fass D, Thorpe C. Chemistry and Enzymology of Disulfide Cross-Linking in Proteins. *Chem Rev* (2018) 118(3):1169–98. doi: 10.1021/acs.chemrev.7b00123
39. Hwang J, Qi L. Quality Control in the Endoplasmic Reticulum: Crosstalk Between ERAD and UPR Pathways. *Trends Biochem Sci* (2018) 43(8):593–605. doi: 10.1016/j.tibs.2018.06.005
40. Ushioda R, Nagata K. Redox-Mediated Regulatory Mechanisms of Endoplasmic Reticulum Homeostasis. *Cold Spring Harb Perspect Biol* (2019) 11(5):a033910. doi: 10.1101/cshperspect.a033910
41. Phillips BP, Gomez-Navarro N, Miller EA. Protein Quality Control in the Endoplasmic Reticulum. *Curr Opin Cell Biol* (2020) 65:96–102. doi: 10.1016/j.ceb.2020.04.002
42. Robinson PJ, Bulleid NJ. Mechanisms of Disulfide Bond Formation in Nascent Polypeptides Entering the Secretory Pathway. *Cells* (2020) 9 (9):1994. doi: 10.3390/cells9091994
43. Guo Z-Y, Qiao Z-S, Feng Y-M. The *In Vitro* Oxidative Folding of the Insulin Superfamily. *Antioxid Redox Signal* (2008) 10(1):127–40. doi: 10.1089/ars.2007.1860
44. Lazaridis T, Karplus M. "New View" of Protein Folding Reconciled With the Old Through Multiple Unfolding Simulations. *Science* (1997) 278 (5345):1928–31. doi: 10.1126/science.278.5345.1928
45. Brooks CL, Gruebele M, Onuchic JN, Wolynes PG. Chemical Physics of Protein Folding. *Proc Natl Acad Sci USA* (1998) 95(19):11037–8. doi: 10.1073/pnas.95.19.11037
46. Kim PS, Baldwin RL. Intermediates in the Folding Reactions of Small Proteins. *Annu Rev Biochem* (1990) 59(1):631–60. doi: 10.1146/annurev.bi.59.070190.003215
47. Creighton TE. Protein Folding Coupled to Disulphide Bond Formation. *Biol Chem Hoppe Seyler* (1997) 378(8):731–44. doi: 10.1515/bchm.1997.378.8.731
48. Xiao S, Bi Y, Shan B, Raleigh DP. Analysis of Core Packing in a Cooperatively Folded Miniature Protein: The Ultrafast Folding Villin Headpiece Helical Subdomain. *Biochemistry* (2009) 48(21):4607–16. doi: 10.1021/bi8021763
49. Clarke J, Fersht AR. Engineered Disulfide Bonds as Probes of the Folding Pathway of Barnase: Increasing the Stability of Proteins Against the Rate of Denaturation. *Biochemistry* (1993) 32(16):4322–9. doi: 10.1021/bi00067a022
50. Zaykov AN, Mayer JP, Gelfanov VM, DiMarchi RD. Chemical Synthesis of Insulin Analogs Through a Novel Precursor. *ACS Chem Biol* (2014) 9(3):683–91. doi: 10.1021/cb400792s
51. Hua QX, Mayer J, Jia W, Zhang J, Weiss MA. The Folding Nucleus of the Insulin Superfamily: A Flexible Peptide Model Foreshadows the Native State. *J Biol Chem* (2006) 281:28131–42. doi: 10.1074/jbc.M602616200
52. Narhi LO, Hua QX, Arakawa T, Fox GM, Tsai L, Rosenfeld R, et al. Role of Native Disulfide Bonds in the Structure and Activity of Insulin-Like Growth Factor 1: Genetic Models of Protein-Folding Intermediates. *Biochemistry* (1993) 32:5214–21. doi: 10.1021/bi00070a033
53. Weiss MA, Hua QX, Jia W, Chu YC, Wang RY, Katsoyannis PG. Hierarchiacal Protein "Un-Design": Insulin's Intrachain Disulfide Bridge Tethers a Recognition α-Helix. *Biochemistry* (2000) 39:15429–40. doi: 10.1021/bi001905s
54. Hua QX, Nakagawa SH, Jia W, Hu SQ, Chu YC, Katsoyannis PG, et al. Hierarchical Protein Folding: Asymmetric Unfolding of an Insulin Analogue Lacking the A7-B7 Interchain Disulfide Bridge. *Biochemistry* (2001) 40:12299–311. doi: 10.1021/bi011021o
55. Jia XY, Guo ZY, Wang Y, Xu Y, Duan SS, Feng YM. Peptide Models of Four Possible Insulin Folding Intermediates With Two Disulfides. *Protein Sci* (2003) 12:2412–9. doi: 10.1110/ps.0389303
56. Neuhof A, Rolls MM, Jungnickel B, Kalies K-U, Rapoport TA. Binding of Signal Recognition Particle Gives Ribosome/Nascent Chain Complexes a Competitive Advantage in Endoplasmic Reticulum Membrane Interaction. *Mol Biol Cell* (1998) 9(1):103–15. doi: 10.1091/mbc.9.1.103
57. Waudby CA, Dobson CM, Christodoulou J. Nature and Regulation of Protein Folding on the Ribosome. *Trends Biochem Sci* (2019) 44(11):914–26. doi: 10.1016/j.tibs.2019.06.008
58. Kaarsholm NC, Norris K, Jorgensen RJ, Mikkelsen J, Ludvigsen S, Olsen OH, et al. Engineering Stability of the Insulin Monomer Fold With Application to Structure-Activity Relationships. *Biochemistry* (1993) 32:10773–8. doi: 10.1021/bi00091a031
59. Weiss MA, Hua Q-X, Jia W, Nakagawa SH, Chu Y-C, Hu S-Q, et al. Activities of Monomeric Insulin Analogs at Position A8 Are Uncorrelated With Their Thermodynamic Stabilities. *J Biol Chem* (2001) 276(43):40018–24. doi: 10.1074/jbc.M104634200
60. Baker EN, Blundell TL, Cutfield JF, Dodson EJ, Dodson GG, Hodgkin DMC, et al. The Structure of 2Zn Pig Insulin Crystals at 1.5 Å Resolution. *Philos Trans R Soc Lond B Biol Sci* (1988) 319(1195):369–456. doi: 10.1098/rstb.1988.0058
61. Shoelson S, Polonsky K, Zeidler A, Rubenstein A, Tager H. Human Insulin B24 (Phe—-Ser). Secretion and Metabolic Clearance of the Abnormal Insulin in Man and in a Dog Model. *J Clin Invest* (1984) 73(5):1351–8. doi: 10.1172/JCI111338
62. Hua QX, Shoelson SE, Inouye K, Weiss MA. Paradoxical Structure and Function in a Mutant Human Insulin Associated With Diabetes Mellitus. *Proc Natl Acad Sci USA* (1993) 90(2):582–6. doi: 10.1073/pnas.90.2.582
63. Pandyarajan V, Smith BJ, Phillips NB, Whittaker L, Cox GP, Wickramasinghe N, et al. Aromatic Anchor at an Invariant Hormone-Receptor Interface: Function of Insulin Residue B24 With Application to Protein Design. *J Biol Chem* (2014) 289(50):34709–27. doi: 10.1074/jbc.M114.608562
64. Yang Y, Glidden MD, Dhayalan B, Zaykov A, Chen Y-S, Wickramasinghe NP, et al. Peptide Model of the Mutant Proinsulin Syndrome. II. Nascent Structure and Biological Implications. *Front Endocrinol* (2022) 13:821091. doi: 10.3389/fendo.2022.821091
65. Glidden MD, Aldabbagh K, Phillips NB, Carr K, Chen Y-S, Whittaker J, et al. An Ultra-Stable Single-Chain Insulin Analog Resists Thermal Inactivation and Exhibits Biological Signaling Duration Equivalent to the Native Protein. *J Biol Chem* (2018) 293(1):47–68. doi: 10.1074/jbc.M117.808626
66. Sreerama N, Woody RW. A Self-Consistent Method for the Analysis of Protein Secondary Structure From Circular Dichroism. *Anal Biochem* (1993) 209(1):32–44. doi: 10.1006/abio.1993.1079
67. Sreerama N, Woody RW. Poly (Pro) II Helixes in Globular Proteins: Identification and Circular Dichroic Analysis. *Biochemistry* (1994) 33 (33):10022–5. doi: 10.1021/bi00199a028
68. Johnson WC. Analyzing Protein Circular Dichroism Spectra for Accurate Secondary Structures. *Proteins: Struct Funct Bioinform* (1999) 35(3):307–12. doi: 10.1002/(SICI)1097-0134(19990515)35:3<307::AID-PROT4>3.0.CO;2-3
69. Gasteiger E, Hoogland C, Gattiker A, Wilkins MR, Appel RD, Bairoch A. Protein Identification and Analysis Tools on the ExPASy Server. *Proteomics Protoc Handbook* (2005) 571–607. doi: 10.1385/1-59259-890-0:571
70. Sosnick TR, Fang X, Shelton VM. Application of Circular Dichroism to Study RNA Folding Transitions. *Methods Enzymol* (2000) 317:393–409. doi: 10.1016/S0076-6879(00)17026-0

71. Pace CN, Shaw KL. Linear Extrapolation Method of Analyzing Solvent Denaturation Curves. *Proteins: Struct Funct Bioinform* (2000) 41(S4):1–7. doi: 10.1002/1097-0134(2000)41:4+<1::AID-PROT10>3.0.CO;2-2
72. Harding HP, Novoa I, Zhang Y, Zeng H, Wek R, Schapira M, et al. Regulated Translation Initiation Controls Stress-Induced Gene Expression in Mammalian Cells. *Mol Cell* (2000) 6(5):1099–108. doi: 10.1016/S1097-2765(00)00108-8
73. Yan W, Frank CL, Korth MJ, Sopher BL, Novoa I, Ron D, et al. Control of PERK Eif2α Kinase Activity by the Endoplasmic Reticulum Stress-Induced Molecular Chaperone P58IPK. *Proc Natl Acad Sci USA* (2002) 99(25):15920–5. doi: 10.1073/pnas.252341799
74. Nilges M, Clore GM, Gronenborn AM. Determination of Three-Dimensional Structures of Proteins From Interproton Distance Data by Hybrid Distance Geometry-Dynamical Simulated Annealing Calculations. *FEBS Lett* (1988) 229(2):317–24. doi: 10.1016/0014-5793(88)81148-7
75. Schwieters CD, Kuszewski JJ, Tjandra N, Clore GM. The Xplor-NIH NMR Molecular Structure Determination Package. *J Magn Reson* (2003) 160(1):65–73. doi: 10.1016/S1090-7807(02)00014-9
76. Schwieters CD, Kuszewski JJ, Clore GM. Using Xplor–NIH for NMR Molecular Structure Determination. *Prog Nucl Magn Reson Spectrosc* (2006) 48(1):47–62. doi: 10.1016/j.pnmrs.2005.10.001
77. Hua Q-x, Weiss MA. Mechanism of Insulin Fibrillation: The Structure of Insulin Under Amyloidogenic Conditions Resembles a Protein-Folding Intermediate. *J Biol Chem* (2004) 279(20):21449–60. doi: 10.1074/jbc.M314141200
78. Shoelson SE, Lu ZX, Parlautan L, Lynch CS, Weiss MA. Mutations at the Dimer, Hexamer, and Receptor-Binding, Surfaces of Insulin Independently Affect Insulin-Insulin and Insulin-Receptor Interactions. *Biochemistry* (1992) 31:1757–67. doi: 10.1021/bi00121a025
79. Jacoby E, Hua QX, Stern AS, Frank BH, Weiss MA. Structure and Dynamics of a Protein Assembly. 1H-NMR Studies of the 36 kDa R6 Insulin Hexamer. *J Mol Biol* (1996) 258(1):136–57. doi: 10.1006/jmbi.1996.0239
80. Dobson CM. Protein Folding and Misfolding. *Nature* (2003) 426(6968):884–90. doi: 10.1038/nature02261
81. Dodson G, Steiner D. The Role of Assembly in Insulin's Biosynthesis. *Curr Opin Struct Biol* (1998) 8(2):189–94. doi: 10.1016/S0959-440X(98)80037-7
82. Flanagan SE, De Franco E, Allen HL, Zerah M, Abdul-Rasoul MM, Edge JA, et al. Analysis of Transcription Factors Key for Mouse Pancreatic Development Establishes NKX2-2 and MNX1 Mutations as Causes of Neonatal Diabetes in Man. *Cell Metab* (2014) 19(1):146–54. doi: 10.1016/j.cmet.2013.11.021
83. Ortolani F, Piccinno E, Grasso V, Papadia F, Panzeca R, Cortese C, et al. Diabetes Associated With Dominant Insulin Gene Mutations: Outcome of 24-Month, Sensor-Augmented Insulin Pump Treatment. *Acta Diabetol* (2016) 53(3):499–501. doi: 10.1007/s00592-015-0793-1
84. Chakrabartty A, Kortemme T, Baldwin RL. Helix Propensities of the Amino Acids Measured in Alanine-Based Peptides Without Helix-Stabilizing Side-Chain Interactions. *Protein Sci* (1994) 3:843–52. doi: 10.1002/pro.5560030514
85. Hua QX, Gozani SN, Chance RE, Hoffmann JA, Frank BH, Weiss MA. Structure of a Protein in a Kinetic Trap. *Nat Struct Biol* (1995) 2:129–38. doi: 10.1038/nsb0295-129
86. Hua QX, Jia W, Frank BH, Phillips NB, Weiss MA. A Protein Caught in a Kinetic Trap: Structures and Stabilities of Insulin Disulfide Isomers. *Biochemistry* (2002) 41:14700–15. doi: 10.1021/bi0202981

Conflict of Interest: This study received partial funding from Calibrium, LLC. The funder was not involved in the study design, collection, analysis, interpretation of data, the writing of this article or the decision to submit it for publication. All authors declare no other competing interests.

frontiers in Endocrinology

CASE REPORT
published: 17 March 2022
doi: 10.3389/fendo.2022.842937

Case Report: Hypoglycemia Due to a Novel Activating Glucokinase Variant in an Adult — a Molecular Approach

Anojian Koneshamoorthy[1], Dilan Seniveratne-Epa[1], Genevieve Calder[1], Matthew Sawyer[1], Thomas W. H. Kay[1,2,3], Stephen Farrell[4], Thomas Loudovaris[2], Lina Mariana[2], Davis McCarthy[2,5], Ruqian Lyu[2], Xin Liu[2,5], Peter Thorn[6], Jason Tong[6], Lit Kim Chin[7], Margaret Zacharin[7], Alison Trainer[8], Shelby Taylor[8], Richard J. MacIsaac[1,3], Nirupa Sachithanandan[1,3], Helen E. Thomas[2,3†] and Balasubramanian Krishnamurthy[1,2,3†]*

[1] Department of Endocrinology and Diabetes, St. Vincent's Hospital, Melbourne, VIC, Australia, [2] St. Vincent's Institute of Medical Research, Melbourne, VIC, Australia, [3] Department of Medicine, St. Vincent's Hospital, Melbourne, VIC, Australia, [4] Department of Surgery, St. Vincent's Hospital, Melbourne, VIC, Australia, [5] Melbourne Integrative Genomics, Faculty of Science, University of Melbourne, Melbourne, VIC, Australia, [6] Charles Perkins Centre, School of Medical Sciences, University of Sydney, Sydney, NSW, Australia, [7] Department of Diabetes and Endocrinology, Royal Children's Hospital, Melbourne, VIC, Australia, [8] Department of Genomic Medicine, Royal Melbourne Hospital, Melbourne, VIC, Australia

OPEN ACCESS

Edited by:
Simone Baltrusch, University Hospital Rostock, Germany

Reviewed by:
Charles Alfred Stanley, Children's Hospital of Philadelphia, United States
Balamurugan Dhayalan, Indiana University School of Medicine, United States
Xin Li, Tianjin Medical University, China
Sara Langer, University Hospital Rostock, Germany

***Correspondence:**
Balasubramanian Krishnamurthy
bmurthy@svi.edu.au

†These authors have contributed equally to this work and share last authorship

Specialty section:
This article was submitted to Clinical Diabetes, a section of the journal Frontiers in Endocrinology

Received: *24 December 2021*
Accepted: *17 February 2022*
Published: *17 March 2022*

Citation:
Koneshamoorthy A, Seniveratne-Epa D, Calder G, Sawyer M, Kay TWH, Farrell S, Loudovaris T, Mariana L, McCarthy D, Lyu R, Liu X, Thorn P, Tong J, Chin LK, Zacharin M, Trainer A, Taylor S, MacIsaac RJ, Sachithanandan N, Thomas HE and Krishnamurthy B (2022) Case Report: Hypoglycemia Due to a Novel Activating Glucokinase Variant in an Adult — a Molecular Approach. Front. Endocrinol. 13:842937. doi: 10.3389/fendo.2022.842937

We present a case of an obese 22-year-old man with activating *GCK* variant who had neonatal hypoglycemia, re-emerging with hypoglycemia later in life. We investigated him for asymptomatic hypoglycemia with a family history of hypoglycemia. Genetic testing yielded a novel *GCK* missense class 3 variant that was subsequently found in his mother, sister and nephew and reclassified as a class 4 likely pathogenic variant. Glucokinase enables phosphorylation of glucose, the rate-limiting step of glycolysis in the liver and pancreatic β cells. It plays a crucial role in the regulation of insulin secretion. Inactivating variants in *GCK* cause hyperglycemia and activating variants cause hypoglycemia. Spleen-preserving distal pancreatectomy revealed diffuse hyperplastic islets, nuclear pleomorphism and periductular islets. Glucose stimulated insulin secretion revealed increased insulin secretion in response to glucose. Cytoplasmic calcium, which triggers exocytosis of insulin-containing granules, revealed normal basal but increased glucose-stimulated level. Unbiased gene expression analysis using 10X single cell sequencing revealed upregulated *INS* and *CKB* genes and downregulated *DLK1* and *NPY* genes in β-cells. Further studies are required to see if alteration in expression of these genes plays a role in the metabolic and histological phenotype associated with glucokinase pathogenic variant. There were more large islets in the patient's pancreas than in control subjects but there was no difference in the proportion of β cells in the islets. His hypoglycemia was persistent after pancreatectomy, was refractory to diazoxide and improved with pasireotide. This case highlights the variable phenotype of *GCK* mutations. In-depth molecular analyses in the islets have revealed possible mechanisms for hyperplastic islets and insulin hypersecretion.

Keywords: hypoglycemia, glucokinase, congenital hyperinsulinism, hyperplastic islets, MODY

INTRODUCTION

Glucokinase (also known as hexokinase IV, encoded by the *GCK* gene) enables phosphorylation of glucose, the rate-limiting step of glycolysis in the liver and pancreatic β cells (1). It plays a crucial role in the regulation of insulin secretion (2). GCK is the primary glucose sensor as small fluctuations in its activity alter glucose-stimulated insulin secretion from pancreatic β cells (3). GCK's midpoint of glucose responsiveness is 7 mM (as compared to ~0.2 mmol/L for homologous isozymes hexokinases I-III), which closely matches physiological, circulatory glucose concentrations (3). Unlike the other hexokinases, GCK is not susceptible to feedback inhibition by physiological concentrations of its product, glucose 6-phosphate (3). The importance of precise control over GCK activity is emphasized by disease phenotypes resulting from variants in the human GCK locus (3). Inactivating variants in *GCK* cause hyperglycemia (4) and activating variants cause hypoglycemia (5).

Here we report detailed clinical, functional, and molecular analysis of a man who presented with hypoglycemia due to an activating variant in *GCK*. The patient underwent spleen-preserving distal pancreatectomy with a curative intent for his hypoglycemia. Histology revealed diffuse larger islets, nuclear pleomorphism and periductular islets. Genetic testing revealed a novel activating *GCK* variant that was subsequently also found in his mother, sister and nephew. Islets were isolated from his pancreas and subjected to functional analysis and single cell RNA sequencing to reveal possible mechanisms for the metabolic effects of the activating glucokinase variant and associated morphological changes in islets.

Clinical Case

A 22-year-old man was referred for evaluation of asymptomatic hypoglycemia (plasma glucose 2.4 mmol/L) which was found incidentally during investigation for obesity (BMI 49.1 kg/m^2). He has no history of bariatric surgery, liver or kidney disease or excess alcohol consumption. His mother had a pancreatectomy (of unknown extent) at age 6 for hypoglycemic seizures. She developed diabetes mellitus in her fifth decade and she is on insulin. There was no history of glucose homeostasis related issues in his father. His sister was asymptomatic when the patient was first evaluated, but she had hypoglycemia when she was monitoring her glucose after diagnosis of gestational diabetes mellitus (described in detail later).

His initial investigation is shown in **Table 1**. A prolonged fast demonstrated endogenous hyperinsulinemic hypoglycemia (**Table 2**). The test was terminated at 10 hours of fasting when the patient's blood glucose was < 2.5mM. Imaging of the pancreas with triple phase computed tomography (CT), magnetic resonance imaging (MRI), endoscopic ultrasound, ^{68}Ga-DOTA-octreotate PET/CT (Dotatate scan, targeting somatostatin receptor subtype 2) and ^{68}Ga-DOTA-exendin-4 PET/CT (GLP-1R scan, targeting glucagon-like peptide-1 receptor) did not reveal a pancreatic lesion (not shown). A selective arterial calcium stimulation test suggested focal abnormal insulin production in the body and tail region (distal splenic artery territory) of the pancreas (**Figure 1A**). Hence he underwent spleen-preserving distal pancreatectomy with resection of the body and tail of the pancreas to the left of the superior mesenteric vein–portal vein confluence with a curative intent for his hypoglycemia. At the time of surgery, we were unaware of the genetic cause for hypoglycemia in the patient. An intraoperative ultrasound did not reveal any pancreatic lesions. Histopathology revealed mildly hyperplastic islets, nuclear pleomorphism and periductular islets (**Figures 1B, C**). There was no increase in Ki67 expressing islet cells in the patient as compared to control islets (**Figure 1C**). The distal pancreatectomy, however, did not correct hypoglycemia, as demonstrated with continuous glucose monitoring (CGM). During the diagnostic evaluation and postoperatively, he had no improvement in his hypoglycemia with continuous glucose monitoring revealing about 50-70% of time below 3.9 mm, with verapamil (80 mg oral, twice daily), a calcium channel blocker, and diazoxide (100 mg oral, three times a day, he could not tolerate a higher dose as he gained 14 kg of weight in 6 weeks with diazoxide), which inhibits insulin release by opening β-cell ATP-sensitive potassium channels. Similarly, octreotide (200 mcg sc three times a day), a somatostatin analogue which inhibits insulin release by activating somatostatin receptors 2 and 5 did not improve his hypoglycemia. There was improvement in hypoglycemia with pasireotide (900 mcg sc twice a day), another somatostatin analogue that activates somatostatin receptors 1, 2, 3 and 5 and has much higher binding affinity for somatostatin receptors 1, 3 and 5 than octreotide. While there was decrease in time below 3.9 mM to 20%, the time above 7.8 mM increased to about 30% with pasereotide (**Supplementary Figures 1**, **2**). There was little change in his insulin or c-peptide values after the surgery. His weight decreased from 141.0 kg before surgery to 123 kg after surgery. His plasma triglyceride was normal (1.9 mM).

The index case's pediatrician was later identified during the discussion on management of his nephew. Discussion with his pediatrician revealed that the index case's birth weight was 4.2 kg. He had a history of severe, recurrent, neonatal hyperinsulinemic hypoglycemia, treated effectively with diazoxide. His hypoglycemia improved and he was weaned off diazoxide by the age of 3 years. He developed obesity within the first 2 years of life. He was lost to follow up after 3 years.

Family Pedigree

The patient's sister developed gestational diabetes based on oral glucose tolerance test with 75 g of glucose during the second trimester. During the pregnancy, home glucose monitoring showed fasting glucose levels between 3.5 and 4.5 mmol/L along with post-prandial hypoglycemia despite not being on insulin. She delivered a male baby with birth weight of 3026g (25^{th} percentile). He developed hypoglycemia with plasma glucose of 1.3 mmol/L at 6 hours of life. The infant had recurrent hypoglycemia, requiring intravenous dextrose and glucagon. He was responsive to diazoxide and was discharged from hospital at 5 weeks of age with regular feeding intervals and

TABLE 1 | Initial biochemical parameters*.

Test	Value	Reference range
Plasma Glucose	2.3	3.0 – 7.7 mmol/L
C-Peptide	904	268-1275 pmol/L[1]
Insulin	17.8	3- 25 mU/L[1]
Pro-Insulin	37.1	<13 pmol/L
Betahydroxybutyrate	<0.01	0 – 0.61 mmol/L[1,2]
HbA1c	3.6	4.0-6.0%
Sulphonylurea screen	Negative	
Insulin antibodies	Negative	
Thyroid stimulating hormone	3.65	0.5-4.7 mIU/L
Free T4	13.9	11.5-22.7 pmol/L
Cortisol	265	100-535 nmol/L
Insulin-like growth factor-1	18	12-42 nmol/L
Human growth hormone	<0.1	0-1.7 ug/L
Amino acids	Non diagnostic profile	
Lactate	1.5	0.5-2.2 mmol/L
Ammonia	55	16-53 μmol/L

**The patient blood sample was drawn in non-fasted state at 11.30 am.*
[1]Reference range for normoglycemia in fasted state.
[2]Betahydroxybutyrate in fasted, hypoglycaemic state would be 2-4 mmol/L.

TABLE 2 | Prolonged fasting test.

Time	Glucose (mmol/L)	Insulin (mU/L)	C-peptide (pmol/L)	Pro insulin (pmol/L)	B-hydroxy butyrate (mmol/L)	Comments
1200 (+0 hrs)	3.8					Fasting from 1200
1800 (+6 hrs)	2.5	24	126	>100	0.08	
2000 (+8 hrs)	2.3	7	94	37.1	0.05	
2200 (+10 hrs)	1.9	7	359	–	0.05	No symptoms Given glucagon 1mg
2210 (+1010 hrs)	6.1					
2220 (+1020 hrs)	5.2					

a diazoxide regimen of 12mg/kg/day. The family pedigree is shown in **Figure 1D**.

RESULTS

Genetic Analysis Reveals an Activating Glucokinase Variant

Genetic testing by analysis of the genes known to cause hypoglycemia by targeted next generation sequencing was performed in the patient and his mother (Exeter laboratory). This revealed a novel heterozygous glucokinase (*GCK*) variant (c.269A>C p.(Lys90Thr), which was predicted to be a pathological mutation using tools including Sorting Intolerant From Tolerant (SIFT), Grantham Variation and Grantham Deviation (Align-GVGD) and Polymorphism Phenotyping v2 (PolyPhen-2). Based on international ACMG guidelines, this variant was originally classified as a class 3 variant of uncertain significance. Segregation analysis for the variant in the index case's sister and her son revealed the same *GCK* c.269A>C p.(Lys90Thr) variant and the variant was re-classified as a class 4 likely pathogenic variant. This case report highlights the importance of awareness of the possibility of genetic forms of hyperinsulinism in adults with hypoglycemia especially when imaging is uninformative and the need to search for clues in the past medical and family histories.

Pancreatic Islet Analysis

Increased Intracellular Calcium in Response to Glucose

Islets were isolated from a part of the removed pancreas for functional studies. Glucose stimulated insulin secretion (GSIS) was higher in patient's islets as compared to control islets (**Figure 2A**). Cytoplasmic calcium ($[Ca^{2+}]_c$), which triggers exocytosis of insulin-containing granules and insulin secretion, was measured in islets from the patient, and control islets from a normal donor by Fura-2 live-cell calcium imaging. Basal $[Ca2+]_c$ (*0–180 s*) did not significantly differ between patient and control islets (**Figures 2B, C**). $[Ca^{2+}]_c$ was significantly elevated in the patient's islets in response to 15 mM glucose (*181–2700 s*), compared to the control (**Figures 2B, D**). In normal islets, intracellular concentrations of calcium are maintained at approximately 100 nM in unstimulated islets and increase to approximately 500 nM following stimulation with secretagogues (6). It is possible that the high cytosolic calcium in response to glucose could be due to the patient's obesity.

Single Cell Transcriptomics Reveals Increased INS Expression and Downregulation of Genes That Control β-Cell Maturation

To investigate the molecular basis for the altered metabolism and larger islet noted in histology, we examined whole transcriptome gene expression changes using 10X single cell sequencing from the

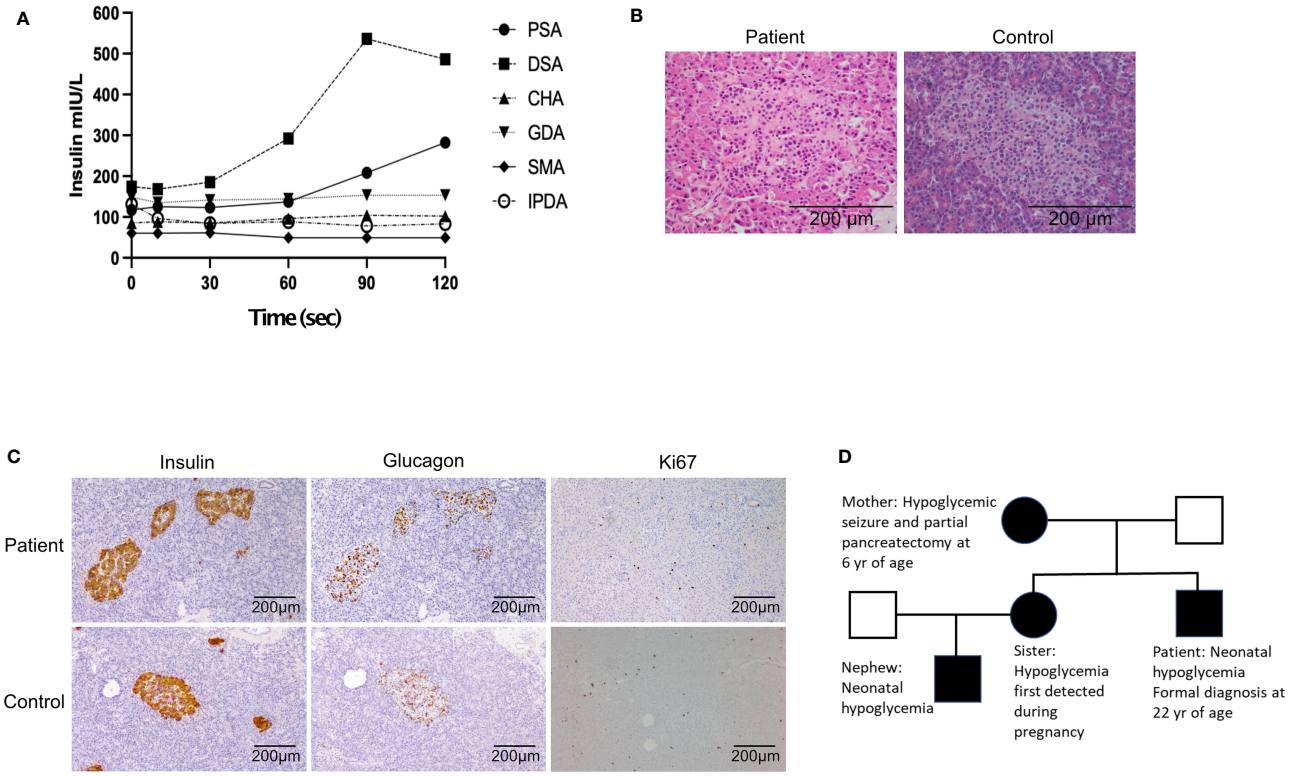

FIGURE 1 | **(A)** Selective arterial calcium stimulation test: Insulin level obtained during a selective arterial calcium stimulation test. Increased hepatic vein insulin when calcium gluconate (0.025 mEq Ca^{2+}/kg diluted to a 5-mL in normal saline, given as rapid bolus) was injected into the distal splenic artery suggested a focal abnormal insulin production in the region the body and tail of the pancreas. PSA, proximal splenic artery; DSA, distal splenic artery; CHA, common hepatic artery; GDA, gastro duodenal artery; SMA, superior mesenteric artery; IPDA, inferior pancreatico duodenal artery. **(B)** Hematoxylin and eosin high power (x200) - variation in size of islet cell nuclei. **(C)** Representative histology of patient (top panels) and control (bottom panels) pancreas sections stained with antibodies recognizing insulin, glucagon and Ki67. **(D)** Pedigree of patient. Black represents individuals with confirmed GCK mutation.

patient's islets compared with control islets. There were 1,191 genes significantly upregulated and 1,636 genes significantly downregulated in the patient's b cells compared with the control b cells (FDR < 0.01 using edgeR's quasi-likelihood F-test). There was no difference in the proportion of islet cell types, including β cells, in the islets from the patient as compared to control islets (**Figure 2E**). There were more islets per gram of pancreatic tissue in the patient. We isolated 13,292 islet equivalent (IEQ) per gram of digested pancreas from the patient's pancreas as compared to 5,209 IEQ ± 2,125 IEQ in controls (mean ± SD of 20 donors aged between 18-26 years of age). The islets were also larger; large islets (>250µm) from the patient contributed 52% of the total islet mass compared to mean ± SD of 29.43 ± 10.53% (range 15-46.3%) from 10 nondiabetic donors between 18 and 26 years of age. The control subjects were matched to the patient for age but the average BMI of the control donors was 27 ± 4.8 kg/m^2. If we only consider control subjects with BMI>27 (n=5), the mean contribution to IEQ by islet >250 µm is 29.48 ± 11.89%. While large islets in patients with activating glucokinase mutation have been described previously (7), it is likely that the patient's obesity contributed to the greater islet size. Single cell RNA sequencing revealed that the patient's β cells expressed significantly more *INS* (insulin) than the control β cells. Creatine kinase B (CKB) reversibly catalyzes the transfer of phosphate between ATP and creatine or between phosphocreatine and ADP. *CKB* was highly expressed in the patient's β cells (**Figure 2F**).

To investigate the underlying mechanisms for larger islets in the patient, we checked if the islets are maintained in a more proliferative stage, similar to neonatal islets. *DLK1* and *NPY* are highly expressed in neonatal islets and both function in β cells to inhibit the switch from immature proliferating cells to a mature differentiated state (8, 9). We found both *DLK1* and *NPY* to be significantly downregulated in the patient's β cells (**Figure 2F**). In addition, expression of genes involved in glycolysis, cell cycle determination or β cell differentiation was not different in the patient's β cells as compared to control β cells (data not shown). As there was increased insulin expression in the patient, we checked if autocrine insulin receptor (IR) signalling in β cells or the high local insulin concentration in islets could bind to IGF-1 to induce β cell proliferation (10–13). We did not find a difference in *IR*, *IGF-1R*, the downstream *IRS-1* and *IRS-2* or the negative regulator *KIAA1324* (Inceptor) gene expression (14) in the patient's β cells as compared to the control β cells. The level of hexokinase subtypes was low in the β cells in patient and control sample and there was

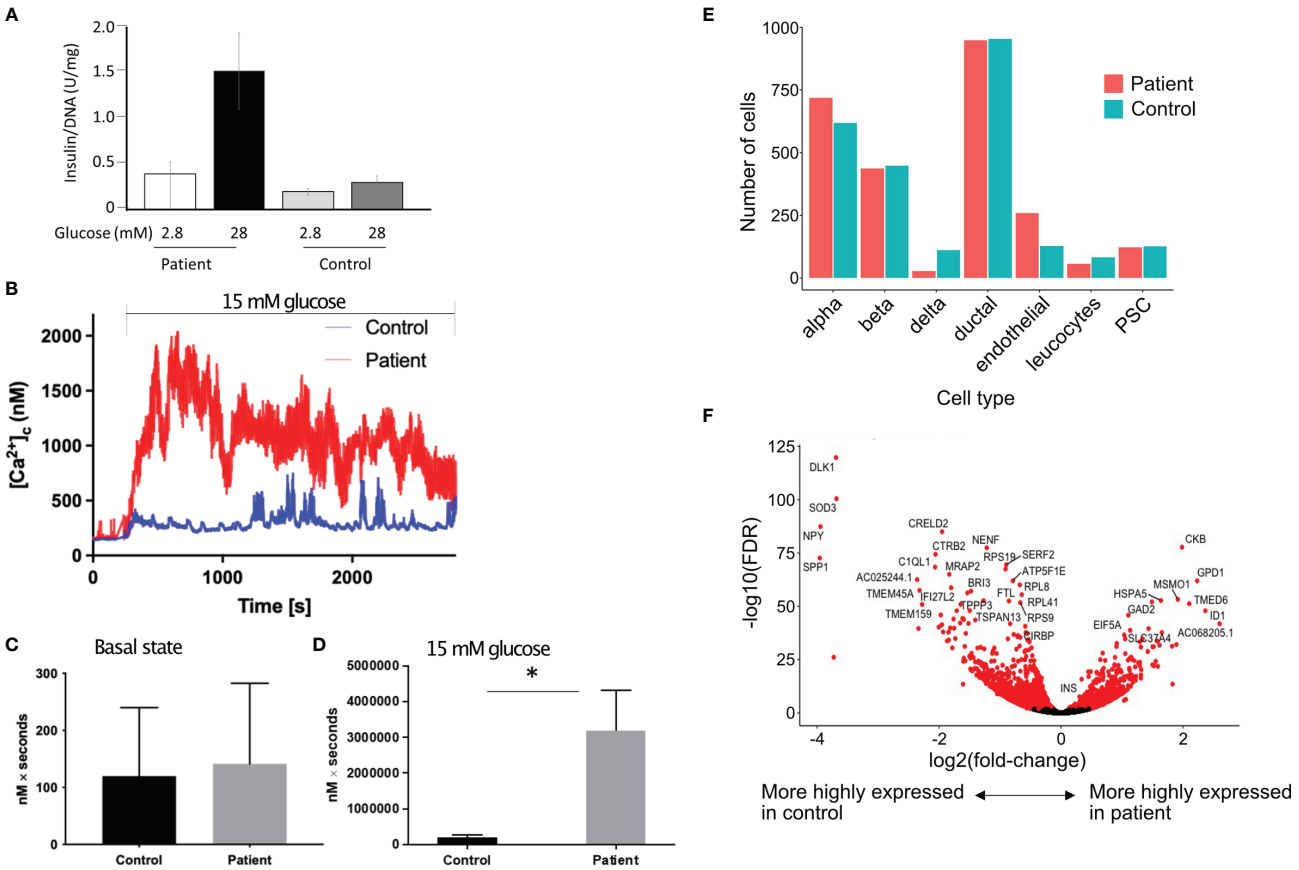

FIGURE 2 | Increased insulin secretion by the islets. **(A)** *In vitro* glucose stimulated insulin secretion of isolated islets cells. Data show mean ± SD of 3 replicates. **(B)** Increase in cytoplasmic calcium level (which triggers degranulation of insulin granules) in response to 15 mM glucose in patient's islets (red) as compared to control islets (blue). **(C, D)** Area under the curve (expressed as nM x seconds) of cytoplasmic calcium in islets in the basal state **(C)** and during stimulation with 15 mM of glucose **(D).** Data show mean ± SD of 3 replicates. *p=0.0289, 2 tailed unpaired t test. **(E)** Proportion of different cell types in the islets from the patient as compared to a single control using 10X single cell sequencing. **(F)** Volcano plot showing differentially expressed genes in the β cells of patient's islets as compared to control islets.

no difference in expression levels between the patient and control β cells.

DISCUSSION

We report a family with hyperinsulinemic hypoglycemia due to a novel activating *GCK* variant. The metabolic effects of activating glucokinase are due to changes in the threshold for insulin release. In-depth molecular analysis of β cells revealed genes that possibly contribute to the process of lowering the threshold for insulin release and associated morphological changes in pancreatic islets in activating glucokinase variant. His massive obesity may also have contributed to the morphological changes in the islets and increased calcium responses to glucose. We noted increased glucose stimulated insulin secretion in the patient's β cells. *INS* and *CKB* were highly expressed while *DLK1* and *NPY* were prominently downregulated in the patient's β cells.

GCK has been detected in the pancreas, liver, gut, and brain and is shown to play a key role in the regulation of carbohydrate metabolism. It acts as a glucose sensor in pancreatic β cells and promotes the synthesis of glycogen and triglycerides in the liver (15, 16). A patient with *GCK* c.269A>G, p.(Lys90Arg) variant, which is similar to the variant in our patient was described recently (17). Adults who are identified with activating *GCK* variants are usually diagnosed with hyperinsulinemic hypoglycemia as part of family screening following an identified neonate (18). Despite carrying the same *GCK* variant, the clinical presentation in this family varied significantly between affected relatives. Several studies have noted variation in clinical presentation within families with activating glucokinase variants (5, 19). Although speculative, one possible explanation for this phenomenon is individual differences in the way liver-specific glucokinase regulatory protein (GKRP), the regulator of GCK activity in the liver, mediates GCK inhibition in individuals.

Functional and transcriptomic analysis of islets isolated from the patient and a control pancreas suggested an increase in β-cell function rather than increased β-cell proliferation. While the number of islets per gram of pancreatic tissue was more in the patient than in control subjects, single cell analysis showed no

difference in the proportion of β cells in the patient compared to control islets. However, in addition to the larger islets, many single chromogranin A positive cells were seen throughout the pancreas (data not shown), a phenomenon not usual in normal adult human pancreas. Thus, while the proportion of β cells was not different in the isolated islets, overall, the number of β cells in the patient's pancreas was likely higher because these single β cells would have been lost during islet isolation.

Glucose stimulated insulin secretion (GSIS) was increased in the patient's islets. *CKB* and *INS* were highly expressed in the patient's β cells and intracellular Ca^{2+} levels were increased. *CKB* is important for regeneration of ATP and thus for GSIS. Insulin potentiates GSIS *in vivo* in healthy humans (20). *In vitro* stimulation of β cells with insulin leads to an increase in intracellular Ca^{2+} levels and insulin secretion (21) (22),. While glucose is the predominant insulin secretagogue, insulin mediated increase in intracellular Ca^{2+} may also amplify insulin secretion (21, 22),. Increased GSIS by the patient's β cells may also be explained by low expression of *NPY*. *NPY* regulates insulin release from β cells by reducing cAMP levels. Knockdown of *Npy* expression in neonatal mouse islets enhances insulin secretion in response to high glucose (8). Thus, increased expression of *INS* and *CKB* and decreased expression of *NPY* potentially contribute to the lower threshold for glucose stimulated insulin release.

DLK1 was reduced in the patient's β cells. *DLK1* is highly expressed in normal β cells and may regulate local insulin action (23, 24), by inhibiting insulin signaling (25). *Dlk1* knockout mice are insulin sensitive and have increased β cell mass, while transgenic mice overexpressing DLK1 under control of the collagen promoter have impaired insulin sensitivity (25). Decreased DLK1 may allow unrestrained insulin signaling leading to β-cell hypertrophy. However, mice with β-cell specific DKL1 deficiency do not have larger islets (26). Interestingly, DLK1 mutation has been linked to central precocious puberty and obesity in humans (27). Accelerated weight gain was also noted in *Dlk1* null mice (28). It is not clear how a gain of function in glucokinase modulates the expression of *DLK1*.

CONCLUSION

Our study highlights that genetic hyperinsulinemic hypoglycemia should be considered as a differential diagnosis in adults with hypoglycemia, especially when imaging is uninformative. Single cell transcriptome analysis revealed changes in gene expression in the islets with activating glucokinase variant. Further studies are required to see if alteration in gene expression plays a role in the metabolic and histological phenotype associated with the pathogenic glucokinase variant.

MATERIALS AND METHODS

Human Islets Isolation and Single Cell RNA Sequencing

Pancreas following distal pancreatectomy was obtained, with informed consent, following research approval from the Human Research Ethics Committee at St. Vincent's Hospital Melbourne (HREC-011-04). Human islets were isolated from the pancreas of the index case using standard procedures (29). We also isolated islet from a control subject whose pancreas was donated at the time we isolated the patient's islets. We quantified the isolated islets using the standard islet equivalency (IEQ) method for islet volume measurements used in islet transplantation. One IEQ is equal to a single spherical islet of 150 μm in diameter, estimated microscopically after dithizone staining (30). Islets were dispersed with accutase then rested in Connaught Medical Research Laboratories (CMRL) 1066 medium (Invitrogen) supplemented with 4% human serum albumin, 100 U/ml penicillin, 100 mg/ml streptomycin and 2 mM L-glutamine (complete CMRL), in a 37° C, 5% CO2 humidified incubator for 2 hours. Cells were processed for single cell RNAseq using the Chromium 10x genomics platform and sequenced using the Illumina NextSeq platform at the Australian Genome Research Facility (Melbourne, Australia).

Data Preprocessing

Patient and control subject's single-cell libraries were multiplexed and sequenced across 4 lanes. The raw sequencing files (.BCL) were first converted into fastq files using "cellranger mkfastq" (v3.02), were then processed using "cellranger count" (3.0.2) pipeline to align sequencing reads in fastq files to reference genome GRCh38 and generate the raw gene count matrices for single cells in each sample.

Normalisation and Clustering

The cells from two samples (patient and control islets) were pooled together for clustering and cell type identification. The filtered feature matrices from two samples (output by cellranger count) were imported into R (3.6) as a Single Cell Experiment (31) object (9,673 cells in total). Normalised gene expression was obtained by applying sctransform (v0.2.0) (32). Principle Component Analysis was performed on normalised data using the top 3,000 highly variable genes selected by their residual variance from fitting sctransform and the top 10 PCs were used for clustering using the SNN-based (shared-nearest-neighbour) clustering function from scran (v1.12.1) (33). The highly expressed genes from each cluster were used as cluster markers and compared to cell type markers found from the literature (34) for cell type identification. Cell type composition plots were generated by ggplot2 (3.1.1).

Differential Gene Expression

Differential gene expression analysis was conducted within identified cell type groups contrasting the cells from case versus from control sample using edgeR(3.26.4) (35) based on a quasi-likelihood F-test (30) and including the cellular detection rate (the fraction of detected genes per cell) as a covariate (36). The genes had log10_total_counts lower than 1.5 were excluded. The significance determined using an FDR (false discovery rate) threshold of 0.01. Note that with only one patient sample and one control sample processed in separate batches, differential expression p-values should be taken as indicative only and will not be calibrated at the nominal significance level.

Glucose Stimulated Insulin Secretion

Islets (200 IEQ) were pre-incubated for 1 hour in HEPES-buffered-KREBS buffer containing 0.1% BSA and 2.8 mmol/L D-glucose in triplicate. Islets were then incubated at 37°C for another 1 hour in KREBS buffer containing either 2.8 mmol/L or 28 mmol/L D-glucose. Culture medium was collected, and insulin secretion was measured by ELISA (Mercodia, Uppsala, Sweden) and values normalized to extracted islet DNA.

Cytoplasmic Calcium Ion Response to Glucose

The $[Ca^{2+}]_c$ in islets was determined by live cytosolic calcium imaging as previously described (37, 38).

Immununohistochemistry

Pancreatic specimens were fixed in 10% neutral buffered formalin. Antibodies for immunohistochemistry were guinea pig anti-insulin (Dako, Carpinteria, CA, USA), mouse anti-glucagon (Sigma-Aldrich, St. Louis, MO), mouse anti human Ki-67 (Dako), mouse anti human chromogranin A (AbDSerotec, Raleigh, NC), rabbit anti guinea pig HRP (Dako), rabbit anti-mouse HRP (Dako). Sections (5 μm) were stained using a Dako autostainer, detected with a peroxidase substrate containing 3,3-diaminobenzidine (brown) (Dako) and counterstained with haematoxylin.

Genetic Testing

Whole blood from the patient and his mother was sent to the Exeter Clinical Laboratory for genetic testing for analysis of the coding regions and exon/intron boundaries of the *KCNJ11, ABCC8, AKT2, GLUD1, GCK, GPC3, HADH, HNF4A, INSR, KDM6A, KMT2D, SLC16A1, CACNA1D, PMM2, TRMT10A* and *HNF1A* genes by targeted next generation sequencing (Agilent custom capture v5.3/Illumina NextSeq500).

DATA AVAILABILITY STATEMENT

The single cell RNA seq data have been uploaded to GEO (https://www.ncbi.nlm.nih.gov/geo/) with the accession number GSE193693.

ETHICS STATEMENT

Human islet studies were approved by the St Vincent's Hospital Human Research Ethics Committee (HREC-011-04). The patients/participants provided their written informed consent to participate in this study.

AUTHOR CONTRIBUTIONS

Conceptualization, BK, TK, PT, and HT. Methodology, TL, LM, RL, XL, and JT Formal analysis, BK, HT, RL, and DM. Investigation, AK, DS, GC, MS, SF, LC, MZ, AT, RM, and NS. Writing—original draft preparation, AK and BK. Writing—review and editing, TK, PT, MZ, HT, and BK. Funding acquisition, TK and HT. All authors have read and agreed to the published version of the manuscript.

FUNDING

This research was funded by The National Health and Medical Research Council of Australia, Grant number 1150425.

ACKNOWLEDGMENTS

We thank Cameron Kos, Tara Catterall and Evan Pappas (St Vincent's Institute), Stephen Wilcox and Casey Anttila (Walter and Eliza Hall Institute) for technical assistance. We thank the individual who provided consent for the publication of his clinical case. We thank all organ donors and their families, DonateLife and the staff of St Vincent's Institute involved in the human islet isolation program.

SUPPLEMENTARY MATERIAL

The Supplementary Material for this article can be found online at: https://www.frontiersin.org/articles/10.3389/fendo.2022.842937/full#supplementary-material

REFERENCES

1. Irwin DM, Tan H. Evolution of Glucose Utilization: Glucokinase and Glucokinase Regulator Protein. *Mol Phylogenet Evol* (2014) 70:195–203. doi: 10.1016/j.ympev.2013.09.016
2. Matschinsky FM. Glucokinase as Glucose Sensor and Metabolic Signal Generator in Pancreatic Beta-Cells and Hepatocytes. *Diabetes* (1990) 39:647–52. doi: 10.2337/diabetes.39.6.647
3. Sternisha SM, Miller BG. Molecular and Cellular Regulation of Human Glucokinase. *Arch Biochem Biophys* (2019) 663:199–213. doi: 10.1016/j.abb.2019.01.011
4. Froguel P, Zouali H, Vionnet N, Velho G, Vaxillaire M, Sun F, et al. Familial Hyperglycemia Due to Mutations in Glucokinase. Definition of a Subtype of Diabetes Mellitus. *New Engl J Med* (1993) 328:697–702. doi: 10.1056/NEJM199303113281005
5. Glaser B, Kesavan P, Heyman M, Davis E, Cuesta A, Buchs A, et al. Familial Hyperinsulinism Caused by an Activating Glucokinase Mutation. *New Engl J Med* (1998) 338:226–30. doi: 10.1056/NEJM199801223380404
6. Draznin B. Intracellular Calcium, Insulin Secretion, and Action. *Am J Med* (1988) 85:44–58. doi: 10.1016/0002-9343(88)90397-X
7. Kassem S, Bhandari S, Rodriguez-Bada P, Motaghedi R, Heyman M, Garcia-Gimeno MA, et al. Large Islets, Beta-Cell Proliferation, and a Glucokinase Mutation. *New Engl J Med* (2010) 362:1348–50. doi: 10.1056/NEJMc0909845
8. Rodnoi P, Rajkumar M, Moin ASM, Georgia SK, Butler AE, Dhawan S. Neuropeptide Y Expression Marks Partially Differentiated Beta Cells Mice Humans. *JCI Insight* (2017) 2(12):e94005. doi: 10.1172/jci.insight.94005
9. Martens GA, Motte E, Kramer G, Stange G, Gaarn LW, Hellemans K, et al. Functional Characteristics of Neonatal Rat Beta Cells With Distinct Markers. *J Mol Endocrinol* (2014) 52:11–28. doi: 10.1530/JME-13-0106

10. Johnson JD, Bernal-Mizrachi E, Alejandro EU, Han Z, Kalynyak TB, Li H, et al. Insulin Protects Islets From Apoptosis *via* Pdx1 and Specific Changes in the Human Islet Proteome. *Proc Natl Acad Sci United States America* (2006) 103:19575–80. doi: 10.1073/pnas.0604208103
11. Alejandro EU, Kalynyak TB, Taghizadeh F, Gwiazda KS, Rawstron EK, Jacob KJ, et al. Acute Insulin Signaling in Pancreatic Beta-Cells Is Mediated by Multiple Raf-1 Dependent Pathways. *Endocrinology* (2010) 151:502–12. doi: 10.1210/en.2009-0678
12. Kulkarni RN, Bruning JC, Winnay JN, Postic C, Magnuson MA, Kahn CR. Tissue-Specific Knockout of the Insulin Receptor in Pancreatic Beta Cells Creates an Insulin Secretory Defect Similar to That in Type 2 Diabetes. *Cell* (1999) 96:329–39. doi: 10.1016/S0092-8674(00)80546-2
13. Kim MH, Hong SH, Lee MK. Insulin Receptor-Overexpressing Beta-Cells Ameliorate Hyperglycemia in Diabetic Rats Through Wnt Signaling Activation. *PloS One* (2013) 8:e67802. doi: 10.1371/journal.pone.0067802
14. Ansarullah C, Jain FF, Far S, Homberg K, Wissmiller FG, von Hahn A, et al. Inceptor Counteracts Insulin Signalling in Beta-Cells to Control Glycaemia. *Nature* (2021) 590:326–31. doi: 10.1038/s41586-021-03225-8
15. Morishita K, Kyo C, Yonemoto T, Kosugi R, Ogawa T, Inoue T. Asymptomatic Congenital Hyperinsulinism Due to a Glucokinase-Activating Mutation, Treated as Adrenal Insufficiency for Twelve Years. *Case Rep Endocrinol* (2017) 2017:4709262. doi: 10.1155/2017/4709262
16. Postic C, Shiota M, Niswender KD, Jetton TL, Chen Y, Moates JM, et al. Dual Roles for Glucokinase in Glucose Homeostasis as Determined by Liver and Pancreatic Beta Cell-Specific Gene Knock-Outs Using Cre Recombinase. *J Biol Chem* (1999) 274:305–15. doi: 10.1074/jbc.274.1.305
17. Ping F, Wang Z, Xiao X. Clinical and Enzymatic Phenotypes in Congenital Hyperinsulinemic Hypoglycemia Due to Glucokinase-Activating Mutations: A Report of Two Cases and a Brief Overview of the Literature. *J Diabetes Investig* (2019) 10:1454–62. doi: 10.1111/jdi.13072
18. Challis BG, Harris J, Sleigh A, Isaac I, Orme SM, Seevaratnam N, et al. Familial Adult Onset Hyperinsulinism Due to an Activating Glucokinase Mutation: Implications for Pharmacological Glucokinase Activation. *Clin Endocrinol* (2014) 81:855–61. doi: 10.1111/cen.12517
19. Gilis-Januszewska A, Boguslawska A, Kowalik A, Rzepka E, Soczowka K, Przybylik-Mazurek E, et al. Hyperinsulinemic Hypoglycemia in Three Generations of a Family With Glucokinase Activating Mutation, C.295T>C (P.Trp99Arg). *Genes (Basel)* (2021) 12. doi: 10.3390/genes12101566
20. Bouche C, Lopez X, Fleischman A, Cypess AM, O'Shea S, Stefanovski D, et al. Insulin Enhances Glucose-Stimulated Insulin Secretion in Healthy Humans. *Proc Natl Acad Sci United States America* (2010) 107:4770–5. doi: 10.1073/pnas.1000002107
21. Aspinwall CA, Qian WJ, Roper MG, Kulkarni RN, Kahn CR, Kennedy RT. Roles of Insulin Receptor Substrate-1, Phosphatidylinositol 3-Kinase, and Release of Intracellular Ca2+ Stores in Insulin-Stimulated Insulin Secretion in Beta -Cells. *J Biol Chem* (2000) 275:22331–8. doi: 10.1074/jbc.M909647199
22. Roper MG, Qian WJ, Zhang BB, Kulkarni RN, Kahn CR, Kennedy RT. Effect of the Insulin Mimetic L-783,281 on Intracellular Ca2+ and Insulin Secretion From Pancreatic Beta-Cells. *Diabetes* (2002) 51(Suppl 1):S43–9. doi: 10.2337/diabetes.51.2007.S43
23. Carlsson C, Tornehave D, Lindberg K, Galante P, Billestrup N, Michelsen B, et al. Growth Hormone and Prolactin Stimulate the Expression of Rat Preadipocyte Factor-1/Delta-Like Protein in Pancreatic Islets: Molecular Cloning and Expression Pattern During Development and Growth of the Endocrine Pancreas. *Endocrinology* (1997) 138:3940–8. doi: 10.1210/endo.138.9.5408
24. Friedrichsen BN, Carlsson C, Moldrup A, Michelsen B, Jensen CH, Teisner B, et al. Expression, Biosynthesis and Release of Preadipocyte Factor-1/Delta-Like Protein/Fetal Antigen-1 in Pancreatic Beta-Cells: Possible Physiological Implications. *J Endocrinol* (2003) 176:257–66. doi: 10.1677/joe.0.1760257
25. Abdallah BM, Ditzel N, Laborda J, Karsenty G, Kassem M. DLK1 Regulates Whole-Body Glucose Metabolism: A Negative Feedback Regulation of the Osteocalcin-Insulin Loop. *Diabetes* (2015) 64:3069–80. doi: 10.2337/db14-1642
26. Appelbe OK, Yevtodiyenko A, Muniz-Talavera H, Schmidt JV. Conditional Deletions Refine the Embryonic Requirement for Dlk1. *Mech Dev* (2013) 130:143–59. doi: 10.1016/j.mod.2012.09.010
27. Gomes LG, Cunha-Silva M, Crespo RP, Ramos CO, Montenegro LR, Canton A, et al. DLK1 is a Novel Link Between Reproduction and Metabolism. *J Clin Endocrinol Metab* (2019) 104:2112–20. doi: 10.1210/jc.2018-02010
28. Moon YS, Smas CM, Lee K, Villena JA, Kim KH, Yun EJ, et al. Mice Lacking Paternally Expressed Pref-1/Dlk1 Display Growth Retardation and Accelerated Adiposity. *Mol Cell Biol* (2002) 22:5585–92. doi: 10.1128/MCB.22.15.5585-5592.2002
29. Barbaro B, Salehi P, Wang Y, Qi M, Gangemi A, Kuechle J, et al. Improved Human Pancreatic Islet Purification With the Refined UIC-UB Density Gradient. *Transplantation* (2007) 84:1200–3. doi: 10.1097/01.tp.0000287127.00377.6f
30. Lund SP, Nettleton D, McCarthy DJ, Smyth GK. Detecting Differential Expression in RNA-Sequence Data Using Quasi-Likelihood With Shrunken Dispersion Estimates. *Stat Appl Genet Mol Biol* (2012) 11. doi: 10.1515/1544-6115.1826
31. McCarthy DJ, Campbell KR, Lun AT, Wills QF. Scater: Pre-Processing, Quality Control, Normalization and Visualization of Single-Cell RNA-Seq Data in R. *Bioinformatics* (2017) 33:1179–86. doi: 10.1093/bioinformatics/btw777
32. Hafemeister C, Satija R. Normalization and Variance Stabilization of Single-Cell RNA-Seq Data Using Regularized Negative Binomial Regression. *Genome Biol* (2019) 20:296. doi: 10.1186/s13059-019-1874-1
33. Lun AT, McCarthy DJ, Marioni JC. A Step-by-Step Workflow for Low-Level Analysis of Single-Cell RNA-Seq Data With Bioconductor. *F1000Res* (2016) 5:2122. doi: 10.12688/f1000research.9501.2
34. Segerstolpe A, Palasantza A, Eliasson P, Andersson EM, Andreasson AC, Sun X, et al. Single-Cell Transcriptome Profiling of Human Pancreatic Islets in Health and Type 2 Diabetes. *Cell Metab* (2016) 24:593–607. doi: 10.1016/j.cmet.2016.08.020
35. McCarthy DJ, Chen Y, Smyth GK. Differential Expression Analysis of Multifactor RNA-Seq Experiments With Respect to Biological Variation. *Nucleic Acids Res* (2012) 40:4288–97. doi: 10.1093/nar/gks042
36. Soneson C, Robinson MD. Bias, Robustness and Scalability in Single-Cell Differential Expression Analysis. *Nat Methods* (2018) 15:255–61. doi: 10.1038/nmeth.4612
37. Parkash J, Chaudhry MA, Amer AS, Christakos S, Rhoten WB. Intracellular Calcium Ion Response to Glucose in Beta-Cells of Calbindin-D28k Nullmutant Mice and in Betahc13 Cells Overexpressing Calbindin-D28k. *Endocrine* (2002) 18:221–9. doi: 10.1385/ENDO:18:3:221
38. Low JT, Shukla A, Behrendorff N, Thorn P. Exocytosis, Dependent on Ca2+ Release From Ca2+ Stores, Is Regulated by Ca2+ Microdomains. *J Cell Sci* (2010) 123:3201–8. doi: 10.1242/jcs.071225

Conflict of Interest: The authors declare that the research was conducted in the absence of any commercial or financial relationships that could be construed as a potential conflict of interest.

Publisher's Note: All claims expressed in this article are solely those of the authors and do not necessarily represent those of their affiliated organizations, or those of the publisher, the editors and the reviewers. Any product that may be evaluated in this article, or claim that may be made by its manufacturer, is not guaranteed or endorsed by the publisher.

frontiers | Frontiers in Endocrinology

ORIGINAL RESEARCH
published: 03 May 2022
doi: 10.3389/fendo.2022.827325

Identification of Variants Responsible for Monogenic Forms of Diabetes in Brazil

Gabriella de Medeiros Abreu[1*], *Roberta Magalhães Tarantino*[2], *Ana Carolina Proença da Fonseca*[1,3], *Juliana Rosa Ferreira de Oliveira Andrade*[1,4], *Ritiele Bastos de Souza*[1], *Camila de Almeida Pereira Dias Soares*[1], *Amanda Cambraia*[1], *Pedro Hernan Cabello*[1,4], *Melanie Rodacki*[2], *Lenita Zajdenverg*[2], *Verônica Marques Zembrzuski*[1] *and Mário Campos Junior*[1]

[1] Laboratory of Human Genetics, Oswaldo Cruz Institute, Oswaldo Cruz Foundation, Rio de Janeiro, Brazil, [2] Diabetes and Nutrology Section, Internal Medicine Department, Federal University of Rio de Janeiro, Rio de Janeiro, Brazil, [3] Laboratory of Immunopharmacology, Oswaldo Cruz Institute, Oswaldo Cruz Foundation, Rio de Janeiro, Brazil, [4] Laboratory of Genetics, School of Health Science, University of Grande Rio, Rio de Janeiro, Brazil

OPEN ACCESS

Edited by:
Jiajun Zhao,
Shandong Provincial Hospital, China

Reviewed by:
Rochelle Naylor,
The University of Chicago, United States
Barbara Zapała,
Jagiellonian University, Poland

***Correspondence:**
Gabriella de Medeiros Abreu
gabriella_bio@yahoo.com.br

Specialty section:
This article was submitted to Clinical Diabetes, a section of the journal Frontiers in Endocrinology

Received: 01 December 2021
Accepted: 24 March 2022
Published: 03 May 2022

Citation:
Abreu GM, Tarantino RM, da Fonseca ACP, Andrade JRFO, de Souza RB, Soares CAPD, Cambraia A, Cabello PH, Rodacki M, Zajdenverg L, Zembrzuski VM and Campos Junior M (2022) Identification of Variants Responsible for Monogenic Forms of Diabetes in Brazil. Front. Endocrinol. 13:827325. doi: 10.3389/fendo.2022.827325

Monogenic forms of diabetes mellitus may affect a significant number of patients of this disease, and it is an important molecular cause to be investigated. However, studies of the genetic causes of monogenic diabetes, especially in populations with mixed ethnic backgrounds, such as the one in Brazil, are scarce. The aim of this study was to screen several genes associated with monogenic diabetes in fifty-seven Brazilian patients with recurrence of the disease in their families and thirty-four relatives. Inclusion criteria were: Age of onset ≤ 40 years old, BMI < 30 kg/m², at least two affected generations and negative anti-GAD and anti-IA2 antibodies. MODY genes *HNF4A*, *GCK*, *HNF1A*, *HNF1B*, *NEUROD1*, *KLF11*, *PAX4*, *INS*, *KCNJ11*, and *MT-TL1* were sequenced by Sanger sequencing. We identified a total of 20 patients with variants, 13 GCK-MODY, four HNF1A-MODY, and one variant in each of the following genes, *HNF4A*, *HNF1B* and *MT-TL1*. Segregation analysis was performed in 13 families. Four variants were novel, two in *GCK* (p.(Met115Val) [c.343A>G] and p.(Asp365GlufsTer95) [c.1094_1095insGCGA]) and two in *HNF1A* (p.(Tyr163Ter) [c.489C>G] and p.(Val380CysfsTer39) [c.1136_1137insC]). Here we highlight the importance of screening for monogenic diabetes in admixed populations.

Keywords: monogenic diabetes, MODY, mitochondrial disease, genetic diagnosis, rare disorders, variants

INTRODUCTION

Diabetes is a clinically and genetically variable group of metabolic diseases characterized by hyperglycemia. It is estimated that monogenic forms of DM represent approximately 2% of cases with early onset diabetes (1, 2). These patients are frequently undiagnosed or misclassified as having type 1 DM (T1DM) or type 2 DM (T2DM). Monogenic diabetes includes different types of the disease: Neonatal diabetes mellitus (NDM) is a rare form of diabetes, characterized by the onset before six months of life (3). Mitochondrial diabetes, caused by a single alteration in the *MT-TL1*

gene in mtDNA, in most cases by the m.3243A>G (4). And the most common form of monogenic diabetes, which is the Maturity-Onset Diabetes of the Young (MODY).

MODY is classically defined as a mild diabetes with autosomal dominant inheritance, early age at onset and impaired insulin secretion. In some cases, there is no insulin dependence (5). Since its first clinical description, variants in fourteen genes (*HNF4A*, *GCK*, *HNF1A*, *PDX1*, *HNF1B*, *NEUROD1*, *KLF11*, *CEL*, *PAX4*, *INS*, *BLK*, *ABCC8*, *KCNJ11* and *APPL1*) were described associated to this condition, presenting phenotypic, metabolic and genetic heterogeneity [review in (6)]. However, variants in *BLK*, *KLF11* and *PAX4* genes have been recently been challenged as causes of MODY (7). The frequency of variants in each gene is variable, according to the genetic background of the population and the methodology applied. In this study, we aimed to screen for variants in nine important genes associated to MODY, and the mitochondrial *MT-TL1*, in a sample with clinical characteristics of monogenic diabetes from Rio de Janeiro, Brazil to understand the contribution of each one of these genes in this cohort.

MATERIALS AND METHODS

Patients

In this cross-sectional observational study were included patients who were treated at the Clementino Fraga Filho University Hospital and at the State Institute for Diabetes and Endocrinology Luiz Capriglione, from Rio de Janeiro, Brazil and their relatives. The inclusion criteria were patients with age at diagnosis (AAD) equal or less than 40 years old; positive family history of DM in at least two other generations in the family, or two or more first degree relatives at the same side of the family; and negative anti-GAD (Glutamic Acid Decarboxylase) and anti-IA2 (Islet Antigen 2) antibodies. The exclusion criteria were patients with T1DM with positive antibodies, obesity (Body Mass Index [BMI] $\geq$ 30 kg/m^2 or $\geq$ 95th percentile at AAD), history of diabetic ketoacidosis at diabetes onset, clinical signs of insulin resistance and presence of secondary causes the disease. Patients were divided into two groups, *GCK* or *HNF1A*, according to their clinical manifestation, since these two genes represents together the major cause of MODY. The GCK group (tested for the *GCK* gene) comprised patients most often asymptomatic that presented mild fasting hyperglycemia since birth ranging from 100 to 154 mg/dL, increase in glycaemia < 54 mg/dL after 75 g anhydrous dextrose and HbA1c < 7.5% (58 mmol/mol); and a evolutionarily stable disease (even without antidiabetic drugs); the remaining patients were included in HNF1A group (tested for the *HNF1A* gene).

Medical records were reviewed and participants were interviewed in order to obtain the following clinical information: AAD, duration of the disease, familiar history of DM, current and previous treatment, anthropometric measurements (height, weight and BMI), blood pressure, laboratory blood tests (Fasting Plasma Glucose [FPG], HbA1c, anti-GAD, anti-IA2, C-reactive protein [CRP], thyroid-stimulating hormone [TSH], free thyroxine 4 [Ft4], thyroid anti-peroxidase [TPO]), and presence of retinopathy, nephropathy, neuropathy and renal cysts. This study protocol was approved by The Ethics and Research Committee of the Clementino Fraga Filho University Hospital (CAAE n° 04232512.4.0000.5257) and by the State Institute for Diabetes and Endocrinology Luiz Capriglione (CAAE n° 04232512.4.3001.5266). All participants were informed about the aim of this study and provided a written informed consent.

Nineteen probands were enrolled in *GCK* screening and 16 were studied for *HNF1A*. In addition, twenty-one negative patients for *HNF1A* and one patient negative for *GCK*, previous reported by our group (8), were included for the screening of the other MODY genes. All negative patients for *GCK* variants were analyzed for *HNF1A* gene. After *GCK* and *HNF1A* sequencing, 40 patients with no detected variants were screened for mutations in *HNF4A*, *HNF1B*, *NEUROD1*, *KLF11*, *PAX4*, *INS*, *KCNJ11* and *MT-TL1*. A total of 34 relatives from 13 families were recruited 40 - 2.5%) (8 men and 16 women; average age 36.3 ± 20.7 years, ranging from 0 to 74 years), in which 21 presented DM and 13 did not report hyperglycemia. In total, 57 Brazilian probands were studied **(Table 1)**. The study sample formation is show in the **Figure 1**.

Molecular Genetic Analysis

Genomic DNA from the probands was isolated from peripheral blood leukocytes using QIAamp DNA Blood Mini Kit (Qiagen, Hilden, Germany) and the genomic DNA from their relatives was collected and extracted from buccal epithelial cells according to the protocol in the literature (9). Primers were designed for all coding regions of 10 genes (*HNF4A*, *GCK*, *HNF1A*, *HNF1B*, *NEUROD1*, *KLF11*, *PAX4*, *INS*, *KCNJ11* and *MT-TL1*) using Primer3Plus software (http://www.bioinformatics.nl/cgi-bin/primer3plus/primer3plus.cgi). The information of the primers, PCR reagents and cycling conditions were summarized in **Supplementary Table S1**. PCR products were purified by ExoSAP-IT® Reagent (Applied Biosystems, Vilnius, Lithuania), followed by Sanger sequencing reaction using the Big Dye Terminator Kit v3.1 (Applied Biosystems, Austin, TX, USA), conducted on an ABI 3130 Automatic Genetic Analyzer (Applied Biosystems). For variants considered to be likely pathogenic, orthogonal methodology was executed, including re-extraction of the sample, testing and sequencing of the forward and reverse strands of the area of interest a second time, and sequencing of the exon containing the variant identified in family members samples.

Classification of Variants

Previous occurrence of all variants identified were checked in the follow public databases: PubMed, Clinvar, dbSNP (https://www.ncbi.nlm.nih.gov/), HGMD (http://www.hgmd.cf.ac.uk/ac/), gnomAD (https://gnomad.broadinstitute.org/) and the Online Archive of Brazilian Mutations (ABraOM; http://abraom.ib.usp.br/) (10). We classified the variants identified by our group according the published criteria of pathogenicity of the American College of Medical Genetics and Genomics and the Association for Molecular Pathology (ACMG/AMP) (Richards et al., 2015) available on VarSome (https://varsome.com/) (11).

TABLE 1 | Clinical description of the sample studied.

Variables	n	GCK-MODY group (n=20)	n	HNF1A-MODY group (n=37)
Sex	20		37	
women		10		22
men		10		15
Age of diagnose (years)	20	16.45 ± 11.53 (0,38)	37	18.16 ± 10.88 (2,37)
Current BMI (kg/m²)	19	21.54 ± 3.99	33	24.38 ± 3.44
Fasting glucose (mg/dL)	15	127.72 ± 23.08	17	150.64 ± 65.41
Glycated hemoglobin (%)	13	6.29 ± 0.66	31	7.73 ± 2.01
Treatment	20		37	
Insulin				
Yes		5		26
No		15		11
Oral hypoglycemic agents				
Yes		5		21
No		15		16
Clinical diagnose suspicion	18		35	
Without classification		2		6
Prediabetes		1		0
DM type 1		8		19
DM type 2		0		8
MODY		7		2

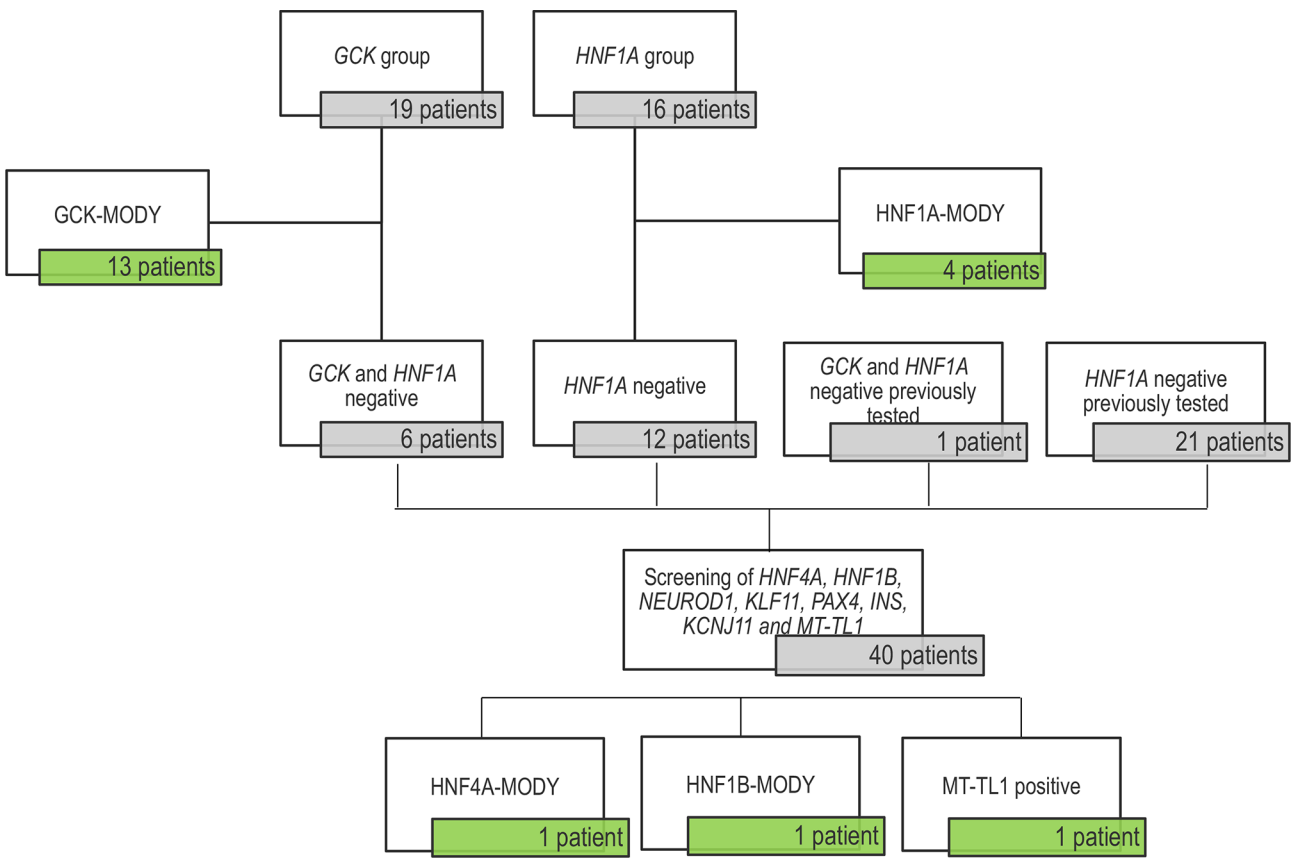

FIGURE 1 | Flow diagram of the sample tested in this study. The untested patients included 19 patients in the GCK-MODY group and 16 patients for being tested for *HNF1A* variants. We found 13 *GCK* carriers and 4 patients with HNF1A-MODY. The 6 GCK negatives probands were screened for HNF1A variants and they were all negatives. This study also included a cohort previously search for variants in in the *HNF1A* gene (21 patients) with negative results; and one patient negative for both genes. Forty patients presented no variant in the two major genes (GCK and HNF1A) and were tested for *HNF4A*, *HNF1B*, *NEUROD1*, *KLF11*, *PAX4*, *INS*, *KCNJ11* and *MT-TL1*, resulting in the identification of three patients with variants.

Variant nomenclature followed the recommendations by the Human Genome Variation Society (http://www.hgvs.org/mutnomen/). Mitochondrial DNA nomenclature followed the Revised Cambridge reference sequence (rCRS) (http://www.mitomap.org/MITOMAP/HumanMitoSeq). Polymorphisms or synonymous variants reported are not included in this study. Variants not described in databases or published in scientific articles were referred as novel.

Bioinformatics Analysis

The potential impact of the identified variants was tested by calculating prediction scores using eight prediction software: MutPred, FATHMM (v.2.3), VEST (v.4.0), SIFT, PolyPhen-2, Mutation Taster, PROVEAN, and Mutation Assessor. Conservation scores were calculated by five software: LRT, GERP++, SiPhy, PhastCons, and PhyloP. Revel was also used to scores of these thirteen software. All analysis were done by the Ensembl Variant Effect Predictor (VEP) and the results were retrieved from the dbNSFP.

More details of each software are present in **Supplemental Information**.

RESULTS

Molecular Screening Findings

In the present study, we identified 20 patients with variants in our cohort: thirteen patients with variants in the *GCK* 40 - 2.5%) (3/19 - 68.4%), four patients with variants in the *HNF1A* (4/16 - 25%) and one variant in each of the following genes *HNF4A*, *HNF1B* and *MT-TL1* 40 - 2.5%) (/40 - 2.5%) (**Table 2**; **Supplementary Figure S1**). Clinical characteristics of the patients with variants described by our group are presented in **Supplemental Table 2**. We did not observe any variants in *KCNJ11*, *KLF11* and *INS* genes. Concerning the segregation study, 24 individuals from the 34 relatives showed the variant described in this study present in the probands. Among them, 20 individuals presented DM. Four relatives with variants in the *GCK* gene did not report DM at the moment of this study. Among the remaining ten relatives, one reported DM. Segregation analyses are shown in the **Figure 2**.

GCK-MODY (OMIM # 125851)

GCK screening showed 11 different variants in 13 probands: seven men and six women. Two of the observed *GCK* variants were novel, the p.(Met115Val) (c.343A>G) and the p.(Asp365GlufsTer95) (c.1094_1095insGCGA); variant p.(Met115Val) was reported in gnomAD (Frequency: 0.00001193), however, no phenotype characteristics were available. The *missense* p.(Met115Val) variant was observed in a female patient (P46) (**Figure 2E**; individual III-3) diagnosed in her first pregnancy at the age of 25 years. This variant was observed segregating from her father (**Figure 2E**; individual II-2) with diabetes and was found in her two brothers (**Figure 2E**; individuals III-1 and III-2). The patient P55 (**Figure 2G**; individual II-3), harboring the *frameshift* p.(Asp365GlufsTer95) variant, was diagnosed at 26 years of age in a routine exam (BMI at diagnosis: 22.3 kg/m^2). At the age of 32 years, when he entered in this study, he showed FPG varying from 109 to 128 mg/dL and HbA1c of 6.1% and he was controlling his hyperglycemia with diet. This variant was also observed in his father (**Figure 2G**; individual I-1) diagnosed at 40 years old and in his 5-year-old son (**Figure 2G**; individual III-3), diagnosed at birth. His son was born prematurely, before 32 weeks of gestation. Both, the proband and his son, control their glycemic level with nutritional diet.

TABLE 2 | Variants identified in the Brazilian sample described by our group.

Patient	Gene	GRCh38 location	Exon	RefSeq Gene position	Variant cDNA level	Variant protein level	Reference
P53	*GCK*	7:44153403	2	g.49768C>T	c.106C>T	p.(Arg36Trp)	(33)
P67	*GCK*	7:44153394	2	g.49777_49779del	c.115_117delAAG	p.(Lys39del)	(34)
P75	*GCK*	7:44153381	2	g.49790G>A	c.128G>A	p.(Arg43His)	(35)
P50	*GCK*	7:44153379	2	g.49792G>A	c.130G>A	p.(Gly44Ser)	(36)
P46	*GCK*	7:44152291	3	g.50880A>G	c.343A>G	p.(Met115Val)	Novel
P48	*GCK*	7:44149986	5	g.53185G>A	c.562G>A	p.(Ala188Thr)	(37)
P59	*GCK*	7:44149813	6	g.53358C>G	c.626C>G	p.(Thr209Arg)	(38)
P79	*GCK*	7:44149778	6	g.53393G>A	c.661G>A	p.(Glu221Lys)	(39)
P68	*GCK*	7:44145674	9	g.57497C>T	c.1076C>T	p.(Pro359Leu)	(40)
P55	*GCK*	7:44145666	9	g.57515_57518C>TinsGCGA	c.1094_1095insGCGA	p.(Asp365GlufsTer95)	Novel
P45, P58, P63	*GCK*	7:44145266	10	g.57905T>A	c.1268T>A	p.(Phe423Tyr)	(41)
P52	*HNF1A*	12:120988993	2	g.15248T>C	c.489C>G	p.(Tyr163Ter)	Novel
P44, P70	*HNF1A*	12:120994261	4	g.20516C>T	c.811C>T	p.(Arg271Trp)	(42)
P56	*HNF1A*	12:120996571	6	g.22826_22827insC	c.1136_1137insC	p.(Val380CysfsTer39)	Novel
P23	*HNF4A*	20:44413795	4	g.62995C>T	c.487C>T	p.(Arg163Ter)	(27)
P65	*HNF1B*	17:37731814	4	g.18293C>T	c.826C>T	p.(Arg276Ter)	(30)
P26	*MT-TL1*	m.3243A>G	-	-	-	-	(43)

Ensembl HGVS: GCK: ENSG00000106633.17, ENST00000403799.8, NM_000162.5, NP_000153.1, NG_008847.2; HNF1A: ENSG00000135100, ENST00000257555.11, NG_011731.2, NM_000545.8, NP_000536.5; HNF4A: ENSG00000101076, ENST00000316099.9, NG_009818.1, NM_000457.5, NP_000448.3; HNF1B: ENSG00000275410, ENST00000617811.5, NG_013019.2, NM_000458.4, NP_000449.1; MT-TL1: NC_012920, gi:251831106, AC_000021.2.

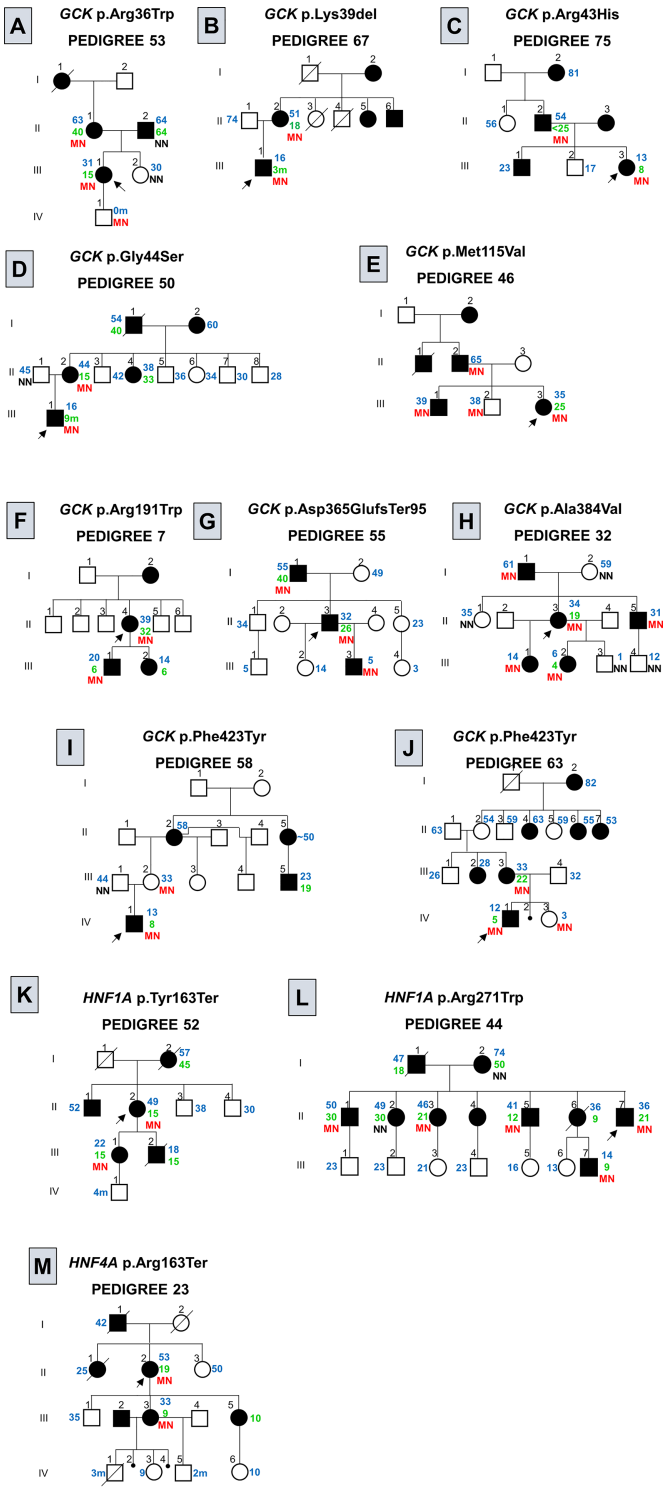

FIGURE 2 | Pedigree of families with variants in genes associated to monogenic diabetes. Filled black symbols, grey symbols and empty symbols represent diabetic patients, impaired tolerance glucose patients and healthy individuals, respectively. Small black circles represent miscarriage [**(J)**, individual IV-2; **(M)**, individuals IV-2 and IV-4]. The present age of the individuals are show in blue and age at diagnosis in green, both are represent in years or months (m) when the age is followed by the **(M)**. Genotypes are expressed by homozygous normal allele (NN) and heterozygous mutated allele (MN) in red. Oblique lines through symbols represent deceased individuals. An arrow indicates the index case. In the pedigree 75 **(C)** < 25 indicates that the AAD was prior to the AAD usually observed for clinical criteria for MODY. In the pedigree 58 **(I)** the age of the individual II-5 was informed to be approximately (~) 50 years old. In the pedigree 23 **(M)** the family reported that the subject III-2 was diagnosed with MODY, although we are not able to confirm this information.

HNF1A-MODY (OMIM # 600496)

Among the 16 patients screened for *HNF1A*, four presented variants, one man and three women. The screening of *HNF1A* revealed two novel variants, one *frameshift*, p.(Val380CysfsTer39) (c.1136_1137insC), and one *nonsense*, p.(Tyr163Ter) (c.489C>G). They were absent in gnomAD and ABraOM population databases. The p.(Val380CysfsTer39) *frameshift* variant was found in a patient (P56) diagnosed at 35 years, with a BMI at diagnostic of 28.2 kg/m². At the time of this study, at the age of 36 years (BMI: 25.3 kg/m²), she showed a FPG of 133 mg/dL and HbA1c of 6.9%, (TSH 0.73 mIU/L; Ft4 of 1.4 ng/dL). She has been treated with alogliptin (25 mg/day). She reported eight family members with DM: her father and her mother (AAD: 30 and 50 years old, respectively), one brother (AAD: 40 years old), two sisters (AAD: 32 and 36 years old), two nieces and one nephew with AAD before the age of 25 years. The family members were not available to participate in our study. The novel *nonsense* p.(Tyr163Ter) variant was observed segregating from the patient P52 (**Figure 2K**; individual II-2) to her daughter (**Figure 2K**; individual III-1). The patient AAD was 15 years old. She presented polyuria, polydipsia and weight loss. Glyburide was initiated and she maintained good glycemic control for almost 26 years and at the age of 41 years, her treatment was switched for insulin (NPH and Regular) and Metformin XR (2000 g/day). At the time of this study, at the age of 49 years, she had a BMI of 25.8 kg/m², and HbA1c of 8.34%. She presented retinopathy and hypertension. The patient had continued the treatment with insulin (0.76 U/kg/day), and Metformin XR (2000 g/day) and gliclazide was started (60 mg/day). The patient's daughter was diagnosed at 15 years old and has been treated with gliclazide (120 mg/day) and insulin (30 U/day).

HNF4A-MODY (OMIM # 125850)

A *nonsense* variant in the exon 4 of *HNF4A*, p.(Arg163Ter) (c.487C>T) was found in a woman (P23), the AAD was 19 years in a routine exam (BMI at diagnosis: 20 kg/m²) (**Figure 2M**; individual II-2). At the age of 49 years, she presented a FPG of 294 mg/dL, managed with OAD (Glimepiride 4 mg/day) and, at the age of 53 years, she was initiated on insulin therapy. The variant segregated to her daughter (**Figure 2M**; individual III-3), with AAD of 9 years old, and FPG of 125 mg/dL. The proband's daughter has 24 years of diagnosis and presents polyneuropathy, renal insufficiency and retinopathy, and has been treated with insulin therapy (10 U/day) with poor glycemic control. The proband's daughter gave birth to a baby (**Figure 2M**; individual IV-1) with congenital heart malformation who died with three months of life. Later she also had two miscarriages (**Figure 2M**; individuals IV-2 and IV-4) and two children (**Figure 2M**; individuals IV-3 and IV-5). Her son (**Figure 2M**; individual IV-5) was born with birth weight of 1.400 g and breathing problems. The children and their fathers were not available for testing. The proband's younger daughter (**Figure 2M**; individual III-5) also presents DM, diagnosed at the age of 10 years old. However, she was not available for test.

HNF1B-MODY (OMIM # 137920)

The screening of the entire coding region of *HNF1B* showed a *nonsense* variant in the exon 4, p.(Arg276Ter) (c.826C>T). The patient (P65) is a woman of 19 years old, clinically diagnosed with T1DM at 14 years old with symptoms of decompensated diabetes (at diagnosis: FPG > 500 mg/dL; BMI 23.6 kg/m²). At the moment of this study, she presented a BMI of 21.9 kg/m², a HbA1c of 12.1%, and she was on insulin therapy (1.7 U/kg/day). The patient was initiated on insulin therapy since her diagnosis and presents no complications of DM; she reports nephrolithiasis. Furthermore, it was informed that her father, uncle and grandfather had DM, and both her uncle and grandfather deceased in young age from DM complications.

MT-TL1 (OMIM * 590050)

The variant m.3243A>G in the *MT-TL1* gene was identified in a male patient (P26) with clinical diagnosis of T1DM at 28 years old (BMI at diagnosis: 21.9 kg/m²). At entry in the study, he was 30 years old, showing an HbA1c of 5.6%, FPG of 116 mg/dL (2-hour postprandial glucose: 145 mg/dL), plasmatic fasting insulin of 5.1 mcU/mL (postprandial insulin: 17.7 mcU/mL) and C-peptide of 2.1 ng/mL. He reported that his mother, father and eight siblings had DM. He did not show any sensorineural hearing loss. At the age of 37 years, he has been treated with insulin (0.12 U/kg/day) and gliclazide (60 mg/day). His family was not available for testing.

Bioinformatics Analysis

The 16 different variants identified in genomic DNA in this study were evaluated through *in silico* predictions algorithms. All ten *missense* variants were predicted as pathogenic at least for seven of the nine programs used to predict the pathogenicity. Besides, they were predicted as conserved at least for three out of four conservation predictions algorithms (**Supplemental Table S3**). According to the ACMG classification of pathogenicity, from the 16 variants in genomic DNA described by our group, ten were characterized as pathogenic and 6 variants as likely pathogenic (**Supplemental Table S4**).

DISCUSSION

In this study, patients were screened firstly for the *GCK* or *HNF1A* genes, according with their phenotypic manifestation, and then for *HNF4A*, *HNF1B*, *NEUROD1*, *KLF11*, *PAX4*, *INS*, *KCNJ11* and *MT-TL1*. We observed 13 cases of GCK-MODY and 4 cases of HNF1A-MODY, respectively. Concerning the others MODY subtypes, we found one variant in each *HNF4A*, *HNF1B*, and *MT-TL1* (**Table 1**).

Until now, variants in 14 genes have been recognized to cause monogenic diabetes type MODY, and variants on *GCK* and *HNF1A* represent the major cause worldwide. The frequency of each MODY subtype varies according to recruitment criteria and genetic background (6). In UK, variants in *HNF1A* were responsible for 52% of all MODY cases, followed by 32% of GCK-MODY (12). A retrospective database study of MODY cases reported in Brazil described GCK-MODY as the most common form, followed by HNF1A-MODY (13). Depending on the genetic cause, each MODY subtype may present a different clinical profile, with variable age at onset, treatment response,

and with some subtypes having a higher risk of long-term complications of DM, and extra pancreatic manifestations (14).

In our GCK-MODY cohort, the age at diagnosis ranged from 9 months to 26 years (**Supplemental Table S1**) and the majority of the patients were diagnosed in routine exams. This findings was expected since the diagnosis is usually incidental and at any age (15). Among our 13 GCK-MODY patients, four were diagnosed in their childhood as having T1DM, three of them were treated with insulin therapy. Out of these 13, four patients were being treated with OAD at the moment of the study. Misdiagnosis of GCK-MODY patients or misclassification as T1DM are frequent (16), which reinforce the importance to screen patients with clinical phenotype for GCK-MODY. Therefore, after our molecular diagnostic analysis, six patients stopped allpharmacological treatment. Typically, patients with GCK-MODY with less than 40 years old show an HbA1c ranging from 5.6 to 7.3% and a FPG range of 5.6 to 8.0 mmol/L (17). Our patients had the HbA1c (6-7.2%) and FPG (6-7.7 mmol/L) within these ranges.

The screening of the coding region of *GCK* revealed 11 different variants; the likely pathogenic missense variants p.(Arg36Trp), p.(Ala188Thr), p.(Glu221Lys), and p.(Phe423Tyr) were previously described by other groups in Brazilian probands (13, 18–20). The p.(Phe423Tyr) was the only one to appear in more than one patient, it was found in three unrelated probands (P45, P58 and P63). To the best of our knowledge, this is the first report of the *GCK* p.(Arg43His), p.(Gly44Ser), p.(Thr209Arg), and p.(Pro359Leu) *missense* variants in Brazilian patients. We observed the first two segregating in their families (**Figures 2C, D**). Unfortunately, both P59 (p.(Thr209Arg)) and P68 (p.(Pro359Leu)) proband's families were not available for analysis. Among the observed variants in the *GCK*, two were novel, the *missense* p.(Met115Val) (c.343A>G) and the *frameshift* p.(Asp365GlufsTer95) (c.1094_1095insGCGA). The p.(Met115Val) is registered in dbSNP under the number rs771677681 and is found in gnomAD with an allele frequency of 0.00001193; however, this variant was not reported associated to diabetes in the databases. This variant was observed in the proband P46 (**Figure 2E** individual III-3) and in her two older brothers, inherited from their father with diabetes; the proband's middle brother did not report hyperglycemia, and his blood tests were not available. The p.(Asp365GlufsTer95) was observed segregating with DM through three generations (**Figure 2G**).

Variants in the *HNF1A* gene usually have high penetrance and patients are usually diagnosed between the ages of nine to 40 years (21, 22). The age at diagnosis of our patients ranged from 14 to 35 years old (**Table 1**). Patients with hyperglycemia caused by *HNF1A* variant can remain sulfonylurea responsive for many years (23). Patients P44 and P56 were switched from insulin to OAD, after 15 years and 1 year since their diagnosis, respectively. However, some patients require insulin treatment, as is the case for patient P52.

The screening of *HNF1A* showed three different variants;. The *HNF1A* p.(Arg271Trp) (c.811C>T), found in two unrelated patients (P44 and P70) segregates among several individuals with DM from the P44 proband's family (**Figure 2L**). The P70 proband's family was not available. This variant seems to decrease the HNF1A affinity and binding to DNA (24, 25). We also found a novel *nonsense* variant p.(Tyr163Ter) (c.489C>G), segregating from the patient P52 to her daughter with diabetes (**Figure 2K**), both diagnosed at the age of 15 years old. Additionally, we found a novel *frameshift* variant p.(Val380CysfsTer39) (c.1136_1137insC) in the patient P56; the P56 patient' family was not available. According to ACMG guidelines the HNF1A p.(Tyr163Ter) and p.(Val380CysfsTer39) are classified as pathogenic and p.(Arg271Trp) as likely pathogenic, supporting the evidence of these variants as the cause of diabetes in these families.

Variants in the *HNF4A* gene seem to be a rare cause of monogenic diabetes in Brazil (26). The *nonsense* variant p.(Arg163Ter) was described by Lindner and coworkers (1997) as the second variant found in the *HNF4A* associated to MODY in a family from German ancestry (27). The patients from the reported family were treated by OAD or insulin, and patients with longer time of the disease showed retinopathy and peripheral polyneuropathy (27). This variant was found in our study in the proband P23 (**Figure 2M**; individual II-2), segregating to her daughter (**Figure 2M**; individual III-3). The HNF4A works as a heterodimer and the premature stop codon results in a truncated protein that loses the transactivation domain (27, 28) and the ability to form heterodimers (29). Laine and coworkers (2000) observed the same variant with a dominant-negative effect (28). Lindner and coworkers (1997) reported patients with the same variant with coronary heart disease and no nephropathy (27). The family members in our study reported renal insufficiency and no heart disease. The proband's daughter (**Figure 2M**; individual III-3) presented peripheral polyneuropathy.

The *nonsense HNF1B* p.(Arg276Ter) was described in two Japanese patients with small kidneys and multiple renal cysts (30, 31). More information from this patients and renal ultrasound was not available, however a review of her medical chart revealed nephrolithiasis.

In this study, we also described one male patient carrying the *MT-TL1* m.3243A>G variant. The patient did not present any other clinical manifestations of MIDD, as sensorineural hearing loss. It has been described a wide spectrum of clinical variability for *MT-TL1* m.3243A>G variant, ranging from asymptomatic carriers to lethal multisystem disorders (32). These findings highlight the importance of screening this genetic variant in patients with familiar recurrence of diabetes despite the lack of other clinical characteristics related to MIDD and MELAS syndrome.

This study has some limitations worth noting: 1) small sample size; 2) DNA samples from relatives were extracted from saliva, different from the DNA source of the patients (blood) and it may cause false negatives due to somatic mosaicism; 3) segregation analysis of *HNF1A* p.(Val380CysfsTer39) and *GCK* p.(Met115Val) were not possible in unaffected relatives to ensure absence of variant and were also not possible in some of the families; 4) by using sanger sequencing instead of NGS we were unable to test other rare genes associated to monogenic diabetes commonly present in NGS panels and we cannot rule out the presence of large duplications and deletions; 5) not all rare forms of diabetes were included here, e.g. neonatal diabetes;

Here we highlight the importance of screening for monogenic forms of diabetes in patients with familial history of diabetes. An

accurate diagnosis with molecular confirmation of monogenic diabetes can improve the choice for a better therapeutic management of patients and their families.

DATA AVAILABILITY STATEMENT

The datasets presented in this study can be found in online repositories. The names of the repository/repositories and accession number(s) can be found in the article/**Supplementary Material**.

ETHICS STATEMENT

The studies involving human participants were reviewed and approved by The Ethics and Research Committee of the Clementino Fraga Filho University Hospital (CAAE n° 04232512.4.0000.5257) and by the State Institute for Diabetes and Endocrinology Luiz Capriglione (CAAE n° 04232512.4.3001.5266). Written informed consent to participate in this study was provided by the participants' legal guardian/next of kin.

AUTHOR CONTRIBUTIONS

GA: Conceptualization, methodology, validation, formal analysis, investigation, writing- original draft, and project administration. RT: conceptualization, methodology, resources, writing - review and editing, supervision, and project administration. AF: Resources, writing - review and editing. JA: Methodology and investigation; RBS: Software, formal analysis, and writing - review and editing. CS: Investigation and writing - review and editing. AC: Writing - review and editing. PC: Resources, writing - review and editing, funding acquisition, and supervision. MR: Resources, writing - review and editing, funding acquisition, and supervision. LZ: Resources, writing - review and editing, funding acquisition. VZ: Resources, writing - review and editing, and funding acquisition. MCJ: Resources, writing - review and editing, supervision, funding acquisition, and project administration. All authors contributed to the article and approved the submitted version.

ACKNOWLEDGMENTS

Authors are grateful to patients and their families and to Network of Technological Platforms from Oswaldo Cruz Foundation. The National Council for Scientific and Technological Development (CNPq), Coordination for the Improvement of Higher Education Personnel (CAPES), Carlos Chagas Filho Foundation for Research Support of the State of Rio de Janeiro (FAPERJ) and Oswaldo Cruz Institute (IOC) supported this work.

SUPPLEMENTARY MATERIAL

The Supplementary Material for this article can be found online at: https://www.frontiersin.org/articles/10.3389/fendo.2022.827325/full#supplementary-material

Supplementary Figure 1 | Electropherograms of variants probably pathogenic found by Sanger sequencing among Brazilian patients with suspicious of monogenic diabetes. Novel variants are showed in blue. An arrow indicates the position of the variant in the electropherogram.

REFERENCES

1. Shepherd M, Shields B, Hammersley S, Hudson M, McDonald TJ, Colclough K, et al. Systematic Population Screening, Using Biomarkers and Genetic Testing, Identifies 2.5% of the U.KPediatric Diabetes Population With Monogenic Diabetes. *Diabetes Care* (2016) 39(11):1879–88. doi: 10.2337/dc16-0645
2. Bansal V, Gassenhuber J, Phillips T, Oliveira G, Harbaugh R, Villarasa N, et al. Spectrum of Mutations in Monogenic Diabetes Genes Identified From High-Throughput DNA Sequencing of 6888 Individuals. *BMC Med* (2017) 15 (1):1–14. doi: 10.1186/s12916-017-0977-3
3. De Franco E, Flanagan SE, Houghton JAL, Allen HL, MacKay DJG, Temple IK, et al. The Effect of Early, Comprehensive Genomic Testing on Clinical Care in Neonatal Diabetes: An International Cohort Study. *Lancet* (2015) 386 (9997):957–63. doi: 10.1016/S0140-6736(15)60098-8
4. Yeung RO, Al Jundi M, Gubbi S, Bompu ME, Sirrs S, Tarnopolsky M, et al. Management of Mitochondrial Diabetes in the Era of Novel Therapies. *J Diabetes Complic* (2021) 35(1):107584.doi: 10.1016/j.jdiacomp.2020.107584
5. Tattersall RB. Mild Familial Diabetes With Dominant Inheritance. *Quartely J Med* (1974) 43(2):339–57. doi: 10.1136/jnnp-2012-303528
6. Firdous P, Nissar K, Ali S, Ganai BA, Shabir U, Hassan T, et al. Genetic Testing of Maturity-Onset Diabetes of the Young Current Status and Future Perspectives. *Front Endocrinol (Lausanne)* (2018) 9:253/full(MAY). doi: 10.3389/fendo.2018.00253/full
7. Zhang H, Colclough K, Gloyn AL, Pollin TI. Monogenic Diabetes: A Gateway to Precision Medicine in Diabetes. *J Clin Invest* (2021) 131(3):1–14. doi: 10.1172/JCI142244
8. Tarantino RM, Abreu G de M, de Foncesca ACP, Kupfer R, Pereira M de FC, Campos M, et al. MODY Probability Calculator for GCK and HNF1A Screening in a Multiethnic Background Population. *Arch Endocrinol Metab* (2019) 1(8):1–7. doi: 10.20945/2359-3997000000173
9. Aidar M, Line SRP. A Simple and Cost-Effective Protocol for DNA Isolation From Buccal Epithelial Cells. *Braz Dent J* (2007) 18(2):148–52. doi: 10.1007/BF01811861
10. Naslavsky MS, Yamamoto GL, de Almeida TF, Ezquina SAM, Sunaga DY, Pho N, et al. Exomic Variants of an Elderly Cohort of Brazilians in the ABraOM Database. *Hum Mutat* (2017) 38(7):751–63. doi: 10.1002/humu.23220
11. Kopanos C, Tsiolkas V, Kouris A, Chapple CE, Albarca Aguilera M, Meyer R, et al. VarSome: The Human Genomic Variant Search Engine. Wren J, editor. *Bioinformatics* (2019) 35(11):1978–80. doi: 10.1093/bioinformatics/bty897
12. Shields BM, Hicks S, Shepherd MH, Colclough K, Hattersley AT, Ellard S. Maturity-Onset Diabetes of the Young (MODY): How Many Cases are We Missing? *Diabetologia* (2010) 53(12):2504–8. doi: 10.1007/s00125-010-1799-4
13. Giuffrida FMA, Moises RS, Weinert LS, Calliari LE, Della MT, Dotto RP, et al. Maturity-Onset Diabetes of the Young (MODY) in Brazil: Establishment of a National Registry and Appraisal of Available Genetic and Clinical Data. *Diabetes Res Clin Pract* (2017) 123:134–42. doi: 10.1016/j.diabres.2016.10.017
14. Vaxillaire M, Froguel P. Monogenic Diabetes: Implementation of Translational Genomic Research Towards Precision Medicine. *J Diabetes* (2016) 8(6):782–95. doi: 10.1111/1753-0407.12446

15. Chakera AJ, Steele AM, Gloyn AL, Shepherd MH, Shields B, Ellard S, et al. Recognition and Management of Individuals With Hyperglycemia Because of a Heterozygous Glucokinase Mutation. *Diabetes Care* (2015) 38(7):1383–92. doi: 10.2337/dc14-2769
16. Petruzelkova L, Dusatkova P, Cinek O, Sumnik Z, Pruhova S, Hradsky O, et al. Substantial Proportion of MODY Among Multiplex Families Participating in a Type 1 Diabetes Prediction Programme. *Diabetes Med* (2016) 33(12):1712–6. doi: 10.1111/dme.13043
17. Steele AM, Wensley KJ, Ellard S, Murphy R, Shepherd M, Colclough K, et al. Use of HbA1c in the Identification of Patients With Hyperglycaemia Caused by a Glucokinase Mutation: Observational Case Control Studies. *PloS One* (2013) 8(6):e65326. doi: 10.1371/journal.pone.0065326
18. Caetano LA, Jorge AAL, Malaquias AC, Trarbach EB, Queiroz MS, Nery M, et al. Incidental Mild Hyoerglycemia in Children : Two MODY 2 Families Identified in Brazilian Subjects. *Arq Bras Endocrinol Metabol* (2012) 56 (8):519–24. doi: 10.1590/S0004-27302012000800010
19. Giuffrida FMA, Calliari LE, Della MT, JG F, Saddi-Rosa P, Kunii IS, et al. A Novel Glucokinase Deletion (P.Lys32del) and Five Previously Described Mutations Co-Segregate With the Phenotype of Mild Familial Hyperglycaemia (MODY2) in Brazilian Families. *Diabetes Res Clin Pract* (2013) 100(2):e42–5. doi: 10.1016/j.diabres.2013.01.029
20. Santana LS, Caetano LA, Costa-Riquetto AD, Quedas EPS, Nery M, Collett-Solberg P, et al. Clinical Application of ACMG-AMP Guidelines in HNF1A and GCK Variants in a Cohort of MODY Families. *Clin Genet* (2017) 92 (4):388–96. doi: 10.1111/cge.12988
21. Yorifuji T, Fujimaru R, Hosokawa Y, Tamagawa N, Shiozaki M, Aizu K, et al. Comprehensive Molecular Analysis of Japanese Patients With Pediatric-Onset MODY-Type Diabetes Mellitus. *Pediatr Diabetes* (2012) 13(1):26–32. doi: 10.1111/j.1399-5448.2011.00827.x
22. Frayling TM, Bulman M, Ellard S, Appeton M, Dronsfield MJ, Mackie ADR, et al. Mutations in Hepatocyte Nuclear Factor 1beta are Not a Common Cause of Maturity-Onset Diabetes of the Young in the U.K. *Diabetes* (1998) 47 (7):1152–4. doi: 10.2337/diabetes.47.7.1152
23. Brunerova L, Rahelić D, Ceriello A, Broz J. Use of Oral Antidiabetic Drugs in the Treatment of Maturity-Onset Diabetes of the Young: A Mini Review. *Diabetes Metab Res Rev* (2018) 34(1):e2940. doi: 10.1002/dmrr.2940
24. Galan M, Garcia-Herrero C-M, Azriel S, Gargallo M, Durán M, Gorgojo J-J, et al. Differential Effects of HNF-1α Mutations Associated With Familial Young-Onset Diabetes on Target Gene Regulation. *Mol Med* (2011) 17(3–4):256–65. doi: 10.2119/molmed.2010.00097
25. Bjørkhaug L, Sagen JV, Thorsby P, Søvik O, Molven A, Njølstad PR. Hepatocyte Nuclear Factor-1α Gene Mutations and Diabetes in Norway. *J Clin Endocrinol Metab* (2003) 88(2):920–31. doi: 10.1210/jc.2002-020945
26. Santana LS, Caetano LA, Costa-Riquetto AD, Franco PC, Dotto RP, Reis AF, et al. Targeted Sequencing Identifies Novel Variants in Common and Rare MODY Genes. *Mol Genet Genomic Med* (2019) 7(12):1–17. doi: 10.1002/mgg3.962
27. Lindner T, Gragnoli C, Furuta H, Cockburn BN, Petzold C, Rietzsch H, et al. Hepatic Function in a Family With a Nonsense Mutation (R154X) in the Hepatocyte Nuclear Factor-4alpha/MODY1 Gene. *J Clin Invest* (1997) 100 (6):1400–5. doi: 10.1172/JCI119660
28. Laine B, Eeckhoute J, Suaud L, Briche I, Furuta H, Bell GI, et al. Functional Properties of the R154X HNF-4α Protein Generated by a Mutation Associated With Maturity-Onset Diabetes of the Young, Type 1. *FEBS Lett* (2000) 479(1–2):41–5. doi: 10.1016/S0014-5793(00)01864-0
29. Ogata M, Awaji T, Iwasaki N, Fujimaki R, Takizawa M, Maruyama K, et al. Localization of Hepatocyte Nuclear Factor-4α in the Nucleolus and Nucleus is Regulated by its C-Terminus. *J Diabetes Investig* (2012) 3(5):449–56. doi: 10.1111/j.2040-1124.2012.00210.x
30. Furuta H, Furuta M, Sanke T, Ekawa K, Hanabusa T, Nishi M, et al. Nonsense and Missense Mutations in the Human Hepatocyte Nuclear Factor-1β Gene (TCF2) and Their Relation to Type 2 Diabetes in Japanese. *J Clin Endocrinol Metab* (2002) 87(8):3859–63. doi: 10.1210/jcem.87.8.8776
31. Fujimoto K, Sasaki T, Hiki Y, Nemoto M, Utsunomiya Y, Yokoo T, et al. *In Vitro* and Pathological Investigations of MODY5 With the R276X-Hnf1β (TCF2) Mutation. *Endocr J* (2007) 54(5):757–64. doi: 10.1507/endocrj.K07-051
32. Mancuso M, Orsucci D, Angelini C, Bertini E, Carelli V, Comi Pietro G, et al. The M.3243A>G Mitochondrial DNA Mutation and Related Phenotypes. A Matter of Gender? *J Neurol* (2014) 261(3):504–10. doi: 10.1007/s00415-013-7225-3
33. Hager J, Blanché H, Sun F, Vaxillaire NVM, Poller W, Cohen D, et al. Six Mutations in the Glucokinase Gene Identified in MODY by Using a Nonradioactive Sensitive Screening Technique. *Diabetes* (1994) 43(5):730–3. doi: 10.2337/diab.43.5.730
34. Zubkova NA, Gioeva OA, Tikhonovich YV, Petrov VM, Vasilyev EV, Timofeev AV, et al. Clinical and Molecular Genetic Characteristics of MODY1—3 Cases in the Russian Federation as Shown by NGS. *Probl Endocrinol* (2018) 63(6):369–78. doi: 10.14341/probl2017636369-378
35. Ziemssen F, Bellanné-Chantelot C, Osterhoff M, Schatz H, Pfeiffer AFH, Lindner T, et al. Molecular Genetics of MODY in Germany. Diabetologia 42: 121–123. *Diabetologia* (2002) 45(2):286–7. doi: 10.1007/s00125-001-0738-9
36. Gragnoli C, Cockburn BN, Chiaramonte F, Gorini A, Marietti G, Marozzi G, et al. Early-Onset Type II Diabetes Mellitus in Italian Families Due to Mutations in the Genes Encoding Hepatic Nuclear Factor 1α and Glucokinase. *Diabetologia* (2001) 44(10):1326–9. doi: 10.1007/s001250100644
37. Takeda J, Gidh-jain M, Xu LZ, Froguel P, Velho G, Vaxillaire M, et al. Structure/Function Studies of Human Beta-Cell Glucokinase. Enzymatic Properties of a Sequence Polymorphism, Mutations Associated With Diabetes, and Other Site-Directed Mutants. *J Biol Chem* (1993) 268 (20):15200–4. doi: 10.1016/S0021-9258(18)82456-5
38. Borowiec M, Fendler W, Antosik K, Baranowska A, Gnys P, Zmyslowska A, et al. Doubling the Referral Rate of Monogenic Diabetes Through a Nationwide Information Campaign - Update on Glucokinase Gene Mutations in a Polish Cohort. *Clin Genet* (2012) 82(6):587–90. doi: 10.1111/j.1399-0004.2011.01803.x
39. Guazzini B, Gaffi D, Mainieri D, Multari G, Cordera R, Bertolini S, et al. Three Novel Missense Mutations in the Glucokinase Gene (G80S; E221K; G227C) in Italian Subjects With Maturity-Onset Diabetes of the Young (MODY). *Hum Mutat* (1998) 12(2):136–6. doi: 10.1002/%28SICI%291098-1004%281998%2912%3A2%3C136%3A%3AAID-HUMU13%3E3.3.CO%3B2-M
40. Garin I, Rica I, Estalella I, Oyarzabal M, Rodríguez-Rigual M, Pedro JIS, et al. Haploinsufficiency at GCK Gene is Not a Frequent Event in MODY2 Patients. *Clin Endocrinol (Oxf)* (2008) 68(6):873–8. doi: 10.1111/j.1365-2265.2008.03214.x
41. Almeida C, Silva SR, Garcia E, Leite AL, Teles A, Campos RA. A Novel Genetic Mutation in a Portuguese Family With GCK-MODY. *J Pediatr Endocrinol Metab* (2014) 27(1–2):129–33. doi: 10.1515/jpem-2013-0056
42. Chèvre J-C, Hani EH, Boutin P, Vaxillaire M, Blanché H, Vionnet N, et al. Mutation Screening in 18 Caucasian Families Suggest the Existence of Other MODY Genes. *Diabetologia* (1998) 41(9):1017–23. doi: 10.1007/s001250051025
43. Goto Y, Nonaka I, Horai S. A Mutation in the Trnaleu(UUR) Gene Associated With the MELAS Subgroup of Mitochondrial Encephalomyopathies. *Nature* (1990) 348(6302):651–3. doi: 10.1038/348651a0

Conflict of Interest: The authors declare that the research was conducted in the absence of any commercial or financial relationships that could be construed as a potential conflict of interest.

frontiers | Frontiers in Endocrinology

ORIGINAL RESEARCH
published: 20 June 2022
doi: 10.3389/fendo.2022.900489

Clinical Characteristics of Patients With *HNF1-alpha* MODY: A Literature Review and Retrospective Chart Review

Qinying Zhao[1†], *Li Ding*[1†], *Ying Yang*[1], *Jinhong Sun*[1], *Min Wang*[1], *Xin Li*[1*] and *Ming Liu*[1,2,3*]

[1] Department of Endocrinology and Metabolism, Tianjin Medical University General Hospital, Tianjin, China, [2] National Health Commission (NHC) Key Laboratory of Hormones and Development, Tianjin Medical University, Tianjin, China, [3] Tianjin Institute of Endocrinology, Tianjin, China

OPEN ACCESS

Edited by:
Åke Sjöholm,
Gävle Hospital, Sweden

Reviewed by:
Stefano Passanisi,
University of Messina, Italy
Mariëlle Schroijen,
Leiden University Medical Center, Netherlands

***Correspondence:**
Xin Li
lixin920616@163.com
Ming Liu
mingliu@tmu.edu.cn

[†]These authors have contributed equally to this work and share first authorship

Specialty section:
This article was submitted to Diabetes: Molecular Mechanisms, a section of the journal Frontiers in Endocrinology

Received: 20 March 2022
Accepted: 02 May 2022
Published: 20 June 2022

Citation:
Zhao Q, Ding L, Yang Y, Sun J, Wang M, Li X and Liu M (2022) Clinical Characteristics of Patients With HNF1-alpha MODY: A Literature Review and Retrospective Chart Review. Front. Endocrinol. 13:900489. doi: 10.3389/fendo.2022.900489

The clinical manifestation of hepatocyte nuclear factor-1-alpha (*HNF1-alpha*) maturity-onset diabetes of the young (MODY) is highly variable. This study aims to investigate the clinical characteristics of patients with *HNF1-alpha* MODY in general, by geographical regions (Asian or non-Asian), *HNF1-alpha* mutations, and islet autoantibody status. A literature review and a chart review of patients with *HNF1-alpha* MODY were performed. The means and proportions from studies were pooled using the inverse variance method for pooling, and subgroup analyses were performed. A total of 109 studies involving 1,325 patients [41.5%, 95% confidence interval (CI): 35.2, 48.1; male] were identified. The mean age of diagnosis was 20.3 years (95% CI: 18.3–22.2), and the mean glycated hemoglobin was 7.3% (95% CI: 7.2–7.5). In comparison, Asian patients exhibited significantly higher HbA1c ($p = 0.007$) and 2-h post-load C-peptide ($p = 0.012$) levels and lower levels of triglyceride (TG) ($p < 0.001$), total cholesterol (TC) ($p < 0.001$), and high-density lipoprotein cholesterol (HDL-c) ($p < 0.001$) and less often had macrovascular complications ($p = 0.014$). The age of diagnosis was oldest in patients with mutations in the transactivation domain ($p < 0.001$). The levels of 2-h post-load C-peptide ($p < 0.001$), TG ($p = 0.007$), TC ($p = 0.017$), and HDL-c ($p = 0.001$) were highest and the prevalence of diabetic neuropathy was lowest ($p = 0.024$) in patients with DNA-binding domain mutations. The fasting ($p = 0.004$) and 2-h post-load glucose ($p = 0.003$) levels and the prevalence of diabetic neuropathy ($p = 0.010$) were higher among patients with positive islet autoantibodies. The study demonstrated that the clinical manifestations of *HNF1-alpha* MODY differed by geographical regions, *HNF1-alpha* mutations, and islet autoantibody status.

Keywords: *HNF1-alpha* MODY, diabetes, *HNF1-alpha* mutations, pancreatic islet autoantibody, diabetic complication

INTRODUCTION

Maturity-onset diabetes of the young (MODY) is a monogenic diabetes syndrome, characterized by onset before 25–35 years of age, autosomal dominant inheritance, negative islet autoimmunity, and lack of the typical features of type 2 diabetes (T2DM). Mutation in the hepatocyte nuclear factor-1-alpha (*HNF1-alpha*) gene is one of the most common causes of MODY (1–5). The *HNF1-alpha* MODY phenotype is characterized by early-onset diabetes and progressive β-cell dysfunction with defective insulin secretion (6). *HNF1-alpha* MODY is caused by the mutation of the *HNF1-alpha* gene, consisting of dimerization domain, DNA-binding domain, and transactivation domain, which regulates multiple genes involved in glucose metabolism in the pancreas, kidney, and liver (7, 8). Though the clinical manifestations of *HNF1-alpha* MODY overlap with type 1 diabetes mellitus (T1DM) and T2DM, patients with *HNF1-alpha* MODY are generally more sensitive to sulfonylureas (9, 10). Thus, the accurate identification of *HNF1-alpha* MODY is of utmost importance for the optimal management and prevention of diabetes-associated micro- and macrovascular complications, which are not infrequent in *HNF1-alpha* MODY.

About 1–5% diabetes and 0.83–6.5% of diabetic children and adolescents were identified as MODY (2, 11–16). The prevalence of *HNF1-alpha* MODY varies among nations and healthcare systems. In a study involving 101 families (95% Caucasian in the United Kingdom), Frayling *et al.* found that 63% of patients with MODY fit the *HNF1-alpha* MODY criteria (17). In a retrospective observational study involving 565 children and adolescents with newly diagnosed diabetes in Southern Italy, *HNF1-alpha* MODY accounted for 13.5% of MODY cases (2). The detection rate of *HNF1-alpha* MODY was 13.9% in Japanese (18) and 15.79% in Chinese pedigree MODY genetic screening studies (19). Previous studies showed that genetic modifiers and *in utero* exposure to hyperglycemia led to a variability in the clinical presentation of *HNF1-alpha* MODY (20, 21). It is unclear if the genetic and environmental factors of different geographic regions may result in different phenotypes of patients with *HNF1-alpha* MODY.

Severe hyperglycemia usually occurs after puberty in patients with *HNF1-alpha* MODY, which may lead to the misdiagnosis of T1DM. Genetic testing that is required for the diagnosis of *HNF1-alpha* MODY is usually sought only in individuals negative for islet autoantibodies, including glutamic acid decarboxylase antibody (GAD), protein tyrosine phosphatase antibody (IA2), and islet cell antibody (ICA) (22), and individuals originally considered as T1DM but who were negative for islet autoantibodies (12). However, some studies reported that a proportion of patients with *HNF1-alpha* MODY were positive for islet autoantibodies (15, 23–30). There is currently a lack of research on whether the clinical phenotype of *HNF1-alpha* MODY differs by geographic regions, *HNF1-alpha* mutations, and islet autoantibody status. In this study, we analyzed the clinical characteristics of patients with *HNF1-alpha* MODY in general and by geographical regions, *HNF1-alpha* mutations, and islet autoantibody status through literature and chart review.

MATERIALS AND METHODS

Study Selection

A literature search was conducted through Pubmed, Web of Science, Embase, Wanfang, and the China National Knowledge Infrastructure Databases from inception of the database to December 2021 using medical subject headings or Emtree thesaurus as well the following key terms: "Maturity-Onset Diabetes of the Young, Type 3", "MODY3", "MODY, Type 3", "hepatic nuclear factor 1 alpha", "*HNF1A*", "*HNF1-alpha*", "nuclear protein LF-B1", "LF-B1 transcription factor, human", and "HNF1 homeobox A protein, human". A detailed search strategy for database is listed in the **Supplementary Material**. The search results were imported into endnote software where duplicated results were identified based on the title, journal, publication year, and authors and were removed automatically. The remaining references were screened through the title and abstract for relevance to this study. Studies dedicated to animal or *in vitro* experiments were excluded. The relevant studies identified, *i.e.*, studies reporting the clinical characteristics of patients with *HNF1-alpha* MODY, were subjected to full-text review for eligibility. The eligible studies met the following criteria: (1) the diagnosis of *HNF1-alpha* MODY was confirmed by genetic testing and (2) individual-level or aggregate data were reported for at least one of the following: fasting plasma glucose (FPG), 2-h post-load glucose (2h PG) in an oral glucose tolerance test, or glycated hemoglobin (HbA1c).

Data Extraction

Clinical data, including the geographical region, gender, age of diagnosis, body mass index (BMI), familial history, HbA1c, FPG, 2h PG, fasting and 2-h post-load C-peptide, triglyceride (TG), total cholesterol (TC), high-density lipoprotein cholesterol (HDL-c), low-density lipoprotein cholesterol (LDL-c), islet autoantibody status, diabetic complications, and anti-diabetic therapies, were abstracted. Besides this, information regarding amino acid substitution, position, and type of mutations in the *HNF1-alpha* gene were abstracted. Literature search, study selection, and data extraction were conducted by two independent reviewers, and disagreement was resolved by consensus with a third reviewer.

Statistical Analysis

Statistical analysis was conducted using R, version 3.5.3 (http://www.r-project.org/). The means and percentages from case reports were calculated and pooled with aggregated data from cohort studies and case series using the inverse variance method for pooling in random effect models with the metamean and metaprop function in the meta package in R. The results were presented with means, proportions, and respective 95%

confidence intervals. A comparison among subgroups was performed. *P*-value less than 0.05 was statistically significant.

RESULTS

Among 5,970 publications identified, 1,153 articles were excluded due to duplication, and 2,660 articles were excluded due to being irrelevant after screening through the title and the abstract. After a full-text review, 109 studies involving 1,325 patients were identified (**Figure 1**). Detailed information and citations of these included studies are provided in the supplementary material (**Supplementary Table S1**).

Clinical Manifestations of *HNF1-alpha* MODY in General

A total of 1,325 patients [41.5%, 95% confidence interval (CI): 35.2, 48.1; male] with *HNF1-alpha* MODY were included in our study. The mean values of the clinical data were as follows: age, 32.6 years (95% CI: 28.5–36.7); age of diagnosis, 20.3 years (95% CI: 18.3–22.2); BMI, 23.1 kg/m^2 (95% CI: 22.3–23.9); HbA1c, 7.3% (95% CI: 7.2–7.5); and FPG, 8.1 mmol/L (95% CI: 7.6–8.5). Among the patients identified, 89.8% (95% CI: 54.1–98.5) had a family history of diabetes, 47.6% (95% CI: 30.6–65.2) had microvascular complications, 21.5% (95% CI: 14.5–30.8) had diabetic retinopathy, 16.6% (95% CI: 10.3–25.5) had diabetic kidney disease, 11.8% (95% CI: 6.2–21.2) had diabetic neuropathy, 11.1% (95% CI: 7.3–16.6) had macrovascular complications, 17.0% (95% CI: 13.2–21.6) received lifestyle management, 40.3% (95% CI: 32.4–48.6) were prescribed with oral hypoglycemic drugs, 35.5% (95% CI: 31.3–40.0) were prescribed with insulin, and 9.5% (95% CI: 5.4–16.2) were prescribed with oral hypoglycemic drugs plus insulin.

Clinical Manifestations of *HNF1-alpha* MODY by Geographical Regions

Among 109 studies identified, 37 studies involving 183 patients were from Asia, while 72 studies including 1,142 patients were from geographic regions other than Asia. Compared to non-Asian patients, BMI [20.8 kg/m^2 (95% CI: 20.3–21.3) vs. 24.1 kg/m^2 (95% CI: 23.6–24.6), $p < 0.001$], TG [1.14 mmol/L (95% CI: 0.81–1.48) vs. 2.09 mmol/L (95% CI: 1.69–2.49), $p < 0.001$], TC [4.70 mmol/L (95% CI: 4.46–4.94) vs. 5.76 mmol/L (95% CI: 5.23–6.29), $p < 0.001$], and HDL-c [1.37 mmol/L (95% CI: 1.29–1.45) vs. 1.75 mmol/L (95% CI: 1.59–1.92), $p < 0.001$] were lower in Asian patients. Their HbA1c [7.9% (95% CI: 7.5–8.4) vs. 7.3% (95% CI: 7.1–7.4), $p = 0.007$] and 2-h post-load C-peptide levels were higher [2.16 ng/ml (95% CI: 1.61–2.72) vs. 1.44 ng/ml (95% CI: 1.34–1.54), $p = 0.012$]. They less often had macrovascular complications [2.7% (95% CI: 0.7–10.0) vs. 14.3% (95% CI: 10.7–18.9), $p = 0.014$], while age, age of diagnosis, diabetes duration, gender, family history, the prevalence of microvascular complications, diabetic retinopathy, diabetic kidney disease, diabetic neuropathy, and anti-diabetic therapies did not differ by geographical regions (**Table 1**).

Clinical Manifestations of *HNF1-alpha* MODY by Mutations

Among those reporting the site and type of mutations of the *HNF1-alpha* gene, 432 patients had mutations in coding regions, consisting of 15 (3.5%) in the dimerization domain, 179 (41.4%) in the DNA-binding domain, and 238 (55.1%) in the transactivation domain (**Figure 2**). Age of diagnosis was oldest in patients with mutations in the transactivation domain [26.0 years (95% CI: 21.7–30.3) vs. 18.9 years (95% CI: 11.5–26.3) for the dimerization domain and 20.5 years (95% CI: 17.3–23.7) for the DNA-binding domain, $p < 0.001$]. The levels of 2-h post-load C-peptide [4.22 ng/ml (95% CI: 2.17–6.26) vs. 2.71 ng/ml for the dimerization domain and 1.92 ng/ml (95% CI: 1.17–2.67) for the transactivation domain, $p < 0.001$], TG [1.82 mmol/L (95% CI: 0.27–3.36) vs. 1.70 mmol/L for the dimerization domain and 1.23 mmol/L (95% CI: 0.81–1.64) for the transactivation domain, $p = 0.007$], TC [5.39 mmol/L (95% CI: 2.07–8.71) *vs*. 3.96 mmol/L for the dimerization domain and 4.54 mmol/L (95% CI: 3.59–5.49) for the transactivation domain, $p = 0.017$], and HDL-c [1.59 mmol/L (95% CI: 0.64–2.54) vs. 0.72 mmol/L for the

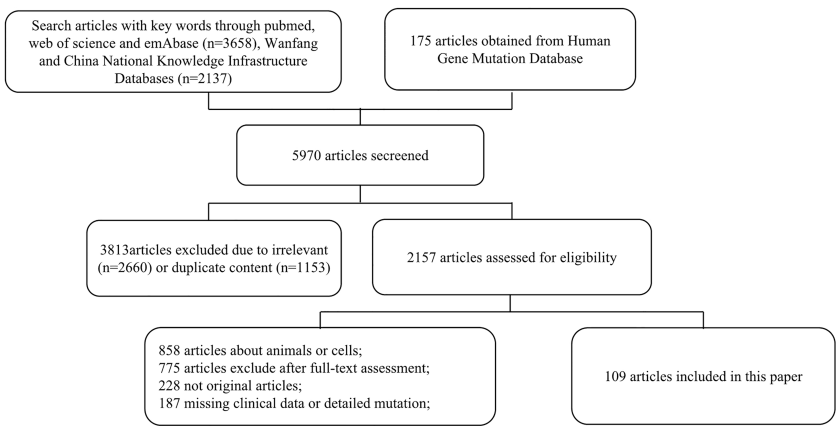

FIGURE 1 | Flow chart.

TABLE 1 | Characteristics of patients with *HNF1-alpha* MODY by geographical regions.

Subject	Total (*n* = 1,325)	Asian (*n* = 183)	Non-Asian (*n* = 1,142)	*P*-value
Age (years)	32.6 (28.5, 36.7)	29.4 (24.9, 33.9)	33.5 (28.6, 38.5)	0.229
Age of diagnosis (years)	20.3 (18.3, 22.2)	18.0 (14.8, 21.3)	20.9 (18.8, 23.0)	0.153
Duration (years)	13.1 (10.5, 15.6)	13.6 (9.3, 18.0)	13.0 (10.0, 16.0)	0.809
BMI (kg/m^2)	23.1 (22.3, 23.9)	20.8 (20.2, 21.3)	24.1 (23.6, 24.6)	<0.001*
HbA1c (%)	7.3 (7.2, 7.5)	7.9 (7.5, 8.4)	7.3 (7.1, 7.4)	0.007*
FPG (mmol/L)	8.1 (7.6, 8.5)	7.9 (7.0, 8.8)	8.1 (7.5, 8.7)	0.618
2h PG (mmol/L)	15.6 (14.8, 16.5)	16.1 (14.5, 17.8)	15.3 (14.4, 16.3)	0.432
Fasting C-peptide (ng/ml)	1.15 (0.84, 1.46)	0.96 (0.46, 1.46)	1.25 (0.86, 1.65)	0.360
2-hour post-load C-peptide (ng/ml)	2.00 (1.40, 2.59)	2.16 (1.61, 2.72)	1.44 (1.34, 1.54)	0.012*
TG (mmol/L)	1.79 (1.49, 2.09)	1.14 (0.81, 1.48)	2.09 (1.69, 2.49)	<0.001*
TC (mmol/L)	5.46 (5.04, 5.88)	4.70 (4.46, 4.94)	5.76 (5.23, 6.29)	<0.001*
HDL-c (mmol/L)	1.66 (1.52, 1.79)	1.37 (1.29, 1.45)	1.75 (1.59, 1.92)	<0.001*
LDL-c (mmol/L)	2.83 (2.60, 3.06)	2.63 (2.40, 2.87)	2.94 (2.58, 3.31)	0.161
Male (%)	41.5 (35.2, 48.1)	43.0 (33.5, 53.1)	41.0 (33.7, 48.7)	0.751
Family history (%)	89.8 (54.1, 98.5)	92.6 (22.2, 99.8)	87.4 (41.5, 98.5)	0.794
Microvascular complications (%)	47.6 (30.6, 65.2)	31.7 (5.1, 79.9)	51.6 (33.3, 69.5)	0.474
Diabetic retinopathy (%)	21.5 (14.5, 30.8)	22.2 (6.0, 56.2)	20.7 (13.9, 29.7)	0.913
Diabetic kidney disease (%)	16.6 (10.3, 25.5)	10.7 (2.8, 32.9)	18.4 (11.0, 29.1)	0.417
Diabetic neuropathy (%)	11.8 (6.2, 21.2)	6.8 (0.7, 43.5)	13.1 (7.2, 22.7)	0.559
Macrovascular complications (%)	11.1 (7.3, 16.6)	2.7 (0.7, 10.0)	14.3 (10.7, 18.9)	0.014*
Lifestyles (%)	17.0 (13.2, 21.6)	15.5 (10.6, 22.3)	16.8 (12.3, 22.5)	0.759
OHA (%)	40.3 (32.4, 48.6)	41.9 (34.2, 50.0)	40.5 (30.8, 51.0)	0.829
INS (%)	35.5 (31.3, 40.0)	35.8 (28.5, 43.8)	35.1 (30.3, 40.3)	0.882
OHA + INS (%)	9.5 (5.4, 16.2)	8.1 (3.7, 16.9)	9.9 (4.7, 19.6)	0.717

*BMI, body mass index; HbA1c, glycated hemoglobin; FPG, fasting plasma glucose; 2h PG, 2-h post-load glucose; TG, triglyceride; TC, total cholesterol; HDL-c, high-density lipoprotein cholesterol; LDL-c, low-density lipoprotein cholesterol; OHA, oral hypoglycemic drugs; INS, insulin; *p < 0.05.*

dimerization domain and 1.12 mmol/L (95% CI: 0.89–1.35) for the transactivation domain, p = 0.001] were highest, while the prevalence of diabetic neuropathy was lowest [10.9% (95% CI: 5.0–22.2) vs. 33.3% (95% CI: 8.4–73.2) for the dimerization domain and 37.0% (95% CI: 21.2–56.2) for the transactivation domain, p = 0.024] in patients with DNA-binding domain mutations. BMI, HbA1c, FPG, 2h PG, fasting C-peptide, LDL-c, family history, gender, diabetic retinopathy, diabetic kidney disease, macrovascular complications and anti-diabetic therapies did not differ significantly (**Table 2**). The mutation domain did not differ significantly between Asian and non-Asian patients (**Table 3**).

In our study, the *HNF1-alpha* mutations included missense mutations (n = 227, 46.1%), frameshift mutations (n = 198, 40.2%), nonsense mutations (n = 30, 6.1%), synonym mutations (n = 2, 0.4%), and non-coding mutations (n = 35, 7.1%). Patients

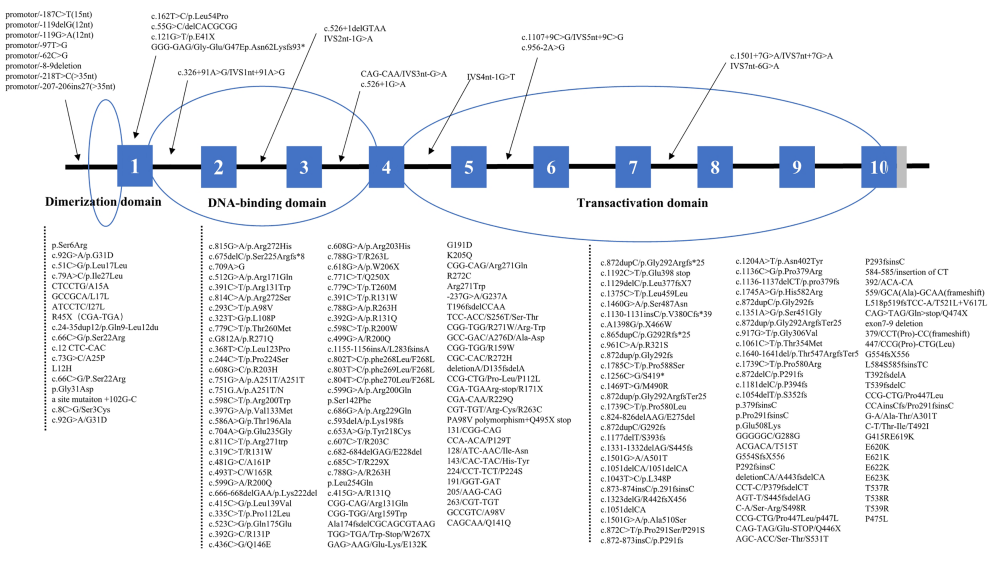

FIGURE 2 | Distribution of *HNF1-alpha* mutations. *means nucleotide number and indicates translation stop codon.

TABLE 2 | Characteristics of patients with *HNF1-alpha* MODY by genetic domains.

Subject	Total (*n* = 432)	Dimerization domain (*n* = 15)	DNA-binding domain (*n* = 179)	Transactivation domain (*n* = 238)	*P*-value
Age of diagnosis (years)	19.7 (17.6, 21.8)	18.9 (11.5, 26.3)	20.5 (17.3, 23.7)	26.0 (21.7, 30.3)	<0.001*
BMI (kg/m^2)	22.8 (22.1, 23.6)	22.8 (20.9, 24.7)	23.6 (22.2, 25.1)	22.1 (20.8, 23.5)	0.227
HbA1c (%)	8.0 (7.6, 8.4)	8.0 (6.5, 9.5)	8.2 (7.4, 9.0)	7.8 (7.2, 8.5)	0.641
FPG (mmol/L)	9.3 (8.0, 10.5)	12.4 (4.6, 20.3)	9.1 (7.2, 11.0)	8.7 (7.6, 9.8)	0.126
2h PG (mmol/L)	15.9 (14.9, 16.9)	16.8 (8.6, 25.1)	16.1 (12.8, 19.4)	15.5 (13.0, 18.0)	0.751
Fasting C-peptide (ng/ml)	1.14 (1.03, 1.25)	1.28 (0.71, 1.85)	1.13 (0.87, 1.40)	1.04 (0.73, 1.35)	0.370
2-h post-load C-peptide (ng/ml)	3.06 (0.81, 5.32)	2.71	4.22 (2.17, 6.26)	1.92 (1.17, 2.67)	<0.001*
TG (mmol/L)	1.51 (0.93, 2.08)	1.70	1.82 (0.27, 3.36)	1.23 (0.81, 1.64)	0.007*
TC (mmol/L)	4.97 (4.13, 5.81)	3.96	5.39 (2.07, 8.71)	4.54 (3.59, 5.49)	0.017*
HDL-c (mmol/L)	1.34 (0.88, 1.81)	0.72	1.59 (0.64, 2.54)	1.12 (0.89, 1.35)	0.001*
LDL-c (mmol/L)	3.01 (2.82, 3.21)	3.02 (1.81, 4.24)	2.89 (1.18, 4.24)	3.19 (2.24, 4.14)	0.662
Male (%)	40.0 (29.1, 52.0)	46.2 (22.4, 71.8)	47.8 (37.7, 58.1)	28.3 (17.8, 41.8)	0.072
Family history (%)	83.9 (75.2, 90.0)	92.9 (63.0, 99.0)	80.4 (55.3, 93.2)	83.0 (75.7, 88.4)	0.618
Microvascular complications (%)	36.6 (26.2, 48.3)	50.0 (16.8, 83.2)	28.9 (17.6, 43.6)	41.5 (24.8, 60.4)	0.406
Diabetic retinopathy (%)	26.1 (16.8, 38.3)	33.3 (8.4, 73.2)	22.0 (11.8, 37.1)	28.6 (12.8, 52.2)	0.760
Diabetic kidney disease (%)	14.0 (7.5, 24.8)	16.7 (2.3, 63.1)	23.5 (12.2, 40.5)	8.4 (3.0, 21.3)	0.209
Diabetic neuropathy (%)	19.8 (9.9, 35.6)	33.3 (8.4, 73.2)	10.9 (5.0, 22.2)	37.0 (21.2, 56.2)	0.024*
Macrovascular complications (%)	5.3 (1.7, 15.1)	0 (0, 100)	8.3 (2.1, 27.9)	3.7 (0.5, 22.1)	0.792
Lifestyles (%)	19.4 (14.7, 25.2)	16.7 (4.2, 47.7)	18.8 (13.4, 25.8)	20.8 (13.7, 30.3)	0.903
OHA (%)	40.4 (29.6, 52.2)	66.7 (37.6, 86.9)	32.6 (15.2, 56.7)	42.6 (34.4, 51.3)	0.192
INS (%)	28.5 (24.2, 33.3)	16.7 (4.2, 47.7)	27.9 (21.4, 35.5)	29.7 (23.9, 36.2)	0.620
OHA + INS (%)	4.2 (1.9, 9.0)	0 (0, 100)	5.9 (2.7, 12.5)	3.5 (0.9, 12.6)	0.799

*BMI, body mass index; HbA1c, glycated hemoglobin; FPG, fasting plasma glucose; 2h PG, 2-h post-load glucose; TG, triglyceride; TC, total cholesterol; HDL-c, high-density lipoprotein cholesterol; LDL-c, low-density lipoprotein cholesterol; OHA, oral hypoglycemic drugs; INS, insulin; *p < 0.05.*

with non-coding mutations had the highest levels of HbA1c [9.5% (95% CI: 8.0–11.0), $p < 0.001$] and 2h PG [20.7 mmol/L (95% CI: 19.7–21.8), $p < 0.001$] and the lowest BMI [20.5 kg/m^2 (95% CI: 19.5–21.6), $p < 0.001$] and fasting C-peptide [0.43 ng/ml (95% CI: 0.33–0.53), $p < 0.001$], and they most often had diabetic kidney disease [80.0% (95% CI: 30.9–97.3), $p = 0.046$]. In terms of lipid profiles, due to the incomplete data of patients with nonsense, synonymous, and non-coding mutations, we only compared the difference of lipid profiles between patients with missense mutations and frameshift mutations. We found that the TC [5.03 mmol/L (95% CI: 4.82–5.24) vs. 4.52 mmol/L (95% CI: 4.10–4.94), $p = 0.034$] and HDL-c [1.36 mmol/L (95% CI: 1.25–1.47) vs. 1.09 mmol/L (95% CI: 0.98–1.20), $p < 0.001$] levels were significantly higher in patients with missense mutations compared with those with frameshift mutations. Age of diagnosis, FPG, TG, LDL-c, gender, diabetic retinopathy, diabetic neuropathy, and anti-diabetic therapies did not differ by types of *HNF1-alpha* mutations (**Supplementary Table S2**).

Clinical Manifestations of *HNF1-alpha* MODY by Islet Autoantibody Status

A total of 15 patients from 9 articles were identified to be positive for islet autoantibodies (GAD, IA2, or ICA). Compared with patients with negative islet autoantibodies, patients with positive islet autoantibodies had higher levels of FPG [12.1 mmol/L (95% CI: 9.9–14.2) vs. 8.6 mmol/L (95% CI: 7.8–9.5), $p = 0.004$] and 2h PG [19.7 mmol/L (95% CI: 17.4–21.9) vs. 16.0 mmol/L (95% CI: 15.0–17.0), $p = 0.003$] and lower levels of HDL-c [0.99 mmol/L (95% CI: 0.85–1.13) vs. 1.49 mmol/L (95% CI: 1.30–1.67), $p < 0.001$], and they more often had diabetic neuropathy [50.0% (95% CI: 20.0–80.0) vs. 11.3% (95% CI: 5.7–21.0), $p = 0.010$]. The levels of TG, TC, and LDL-c and the prevalence of macrovascular complications did not differ by islet autoantibody status (**Table 4**).

DISCUSSION

In this study, we analyzed the clinical characteristics of patients with *HNF1-alpha* MODY through literature review and found that the clinical manifestations of *HNF1-alpha* MODY differed by geographical regions, *HNF1-alpha* mutations, and islet autoantibody status. Asian patients with *HNF1-alpha* MODY had a higher HbA1c or 2-h post-load C-peptide levels, lower lipid profile levels, and, less often, macrovascular complications. Patients with transactivation domain mutations were diagnosed at an older age. The levels of 2-h post-load C-peptide, TG, TC, and HDL-c were highest, while the prevalence of diabetic

TABLE 3 | Differences in domain mutations between Asian patients and non-Asian patients.

Subject	Total (*n* = 1,325)	Asian (*n* = 183)	Non-Asian (*n* = 1,142)	*P*-value
Dimerization domain (%)	6.4 (3.9, 10.4)	3.8 (1.2, 11.0)	7.8 (4.5, 13.2)	0.241
DNA-binding domain (%)	33.0 (17.2, 53.9)	48.8 (38.0, 59.6)	29.2 (12.9, 53.6)	0.144
Transactivation domain (%)	59.9 (40.7, 76.4)	47.5 (36.8, 58.4)	63.0 (40.0, 81.4)	0.231

neuropathy was lowest in patients with DNA-binding domain mutations. Patients with non-coding mutations had higher levels of HbA1c or 2h PG and a higher prevalence of diabetic kidney disease but with lower fasting C-peptide levels. In addition, hyperglycemia and diabetic neuropathy were more frequent in patients with positive islet autoantibodies.

The prevalence of *HNF1-alpha* MODY vary among nations and healthcare systems. We thus hypothesized that the clinical manifestations of *HNF1-alpha* MODY could also vary by geographical regions due to diversity in genetic background and environmental factors. In this study, Asian patients exhibited higher HbA1c levels compared with non-Asian patients despite similar fasting and post-load blood glucose. The genetic factors that determine the correlation between HbA1c levels and blood glucose levels could partially explain this discrepancy. In a meta-analysis involving data from 49,238 individuals without diabetes, the HbA1c values are higher in Asians compared to White persons (31). In addition, the postprandial glycemic responses are higher in Asians compared with Caucasians following the ingestion of breakfast cereal and rice (32–35), which could result in higher post-prandial blood glucose and HbA1c levels, but not reflected in post-load glucose levels. In our study, Asian patients with *HNF1-alpha* MODY had a lower BMI but had higher 2-h post-load C-peptide levels. Asians are more likely to have less muscle mass and more visceral fat and are more insulin resistant at a lower BMI (36). The higher levels of 2-h post-load C-peptide in Asian patients may be associated with insulin resistance. In a study involving 94,952 Chinese adults (37), approximately 24.4% of the incidents of diabetes could be attributed to insulin resistance and 12.4% could be attributed to β-cell dysfunction, which, in part, suggested that insulin resistance show a stronger association with incident diabetes than does β-cell dysfunction in Asia. Asian patients with *HNF1-alpha* MODY had lower TG, TC, and HDL-c levels and less often had macrovascular complications despite a higher HbA1c level. The lower lipid profiles among Asians are associated with lifestyle and dietary factors (38). Some single-nucleotide polymorphisms in Asians are also closely related to dyslipidemia, which could independently influence the occurrence of macrovascular complications (39). Age, age of diagnosis, and diabetes duration did not differ between Asian and non-Asian patients with *HNF1-alpha* MODY. Thus, our study suggested that the macrovascular complications of *HNF1-alpha* MODY may be impacted by race and blood lipid. However, a further study, with individual-level patient data, is needed to discern associations between risk factors and macrovascular complications among patients with *HNF1-alpha* MODY. With respect to microvascular complications, in a study involving 667 affected members of *HNF1-alpha* MODY, the prevalence of proliferative retinopathy and proteinuria was 21 and 19%, respectively, higher than *GCK*-MODY and other MODY types (40). The pooled results of our study were similar to the above-mentioned report. Among *HNF1-alpha MODY* patients identified in our study, the prevalence of microvascular diabetic retinopathy was 21.5% (95% CI: 14.5–30.8), and the prevalence of diabetic kidney disease was 16.6% (95% CI: 10.3–25.5). Isomaa B *et al.* found that the risk of microvascular complications in *HNF1-alpha* MODY was closely

TABLE 4 | Characteristics of patients with *HNF1-alpha* by islet autoantibody status.

Subject	Total (*n* = 1,325)	Negative (*n* = 1,310)	Positive (*n* = 15)	*P*-value
Age of diagnosis (years)	20.1 (16.2, 24.0)	19.8 (15.7, 23.9)	23.4 (18.3, 28.5)	0.282
BMI (kg/m^2)	22.7 (21.5, 23.9)	22.6 (21.4, 23.9)	23.8 (21.3, 26.3)	0.399
HbA1c (%)	7.7 (7.3, 8.0)	7.6 (7.3, 7.9)	8.9 (7.4, 10.3)	0.094
FPG (mmol/L)	8.9 (8.0, 9.8)	8.6 (7.8, 9.5)	12.1 (9.9, 14.2)	0.004*
2-hour PG (mmol/L)	16.6 (14.5, 18.7)	16.0 (15.0, 17.0)	19.7 (17.4, 21.9)	0.003*
Fasting C-peptide (ng/ml)	1.07 (0.54, 1.60)	1.05 (0.48, 1.63)	1.19 (0.63, 1.74)	0.747
2-h post-load C-peptide (ng/ml)	2.11 (1.61, 2.60)	2.17 (1.59, 2.76)	1.83 (1.26, 2.40)	0.407
TG (mmol/L)	1.12 (0.92, 1.32)	1.12 (0.90, 1.35)	1.14 (0.86, 1.41)	0.942
TC (mmol/L)	4.73 (4.43, 5.04)	4.77 (4.44, 5.10)	4.40 (3.67, 5.13)	0.365
HDL-c (mmol/L)	1.42 (1.24, 1.60)	1.49 (1.30, 1.67)	0.99 (0.85, 1.13)	<0.001*
LDL-c (mmol/L)	2.81 (2.54, 3.08)	2.80 (2.05, 3.10)	2.87 (2.33, 3.41)	0.821
Male (%)	41.1 (34.7, 47.9)	41.5 (34.9, 48.4)	30.8 (12.0, 59.1)	0.450
Family history (%)	87.2 (51.5, 97.8)	88.0 (46.3, 98.4)	86.7 (59.5, 96.6)	0.929
Microvascular complications (%)	48.4 (31.0, 66.2)	47.5 (29.3, 66.3)	62.5 (28.5, 87.5)	0.461
Diabetic retinopathy (%)	20.8 (14.2, 29.4)	20.6 (13.8, 29.7)	25.0 (6.3, 62.3)	0.769
Diabetic kidney disease (%)	15.3 (9.0, 24.7)	16.3 (9.7, 25.9)	100 (0, 100)	1.000
Diabetic neuropathy (%)	12.8 (6.7, 23.3)	11.3 (5.7, 21.0)	50.0 (20.0, 80.0)	0.010*
Macrovascular complications (%)	11.5 (7.7, 16.8)	11.4 (7.5, 17.0)	12.5 (1.7, 53.7)	0.925
Lifestyles (%)	17.0 (13.2, 21.6)	17.2 (13.4, 21.9)	9.1 (1.3, 43.9)	0.490
OHA (%)	39.7 (31.7, 48.3)	40.1 (31.9, 49.0)	27.3 (9.1, 58.6)	0.408
INS (%)	36.2 (31.8, 40.9)	35.8 (31.4, 40.5)	54.6 (26.8, 79.7)	0.213
OHA + INS (%)	9.8 (5.1, 18.0)	9.8 (4.7, 19.3)	9.1 (1.3, 43.9)	0.939
Dimerization domain (%)	5.8 (3.5, 9.6)	5.6 (3.3, 9.4)	11.1 (1.5, 50.0)	0.498
DNA-binding domain (%)	22.5 (8.7, 47.1)	28.7 (13.0, 52.2)	0 (0, 100)	1.000
Transactivation domain (%)	68.3 (47.6, 83.7)	64.1 (42.8, 81.1)	88.9 (50.0, 98.5)	0.193

*BMI, body mass index; HbA1c, glycated hemoglobin; FPG, fasting plasma glucose; 2-hour PG, 2-h post-load glucose; TG, triglyceride; TC, total cholesterol; HDL-c, high-density lipoprotein cholesterol; LDL-c, low-density lipoprotein cholesterol; OHA, oral hypoglycemic drugs; INS, insulin; *p < 0.05.*

related to poor glycemic control, diabetes duration, and *HNF1-alpha* mutations (41). In our study, the prevalence of microvascular complications was similar between Asian and non-Asian patients despite the Asian patients having higher HbA1c levels.

HNF1-alpha, as a widely expressed tissue-specific transcription factor located at q24.31 on chromosome 12, is composed of 631 amino acids and contains 10 exons (42). In pancreatic β-cells, *HNF1-alpha* regulates the expression of genes associated with β-cell maturation, growth, and function, including glucose transport/metabolism and insulin secretion (43); in the liver, *HNF1-alpha* regulates the expression of tissue-specific regulatory proteins and participates in the metabolism of glucose, fat, and other substances (44); in the kidney, *HNF1-alpha* regulates the expression of SGLT2 and controls glucose reabsorption in proximal tubules (45). The *HNF1-alpha* protein comprises 3 functional domains: dimerization, DNA-binding, and transactivation domains, of which DNA-binding (41.4%) and transactivation domain (55.1%) were predominant in our research. It has been shown that the transactivation domain was more accommodating to mutations causing minor changes in the *HNF1-alpha* protein structure than the dimerization domain or the DNA-binding domain (46) such that mutations in the transactivation domain may not be associated with overt diabetes or a severe phenotype, in line with the observation in our study that the age of diagnosis of patients with transactivation domain mutations was older. However, in the dimerization domain or the DNA-binding domain, there were some crucial sites for the function of *HNF1-alpha* protein, such as exons 1, 4, and 6 (47). Our study also showed that, in patients with dimerization or DNA-binding domain mutations, the age of diagnosis was younger than those with transactivation domain mutations. Moreover, in our study, different types of mutations of *HNF1-alpha* are spread throughout the entire sequence of the gene, including missense mutations, frameshift mutations, nonsense mutations, synonym mutations, and non-coding mutations. In comparison, patients with non-coding mutations had the highest levels of HbA1c or 2h PG and the highest prevalence of diabetic kidney disease but with the lowest levels of BMI or fasting C-peptide among different types of *HNF1-alpha* mutations. The result of this study suggested that more attention is needed for the clinical characteristics of *HNF1-alpha* MODY in different mutations, especially the rare mutations in non-coding regions.

In patients with *HNF1-alpha* MODY, severe hyperglycemia usually occurs before 25–35 years of age and may lead to the misdiagnosis of T1DM. Islet autoantibodies, as an important basis for the diagnosis of T1DM, can be detected in 87–94% of T1DM but are less common in other diabetes (48). In current guidelines for the molecular genetic diagnosis of MODY, absence of islet autoantibodies is one of the criteria for testing for MODY in children and young adults with diabetes and a strong family history of diabetes (49). However, some studies have shown that the islet autoantibodies can be detected in parts of patients with T2DM or MODY and the general population. The initial publication reported that less than 4% of the general population had positive autoantibodies (50). Some studies found islet autoantibodies in 21–33% of children and young people with a clinical diagnosis of T2DM (51, 52). In a study involving 508 patients with MODY (including 229 *HNF1-alpha* MODY patients), GAD positivity, defined as >99th centile of 500 adult control subjects, was detected in 5 patients (<1%, 3 of which were *HNF1-alpha* MODY patients). Among the 5 MODY patients with positive autoantibodies, 4 patients had a clinical course consistent with MODY, while 1 patient was consistent with T1DM (53). In our study, 15 out of 1,325 *HNF1-alpha* MODY patients were found to have positive islet autoantibodies, which was consistent with the above-mentioned reports. Then, we further investigated the special characteristics of patients with positive islet autoantibodies in *HNF1-alpha* MODY. It was noted that patients with positive islet autoantibodies had higher blood glucose levels and more likely had diabetic neuropathy in our study, suggesting that the features of T1DM is present in some MODY patients with positive autoantibodies. In this subset of patients, double diabetes may be the appropriate diagnosis rather than either MODY or T1DM (53). However, there was only approximately 1% of patients with double DM; hence, conducting islet autoantibody testing for all patients with *HNF1-alpha* MODY may be not necessary. Thus, further studies are needed to explore and determine whether islet autoantibody testing is necessary for patients with *HNF1-alpha* MODY.

The intent of this study was to summarize the available published information regarding the clinical characteristics of *HNF1-alpha* MODY. The study has the following limitations: firstly, some studies identified were not included due to the unavailability of key clinical information indicated in the eligible study criteria. Secondly, not all geographic regions were represented in the results—for example, no studies reporting *HNF1-alpha* MODY patients in Africa were identified. Thirdly, the ethnicity of the majority of participants was not specified. Fourthly, due to the limited clinical data in enrolled studies, there was a restriction of further statistical analyses like regression analysis to investigate the association between clinical variables (*e.g.*, diabetes duration and type of treatment) and chronic complications. More studies with individual-level patient data are needed in the future. Lastly, although we observed more severe clinical characteristics in patients with dimerization/DNA-binding domain mutations or non-coding mutations, further studies are needed to explore the effect of variants in dimerization/DNA-binding domain or non-coding regions for the purpose of understanding the precise molecular mechanism of *HNF1-alpha* MODY.

In conclusion, our study demonstrated that the clinical manifestations of *HNF1-alpha* MODY differed by geographical regions, *HNF1-alpha* mutations, and islet autoantibody status. Asian patients with *HNF1-alpha* MODY had a lower prevalence of macrovascular complications despite higher HbA1c or 2-h post-load C-peptide levels. Patients with transactivation domain mutations were diagnosed at an older age. The levels of 2-h post-load C-peptide, TG, TC, and HDL-c were highest and the prevalence of diabetic neuropathy was lowest in patients with

DNA-binding domain mutations. Patients with non-coding mutations had higher levels of HbA1c or 2h PG and a higher prevalence of diabetic kidney disease but with a lower fasting C-peptide level. Hyperglycemia and diabetic neuropathy were more frequent in patients with positive islet autoantibodies.

DATA AVAILABILITY STATEMENT

The original contributions presented in the study are included in the article/**Supplementary Material**. Further inquiries can be directed to the corresponding authors.

AUTHOR CONTRIBUTIONS

QZ and LD researched the data. QZ wrote the manuscript. YY, JS, MW, and XL contributed to the discussion and reviewed/edited the manuscript. ML initiated and designed the research project, reviewed the data, and wrote the manuscript. ML is the guarantor of this work and, as such, had full access to all the data in the study and take responsibility for the integrity of the data and the accuracy of the data analysis. All authors contributed to the article and approved the submitted version.

FUNDING

This work was supported by the National Key R&D Program of China (2019YFA0802502) and the National Natural Science Foundation of China (81830025, 81620108004, and 82100865). We acknowledge the support of the Tianjin Municipal Science and Technology Bureau (18JCYBJC93900) and the Tianjin Key Medical Discipline (Specialty) Construction Project.

SUPPLEMENTARY MATERIAL

The Supplementary Material for this article can be found online at: https://www.frontiersin.org/articles/10.3389/fendo.2022.900489/full#supplementary-material

REFERENCES

1. Fajans SS, Bell GI, Polonsky KS. Molecular Mechanisms and Clinical Pathophysiology of Maturity-Onset Diabetes of the Young. *N Engl J Med* (2001) 345(13):971–80. doi: 10.1056/NEJMra002168
2. Passanisi S, Salzano G, Bombaci B, Lombardo F. Clinical and Genetic Features of Maturity-Onset Diabetes of the Young in Pediatric Patients: A 12-Year Monocentric Experience. *Diabetol Metab Syndr* (2021) 13(1):1–8. doi: 10.1186/s13098-021-00716-6
3. Shields BM, Hicks S, Shepherd MH, Colclough K, Hattersley AT, Ellard S. Maturity-Onset Diabetes of the Young (MODY): How Many Cases are We Missing? *Diabetologia* (2010) 53(12):2504–8. doi: 10.1007/s00125-010-1799-4
4. Kyithar MP, Bacon S, Pannu KK, Rizvi SR, Colclough K, Ellard S, et al. Identification of HNF1A-MODY and HNF4A-MODY in Irish Families: Phenotypic Characteristics and Therapeutic Implications. *Diabetes Metab* (2011) 37(6):512–9. doi: 10.1016/j.diabet.2011.04.002
5. Losekoot M, Broekman A, Breuning M, De Koning E, Romijn J, Maassen J. Molecular Diagnosis on Indication of Maturity Onset Diabetes of the Young; Results From 184 Patients. *Nederlands Tijdschrift Voor Geneeskunde.* (2005) 149(3):139–43.
6. Byrne MM, Sturis J, Menzel S, Yamagata K, Fajans SS, Dronsfield MJ, et al. Altered Insulin Secretory Responses to Glucose in Diabetic and Nondiabetic Subjects With Mutations in the Diabetes Susceptibility Gene MODY3 on Chromosome 12. *Diabetes* (1996) 45(11):1503. doi: 10.2337/diab.45.11.1503
7. Wang H, Maechler P, Hagenfeldt KA, Wollheim CB. Dominant-Negative Suppression of HNF-1alpha Function Results in Defective Insulin Gene Transcription and Impaired Metabolism-Secretion Coupling in a Pancreatic Beta-Cell Line. *EMBO J* (1998) 17(22):6701–13. doi: 10.1093/emboj/17.22.6701
8. Shih DQ, Screenan S, Munoz KN, Philipson L, Pontoglio M, Yaniv M, et al. Loss of HNF-1alpha Function in Mice Leads to Abnormal Expression of Genes Involved in Pancreatic Islet Development and Metabolism. *Diabetes* (2001) 50(11):2472–80. doi: 10.2337/diabetes.50.11.2472
9. Pearson ER, Liddell WG, Shepherd M, Corrall RJ, Hattersley AT. Sensitivity to Sulphonylureas in Patients With Hepatocyte Nuclear Factor-1α Gene Mutations: Evidence for Pharmacogenetics in Diabetes. *Diabetic Med* (2000) 17(7):543–5. doi: 10.1046/j.1464-5491.2000.00305.x
10. Dahl OE. Multicenter Study. *Lancet* (2008) 372(9632):31–9. doi: 10.1016/S0140-6736(08)60880-6
11. Pettitt DJ, Talton J, Dabelea D, Divers J, Imperatore G, Lawrence JM, et al. Prevalence of Diabetes in U.S. Youth in 2009: The SEARCH for Diabetes in Youth Study. *Diabetes Care* (2014) 37(2):402–8. doi: 10.1001/jama.2014.3201
12. Johansson BB, Irgens HU, Molnes J, Sztromwasser P, Aukrust I, Juliusson PB, et al. Targeted Next-Generation Sequencing Reveals MODY in Up to 6.5% of Antibody-Negative Diabetes Cases Listed in the Norwegian Childhood Diabetes Registry. *Diabetologia* (2017) 60(4):625–35. doi: 10.1007/s00125-016-4167-1
13. Kim SH. Maturity-Onset Diabetes of the Young: What Do Clinicians Need to Know? *Diabetes Metab J* (2015) 39(6):468–77. doi: 10.4093/dmj.2015.39.6.468
14. Mozzillo E, Salzano G, Barbetti F, Maffeis C, Lombardo F, Franzese A, et al. Survey on Etiological Diagnosis of Diabetes in 1244 Italian Diabetic Children and Adolescents: Impact of Access to Genetic Testing. *Diabetes Res Clin Pract* (2015) 107(3):e15–8. doi: 10.1016/j.diabres.2015.01.003
15. Thanabalasingham G, Pal A, Selwood MP, Dudley C, Fisher K, Bingley PJ, et al. Systematic Assessment of Etiology in Adults With a Clinical Diagnosis of Young-Onset Type 2 Diabetes Is a Successful Strategy for Identifying Maturity-Onset Diabetes of the Young. *Diabetes Care* (2012) 35(6):1206–12. doi: 10.2337/dc11-1243
16. Hattersley A, Bruining J, Shield J, et al. ISPAD Clinical Practice Consensus Guidelines 2006–2007 The Diagnosis and Management of Monogenic Diabetes in Children. *Pediatr Diabetes* (2006) 7(6):352–60. doi: 10.1111/j.1399-5448.2006.00217.x
17. Frayling TM, Evans JC, Bulman MP, Pearson E, Allen L, Owen K, et al. Beta-Cell Genes and Diabetes: Molecular and Clinical Characterization of Mutations in Transcription Factors. *Diabetes* (2001) 50 Suppl 1:S94–100. doi: 10.2337/diabetes.50.2007.s94
18. Yorifuji T, Fujimaru R, Hosokawa Y, Tamagawa N, Urakami T. Comprehensive Molecular Analysis of Japanese Patients With Pediatric-Onset MODY-Type Diabetes Mellitus. *Pediatr Diabetes* (2013) 13(1):26–32. doi: 10.1111/j.1399-5448.2011.00827.x
19. Liang H, Zhang Y, Li M, Yan J, Yang D, Luo S, et al. Recognition of Maturity-Onset Diabetes of the Young in China. *J Diabetes Investig* (2021) 12(4):501–9. doi: 10.1111/jdi.13378
20. Stride A, Shepherd M, Frayling TM, Bulman MP, Ellard S, Hattersley AT. Intrauterine Hyperglycemia Is Associated With an Earlier Diagnosis of Diabetes in HNF-1alpha Gene Mutation Carriers. *Diabetes Care* (2002) 25(12):2287–91. doi: 10.2337/diacare.25.12.2287
21. Kim S-H, Ma X, Klupa T, Powers C, Pezzolesi M, Warram JH, et al. Genetic Modifiers of the Age at Diagnosis of Diabetes (MODY3) in Carriers of

Hepatocyte Nuclear Factor-1α Mutations Map to Chromosomes 5pl5, 9q22, and 14q24. *Diabetes* (2003) 52(8):2182–6. doi: 10.2337/diabetes.52.8.2182
22. Lucchetta M, Rudilosso S, Costa S, Bruttomesso D, Ruggero S, Toffanin E, et al. Anti-Ganglioside Autoantibodies in Type 1 Diabetes. *Muscle Nerve* (2010) 41(1):50–3. doi: 10.1002/mus.21326
23. Wang T, Zhang M, Shi L, et al. A Novel Hepatocyte Nuclear Factor-1a Genetic Mutation in a Chinese Pedigree With Maturity-Onset Diabetes of the Young Type 3. *Chin J Diabetes Mellitus* (2014) 6(1):27—31. doi: 10.3760/cma.j.issn.1674-5809.2014.01.006
24. Bonatto N, Nogaroto V, Svidnicki PV, Milléo FQ, Grassiolli S, Almeida MC, et al. Variants of the HNF1α Gene: A Molecular Approach Concerning Diabetic Patients From Southern Brazil. *Genet Mol Biol* (2012) 35(4):737–40. doi: 10.1590/S1415-47572012005000061
25. Rafique I, Saqib M, Fawwad A, Zubaida B, Basit A. Genetic Characterization of Suspected MODY Patients in Pakistan by Next Generation Sequencing—a Pilot Study. *Int J Diabetes Develop Cntr* (2021) 41(4):563–9. doi: 10.1007/s13410-021-00926-8
26. Miura J, Sanaka M, Ikeda Y, Watanabe C, Nakagami T, Iwasaki N, et al. A Case of Type-1 Diabetes Mellitus Formerly Diagnosed as Maturity-Onset Diabetes of the Young (MODY) Carrying Suggestive MODY3 Gene. *Diabetes Res Clin Pract* (1997) 38(2):139–41. doi: 10.1016/S0168-8227(97)00092-2
27. Zhang M, Wang T, Shi L, Yang Y. Hepatocyte Nuclear Factor-α Genetic Mutation in a Chinese Pedigree With Maturity-Onset Diabetes of the Young (MODY3). *Diabetes Metab Res Rev* (2015) 31(7):767–70. doi: 10.1002/dmrr.2678
28. Toaima D, Näke A, Wendenburg J, Praedicow K, Rohayem J, Engel K, et al. Identification of Novel GCK and HNF1A/TCF1 Mutations and Polymorphisms in German Families With Maturity-Onset Diabetes of the Young (MODY). *Hum Mutat* (2005) 25(5):503–4. doi: 10.1002/humu.9334
29. Knebel B, Mack S, Haas J, Herman-Friede MK, Lange S, Schubert O, et al. Divergent Phenotypes in Siblings With Identical Novel Mutations in the HNF-1α Gene Leading to Maturity Onset Diabetes of the Young Type 3. *BMC Med Genet* (2018) 18(1):1–12. doi: 10.1186/s12881-016-0297-z
30. Sacks D, Baxter B, Campbell BCV, Carpenter JS, Cognard C, Dippel D, et al. Multisociety Consensus Quality Improvement Revised Consensus Statement for Endovascular Therapy of Acute Ischemic Stroke. *Int J Stroke* (2018) 13(6):612–32. doi: 10.1177/1747493018778713
31. Cavagnolli G, Pimentel AL, Freitas PA, Gross JL, Camargo JL. Effect of Ethnicity on HbA1c Levels in Individuals Without Diabetes: Systematic Review and Meta-Analysis. *PloS One* (2017) 12(2):e0171315. doi: 10.1371/journal.pone.0171315
32. Venn B, Williams S, Mann J. Comparison of Postprandial Glycaemia in Asians and Caucasians. *Diabetic Med* (2010) 27(10):1205–8. doi: 10.1111/j.1464-5491.2010.03069.x
33. Kataoka M, Venn B, Williams S, Te Morenga L, Heemels I, Mann J. Glycaemic Responses to Glucose and Rice in People of Chinese and European Ethnicity. *Diabetic Med* (2013) 30(3):e101–e7. doi: 10.1111/dme.12080
34. Chiu KC, Cohan P, Lee NP, Chuang LM. Insulin Sensitivity Differs Among Ethnic Groups With a Compensatory Response in Beta-Cell Function. *Diabetes Care* (2000) 23(9):1353–8. doi: 10.2337/diacare.23.9.1353
35. Liew CF, Seah ES, Yeo KP, Lee KO, Wise SD. Lean, Nondiabetic Asian Indians Have Decreased Insulin Sensitivity and Insulin Clearance, and Raised Leptin Compared to Caucasians and Chinese Subjects. *Int J Obes Relat Metab Disord* (2003) 27(7):784–9. doi: 10.1038/sj.ijo.0802307
36. Chan JCN, Malik V, Jia W, Kadowaki T, Yajnik CS, Yoon K-H, et al. Diabetes in Asia: Epidemiology, Risk Factors, and Pathophysiology. *JAMA* (2009) 301(20):2129–40. doi: 10.1001/jama.2009.726
37. Wang T, Lu J, Shi L, Chen G, Xu M, Xu Y, et al. Association of Insulin Resistance and β-Cell Dysfunction With Incident Diabetes Among Adults in China: A Nationwide, Population-Based, Prospective Cohort Study. *Lancet Diabetes Endocrinol* (2020) 8(2):115–24. doi: 10.1016/S2213-8587(19)30425-5
38. Rice Bradley BH. Dietary Fat and Risk for Type 2 Diabetes: A Review of Recent Research. *Curr Nutr Rep* (2018) 7(4):214–26. doi: 10.1007/s13668-018-0244-z
39. Teslovich TM, Musunuru K, Smith AV, Edmondson AC, Stylianou IM, Koseki M, et al. Biological, Clinical and Population Relevance of 95 Loci for Blood Lipids. *Nature* (2010) 466(7307):707–13. doi: 10.1038/nature09270
40. Velho G, Vaxillaire M, Boccio V, Charpentier G, Froguel P. Diabetes Complications in NIDDM Kindreds Linked to the MODY3 Locus on Chromosome 12q. *Diabetes Care* (1996) 19(9):915–9. doi: 10.2337/diacare.19.9.915
41. Isomaa B, Henricsson M, Lehto M, Forsblom C, Karanko S, Sarelin L, et al. Chronic Diabetic Complications in Patients With MODY3 Diabetes. *Diabetologia* (1998) 41(4):467–73. doi: 10.1007/s001250050931
42. Yamagata K, Oda N, Kaisaki PJ, Menzel S, Furuta H, Vaxillaire M, et al. Mutations in the Hepatocyte Nuclear Factor-1alpha Gene in Maturity-Onset Diabetes of the Young (MODY3). *Nature* (1996) 384(6608):455–8. doi: 10.1038/384455a0
43. Wang H, Antinozzi PA, Hagenfeldt KA, Maechler P, Wollheim CB. Molecular Targets of a Human HNF1 Alpha Mutation Responsible for Pancreatic Beta-Cell Dysfunction. *EMBO J* (2000) 19(16):4257–64. doi: 10.1093/emboj/19.16.4257
44. Shih D. Bussen M, Sehayek E, Ananthanarayanan M, Shneider BL, Suchy FJ, Shefer S, et al. Hepatocyte Nuclear Factor-1α Is an Essential Regulator of Bile Acid and Plasma Cholesterol Metabolism. *Nat Genet* (2001) 27:375–82. doi: 10.1038/86871
45. Pontoglio M. Hepatocyte Nuclear Factor 1, a Transcription Factor at the Crossroads of Glucose Homeostasis. *J Am Soc Nephrol* (2000) 11 Suppl 16:S140–3. doi: 10.1681/ASN.V11suppl_2s140
46. Ellard S, Colclough K. Mutations in the Genes Encoding the Transcription Factors Hepatocyte Nuclear Factor 1 Alpha (HNF1A) and 4 Alpha (HNF4A) in Maturity-Onset Diabetes of the Young. *Hum Mutation* (2010) 27(9):854–69. doi: 10.1002/humu.20357
47. Awa WL, Thon A, Raile K, Grulich-Henn J, Meissner T, Schober E, et al. Genetic and Clinical Characteristics of Patients With HNF1A Gene Variations From the German-Austrian DPV Database. *Eur J Endocrinol* (2011) 164(4):513–20. doi: 10.1530/EJE-10-0842
48. Leslie R, Atkinson M, Notkins AL. Autoantigens IA-2 and GAD in Type I (Insulin-Dependent) Diabetes. *Diabetologia* (1999) 42(1):3–14. doi: 10.1007/s001250051105
49. Ellard S, Bellanné-Chantelot C, Hattersley AT. Best Practice Guidelines for the Molecular Genetic Diagnosis of Maturity-Onset Diabetes of the Young. *Diabetologia* (2008) 51(4):546–53. doi: 10.1007/s00125-008-0942-y
50. Aanstoot H-J. Identification, Characterization and Application of Autoantigens in Type 1 Diabetes Mellitus. (1993). Available at: http://hdl.handle.net/1765/38447
51. Dabelea D, Bell RA, D'Agostino RBJr., Imperatore G, Johansen JM, Linder B, et al. Incidence of Diabetes in Youth in the United States. *Jama* (2007) 297(24):2716–24. doi: 10.1001/jama.297.24.2716
52. Reinehr T, Schober E, Wiegand S, Thon A, Holl R. β-Cell Autoantibodies in Children With Type 2 Diabetes Mellitus: Subgroup or Misclassification? *Arch Dis Childhood* (2006) 91(6):473–7. doi: 10.1136/adc.2005.088229
53. McDonald TJ, Colclough K, Brown R, Shields B, Shepherd M, Bingley P, et al. Islet Autoantibodies can Discriminate Maturity-Onset Diabetes of the Young (MODY) From Type 1 Diabetes. *Diabetes Med* (2011) 28(9):1028–33. doi: 10.1111/j.1464-5491.2011.03287.x

Conflict of Interest: The authors declare that the research was conducted in the absence of any commercial or financial relationships that could be construed as a potential conflict of interest.

Publisher's Note: All claims expressed in this article are solely those of the authors and do not necessarily represent those of their affiliated organizations, or those of the publisher, the editors and the reviewers. Any product that may be evaluated in this article, or claim that may be made by its manufacturer, is not guaranteed or endorsed by the publisher.

frontiers | Frontiers in Endocrinology

SYSTEMATIC REVIEW
published: 30 June 2022
doi: 10.3389/fendo.2022.911526

The Clinical Characteristics and Gene Mutations of Maturity-Onset Diabetes of the Young Type 5 in Sixty-One Patients

Shenghui Ge[1], Mengge Yang[2], Yuying Cui[3], Jing Wu[1], Lusi Xu[2], Jianjun Dong[4] and Lin Liao[1,5]**

[1] Department of Endocrinology and Metabolology, The First Affiliated Hospital of Shandong First Medical University and Shandong Provincial Qianfoshan Hospital, Jinan, China, [2] Cheeloo College of Medicine, Shandong University, Department of Endocrinology and Metabolology, Shandong Provincial Qianfoshan Hospital, Shandong Key Laboratory of Rheumatic Disease and Translational medicine, Shandong Institute of Nephrology, Jinan, China, [3] College of Traditional Chinese Medicine, Shandong University of Traditional Chinese Medicine, Jinan, China, [4] Division of Endocrinology, Department of Internal Medicine, Qilu Hospital of Shandong University, Jinan, China, [5] Department of Endocrinology and Metabolology, The First Affiliated Hospital of Shandong First Medical University & Shandong Provincial Qianfoshan Hospital, Shandong Key Laboratory of Rheumatic Disease and Translational medicine, Shandong Institute of Nephrology, Jinan, China

OPEN ACCESS

Edited by:
Jiajun Zhao,
Shandong Provincial Hospital, China

Reviewed by:
Lingling Xu,
Peking Union Medical College Hospital (CAMS), China
Gabriella De Medeiros Abreu,
Oswaldo Cruz Institute, Oswaldo Cruz Foundation (Fiocruz), Brazil
Yang Xiao,
Central South University, China

***Correspondence:**
Lin Liao
liaolin@sdu.edu.cn
Jianjun Dong
dongjianjun@sdu.edu.cn

Specialty section:
This article was submitted to Clinical Diabetes, a section of the journal Frontiers in Endocrinology

Received: *02 April 2022*
Accepted: *01 June 2022*
Published: *30 June 2022*

Citation:
Ge S, Yang M, Cui Y, Wu J, Xu L, Dong J and Liao L (2022) The Clinical Characteristics and Gene Mutations of Maturity-Onset Diabetes of the Young Type 5 in Sixty-One Patients. Front. Endocrinol. 13:911526. doi: 10.3389/fendo.2022.911526

Aims: Maturity-onset diabetes of the young type 5 (MODY5), a rare disease, is very easy to be misdiagnosed as type 2 diabetes. To get better understanding of the disease, we analyzed the clinical characteristics and gene mutations of MODY5.

Methods: PubMed, Cochrane, the China National Knowledge Infrastructure, and Wanfang were searched with the following search terms: "MODY5" OR "HNF1B maturity-onset diabetes of the young" OR "maturity-onset diabetes of the young type 5" OR "renal cysts and diabetes syndrome". Clinical characteristics and gene mutations of MODY5 were analyzed. The demography, clinical characteristics, and blood indicators of patients were described utilizing simple summary statistics. Variables were analyzed by t-test, Wilcoxon signed rank test, and Fisher exact test. Spearman's correlation analysis was used for bi-variate analysis. All tests were two-sided, and a p-value < 0.05 was considered statistically significant. Statistical analysis was performed using the Statistical Package for the Social Sciences version 26 for Windows (SPSS).

Results: A total of 48 literatures were included in this study, including 61 eligible patients and 4 different mutations. Of the 39 patients with available body weight index, 15 (38.46%) were underweight, 21 (53.85%) were normal weight and 3 (7.69%) were overweight or obese. Of the 38 patients with available family history, 25 (65.79%) reported a family history of diabetes. Of the 34 patients with available age of diabetes diagnosis, the median age of diabetes diagnosis was 16.00 years old and 88.24% (30/34) of patients were under 25 years old when they were first diagnosed with diabetes. Renal cysts were presented in 72.41%, hypomagnesemia in 91.67%, and pancreatic dysplasia in 71.88% of the patients. Patients with hepatocyte nuclear factor 1B (HNF1B) deletion had lower serum

magnesium, serum creatinine, and higher eGFR than patients with other gene mutations, and the difference was statistically significant.

Conclusions: The young onset of diabetes with low or normal BMI, renal cysts, hypomagnesemia, and pancreatic dysplasia should be recommended to genetic testing in order to differentiate MODY5 from other types of diabetes earlier.

Keywords: MODY5, diagnosis, HNF1B, gene mutation, renal cysts and diabetes syndrome

INTRODUCTION

Globally, diabetes is a widely distributed disease which is a chronic metabolic disease that seriously affects human health. Due to advances in genetic testing technologies, an increasing number of monogenic diabetes are differentiated from type 2 or type 1 diabetes. Maturity-onset diabetes of the young (MODY) is a monogenic diabetes accounting for approximately 1% – 2% of diabetes (1), and currently at least 14 types of genes have been confirmed to be associated with MODY, which include *GCK*, *HNF1A*, *HNF1B*, *HNF4A*, *PDX1*, *NEUROD-1*, *KLF-11*, *CEL*, *PAX4*, *INS*, *BLK*, *ABCC8*, *KCNJ11*, *APPL1* (2). The incidence of MODY5 is low, accounting for less than 5% in MODY (3). MODY5 was first described by Horikawa and noted to be related to *HNF1B* (4). Since there was considerable variability in the clinical features of MODY5, it was often misdiagnosed as type 1 diabetes or type 2 diabetes (5). Unfortunately, no systematic summary of MODY5 has been performed to date. In order to get a better understanding of MODY5, this study analyzed the clinical features and gene mutations of MODY5 to help physicians to differentiate MODY5 from other types of diabetes early.

MATERIALS AND METHODS

Data Sources and Study Patients

PubMed, Cochrane, China National Knowledge Infrastructure (CNKI) and Wanfang were searched from the date of inception to February 27, 2022 using the following search terms: "MODY5", "*HNF1B* maturity-onset diabetes of the young", "maturity-onset diabetes of the young type 5", and "renal cysts and diabetes syndrome". All the enrolled studies met the following criteria: ① the diagnosis of MODY5 was confirmed by genetic test and the mutated sites were described; ② the literature provided the data of FBG or HbA1c; ③ the language of the literature was English or Chinese. The flow chart (**Supplementary Figure 1**) showed the reasons for identification of eligible studies.

The following clinical and laboratory variables were studied: (1) country; (2) gender; (3) age at diagnosis; (4) site and type of gene mutation; (5) family history; (6) BMI; (7) treatment of diabetes; (8) fasting blood-glucose; (9) fasting C-peptide; (10) HbA1c; (11) serum magnesium; (12) other serum indices; (13) renal manifestations; (14) pancreatic manifestations; (15) reproductive manifestations.

Statistical Analysis

The demography, clinical characteristics, and blood indicators of patients were described utilizing simple summary statistics. Variables were analyzed by t-test, Wilcoxon signed rank test, and Fisher exact test. Spearman's correlation analysis was used for bi-variate analysis. All tests were two-sided, and a p-value < 0.05 was considered statistically significant. Statistical analysis was performed using the Statistical Package for the Social Sciences version 26 for Windows (SPSS).

RESULTS

General Data

A total of 48 literatures were included in this study, including 61 eligible patients from 15 countries involving 5 continents (**Figure 1**). The top four were China (15/61, 24.59%), Japan (12/61, 19.67%), France (8/61, 13.11%) and The United States (7/61, 11.48%). The patients were distributed in Asia (30/61, 48.2%), Europe (20/61, 32.8%), North America (7/61, 11.5%), South America (3/61, 4.9%) and Oceania (1/61, 1.6%).

Clinical Features

The clinical data of the patients were shown in **Supplementary Table 1**, **Supplementary Table 2** and **Figure 2**. Among the 61 patients, 36 patients (36/61, 59.02%) were male and 25 patients (25/61, 40.98%) were female. Among the 38 patients mentioning family history, 25 patients (25/38, 65.79%) had a family history of diabetes. A total of 39 patients were recorded with the body-mass-index (BMI). The median of BMI was 19.60 kg/m^2. According to WHO standard, 15 patients (15/39, 38.46%) were underweight (< 18.5 kg/m^2), 21 patients (21/39, 53.85%) were normal weight, 2 patients (2/39, 5.13%) were overweight (25~29.9 kg/m^2), and 1 patient (1/39, 2.56%) was obese (≥ 30 kg/m^2).

Fasting blood-glucose (FBG) was recorded in 38 patients with a median of 8.37 mmol/L (normal range 3.9-6.1 mmol/L). In addition, 2-hour postprandial blood glucose (2h-PG) was recorded in 9 patients with a mean of 17.24 mmol/L (normal range 4.4-7.8 mmol/L). Fasting C-peptide (FCP) was recorded in 35 patients with a median of 1.23 ng/mL (normal range 1.1-4.4 ng/mL). HbA1c was recorded in 55 patients with a median of 9.40 (normal range 4-6%). Serum magnesium was recorded in 25 patients, with an average of 0.52 mmol/L (normal range 0.70-1.00 mmol/L) and hypomagnesemia occurred in 91.67% of patients. Esti mated glomerularfiltrationrate (eGFR) was

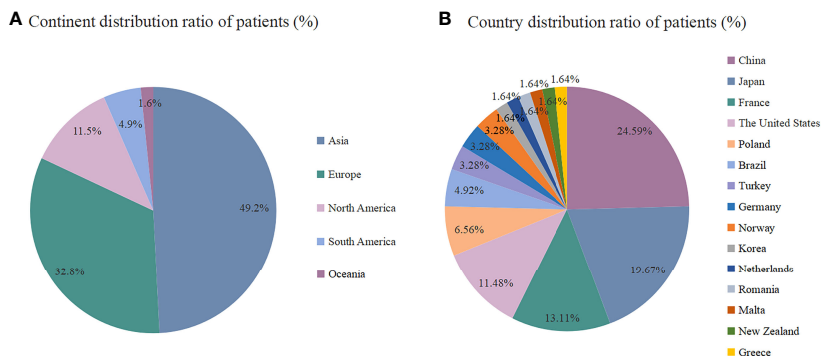

FIGURE 1 | **(A)** Continent distribution ratio among the patients (%), **(B)** Country distribution ratio among the patients (%).

recorded in 26 patients with a median of 72.00 ml/min per 1.73m^2. Serum uric acid level was recorded in 20 patients with an average of 446.01 μmol/L (normal range < 420 μmol/L), of which 13 patients (13/20, 65.00%) had serum uric acid ≥ 420 μmol/L. Serum creatinine was recorded in 34 patients with a median of 96.74 μmol/L (normal range < 106 μmol/L).

Among the 34 patients with recorded age of diabetes diagnosis, the median age of diabetes at diagnosis was 16.00 years old, 88.24% of patients developed diabetes before 25 years old, and 14.71% of patients developed diabetes before 10 years old. There were 10 patients (10/61, 16.39%) had experience of ketoacidosis. Renal morphology was recorded in 58 patients, and 42 patients (42/58, 72.41%) had renal cysts, including left renal cysts (8/42, 19.05%), right renal cysts (3/42, 7.14%), double or multiple renal cysts (25/42, 59.52%), and not classified (6/42, 14.29%). There were 11 patients (11/58, 18.97%) with renal dysplasia, 2 patients (2/58, 3.45%) with

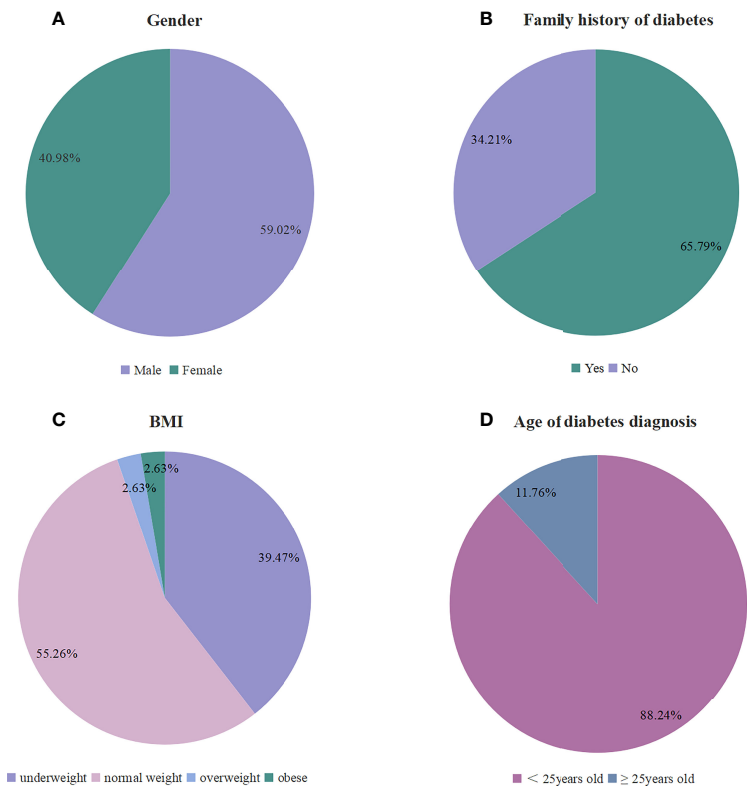

FIGURE 2 | Clinical characteristics of patients with MODY5. **(A–D)** The proportion of several clinical characteristics in enrolled patients: **(A)** gender (N: 61), **(B)** family history of diabetes (N: 38), **(C)** BMI (N: 39), and **(D)** Age of diabetes diagnosis (N: 34).

renal calculus, 1 patient (1/58, 1.72%) with renal cystic nodules. Pancreatic dysplasia was recorded in 23 patients (23/32, 71.88%), including pancreatic atrophy or agenesis (22/32, 68.75%) and annular pancreas (1/32, 3.13%). Exocrine pancreatic insufficiency was described in 9 patients (9/13, 69.23%), with tests including fecal elastase and p-aminobenzoic acid excretion index. Five patients were with reproductive system abnormalities, including saddle uterus, seminal vesicular cyst with azoospermia, double horn uterus, and double uterus.

The treatments regimens were recorded for 51 patients. Forty-one patients (41/51, 80.39%) were treated with insulin, 6 patients (6/51, 11.76%) underwent diet therapy only and 4 patients (4/51, 7.84%) were given oral hypoglycemic agents without insulin. Among the 41 patients receiving insulin, 4 patients (4/41, 9.76%) combined oral hypoglycemic drugs, 1 patient (1/41, 2.44%) combined liraglutide and 36 patients (36/41, 88.80%) received insulin monotherapy.

The clinical data of patients with *HNF1B* deletion and other mutations were shown in **Supplementary Table 3**. In patients with *HNF1B* deletion, the median of FBG was 8.67 mmol/L, FCP was 1.40 ng/mL, serum creatinine was 84.86 μmol/L, and the mean of serum magnesium was 0.48 mmol/L, serum uric acid was 429.15 μmol/L. In patients with other mutations, the median of FBG was 7.82 mmol/L, FCP was 1.08 ng/mL, serum creatinine was 134.37 μmol/L, and the mean of serum magnesium was 0.61 mmol/L, serum uric acid was 466.62 μmol/L. Patients with *HNF1B* deletion had lower serum magnesium, serum creatinine, and higher eGFR than patients with other gene mutations, and the difference was statistically significant. However, there was no significant difference in the incidence of pancreatic dysplasia.

The correlation analysis of renal cysts and serum parameters was shown in **Table 1**. In MODY5, there was no correlation between the occurrence of renal cysts and eGFR, serum creatinine, serum magnesium, and serum uric acid. The proportion of hypomagnesemia in MODY5 patients with or without polycystic kidney disease was presented in **Figure 3**. Hypomagnesemia was presented in 11 patients (11/13, 84.62%) with polycystic kidney disease. And hypomagnesemia was presented in 8 patients (8/9, 88.89%) without polycystic kidney disease. There was no significant correlation between polycystic kidney disease and hypomagnesemia in MODY5.

Gene Mutations

The gene mutations of the patients were shown in **Table 2** and **Figure 4**. Totally 4 types of mutations were identified, which included substitution (29/61, 47.54%), *HNF1B* deletion (28/61, 45.90%), frame shift (3/61, 4.92%) and small deletion (1/61, 1.64%). The genetic information of the patient's parents was recorded in 14 cases, and *de novo* mutations were confirmed in 11 patients (11/14, 78.57%).

TABLE 1 | Spearman's correlation analysis evaluating the association between serum parameters and renal cysts of MODY5 patients.

Subjects	Case	Renal cysts (yes/no)	
		r	P
eGFR	25	0.198	0.344
Serum creatinine	32	-0.087	0.638
Serum magnesium	23	0.329	0.125
Serum uric acid	20	-0.310	0.183

eGFR, estimated glomerularfiltrationrate.

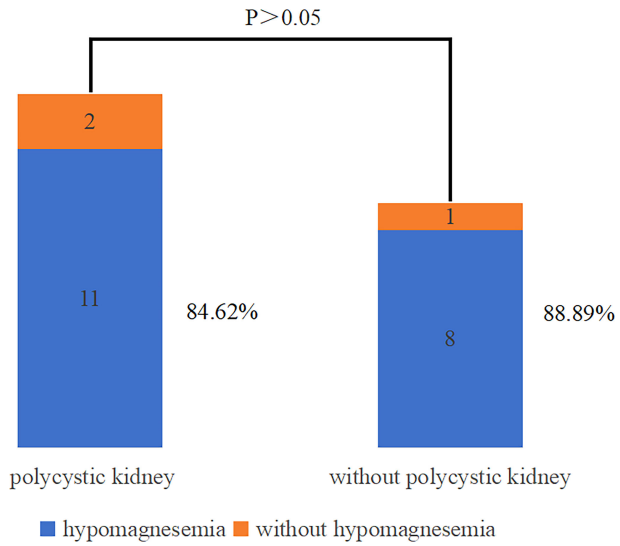

FIGURE 3 | Correlation analysis of hypomagnesemia and polycystic kidney disease in MODY5 patients.

DISCUSSION

MODY5 was caused by *HNF1B* mutations due to changes in its effectors. Since MODY5 was first described, there have been some reports about this disease. However, most reports were case reports. Unlike previous studies, our study summarized the clinical features and genetic mutations of 61 patients with MODY5, and demonstrated the MODY5 patients had the following clinical characteristics: (1) high incidence of renal cysts (72.41%), hypomagnesemia (91.67%), and pancreatic dysplasia (71.88%); (2) early onset of diabetes; (3) normal or underweight (92.31%).

As for diagnosis, most MODY5 patients were misdiagnosed as type 1 diabetes or type 2 diabetes (5). Therefore, it was crucial to identify the clinical features of diabetes in MODY5 patients. Our study showed that most patients (88.24%) developed diabetes before 25 years old, and the median onset age of diabetes in MODY5 patients were 16.00 years old, which was different from previous studies (6–9). A multi-clinical center study showed that the onset age of diabetes in MODY5 patients were more than 25 years old (6). Another multicenter retrospective cohort study of patients with *HNF1B* mutation showed that the mean age of diagnosis of diabetes was 26 years old (7). In the Japanese study (8), only 6% of patients developed diabetes during adolescence. Lim et al. reported 4 patients (29%) developed diabetes before 14.6 years old (9). The reasons for these different conclusions might be as follows: The results might be

TABLE 2 | *HNF1B* mutations of MODY5 patients.

No.	Country	Gender	cDNA	Protein
1	China	F	c.1007A>G	p.His336Arg
2	The United States	F	c.1127C>T	p.Thr376Ile
3	China	M	c.1132C>T	p.Gln378*
4	Japan	M	c.457C>A	p.His153Asn
5	Malta	F	c.1580G>A	p.Arg527Gln
6	Japan	M	c.434T>A	p.Leu145Gln
7	France	F	c.443C>G	p.Ser148Trp
8	China	M	c.443C>T	p.Ser148Leu
9	The United States	M	c.443C>T	p.Ser148Leu
10	Turkey	F	c.443C>T	p.Ser148Leu
11	Germany	M	c.443C>T	p.Ser148Leu
12	Korea	F	c.476C>T	p.Pro159Leu
13	China	F	c.494G>A	p.Arg165His
14	Japan	M	c.503T>C	p.Leu168Pro
15	China	M	c.530G>A	p.Arg177Gln
16	China	F	c.541C>T	p.Arg181*
17	Rumania	M	c.715G>C	p.Gly239Arg
18	Poland	M	c.742C>T	p.Gln248*
19	Poland	M	c.742C>T	p.Gln248*
20	China	F	c.826C>T	p.Arg276*
21	Japan	M	c.826C>T	p.Arg276*
22	France	M	c.884G>A	p.Arg295His
23	France	M	c.884G>A	p.Arg295His
24	France	M	c.143delT	p.Leu48fs
25	Brazil	M	c.983delC	p.Pro328Leufs*48
26	Norway	F	c.409_483del	p.Arg137_Lys161del
27	The United States	F	c.1149delinsTGGCC	p.Arg351Leufs*10
28	Japan	F		p.Leu264Ser
29	Norway	M		p.Phe148Leu
30	Poland	M	c.1046-15T>A	
31	France	M	c.544+4A>C	
32	Japan	F	c.544+1G>T	
33	Japan	M	g.37731831C>G	
34	China	F	*HNF1B* deletion	
35	China	M	*HNF1B* deletion	
36	Japan	F	*HNF1B* deletion	
37	Japan	M	*HNF1B* deletion	
38	The United States	F	*HNF1B* deletion	
39	France	M	*HNF1B* deletion	
40	France	F	*HNF1B* deletion	
41	Brazil	M	*HNF1B* deletion	
42	Brazil	M	*HNF1B* deletion	
43	New Zealand	F	*HNF1B* deletion	
44	China	M	*HNF1B* deletion ◇	
45	China	F	*HNF1B* deletion ◇	
46	China	F	*HNF1B* deletion ◇	
47	China	M	*HNF1B* deletion ◇	
48	China	F	*HNF1B* deletion ◇	
49	Japan	F	*HNF1B* deletion ◇	
50	Japan	F	*HNF1B* deletion ◇	
51	Japan	M	*HNF1B* deletion ◇	
52	The United States	M	*HNF1B* deletion ◇	
53	The United States	M	*HNF1B* deletion ◇	
54	The United States	M	*HNF1B* deletion ◇	
55	France	M	*HNF1B* deletion ◇	
56	Poland	M	*HNF1B* deletion ◇	
57	Turkey	M	*HNF1B* deletion ◇	
58	Germany	F	*HNF1B* deletion ◇	
59	Netherlands	M	*HNF1B* deletion ◇	
60	China	M	*HNF1B* deletion §	
61	Greece	F	*HNF1B* deletion ¶	

Gender: F, female; M, male. § Exon2~9del. ◇HNF1B deletion is accompanied with 17q12 deletion. ¶HNF1B deletion is accompanied with a HNF1A mutation (c.685C>T, p.Arg229).*

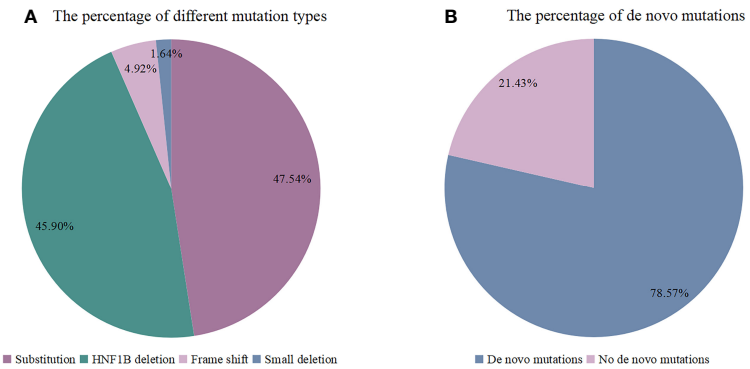

FIGURE 4 | **(A)** The percentage of different mutation types (N: 61), **(B)** The percentage of *de novo* mutations (N: 14).

affected by different inclusion criteria. In our study, glucose-related data must be recorded when data literatures were included. While in the most above-mentioned study, age was set in the inclusion criteria. Notably, although the onset of diabetes in most patients was under 25 years old, only 14.71% of patients developed diabetes before 10 years old. Teo et al. indicated that compensatory mechanisms in the pancreatic transcription factor network due to *HNF1B* mutations (10). Therefore, MODY5 often occurred in adolescence rather than in the neonatal period. Different mechanisms were involved in the development of MODY5 diabetes. Firstly, pancreatic dysplasia was presented in most patients (71.88%). A study in monozygotic twins with MODY5 showed that impaired insulin secretion was not due to pancreatic B cell functional defects, but pancreatic dysplasia (11). It has also been previously reported that pancreatic dorsal dysplasia was associated with *HNF1B* mutations (12). Therefore, pancreatic dysplasia might be involved in the development of diabetes. Secondly, some mutations might be related to changes in GLUT2-related signaling pathways, such as p.Arg276* mutation and p.Pro159Leu mutation (13). Previous studies have shown that glucose-stimulated insulin secretion was significantly reduced when the p.Arg276* mutation occurred (14). However, this change in insulin secretion was not presented in KCl stimulation. Because *HNF1B* might play a role in intracellular ATP production and indirectly regulate K^+ current through ATP-sensitive K^+ channels (14). There were individual differences in diabetes among MODY5 patients. This also explained why MODY5 was easily misdiagnosed as type 1 diabetes or type 2 diabetes.

The renal manifestations were prominent in MODY5 patients. Renal cysts (72.41%) were the most common morphological abnormalities, with the majority presented as multiple renal cysts. Although multiple renal cysts were a common renal phenotype in MODY5 patients, they needed to be differentiated from other polycystic kidney diseases. In a study of children with cystic kidney disease (15), hypomagnesemia appeared to be a marker of differential diagnosis between autosomal dominant polycystic kidney disease (ADPKD), autosomal recessive polycystic kidney disease (ARPKD) and MODY5. Patients with MODY5 often had hypomagnesemia, but it was uncommon in patients with ADPKD or ARPKD. Hypomagnesemia was presented in 84.62% of MODY5 patients with multiple renal cysts. Therefore, multiple renal cysts with hypomagnesemia should raise suspicion for MODY5 diagnosis. In addition, the correlation between hypomagnesemia and multiple renal cysts was analyzed in MODY5 patients. The results showed that there was no significant relationship between hypomagnesemia and multiple renal cysts. At the same time, the correlation between serum magnesium and renal cysts was studied in MODY5 patients, and no association was presented. Therefore, hypomagnesemia might be helpful to differentiate different polycystic kidney diseases. This depended on the high incidence of hypomagnesemia in MODY5 rather than polycystic kidney itself.

The renal function of MODY5 varied greatly from normal to end-stage renal failure (16), but there was no unified conclusion about the correlation between gene mutation types and renal function. In our study, patients with a total gene deletion had a better renal prognosis than those with other gene mutations. Firstly, additional deleted genes within *HNF1B* might include genes that impair renal functional. But the effect has not been reported thus far (6). Secondly, patients with *HNF1B* deletion may be affected by 17q12 deletion. This led to underexpression of certain genes and indirectly reduced kidney damage (17). But another study showed no correlation between genotype and renal functional (9). Although renal malformations appeared to be the common manifestation of *HNF1B* mutations, progression to end-stage renal disease (ESKD) in patients with *HNF1B* mutations seemed to be rare (18). The specific mechanism needs to be further explored. Furthermore, our study did not find an association between renal function and renal cysts. Renal function might not be affected by renal cysts.

Pancreatic abnormalities in MODY5 were mainly dysplasia. Ventral pancreatic dysplasia was the most prominent, because *HNF1B* was related to ventral pancreatic development, its mutation could cause pancreatic dysplasia (19–21). It was also reported that patients might have pancreas divisum, intraductal papillary mucinous tumo, yet these manifestations were extremely rare (6). In MODY5, in addition to insufficient

insulin secretion due to pancreatic dysplasia, pancreatic exocrine function was also often impaired. Pancreatic exocrine dysfunction was also presented in MODY5 patients. These patients might present with abdominal pain, loose stools and weight loss. Fecal elastase was a convenient indicator of pancreatic exocrine function (22). Therefore, fecal elastase test was recommended for patients with suspected MODY5.

Hypomagnesemia was common in patients with MODY5. The deficient *HNF1B* downregulated the expression of *FXYD2*. The downregulated *FXYD2* blocked the encoding of the γ subunit of the Na^+-K^+-ATPase and indirectly led to hypomagnesemia (23–25). Although hypomagnesemia was a common presentation in patients with MODY5, patients had varying degrees of hypomagnesemia in different mutation types. Patients with *HNF1B* deletion had worse hypomagnesemia than those with other mutations. The reason might be that patients with other mutations have worse renal function relative to patients with HNF1B deletion, which might reduce renal magnesium loss (15). Therefore, this should be fully considered in patients with renal insufficiency.

In addition, patients with MODY5 were prone to hyperuricemia, and some patients developed gout. Hyperuricemia is defined as serum uric acid level ≥ 420 μmol/L. In our study, 65.00% of MODY5 patients met the diagnosis of hyperuricemia. Previous studies indicated that hyperuricemia was a common early manifestation of MODY5 in children, but its utility as a predictor of the disease was limited (26). However, hyperuricemia might serve as a supplement to raise our suspicions about MODY5.

In our study, reproductive system abnormalities presented in 5 patients, included saddle uterus, eminal vesicular cyst with azoospermia, double horn uterus, and double uterus. Evaluation of the reproductive system was necessary in patients with reproductive needs or the young people. The correlation between neurological abnormalities and *HNF1B* was still unclear. Currently, it was generally believed that neurological abnormalities were more likely to come from genes other than *HNF1B* (27). Therefore, it was necessary to consider expanding the scope of genetic testing when neurological symptoms were prominent.

Clinical management is critical for MODY5 patients. Our study showed that most of the MODY5 patients (80.39%) received insulin therapy. Only a minority of patients did not use insulin after the onset of diabetes. Sulfonylureas were suitable for patients with a certain reserve of pancreas islet function (28), and they were not suitable for patients with severe pancreatic dysplasia. Notably, recent reports have provided some new therapeutic possibilities. A patient with *HNF1B* deficiency MODY5 who was treated with liraglutide restored endogenous insulin secretion and stopped insulin injection (29). This might be due to the upregulation of *PAX6* by glucagon-like peptide 1 receptor agonists (30), which promoted the regeneration of insulin-secreting cells. In addition, MODY5 patients might benefit from Bacillus Calmette – Guerin (BCG) vaccination (31). Studies showed that BCG treatment might regenerate pancreatic B cell (32, 33). This might compensate for the deficiency caused by pancreatic dysplasia. Management of pancreatic exocrine dysfunction is often neglected. Early pancreatic replacement therapy for these patients can improve their symptoms and normalize their weight (22). For hypomagnesemia patients, inorganic magnesium treatment was less effective, there were side effects of diarrhea. Organomagnesium such as magnesium aspartate was recommended (34). At the same time, thiazide diuretics should be carefully used in patients with hypomagnesemia, which could aggravate hypomagnesemia (35). In MODY5 patients with hyperuricemia, drugs that promote uric acid excretion were prohibited. Allopurinols were recommended to control serum uric acid levels and delay renal damage (36).

Our study has several limitations. Firstly, in order to comprehensively understand the clinical characteristics of MODY5 patients, all articles were limited to at least recording diabetes-related indicators, which might lead to selection bias in our study. Secondly, because of the low incidence of MODY5, some rare clinical manifestations are difficult to analyze. Finally, the mechanism of different mutations leading to various clinical features still remains confused and further studies are needed to explain its molecular mechanism.

In summary, our study shows that MODY5 often has multiple clinical manifestations. Diabetes usually starts before 25 years old and often with pancreatic dysplasia. Patients with *HNF1B* deletion have a better renal prognosis and worse hypomagnesemia than patients with other gene mutations. The young onset of diabetes with low or normal BMI, renal cysts, hypomagnesemia, and pancreatic dysplasia should be recommended to genetic testing earlier in order to differentiate MODY5 from other types of diabetes.

DATA AVAILABILITY STATEMENT

The original contributions presented in the study are included in the article/**Supplementary Material**. Further inquiries can be directed to the corresponding author.

AUTHOR CONTRIBUTIONS

SG: Document Retrieval, Data Extraction, Data analysis, Essay writing, and Paper submission. MY and YC: Data analysis. JW and LX: Data Extraction. JD and LL: Article innovation and Paper submission. All authors contributed to the article and approved the submitted version.

FUNDING

This work was funded by the National Natural Science Foundation of China (82170847).

SUPPLEMENTARY MATERIAL

The Supplementary Material for this article can be found online at: https://www.frontiersin.org/articles/10.3389/fendo.2022.911526/full#supplementary-material

REFERENCES

1. Fajans SS, Bell GI. Mody: History, Genetics, Pathophysiology, and Clinical Decision Making. *Diabetes Care* (2011) 34(8):1878–84. doi: 10.2337/dc11-0035
2. Urakami T. Maturity-Onset Diabetes of the Young (Mody): Current Perspectives on Diagnosis and Treatment. *Diabetes Metab Syndrome Obes* (2019) 12:1047–56. doi: 10.2147/dmso.S179793
3. Firdous P, Nissar K, Ali S, Ganai BA, Shabir U, Hassan T, et al. Genetic Testing of Maturity-Onset Diabetes of the Young Current Status and Future Perspectives. *Front Endocrinol* (2018) 9:253. doi: 10.3389/fendo.2018.00253
4. Horikawa Y, Iwasaki N, Hara M, Furuta H, Hinokio Y, Cockburn BN, et al. Mutation in Hepatocyte Nuclear Factor-1 Beta Gene (Tcf2) Associated With Mody. *Nat Genet* (1997) 17(4):384–5. doi: 10.1038/ng1297-384
5. Kleinberger JW, Pollin TI. Undiagnosed Mody: Time for Action. *Curr Diabetes Rep* (2015) 15(12):110. doi: 10.1007/s11892-015-0681-7
6. Dubois-Laforgue D, Cornu E, Saint-Martin C, Coste J, Bellanné-Chantelot C, Timsit J. Response to Comment on Dubois-Laforgue Et al. Diabetes, Associated Clinical Spectrum, Long-Term Prognosis, and Genotype/Phenotype Correlations in 201 Adult Patients With Hepatocyte Nuclear Factor 1b (Hnf1b) Molecular Defects. *Diabetes Care* (2017) 40:1436–43. doi: 10.2337/dci17-0048
7. Bingham C, Hattersley AT. Renal Cysts and Diabetes Syndrome Resulting From Mutations in Hepatocyte Nuclear Factor-1beta. *Nephrology Dialysis Transplant* (2004) 19(11):2703–8. doi: 10.1093/ndt/gfh348
8. Shields BM, Hicks S, Shepherd MH, Colclough K, Hattersley AT, Ellard S. Maturity-Onset Diabetes of the Young (Mody): How Many Cases Are We Missing? *Diabetologia* (2010) 53(12):2504–8. doi: 10.1007/s00125-010-1799-4
9. Lim SH, Kim JH, Han KH, Ahn YH, Kang HG, Ha IS, et al. Genotype and Phenotype Analyses in Pediatric Patients With Hnf1b Mutations. *J Clin Med* (2020) 9(7):454–5. doi: 10.3390/jcm9072320
10. Teo AK, Lau HH, Valdez IA, Dirice E, Tjora E, Raeder H, et al. Early Developmental Perturbations in a Human Stem Cell Model of Mody5/Hnf1b Pancreatic Hypoplasia. *Stem Cell Rep* (2016) 6(3):357–67. doi: 10.1016/j.stemcr.2016.01.007
11. Ohara Y, Okada Y, Yamada T, Sugawara K, Kanatani M, Fukuoka H, et al. Phenotypic Differences and Similarities of Monozygotic Twins With Maturity-Onset Diabetes of the Young Type 5. *J Diabetes Invest* (2019) 10(4):1112–5. doi: 10.1111/jdi.13004
12. Haldorsen IS, Vesterhus M, Raeder H, Jensen DK, Søvik O, Molven A, et al. Lack of Pancreatic Body and Tail in Hnf1b Mutation Carriers. *Diabetic Med* (2008) 25(7):782–7. doi: 10.1111/j.1464-5491.2008.02460.x
13. Kim EK, Lee JS, Cheong HI, Chung SS, Kwak SH, Park KS. Identification and Functional Characterization of P159l Mutation in Hnf1b in a Family With Maturity-Onset Diabetes of the Young 5 (Mody5). *Genomics Inf* (2014) 12(4):240–6. doi: 10.5808/gi.2014.12.4.240
14. Fujimoto K, Sasaki T, Hiki Y, Nemoto M, Utsunomiya Y, Yokoo T, et al. *In Vitro* and Pathological Investigations of Mody5 With the R276x-Hnf1beta (Tcf2) Mutation. *Endocrine J* (2007) 54(5):757–64. doi: 10.1507/endocrj.k07-051
15. Seeman T, Fořtová M, Sopko B, Průša R, Pohl M, John U. Hypomagnesaemia Is Absent in Children With Autosomal Dominant Polycystic Kidney Disease. *Ann Clin Biochem* (2019) 56(1):90–4. doi: 10.1177/0004563218785190
16. Bingham C, Ellard S, Allen L, Bulman M, Shepherd M, Frayling T, et al. Abnormal Nephron Development Associated With a Frameshift Mutation in the Transcription Factor Hepatocyte Nuclear Factor-1 Beta. *Kidney Int* (2000) 57(3):898–907. doi: 10.1046/j.1523-1755.2000.057003898.x
17. Kampe K, Sieber J, Orellana JM, Mundel P, Jehle AW. Susceptibility of Podocytes to Palmitic Acid Is Regulated by Fatty Acid Oxidation and Inversely Depends on Acetyl-Coa Carboxylases 1 and 2. *Am J Physiol Renal Physiol* (2014) 306(4):F401–9. doi: 10.1152/ajprenal.00454.2013
18. Bockenhauer D, Jaureguiberry G. Hnf1b-Associated Clinical Phenotypes: The Kidney and Beyond. *Pediatr Nephrol (Berlin Germany)* (2016) 31(5):707–14. doi: 10.1007/s00467-015-3142-2
19. Haumaitre C, Barbacci E, Jenny M, Ott MO, Gradwohl G, Cereghini S. Lack of Tcf2/Vhnf1 in Mice Leads to Pancreas Agenesis. *Proc Natl Acad Sci USA* (2005) 102(5):1490–5. doi: 10.1073/pnas.0405776102
20. Kawaguchi Y, Cooper B, Gannon M, Ray M, MacDonald RJ, Wright CV. The Role of the Transcriptional Regulator Ptf1a in Converting Intestinal to Pancreatic Progenitors. *Nat Genet* (2002) 32(1):128–34. doi: 10.1038/ng959
21. Iwasaki N, Tsurumi M, Asai K, Shimuzu W, Watanabe A, Ogata M, et al. Pancreatic Developmental Defect Evaluated by Celiac Artery Angiography in a Patient With Mody5. *Hum Genome variation* (2016) 3:16022. doi: 10.1038/hgv.2016.22
22. Clissold RL, Fulford J, Hudson M, Shields BM, McDonald TJ, Ellard S, et al. Exocrine Pancreatic Dysfunction Is Common in Hepatocyte Nuclear Factor 1β-Associated Renal Disease and Can Be Symptomatic. *Clin Kidney J* (2018) 11(4):453–8. doi: 10.1093/ckj/sfx150
23. Ferrè S, Bongers EM, Sonneveld R, Cornelissen EA, van der Vlag J, van Boekel GA, et al. Early Development of Hyperparathyroidism Due to Loss of Pth Transcriptional Repression in Patients With Hnf1β Mutations? *J Clin Endocrinol Metab* (2013) 98(10):4089–96. doi: 10.1210/jc.2012-3453
24. Adalat S, Woolf AS, Johnstone KA, Wirsing A, Harries LW, Long DA, et al. Hnf1b Mutations Associate With Hypomagnesemia and Renal Magnesium Wasting. *J Am Soc Nephrol* (2009) 20(5):1123–31. doi: 10.1681/asn.2008060633
25. Geering K. Fxyd Proteins: New Regulators of Na-K-Atpase. *Am J Physiol Renal Physiol* (2006) 290(2):F241–50. doi: 10.1152/ajprenal.00126.2005
26. Kołbuc M, Bieniaś B, Habbig S, Kołek MF, Szczepańska M, Kiliś-Pstrusińska K, et al. Hyperuricemia Is an Early and Relatively Common Feature in Children With Hnf1b Nephropathy But Its Utility as a Predictor of the Disease Is Limited. *J Clin Med* (2021) 10(15):712–4. doi: 10.3390/jcm10153265
27. Roehlen N, Hilger H, Stock F, Gläser B, Guhl J, Schmitt-Graeff A, et al. 17q12 Deletion Syndrome as a Rare Cause for Diabetes Mellitus Type Mody5. *J Clin Endocrinol Metab* (2018) 103(10):3601–10. doi: 10.1210/jc.2018-00955
28. Mateus JC, Rivera C, O'Meara M, Valenzuela A, Lizcano F. Maturity-Onset Diabetes of the Young Type 5 a Multisystemic Disease: A Case Report of a Novel Mutation in the Hnf1b Gene and Literature Review. *Clin Diabetes Endocrinol* (2020) 6:16. doi: 10.1186/s40842-020-00103-6
29. Terakawa A, Chujo D, Yasuda K, Ueno K, Nakamura T, Hamano S, et al. Maturity-Onset Diabetes of the Young Type 5 Treated With the Glucagon-Like Peptide-1 Receptor Agonist: A Case Report. *Medicine* (2020) 99(35):e21939. doi: 10.1097/md.0000000000021939
30. Li Y, Zheng J, Shen Y, Li W, Liu M, Wang J, et al. Comparative Study of Liraglutide and Insulin Glargine on Glycemic Control and Pancreatic β-Cell Function in Db/Db Mice. *Med Sci Monitor* (2018) 24:3293–300. doi: 10.12659/msm.907227
31. Ayoub BM, Ramadan E, Ashoush N, Tadros MM, Hendy MS, Elmazar MM, et al. Avoiding Covid-19 Complications With Diabetic Patients Could Be Achieved by Multi-Dose Bacillus Calmette-Guérin Vaccine: A Case Study of Beta Cells Regeneration. *Die Pharmazie* (2020) 75(8):375–80. doi: 10.1691/ph.2020.0494
32. Kühtreiber WM, Tran L, Kim T, Dybala M, Nguyen B, Plager S, et al. Long-Term Reduction in Hyperglycemia in Advanced Type 1 Diabetes: The Value of Induced Aerobic Glycolysis With Bcg Vaccinations. *NPJ Vaccines* (2018) 3:23. doi: 10.1038/s41541-018-0062-8
33. Kodama S, Kühtreiber W, Fujimura S, Dale EA, Faustman DL. Islet Regeneration During the Reversal of Autoimmune Diabetes in Nod Mice. *Science (New York NY)* (2003) 302(5648):1223–7. doi: 10.1126/science.1088949
34. Stiles CE, Thuraisingham R, Bockenhauer D, Platts L, Kumar AV, Korbonits M. *De Novo* Hnf1 Homeobox B Mutation as a Cause for Chronic, Treatment-Resistant Hypomagnesaemia. *Endocrinology Diabetes Metab Case Rep* (2018) 2018:750–1. doi: 10.1530/edm-17-0120
35. Li HJ, Groden C, Hoenig MP, Ray EC, Ferreira CR, Gahl W, et al. Case Report: Extreme Coronary Calcifications and Hypomagnesemia in a Patient With a 17q12 Deletion Involving Hnf1b. *BMC Nephrol* (2019) 20(1):353. doi: 10.1186/s12882-019-1533-5

36. Wang Q, Tan WF, Wang Q, Wang YY, Shen YX, Zhang MJ. A Case of Renal Cyst and Diabetic Syndrome With Gout as Primary Presentation. *Chin J Internal Med* (2017) 56(04):302–3. doi: 10.3760/cma.j.issn.0578-1426.2017.04.014

Conflict of Interest: We declare that the research was conducted in the absence of any commercial or financial relationships that could be construed as a potential conflict of interest.

Publisher's Note: All claims expressed in this article are solely those of the authors and do not necessarily represent those of their affiliated organizations, or those of the publisher, the editors and the reviewers. Any product that may be evaluated in this article, or claim that may be made by its manufacturer, is not guaranteed or endorsed by the publisher.

Advantages of publishing in Frontiers

OPEN ACCESS
Articles are free to read for greatest visibility and readership

FAST PUBLICATION
Around 90 days from submission to decision

HIGH QUALITY PEER-REVIEW
Rigorous, collaborative, and constructive peer-review

TRANSPARENT PEER-REVIEW
Editors and reviewers acknowledged by name on published articles

Frontiers
Avenue du Tribunal-Fédéral 34
1005 Lausanne | Switzerland

Visit us: www.frontiersin.org
Contact us: frontiersin.org/about/contact

REPRODUCIBILITY OF RESEARCH
Support open data and methods to enhance research reproducibility

DIGITAL PUBLISHING
Articles designed for optimal readership across devices

FOLLOW US
@frontiersin

IMPACT METRICS
Advanced article metrics track visibility across digital media

EXTENSIVE PROMOTION
Marketing and promotion of impactful research

LOOP RESEARCH NETWORK
Our network increases your article's readership